

การตัดแปรรูปของไมโครคริสตัลลีนเซลลูโลสจากซีลีเยอไมยางพาราโดยกระบวนการเคมีเชิงกลเพื่อ
เป็นวัสดุเสริมแรงในวัสดุเชิงประกอบพอลิโพรพิลีน



นางสาวพัชรภรณ์ ช่วยปลอด

บทคัดย่อและแฟ้มข้อมูลฉบับเต็มของวิทยานิพนธ์ตั้งแต่ปีการศึกษา 2554 ที่ให้บริการในคลังปัญญาจุฬาฯ (CUIR)
เป็นแฟ้มข้อมูลของนิสิตเจ้าของวิทยานิพนธ์ ที่ส่งผ่านทางบัณฑิตวิทยาลัย

The abstract and full text of theses from the academic year 2011 in Chulalongkorn University Intellectual Repository (CUIR)
are the thesis authors' files submitted through the University Graduate School.

วิทยานิพนธ์นี้เป็นส่วนหนึ่งของการศึกษาตามหลักสูตรปริญญาวิทยาศาสตรดุษฎีบัณฑิต

สาขาวิชาวัสดุศาสตร์ ภาควิชาวัสดุศาสตร์

คณะวิทยาศาสตร์ จุฬาลงกรณ์มหาวิทยาลัย

ปีการศึกษา 2560

ลิขสิทธิ์ของจุฬาลงกรณ์มหาวิทยาลัย

SURFACE MODIFICATION OF MICROCRYSTALLINE CELLULOSE FROM PARAWOOD
SAWDUST VIA MECHANOCHEMICAL PROCESS FOR REINFORCEMENT IN
POLYPROPYLENE COMPOSITES

Miss Patcharaporn Chuayplod



A Dissertation Submitted in Partial Fulfillment of the Requirements
for the Degree of Doctor of Philosophy Program in Materials Science

Department of Materials Science

Faculty of Science

Chulalongkorn University

Academic Year 2017

Copyright of Chulalongkorn University

Thesis Title SURFACE MODIFICATION OF MICROCRYSTALLINE
CELLULOSE FROM PARAWOOD SAWDUST VIA
MECHANOCHEMICAL PROCESS FOR
REINFORCEMENT IN POLYPROPYLENE
COMPOSITES

By Miss Patcharaporn Chuayplod

Field of Study Materials Science

Thesis Advisor Associate Professor Duangdao Aht-Ong, Ph.D.

Accepted by the Faculty of Science, Chulalongkorn University in Partial
Fulfillment of the Requirements for the Doctoral Degree

..... Dean of the Faculty of Science
(Professor Polkit Sangvanich, Ph.D.)

THESIS COMMITTEE

..... Chairman
(Assistant Professor Dujreutai Pongkao Kashima, Ph.D.)

..... Thesis Advisor
(Associate Professor Duangdao Aht-Ong, Ph.D.)

..... Examiner
(Associate Professor Onusa Saravari)

..... Examiner
(Associate Professor Pranut Potiyaraj, Ph.D.)

..... External Examiner
(Roman Strauss, Ph.D.)

5572828023 : MAJOR MATERIALS SCIENCE

KEYWORDS: MICROCRYSTALLINE CELLULOSE / COMPOSITES / ACID HYDROLYSIS / SURFACE MODIFICATION / MECHANOCHEMISTRY / POLYPROPYLENE

PATCHARAPORN CHUAYPLOD: SURFACE MODIFICATION OF MICROCRYSTALLINE CELLULOSE FROM PARAWOOD SAWDUST VIA MECHANOCHEMICAL PROCESS FOR REINFORCEMENT IN POLYPROPYLENE COMPOSITES. ADVISOR: ASSOC. PROF. DUANGDAO AHT-ONG, Ph.D., 187 pp.

The objective of this study is to prepare and modify parawood microcrystalline cellulose (PW-MCC) for applying as reinforced material for polypropylene composites. PW-MCC was prepared from parawood sawdust using acid hydrolysis method with pulp to acid ratio at 1:15 and temperature at 80°C for 2 hours. The obtained PW-MCC exhibited the cellulose type I with CrI at 60%. Moreover, PW-MCC had higher thermal stability than parawood sawdust. PW-MCC was further modified with various types of coupling agent such as maleic anhydride-grafted-polypropylene (PP-G-MA), organosilane, and acid chloride. Vinyltrimethoxysilane and three different acid chlorides such as benzoyl chloride, hexanoyl chloride, and lauroyl chloride were used to modify PW-MCC under mechanochemical method using planetary ball milling at ambient temperature. The optimized condition for each modification and properties of modified PW-MCC were studied and characterized. The functional group from FTIR and surface composition from XPS of silane treated PW-MCC confirmed the chemical bonding between PW-MCC surface and silane coupling agent. The esterified cellulose presented carbonyl stretching of ester peak at 1740 cm⁻¹. Then, PW-MCC and the modified PW-MCC were applied to prepare polypropylene composites at 5-30 wt% loading content without a compatibilizer using an internal mixer for compounding. The compound was fabricated into specimens by injection process. The results of the PP composites revealed that PW-MCC was an effective reinforcing material. The modified PW-MCC enhanced compatibility between PW-MCC and PP matrix resulting in an increasing of mechanical properties, water resistance, and thermal stability of PP composites. Besides, the type of coupling agents was also affected to composites properties. The results indicated that modified PW-MCC with fatty alkyl chain provided a better compatibility than using benzoyl group and organosilane. In addition, using long chain fatty grafted on PW-MCC exhibited a plasticizing effect to composites resulting to the reduction of modulus of the composites. Nevertheless, the suitable content for using modified PW-MCC was 5wt%. Comparatively, cellulose laurate was an effective reinforcing agent for applying in PP composite. Cellulose laurate/PP composite exhibited an increasing of elongation at break and impact strength at 21% and 23%, respectively. In addition, water resistance was increased approximately 80% and thermal stability at T_{d50%} was shifted from 431 to 462°C with char residue at 4.23% which was higher than those of the PW-MCC/PP composites.

Department: Materials Science

Student's Signature

Field of Study: Materials Science

Advisor's Signature

Academic Year: 2017

ACKNOWLEDGEMENTS

I am very glad and so proud that the thesis was completed. I sincerely thank to my thesis advisor, Associate Professor Dr. Duangdao Aht-Ong, who has always supported me and gave me good advice and guidance on my research with her attention, patience, advice and invaluable knowledge. She is very kind and industrious person. She fully supports me and our research group to achieve the goal. This thesis could not be completed without her supports. I really appreciate and respect her. It is my good opportunity to be her advisee.

Besides my advisor, I would like to thank my thesis committee sincerely, Associate Professor Dr. Dujreutai Pongkao Kashima, the chairman of thesis committee and also would like to express my appreciation to the thesis committee members, Associate Professor Onusa Saravari, Associate Professor Dr. Pranut Potiyaraj and Dr. Roman Strauss for taking their valuable time to be the committee for this thesis exam.

In addition, I would like to sincerely thank to Research and Development department, IRPC Public Company Limited for the necessary research instrument and financial support. Special thanks should be given to Mr. Sanchai Thongkham, who has always supported me and suggested me to complete my research. In addition, many thanks for my lovely colleagues who has helped me and encouraged me throughout my critical time. The special person that I would like to sincere appreciation is Mr. Charungkit Jaikew, who is my buddy and gives me spirit entire my study time.

Besides, I would like to thank all the teachers and staffs at the Department of Materials Science, Faculty of Science, Chulalongkorn University for their knowledge and kind assistances. This department gives me a good memory and impression. I am very lucky to have a chance to be a part of this department.

Unforgettably, I would to like to thank my family and my best friends for their kindness and encouraging me to pass the hard time and achieve my goal. They are always besides me. Love them all.

CONTENTS

	Page
THAI ABSTRACT	iv
ENGLISH ABSTRACT	v
ACKNOWLEDGEMENTS	vi
CONTENTS	vii
LIST OF TABLES	xiv
LIST OF FIGURES	xvii
CHAPTER I INTRODUCTION.....	1
CHAPTER II THEORY AND LITERATURE REVIEWS.....	3
2.1 Natural fiber composites	3
2.1.1. Properties of natural fiber composites.....	3
2.1.2. The advantage of natural fiber composites	4
2.1.3 Polymer matrix.....	4
2.1.3.1 Polyethylene	4
2.1.3.2 Polypropylene (PP).....	6
2.1.4 Natural fibers	8
2.1.4.1 Cellulose	9
2.1.4.2 Hemicellulose	10
2.1.4.3 Lignin	10
2.1.4.4 Pectin	11
2.1.5 Advantages of natural fibers.....	14
2.1.6 Disadvantages of natural fibers.....	15
2.2 Literature review of natural plastic composites	15

	Page
2.3 Parawood	16
2.4 Cellulose derivatives	17
2.4.1 Nanocellulose.....	18
2.4.2 Microcrystalline cellulose (MCC).....	20
2.5 Literature review of microcrystalline cellulose preparation	22
2.6 Literature review of microcrystalline cellulose composites	24
2.7 Purification of natural fibers.....	26
2.7.1 Alkaline treatment.....	26
2.7.2. Oxidation agent treatment.....	26
2.8 Surface modification of natural fibers.....	26
2.8.1 Physical modification	27
2.8.1.1 Corona treatment.....	27
2.8.1.2 Plasma treatment.....	27
2.8.2 Chemical modification	27
2.8.2.1 Acetylation.....	27
2.8.2.2 Acylation.....	28
2.8.2.3 Benzoylation.....	30
2.8.2.4 Silanization.....	32
2.8.2.5 Maleated coupling agents	34
2.9 Literature review of modified fiber polymer composites.....	35
2.10 Mechanochemistry.....	37
2.10.1 Ball mill.....	38
CHAPTER III EXPERIMENTAL	41

	Page
3.1 Materials.....	41
3.1.1 Polypropylene (PP).....	41
3.1.2 Parawood sawdust.....	41
3.1.3 Chemicals for preparation of PW-MCC.....	41
3.1.4. Chemical for surface modification	42
3.1.4.1 Modifying agents	42
3.1.4.2 Chemicals and solvents	42
3.1.5 Polypropylene grated maleic anhydride (PP-g-MA).....	43
3.2 Equipment and Instruments.....	43
3.3 Experimental procedure.....	45
3.3.1 Preparation of PW pulp.....	45
3.3.2 Preparation of parawood microcrystalline cellulose (PW-MCC).....	45
3.3.3 Surface modification of PW-MCC.....	47
3.3.3.1 Surface modification of PW-MCC using organosilane.....	47
3.3.3.2 Surface modification of PW-MCC using acid chloride.....	47
3.3.4 Preparation of PP composites.....	48
3.3.5 Injection of composite specimens	50
3.4 Characterization of PW-MCC and modified PW-MCC.....	51
3.4.1 Bulk density.....	51
3.4.2 Chemical constituent analysis.....	51
3.4.3 Crystallinity.....	52
3.4.4 Degree of polymerization.....	53
3.4.5 Degree of substitution.....	54

	Page
3.4.6 Functional group.....	55
3.4.7 Morphology.....	56
3.4.8 Particle size analysis.....	56
3.4.9 Surface composition.....	57
3.4.10 Thermogravimetric analysis.....	58
3.5 Characterization and testing of PP composites.....	58
3.5.1 Mechanical properties.....	58
3.5.1.1 Tensile properties.....	58
3.5.1.2 Flexural properties.....	59
3.5.1.3 Impact strength.....	60
3.5.2 Dynamic mechanical properties.....	60
3.5.3 Physical properties.....	61
3.5.3.1 Density.....	61
3.5.3.2 Melt flow index.....	62
3.5.3.3 Morphology.....	63
3.5.3.4 Water uptake isotherm.....	63
3.5.4 Thermal properties.....	63
3.5.4.1 Thermogravimetric analysis (TGA).....	63
3.5.4.2 Differential scanning calorimetry (DSC).....	64
3.5.4.3 Thermo mechanical analysis.....	65
CHAPTER IV RESULTS.....	66
4.1 Characterization of parawood sawdust (PW).....	66
4.1.1 Chemical composition.....	66

	Page
4.2 Preparation of parawood microcrystalline cellulose (PW-MCC).....	66
4.2.1 Chemical composition of PW-MCC	66
4.2.2 Product yield	67
4.2.3 Bulk density of prepared PW-MCC	68
4.2.4 Particle size of PW-MCC.....	69
4.2.5 Functional group of prepared PW-MCC	70
4.2.6 Degree of polymerization of PW-MCC.....	72
4.2.7 Crystallinity of PW-MC.....	74
4.2.8 Thermogravimetric analysis	75
4.2.9 Morphological analysis	78
4.3 Surface modification of PW-MCC	82
4.3.1 Effect of ball milling speed on crystallinity and structure of PW-MCC.....	82
4.3.2 Effect of ball milling speed on morphology	84
4.3.3 Surface modification of PW-MCC using organosilane	85
4.3.3.1 Functional group of silane treated PW-MCC	85
4.3.3.2 Surface composition of silane treated PW-MCC	86
4.3.3.3 Thermal stability of silane treated PW-MCC.....	91
4.3.3.4 Morphological studies of silane treated PW-MCC	93
4.3.4 Surface modification of PW-MCC using benzoyl chloride	95
4.3.4.1 Chemical structure of cellulose benzoate.....	95
4.3.4.2 Functional group of cellulose benzoate	96
4.3.4.3 Thermal stability of cellulose benzoate	100
4.3.4.4 Morphological properties of cellulose benzoate	102

	Page
4.3.5 Surface modification of PW-MCC using hexanoyl chloride	103
4.3.5.1 Chemical structure of cellulose hexanoate.....	103
4.3.5.2 Functional group of cellulose hexanoate	104
4.3.5.3 Thermal stability of cellulose hexanoate	110
4.3.5.4 Morphological properties of cellulose benzoate	111
4.3.6 Surface modification of PW-MCC using lauroyl chloride	112
4.3.6.1 Chemical structure of cellulose laurate	112
4.3.6.2 Functional group of cellulose laurate	113
4.3.6.3 Thermal stability of cellulose laurate.....	117
4.3.6.4 Morphological properties of cellulose laurate.....	118
4.3.7 Comparison of cellulose ester.....	119
4.4 Mechanical properties of the composites	124
4.4.1 Tensile properties	124
4.4.2 Flexural properties.....	130
4.4.3 Izod impact properties.....	132
4.5 Physical properties of the composites	134
4.5.1 Density.....	134
4.5.2 Melt flow index	136
4.5.3 Morphology of PP composites	137
4.5.4 Water absorption of composites	141
4.6 Dynamic mechanical properties of the composites	143
4.7 Thermal properties of the composites.....	147
4.7.1 Thermal stability of composites.....	147

	Page
4.7.2 Differential scanning calorimetry of composites.....	151
4.7.3 Thermal expansion of composites.....	154
CHAPTER V CONCLUSIONS	156
REFERENCES	162
VITA.....	187



LIST OF TABLES

Table 2.1 Chemical composition from various plants [21].....	12
Table 2.2 Commercial major fiber source [21].....	13
Table 2.3 Comparative properties of natural fibers with synthetic reinforcing fibers.....	14
Table 2.4 Silane type and applied target polymer matrix [60].....	33
Table 3.1 Chemical and supplier used in PW-MCC preparation.....	41
Table 3.2 Modifying agents and suppliers.....	42
Table 3.3 Chemical and supplier used in surface modification PW-MCC.....	42
Table 3.4 Equipment and instruments used to characterize PW-MCC and esterified PW-MCC.....	43
Table 3.5 Equipment and instruments used to prepare modified PW-MCC and composites.....	44
Table 3.6 Equipment and instruments used to characterize composites.....	44
Table 3.7 Reaction condition for preparation of PW-MCC.....	45
Table 3.8 List of prepared parawood sawdust microcrystalline cellulose.....	46
Table 3.9 PP composites using unmodified PW-MCC.....	49
Table 3.10 PP composites using modified PW-MCC.....	50
Table 4.1 Chemical composition of parawood sawdust.....	66
Table 4.2 Chemical composition of PW and PW-MCC.....	67
Table 4.3 Product yield of PW-MCC from acid hydrolysis.....	67
Table 4.4 Bulk density of prepared PW-MCC.....	69

Table 4.5 Particle size of PW-MCC.....	70
Table 4.6 Degree of polymerization of PW-MCC	73
Table 4.7 CrI values of PW-MCC prepared from different acid hydrolysis conditions.....	75
Table 4.8 Thermal stability of PW-MCC prepared from different acid hydrolysis conditions.....	77
Table 4.9 Binding energy and bond type for high-resolution XPS scan of C1s [111]..	87
Table 4.10 Elemental composition of silane treated PW-MCC evaluated by low – resolution XPS scan using 10% vinyltrimethoxy silane at different ball milling times.....	90
Table 4.11 Elemental composition of silane treated PW-MCC evaluated by low – resolution XPS scan.....	91
Table 4.12 The thermal decomposition temperature of silane treated PW-MCC.....	93
Table 4.13 Degree of substitution and %WI for cellulose benzoate at 60 min.....	97
Table 4.14 Degree of substitution and %WI for esterified PW-MCC at benzoyl chloride/AGU ratio at 5 with different reaction time	100
Table 4.15 The decomposition temperature of cellulose benzoate.....	101
Table 4.16 Comparison between the DS values of cellulose hexanoate with and without toluene	105
Table 4.17 Degree of substitution and %WI for cellulose hexanoate at 60 min.....	107
Table 4.18 DS and %WI for cellulose hexanoate using hexanoyl chloride/AGU ratio at 5 with different reaction times	108
Table 4.19 The decomposition temperature of cellulose hexanoate.....	111
Table 4.20 Degree of substitution and %WI for cellulose laurate at 60 min	115
Table 4.21 DS and %WI for cellulose laurate at lauroyl chloride/AGU ratio at 4 with different reaction time.....	116

Table 4.22 The decomposition temperature of cellulose laurate	118
Table 4.23 DS and thermal decomposition temperature of cellulose ester	121
Table 4.24 The thermal decomposition temperature of PP and PP composites.....	148
Table 4.25 Melting and crystallization properties of PP and PP composites	152



LIST OF FIGURES

Figure 2.1 PE Structure	5
Figure 2.2 The structure of a) LDPE with long and short chain branching and b) HDPE with short chain branching only	5
Figure 2.3 The chemical structure of PP	6
Figure 2.4 Tacticity of polypropylene.....	7
Figure 2.5 Types of polypropylene [11].....	8
Figure 2.6 The plant cell wall structure [13]	8
Figure 2.7 Chemical structure of cellulose [16]	9
Figure 2.8 Supramolecular distinction between Cellulose I and Cellulose II [16].....	10
Figure 2.9 Chemical structure of hemicellulose [18]	10
Figure 2.10 Chemical structure of lignin [18]	11
Figure 2.11 Chemical structure of pectin [20]	11
Figure 2.12 a) Para rubber tree and b) parawood sawdust	17
Figure 2.13 Depolymerization of cellulose to obtain cellulose crystalline [13]	18
Figure 2.14 SEM image of corn husk nanocellulose from H ₂ SO ₄ /fiber ratio at 10 using reaction time at a) 30 min and b) 120 min	19
Figure 2.15 The TEM micrographs of cellulose nanocrystals from a) parenchyma and b) vascular bundle	20
Figure 2.16 Preparation MCC steps from cellulose materials [40]	21
Figure 2.17 Life cycle of MCC – based polymer biocomposites [40]	22
Figure 2.18 Acetylation reaction of cellulose with acetic anhydride [53]	28
Figure 2.19 Acylation reaction of cellulose with acid chloride [55].....	29
Figure 2.20 Benzoylation reaction of cellulose with benzoyl chloride [58]	31

Figure 2.21 The chemical reaction of silanization of alkoxysilane with cellulose [62].....	32
Figure 2.22 An interaction of maleated-graft-polypropylene with natural fiber [67]..	35
Figure 2.23 Various applications of mechanochemistry [74].....	37
Figure 2.24 Planetary ball mill with four grinding chambers rotating in opposite direction to sun disc [78]	39
Figure 2.25 Mechanism of acetylation via pan-milling method [79].....	39
Figure 3.1 Planetary ball mill with ceramic chamber and balls (QM-BP, NANJING, Jiangsu, China).....	47
Figure 3.2 Internal mixer (Lab Station, Barbender, Duisburg, Germany).....	48
Figure 3.3 Minijet injection machine (HAAKE MiniJet II,Thermo, Scientific, Karlsruhe, Germany).....	51
Figure 3.4 X-ray diffraction (XRD) (PW3710, Phillips, Almelo, Netherlands)	53
Figure 3.5 Proton nuclear magnetic resonance spectroscopy (¹ H-NMR) (Varian Inova 500 MHZ NMR system, Varian Inc., PaloAlto, CA)	55
Figure 3.6 Fourier transform infrared spectroscopy (Vertex 70, Bruker, Ettlingen, Deutschland).....	55
Figure 3.7 Scanning electron microscopy (LEO1450VP, LEO, Oberkochen, Germany).....	56
Figure 3.8 Particle size analyzer (1180L, Cilas, Wisconsin, United State).....	56
Figure 3.9 a) Principle of XPS technique and b) X-ray photoelectron spectroscopy (AXIS Ultra DLD, Shimadzu, Manchester, United Kingdom)	57
Figure 3.10 Thermogravimetric analyzer (TGA) (TGA/DSC1, Mettler Toledo, Greifensee, Switzerland).....	58

Figure 3.11 a) Tensile specimen dumb-bell shaped following ASTM D638-V and b) universal testing machine (Instron 5566, Instron, Illinois/ United State).....	59
Figure 3.12 a) Dimension of flexural tested specimen and b) three point bending mode testing.....	59
Figure 3.13 a) Dimension of impact tested specimen and b) impact testing machine (IMPACTOR II, CEAST, Pianezza, Italy).....	60
Figure 3.14 Dynamic mechanical analyzer (DMA) (EPLEXOR, GABO, Ahlden, Germany).....	61
Figure 3.15 Density balance (201, Mettler Toledo, Greifensee, Switzerland)	62
Figure 3.16 Melt flow indexer machine (CEAST MF50, Instron, Illinois, United State).....	62
Figure 3.17 Differential scanning calorimetry (DSC) (DSC 204 F1, NETZSCH, Selb, Germany).....	64
Figure 3.18 Thermomechanical analyzer (TMA/SDTA841 ^e , Mettler Toledo, Greifensee, Switzerland) [88].....	65
Figure 4.1 FTIR spectra of raw-PW, bleached PW, PW-MCC, and ref-MCC.....	71
Figure 4.2 FTIR spectra of PW-MCC using HCl hydrolysis and H ₂ SO ₄ hydrolysis at temperature 80°C.....	72
Figure 4.3 X-ray diffraction pattern of raw-PW, PW pulp, and PW-MCC.....	74
Figure 4.4 TGA thermograms of PW-MCC prepared using pulp to acid ratio 1:10 at 80°C for 2 h.....	76
Figure 4.5 SEM micrographs of a) raw PW at 500x, b) raw PW at 1000x, c) PW pulp at 500x, and d) PW pulp at 1000x	78
Figure 4.6 SEM micrographs of the ref-MCC at a) 500x and b) 1000x.....	79

Figure 4.7 SEM micrographs of PW-MCC prepared using pulp to HCl ratio 1:10 at a) 80°C/2h b) 80°C/4h, c) 105°C/2h and e) 105°C/4h.....	80
Figure 4.8 SEM micrographs of PW-MCC prepared using pulp to HCl ratio 1:15 at a) 80°C/2h b) 80°C/4h, c) 105°C/2h, and e) 105°C/4h.....	80
Figure 4.9 SEM micrographs of PW-MCC prepared using pulp to H ₂ SO ₄ acid ratio 1:10 at a) 80°C/2h b) 80°C/4h, c) 105°C/2h, and e) 105°C/4h.....	81
Figure 4.10 SEM micrographs of PW-MCC prepared using pulp to H ₂ SO ₄ acid ratio 1:15 at a) 80°C/2h b) 80°C/4h, c) 105°C/2h, and e) 105°C/4h.....	81
Figure 4.11 The CrI (%) of PW-MCC with different ball milling speed at 60 min.....	83
Figure 4.12 XRD patterns of PW-MCC and milled PW-MCC at rotation speed 400 rpm for 60 min.....	83
Figure 4.13 XRD patterns of milled PW-MCC at a) 100 rpm, b) 200 rpm, c) 300 rpm, and d) 400 rpm.....	84
Figure 4.14 Silanization reaction of silane treated PW-MCC.....	85
Figure 4.15 FTIR spectra of PW-MCC and silane treated PW-MCC.....	86
Figure 4.16 XPS survey spectra of a) PW-MCC and b) silane treated PW-MCC.....	88
Figure 4.17 XPS patterns of carbon peak for a) PW-MCC and b) silane treated PW-MCC.....	89
Figure 4.18 TGA thermogram of PW-MCC and silane treated PW-MCC.....	92
Figure 4.19 SEM micrographs of silane treated PW-MCC at different ball milling times a) 60 min, b) 120 min, c) 180 min, and d) 240 min.....	94
Figure 4.20 SEM micrographs of silane treated PW-MCC at 60 min using silane content at a) 10 wt%, b) 20 wt%, and c) 30 wt%.....	94
Figure 4.21 Acylation reaction of cellulose benzoate.....	95
Figure 4.22 ¹ H-NMR spectrum of cellulose benzoate.....	96
Figure 4.23 FTIR spectra of PW-MCC and cellulose benzoate.....	97

Figure 4.24 FTIR spectra of cellulose benzoate at benzoyl chloride/AGU ratio 3 to 6.	98
Figure 4.25 FTIR spectra of cellulose benzoate at benzoyl chloride/AGU ratio at 5 with reaction time 60 min, 120 min, and 180 min	99
Figure 4.26 TGA curves of PW-MCC and cellulose benzoate.....	101
Figure 4.27 SEM micrographs of cellulose benzoate at ball milling 60 min with benzoyl chloride/AGU ratio a) 3, b) 4, c) 5 and d) 6	102
Figure 4.28 Acylation reaction of cellulose hexanoate	103
Figure 4.29 ¹ H-NMR spectrum of cellulose hexanoate.....	103
Figure 4.30 FTIR spectra of PW-MCC and cellulose hexanoate	104
Figure 4.31 FTIR spectra of cellulose hexanoate with and without toluene.....	106
Figure 4.32 FTIR spectra of cellulose hexanoate at hexanoyl chloride/AGU ratio 3 to 6	108
Figure 4.33 FTIR spectra of cellulose hexanoate using hexanoyl chloride/AGU ratio at 5 with reaction time 60 min, 120 min, and 180 min	109
Figure 4.34 TGA curve of PW-MCC and cellulose hexanoate	110
Figure 4.35 SEM micrographs of cellulose hexanoate at ball milling 60 min with hexanoyl chloride/AGU ratio a) 3, b) 4, c) 5 and d) 6	112
Figure 4.36 Acylation reaction of cellulose laurate.....	112
Figure 4.37 ¹ H-NMR spectrum of cellulose laurate	113
Figure 4.38 FTIR spectra of PW-MCC and cellulose laurate	114
Figure 4.39 FTIR spectra of cellulose laurate at lauroyl chloride/AGU ratio 3 to 5 ..	115
Figure 4.40 FTIR spectra of cellulose laurate at lauroyl chloride/AGU ratio at 4 with reaction time 60 min, 120 min, and 180 min	116
Figure 4.41 TGA curve of PW-MCC and cellulose laurate.....	117

Figure 4.42 SEM micrographs of cellulose laurate at ball milling 60 min with lauoyl chloride/AGU ratio a) 3, b) 4 and c) 5.....	119
Figure 4.43 FTIR spectra of PW-MCC and cellulose ester.....	120
Figure 4.44 TGA curves of PW-MCC and cellulose ester.....	122
Figure 4.45 SEM micrographs at 300x and 1000x of a) PW-MCC, b) cellulose benzoate, c) cellulose hexanoate, and d) cellulose laurate	123
Figure 4.46 Tensile strength of obtained PP composites.....	124
Figure 4.47 Hypothetical chemical structure of MAPP between MCC and PP matrix [137].....	125
Figure 4.48 Hypothetical chemical structure of esterified cellulose and PP matrix [140].....	126
Figure 4.49 Hypothetical chemical structure of silane treated PW-MCC and PP matrix [142].....	127
Figure 4.50 Elongation at break of a) PP and obtained PP composites and b) obtained PP composites	128
Figure 4.51 Young's modulus of obtained PP composites.....	129
Figure 4.52 Flexural modulus of obtained PP composites.....	130
Figure 4.53 Flexural strength of obtained PP composites	132
Figure 4.54 Izod notched impact strength of a) PP and obtained PP composites and b) obtained PP composites	133
Figure 4.55 Density of obtained PP composites	135
Figure 4.56 Melt flow index (MFI) of obtained PP composites	136
Figure 4.57 SEM micrograph at 500 magnification of neat PP.....	137
Figure 4.58 SEM micrographs at 1000 magnification of PW-MCC/PP composites at a) 5 wt%, b) 10 wt%, c) 20 wt%, and d) 30 wt%.....	138

Figure 4.59 SEM micrographs at 1000 magnification of PW-MCC-MA/PP composites at a) 5 wt%, b) 10 wt%, c) 20 wt%, and d) 30%.....	138
Figure 4.60 SEM micrographs at 1000 magnification of silane treated PW-MCC/PP composites at a) 5 wt%, b) 10 wt%, c) 20 wt%, and d) 30 wt%.....	139
Figure 4.61 SEM micrographs at 1000 magnification of cellulose benzoate/PP composites at a) 5 wt%, b) 10 wt%, c) 20 wt%, and d) 30 wt%.....	140
Figure 4.62 SEM micrographs at 1000 magnification of cellulose hexanoate/PP composites at a) 5 wt%, b) 10 wt%, c) 20 wt%, and d) 30 wt%.....	140
Figure 4.63 SEM micrographs at 1000 magnification of cellulose laurate/PP composites at a) 5 wt%, b) 10 wt%, c) 20 wt%, and d) 30 wt%.....	141
Figure 4.64 Water absorption of PP and obtained PP composites	142
Figure 4. 65 Storage modulus of a) PW-MCC/PP, b) PW-MCC-MA/PP, c) silane treated PW-MCC/PP, d) cellulose benzoate/PP, e) cellulose hexanoate/PP, and f) cellulose laurate/PP composites	144
Figure 4.66 Tan δ of a) PW-MCC/PP, b) PW-MCC-MA/PP, c) silane treated PW-MCC/PP, d) cellulose benzoate/PP, e) cellulose hexanoate/PP, and f) cellulose laurate/PP composites	146
Figure 4.67 TGA thermograms of PP and PP composites at 20 wt% PW-MCC content	148
Figure 4.68 DSC thermograms of PP and PP composite at 10wt% a) second endothermic curve and b) first exothermic curve.....	152
Figure 4.69 The coefficient of thermal expansion (CTE) of PP and PP composites ..	155

CHAPTER I

INTRODUCTION

Nowadays, there are many researches in the field of natural fiber composites because of their potential to replace synthetic fiber plastic composites and relieve the negative impacts of petroleum-based industries to the environment. A composite is a multi-phase material consisting of two or more physically distinct components, a continuous (matrix) phase and a dispersed (filler or reinforcement) phase. Polymer composites with naturally reinforcing materials are being prepared widely in order to improve or optimize the mechanical properties as well as to meet the specific requirements or certain applications. Reinforced composites are subjected to several applications such as automotive, aerospace, construction, furniture, and packaging. Natural biopolymers such as plant fibers are the most abundant materials on earth that become attractive reinforcing materials according to their environmental friendliness, low density, high specific strength and stiffness. These advantages allow the production of low-density composites with higher filler concentration. Cellulose-based plant fibers and wood flour have been used extensively as reinforcement in polymer composites. Over the past decades, many plants fibers have been applied on reinforcing materials in polymer composites such as kenaf, rice husk, banana, jute, and etc. The difference in fibers morphology indicates the mechanical properties of the composites. Using long fibers shows better performance in tensile and impact properties than short fibers. Recently, the extraction and utilization of cellulose in term of microcrystalline cellulose (MCC), cellulose nanocrystals (CNC), and nanofibrillated cellulose (NFC) have been widely applied in natural reinforced fiber composites.

Microcrystalline cellulose (MCC) is a purified partially depolymerized non-fibrous form of cellulose that occurs as a white, odourless, tasteless, crystalline powder. Woody plants and cotton are the major sources of MCC production. Normally, MCC can be produced by hydrolysis of cotton or wood pulp using dilute mineral acid. There are many reports on using MCC as a reinforcement in polymeric matrix. In this research, parawood or rubber wood sawdust from local furniture manufacturer was

used as raw material for preparing microcrystalline cellulose. After rubber tree ceases to produce latex sap, the wood can be processed and further made into furniture, inevitably leaving a large amount of sawdust waste from furniture factory. Generally, parawood sawdust serve as a medium for mushroom production or making wood pellets for power generation, residential heating, and cooking. However, using parawood sawdust in composites application, it can minimize the parawood sawdust and maximize the parawood sawdust into a value-added material.

Polyolefins, is a popular polymer matrix for natural fiber composites. Polypropylene (PP) is one of the commodity polymer that has been widely used in many applications such as packaging, household product, furniture, and auto-part. PP has a cheap price, low density, and excellent chemical resistance properties. However, PP has a high thermal expansion coefficient and low stiffness which limits its high temperature applications. Thus, in this research, PP was used as a polymer matrix in natural fiber composites. However, the chemical structure of PP and MCC is different. Natural fibers are high hydrophilicity due to their attraction or interaction between the hydroxyl group of fiber components and water molecules, while polypropylene is a hydrophobic polymer. Their different chemical structures cause incompatibility between natural fibers and polymer matrix. As a result, surface modification of natural fibers is commonly proposed to improve polymer-filler interfacial adhesion.

Hence, this research was focused on the preparation of MCC from parawood sawdust by acid hydrolysis method. Pulping process was performed to parawood sawdust before acid hydrolysis process. The effects of acid type, pulp to acid ratio, and the hydrolysis time on hydrolysis process had been investigated. The obtained MCC was surface-modified with different modifying agents such as acid chloride (i.e. benzoyl chloride, hexanoyl chloride, and lauroyl chloride) and silane (i.e. vinyltrimethoxy silane) via mechanochemical process in order to improve compatibility between MCC and PP matrix. The modified MCC was then applied as fillers to enhance the reinforcing effect of PP composites. The prepared composites with different fiber loadings and modifying agents were investigated in terms of their physical, mechanical, and thermal properties.

CHAPTER II

THEORY AND LITERATURE REVIEWS

2.1 Natural fiber composites

Nowadays, polymer composites with natural fiber reinforcing are being prepared widely in order to improve or optimize the mechanical properties as well as to meet the specific requirements of certain applications. A composite is a multi-phase material consisting of two or more physically distinct components, a continuous (matrix) phase and a dispersed (filler or reinforcement) phase. In addition, natural fiber composites have gained much attention from both academic and industrial research. One of the most well-known natural fiber composites is wood plastic composite (WPCs). Fiber reinforced polymer matrix can be applied to numerous applications because natural fibers provide many advantages such as low cost, low density, low abrasive, and environmentally friendly [1]. There are many applications of using natural fiber composites in field of automotive, construction, furniture, and packaging [2].

2.1.1. Properties of natural fiber composites

Natural fiber reinforced polymer composites (NFPCs) are materials which combine the good properties of both natural fiber and plastic. The properties of NFPCs depends on origin of natural fibers. The fiber constituents vary depending on their origination. In addition, the compatibility between natural fibers and polymer matrix plays the major role in natural fiber composites. The properties of NFPCs can be adjusted by changing types of polymer matrix and filler content. Incorporating the tough and light-weight natural fibers into polymer matrices generates composites with a high specific stiffness and strength. The renewable and biodegradable characteristics of natural fibers facilitate their ultimate disposal by composting or incineration, options not possible with most industrial fibers [3].

2.1.2. The advantage of natural fiber composites

Nowadays, the growing of global population and environmental problems become a big issue for the world. It is of high interested to find solutions to overcome the problem. One solution is using natural fiber to reinforce in polymer matrix instead of synthetic fibers and carbon fibers. Natural fibers are an environmental friendly materials. Using natural fiber composites provide several advantages as follows [4]:

- NFPCs is a hybrid material combining the good properties of natural fibers and polymer matrix together.
- Low cost materials for NFPCs. Natural fiber could be waste from agriculture or manufacturer.
- NFPCs has lower density than synthetic fiber composites which is suitable for automotive industry.

2.1.3 Polymer matrix

There are a lot of polymer matrices which have been used as matrix in natural reinforced composites. Plastic polymers are usually synthetic commonly derived from petrochemicals but many plastics are also made from renewable materials. Polyolefins are a class of polymers produced from olefin monomer such as ethylene and propylene. The commodity polyolefins in market are polyethylene and polypropylene.

2.1.3.1 Polyethylene

Polyethylene (PE) is a thermoplastic polymer which can be used in many application such as extrusion, blow molding, compression, and injection. PE is obtained from polymerization from monomer named ethylene. The property of PE significantly depends on nature of catalyst. The structure of PE molecules compose of carbon (C) and hydrogen (H) atom. They bond together by covalent bond. The chemical structure of PE is presented in Figure 2.1 [5].

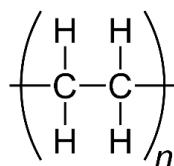


Figure 2.1 PE Structure

PE contains wide range of molecular weight or degree of polymerization. The range of molecular weight of PE is in the range 4,000 – 3,500,000 g/mol. PE can be polymerized with co-monomer for generating branches into PE backbone. PE with low branching leads to high crystallinity. In addition, PE can be classified by density of polymer chain. The major density of PE ranges from low density polyethylene and high density polyethylene as shown in Figure 2.2.



Figure 2.2 The structure of a) LDPE with long and short chain branching and b) HDPE with short chain branching only

Low density polyethylene (LDPE) has density in the range of 0.915-0.940 g/cm³. LDPE is synthesized by free radical polymerization of ethylene using initiators such as oxygen, peroxide or azo-compounds under very high pressure (1500-3000 atm). LDPE has high degree of branching leading to less crystallinity. LDPE is applied for rigid containers and plastic film.

High density polyethylene (HDPE) has density in the range 0.945-0.960 g/cm³. HDPE is polymerized at lower pressure in hydrocarbon solvent such as hexane and heptane using Ziegler-Natta catalysts, chromium/silica catalysts, or metallocene catalysts with small amount of co-monomer. Gas phase polymerization process can be also used. HDPE has a low degree of branching resulting in high crystallinity. HDPE has a good mechanical properties and chemical resistance. HDPE is used for water pipe, container, detergent bottles.

2.1.3.2 Polypropylene (PP)

Polypropylene (PP) is one of the most selective as polymer matrix for producing composites. PP has been reinforced commercially with glass fiber and particle materials (e.g. talc, calcium carbonate) for several decades [6-8]. PP was discovered in 1954 by Giulio Natta. PP is a thermoplastic polymer used in a wide variety of applications including automotive, pipe, textiles, stationery, household product, packaging and labeling. PP has gained a popularity as the lightest homopolymer and excellent chemical resistance properties. PP can be processed by various processing such extrusion, blow molding, and injection [9].

PP is produced via insertion polymerization using propylene as monomer. Propylene monomer is obtained from the cracking of petroleum production. Polymerization of PP requires a catalyst like Ziegler-Natta catalyst and pressurized propylene at temperature 60-70°C. In addition, hydrogen (H₂) has been used as a transfer agent or chain termination for control of molecular weight. The PP molecule consists of carbon (C) and hydrogen (H) atom which are bonded by covalent bond [5]. The chemical structure of PP is presented in Figure 2.3. PP has density around 0.855 – 0.946 g/cm³ with melting temperature at 160-170°C.

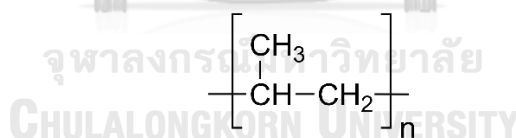


Figure 2.3 The chemical structure of PP

The properties of polypropylene depend on the molecular weight and molecular weight distribution, crystallinity, type and proportion of comonomer and tacticity. Tacticity or stereoisomerism of PP is an effect of orientation of methyl group which is classified into 3 types as shown in Figure 2.4. There are isotactic, syndiotactic, and atactic modifications. The explanation of each tacticity is below;

- Isotactic PP has the arrangement of the methyl groups on the one side of polymer backbone
- Syndiotactic PP has the methyl groups alternating on both side

- Atactic PP has random or irregular the arrangement of methyl groups

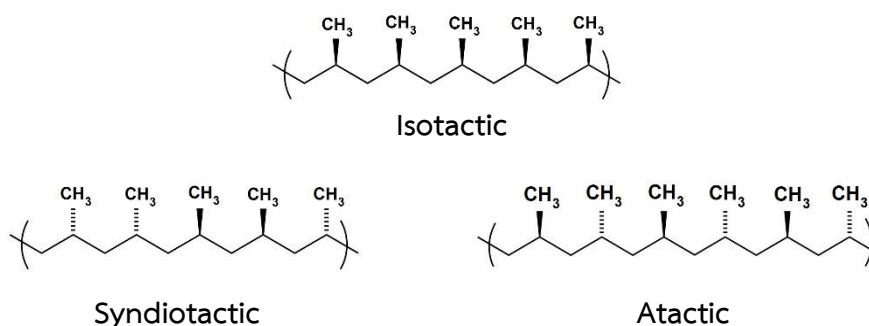


Figure 2.4 Tacticity of polypropylene

The crystallinity of isotactic propylene makes it the sole form with properties of commercial interest. Its high crystallinity imparts to it high tensile strength, stiffness, and hardness. Thus, most of PP production is isotactic. In addition, PP can be synthesized to co-polymer in order to overcome brittleness problem. Block copolymer is a polymerization of propylene with minor proportions (5-15%) of ethylene. The block copolymer are the most impact resistant and are used in injection molding application [5].

Commercial PP type can be categorized into 3 types. There are PP – Homopolymer, PP- Block copolymer, and PP- Random Copolymer as presented in Figure 2.5.

PP - Homopolymer (PP-H) is polymerized by a continuous chain of polypropylene units. The obtained polymer has a high stiffness and clarity.

PP - Block copolymer (PP- B) is synthesized by adding 5-15% ethylene to the polypropylene resulting in improved impact strength. Thus, it has more ductility than PP-H. PP-B can be used under low temperature (-20°C)

PP - Random copolymer (PP-R) is produced by adding 1-7% of ethylene molecules to 99-93% of propylene molecules. The random insertion of ethylene into propylene chains leads to a semi-crystalline polymer which provides properties such as a transparency, better impact strength, high stiffness and good electrical insulation properties.

The market share of PP types is the approximate 65-75% of PP-H, 20-30% of PP-B, and 5-10% of PP-R [10].

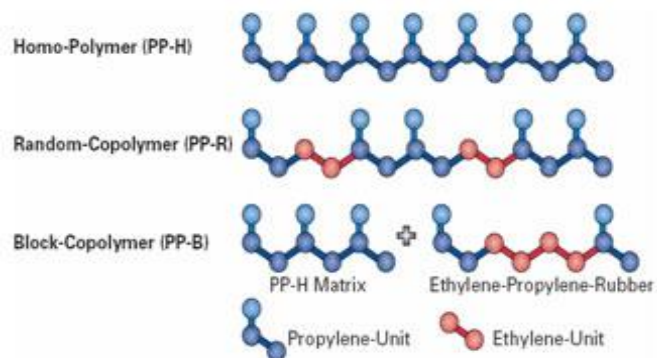


Figure 2.5 Types of polypropylene [11]

2.1.4 Natural fibers

Natural plant fibers are lignocellulose which is composed of cellulose, hemicellulose, lignin, pectin and waxy substances [12]. Lignocellulose is a complex of plant cell wall. Cellulose is coated with hemicellulose to generate amorphous part. While lignin is binder to link the structure together [13]. The plant cell wall structure is presented in Figure 2.6.

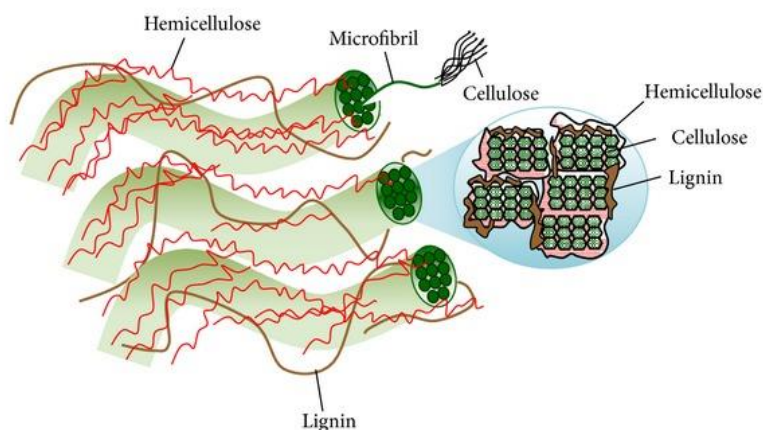


Figure 2.6 The plant cell wall structure [13]

2.1.4.1 Cellulose

Cellulose is the major component of fiber structure. Cellulose provides stiffness, strength, and structural stability of the fiber. Cellulose is a linear homopolymer of glucose ($C_6H_{10}O_5$)_n with repeating units consisting of D-glucose in a 4C_1 conformation [14]. The degree of polymerization (DP) of cellulose is in range about 1,000-10,000. Each unit of anhydroglucose unit (AGU) consists of three hydroxyl groups (OH) at C2, C3, and C6 positions. Two hydroxyl groups form hydrogen bonds within cellulose macromolecules (intramolecular) while the rest of the groups form hydrogen bond with other cellulose molecule (intermolecular). Thus, it causes crystallization in the cellulose structure [15]. The chemical structure of cellulose is presented in Figure 2.7.

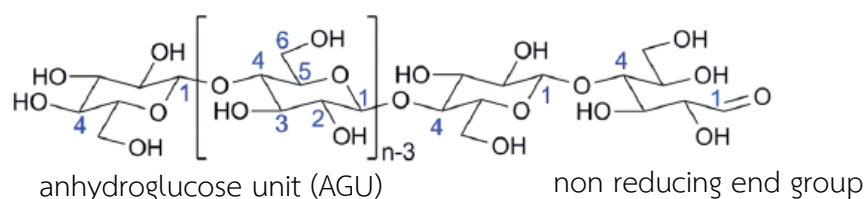


Figure 2.7 Chemical structure of cellulose [16]

Cellulose can be categorized into four types by different polymorphs. Native cellulose in plants and fibers is called cellulose I which are two allomorphs of I_α and I_β . Cellulose I can be changed to cellulose II by using aqueous NaOH solution. Thus, cellulose II is a regenerated cellulose. This method is applied for producing rayon fibers [17]. Cellulose III_i and III_{ii} are obtained from ammonia treatment of cellulose I and II, respectively. In addition, cellulose IV is produced from the modification of cellulose III using heat treatment. The difference between cellulose I and cellulose II is that inter and intramolecular hydrogen bonds leads to different arrangement. Cellulose I has parallel chains while cellulose II is antiparallel chains as presented in Figure 2.8 [16].

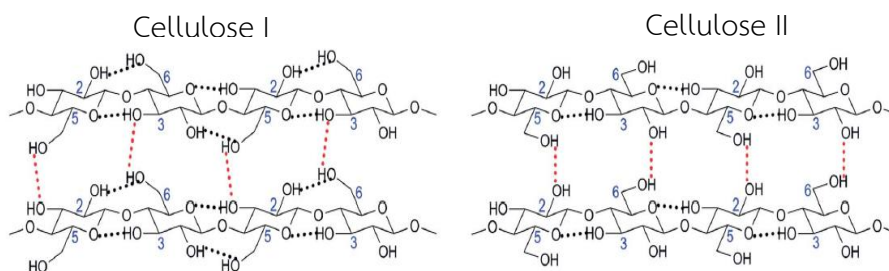


Figure 2.8 Supramolecular distinction between Cellulose I and Cellulose II [16]

2.1.4.2 Hemicellulose

Hemicellulose has branched polymers containing of five and six carbon sugars of varied chemical structure with lower degree of polymerization (DP) at 50-300. It is a water soluble polysaccharides. Hemicellulose consists of different types of cyclic saccharide Hemicelluloses include xylose, xylan, glucuronoxylan, arabinoxylan, glucomannan, and xyloglucan. While cellulose is crystalline in structure, strength and resistant to hydrolysis but hemicellulose has a random, amorphous structure with little strength. Hemicellulose is easily hydrolyzed by dilute acid or base. The chemical structure of hemicellulose is presented in Figure 2.9.

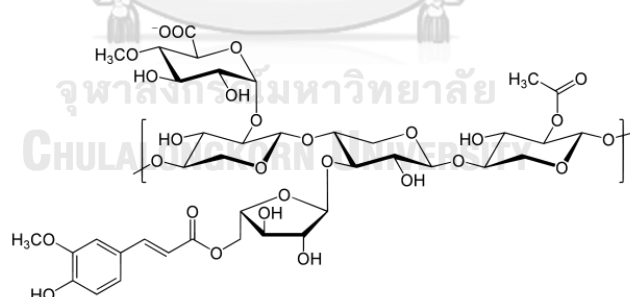


Figure 2.9 Chemical structure of hemicellulose [18]

2.1.4.3 Lignin

Lignin is amorphous and contains an aromatic structure [19]. The chemical structure of lignin is a phenolic compound consisting of an irregular array of various bonded hydroxyl- and methoxy-substituted phenylpropane units (alcohol). The alcohols in the lignin structure are linked with ether and carbon-carbon bonds.

Moreover, lignin is the main component to control water content in cell wall. The chemical structure of lignin is presented in Figure 2.10.

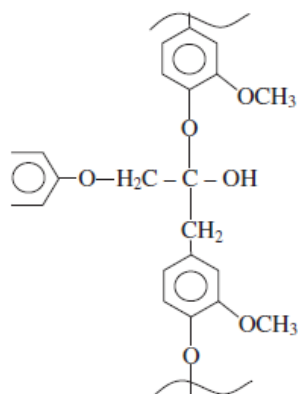


Figure 2.10 Chemical structure of lignin [18]

2.1.4.4 Pectin

Pectin consists of complex polysaccharide. Their side chains are cross-linked with the calcium ions and arabinose sugars. Moreover, there are also small amounts of organic (extractives) and inorganic (ash) components are allocated in fiber structure. Organic extractives affect to color, odor, and decay resistance while inorganic components improve the abrasive nature of fiber [12]. The structure of pectin is presented in Figure 2.11.

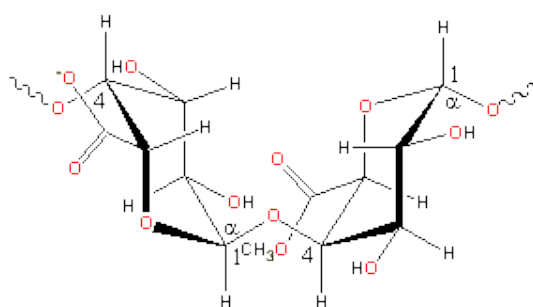


Figure 2.11 Chemical structure of pectin [20]

The chemical composition of lignocellulose depends on origin of plant, region, and country. Table 2.1 presents chemical composition from various plants.

Table 2.1 Chemical composition from various plants [21]

Source	Cellulose (%)	Hemicellulose (%)	Lignin (%)	Waxes (%)
Bagasses	55.2	16.8	25.3	-
Bamboo	26-43	30	21-31	-
Flax	71	18.6-20.6	2.2	1.5
Kenaf	72	20.3	9	-
Jute	61-71	14-20	12-13	0.5
Hemp	68	15	10	0.8
Ramie	68.6-76.2	13-16	0.6-0.7	0.3
Abaca	56-63	20-25	7-9	2
Sisal	65	12	9.9	-
Coir	32-43	0.15-0.25	40-45	-
Oil palm	65	-	29	-
Pineapple	81	-	12.7	-
Curaua	73.6	9.9	7.5	-
Wheat straw	38-45	15-31	12-20	-
Rice husk	35-45	19-25	20	14-17
Rice straw	41-57	33	8-19	8-38

In addition, there are many sources of plant that being use in commercial scale. Normally, plants are divided by their utilization. There are primary and secondary plants. Primary plants are grown for fiber purpose such as jute, kenaf, hemp, and sisal.

The secondary plants has fibers as a by-product such as pineapple, coir, and oil palm. Table 2.2 presents the main fibers applied commercially in composites.

Table 2.2 Commercial major fiber source [21]

Fiber source	World production (10 ³ ton)
Bamboo	30,000
Jute	2,300
Kenaf	970
Flax	830
Sisal	378
Hemp	214
Coir	100
Ramie	100
Abaca	70
Sugar cane bagasse	75,000
Grass	700

Moreover, comparative properties of natural fibers with synthetic reinforcing materials is presented in Table 2.3. [12]

Although natural fibers provide lower strength properties compared to inorganic fibers, the properties such as elongation at break and specific modulus presents the potential to replace inorganic fibers in polymer composites.

Table 2.3 Comparative properties of natural fibers with synthetic reinforcing fibers

Fibers	Density (g/cm ³)	Tensile strength (MPa)	Young's modulus (GPa)	Specific strength (GPa/g/cm ³)	Specific modulus (GPa/g/cm ³)	Elongation @break (%)
Jute	1.3-1.4	393-773	13-26.5	0.3-0.5	10-18.3	1.16-1.5
Flax	1.50	345- 1100	27.6	0.2-0.7	18.4	2.7-3.2
Hemp	1.14	690	30-60	0.6	26.3-52.6	1.6
Ramie	1.50	400-938	61.4-128	0.3-0.6	40.9-85.3	1.2-3.8
Sisal	1.45	468-640	9.4-22.0	0.3-0.4	6.4-15.2	3-7
PALF	1.52	413- 1627	34.5-82.5	0.3-1.1	22.7-54.3	1.6
Cotton	1.5-1.6	287-800	5.5-12.6	0.2-0.5	3.7-7.8	7.8-8.0
E-glass	2.5	2000- 3500	70	0.8-1.4	28	2.5
S-glass	2.5	4570	86	1.8	34.4	2.8
Aramid	1.4	3000- 3150	63-67	2.1-2.2	45-47.8	3.3-3.7

2.1.5 Advantages of natural fibers

Using natural fibers as reinforcing materials provides many advantages. Natural fibers have low specific weight resulting in a higher specific strength and stiffness than synthetic glass fibers. They are a renewable resource and using less energy for production. They are possible to recycle without combustion furnaces and have good thermal and acoustic insulating properties. Moreover, using natural fibers is friendly process for machine and operator [2].

2.1.6 Disadvantages of natural fibers

There are disadvantages of using natural fiber which are their lower impact strength and the quality variation due to source of natural fibers. There is also limitation of process temperature according to poor fire resistance of natural fibers. The big problem of using natural fibers is moisture absorption ability due to hydroxyl group resulting in poor compatibility between natural fiber and polymer matrix [22].

2.2 Literature review of natural plastic composites

Wambua et al. [23] studied the natural fiber composites from sisal, kenaf, hemp, coir, and jute using polypropylene as polymer matrix. The composites were prepared by compression molding using a film stacking method. Kenaf, sisal and hemp composites indicated comparable tensile strength and modulus results. Moreover, sisal and hemp composites also exhibited good impact properties. In case of kenaf, increasing of kenaf content resulting in an improved of tensile modulus, tensile stress and impact strength. Whereas, coir fiber composites gave the lowest mechanical properties but coir fiber composite gave higher impact strength than kenaf fiber composites. However, natural fibers composites showed efficient to replace glass fibers.

Doan et al. [24] investigated the dynamic and thermal properties of jute fiber/polypropylene composites. Short jute fibers were used as reinforcing material for injection molding application. The effect of using maleic anhydride as coupling agent was also studied. The thermal properties of jute fiber/PP using a coupling agent indicated an improvement of thermal stability due to good fiber and matrix interaction. The degradation of PP matrix was shifted to higher temperature. In addition, increment of fiber content leading to increase of thermal stability. For dynamic properties, the storage modulus of composites were higher than neat PP. The composites with high fiber content provided the higher storage modulus. It can be noticed that composites with coupling agent gave slightly higher storage modulus according to better adhesion between fibers and PP.

Yang et al. [25] prepared rice-husk/polypropylene composites using compatibilizing with maleated polypropylene. The addition of rice-husk to PP was 10, 20, 30 and 40 wt%. The results presented that composites without compatibilizing showed the reduction of tensile strength with increasing rice-husk content. In order to improve tensile strength, addition of compatibilizing was necessary. Thus, rice-husk composites with maleated polypropylene exhibited an improvement of mechanical properties and morphology compared with the composites without compatibilizing.

Kuo et al. [26] prepared wood plastic composites with various polymer matrix such as LLDPE, PP, and ABS by using maleic anhydride polypropylene as coupling agent for injection application. The composition of composites were using a ratio of wood flour/polymer matrix/MAPP/zinc stearate of 47:47:3:3. The tensile strength of composites made from PP and LDPE was significantly increased from neat PP and LDPE. However, composites made from ABS showed contrasting results.

Singh et al. [27] investigated hemp fiber reinforced polyethylene composites by using injection molding with fiber content from 10% to 30%. Mechanical testing was performed according to ASTM D638 and ASTM D790. The properties of composites were compared with specimens made of neat PE. It was noticed that increment of hemp fiber content led to reduction of tensile strength compared to neat PE. The flexural strength was increased when using hemp fiber content at 20% compared to neat PE. Moreover, morphology presented fiber delamination implying poor interfacial adhesion between hemp fibers and HDPE causing reduction of tensile strength.

2.3 Parawood

Parawood or rubberwood is a wood from Para rubber tree (*Hevea brasiliensis*) which is one of the most important economic trees in Thailand. Parawood is a light-colored medium-density tropical hardwood that produces latex sap for 25-30 years. After that, the wood is supplied for other application such as furniture, furniture parts, parquet, paneling, wood-based panels, medium-density fiberboards (MDF), and as sawn timber for general utility because it has very little shrinkage making it one of the more stable construction materials available for furniture, toys and kitchen accessories

[28]. There are approximately 3 million cubic meters parawood used per year. Thus, there are huge amounts of parawood sawdust waste from wood processing mills [29]. Nevertheless, parawood is not suitable for outdoor usage because the wood will be warped by the moisture and decayed by fungus and insect. Figure 2.12 presents Para rubber tree and parawood sawdust.

Parawood fibers contain around 50% cellulose, 18% hemicellulose, 21% lignin, and 11% extractives [30]. There are many researches on using parawood fibers as filler in matrix such as using in cement composite board [31] and in highly filled wood-substituted composites where up to 70% of parawood wood flour was mixed with benzoxazine resin (BA-a) and phenolic novolac resin [32].



Figure 2.12 a) Para rubber tree and b) parawood sawdust

2.4 Cellulose derivatives

Cellulose is the most abundant biopolymer on earth. Cellulose is composed of crystalline and amorphous region. Moreover, cellulose can be hydrolyzed by acid or enzyme to obtain cellulose derivative such as nanocellulose (NCC), cellulose nanocrystal, and microcrystalline cellulose (MCC) as presented in Figure 2.13.

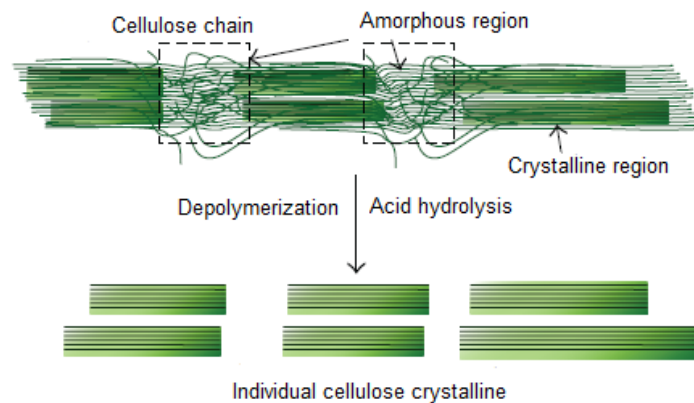


Figure 2.13 Depolymerization of cellulose to obtain cellulose crystalline [13]

Acid hydrolysis is an efficient process to obtain cellulose product. Generally, hydrolysis is performed by using mineral acid such as hydrochloric or sulfuric acid for depolymerization of cellulose. Amorphous parts are low density in native cellulose which is more accessible to acid and more susceptible to hydrolytic action than crystalline regions. Thus, the amorphous parts will break up leading to releasing the individual crystalline cellulose [13].

2.4.1 Nanocellulose

Cellulose can be converted into nano-dimensions which gives promising properties such as high mechanical characteristics, low thermal expansion, low density, and high aspect ratio. Nanocellulose can be produced by different methods from various lignocellulosic sources. Nanocelluloses can be classified in three main subcategories on the basis of their dimensions, functions, and preparation methods such as cellulose nanocrystal (CNC) and nanofibrillated cellulose (NFC) which are obtained from wood or agricultural. The other type of nanocellulose is bacterial nanocellulose (BNC) which is produced by bacteria [33]. However, the diameters of NFC and BNC are similar (<100 nm). But their purity and crystal structure is different. BNC is essentially pure crystalline cellulose while NFC consists of both amorphous and crystalline parts. Nanocellulose properties depend on origin of plant fibers. CNC has a rod-like shape with 5-70 nm width and a length varying from 100 nm to a few micrometers [34]. Nanocellulose can be applied in many applications such as hybrid

composite materials, films, dispersions and foams, and in many other [13]. In addition, nanocellulose has a potential to be applied as a reinforcing material in polymer composites [35].

Mendes et al. [36] produced nanocellulose from corn husk using acid hydrolysis method. The studied conditions were reaction time at 30 and 120 min and using H_2SO_4 to fiber ratio at 10 and 30. The results indicated that the properties of nanocellulose such as particle size, crystalline index, and thermal stability depended on reaction time. In addition, the prepared nanocellulose was dried by spray drying technique. The dried nanocellulose dispersed in aqueous solution exhibited agglomerates of nanocellulose particles with spherical and irregular shapes. The morphology of prepared nanocellulose is presented in Figure 2.14.

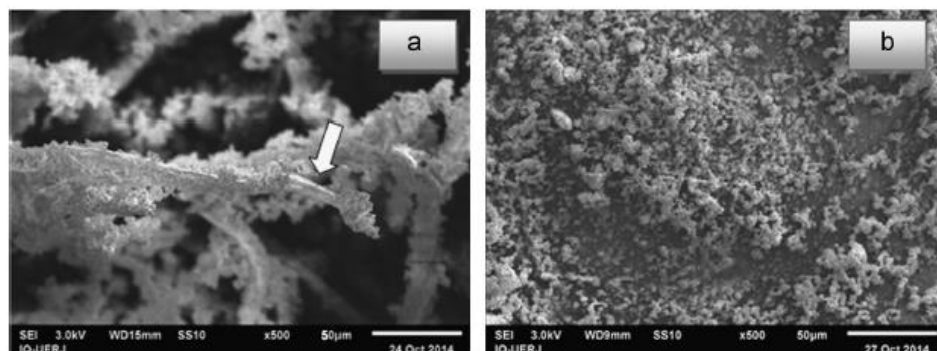


Figure 2.14 SEM image of corn husk nanocellulose from H_2SO_4 /fiber ratio at 10 using reaction time at a) 30 min and b) 120 min

Lamaming et al. [37] prepared nanocrystal via acid hydrolysis method from parenchyma and vascular bundle of oil palm trunk (*Elaeis guineensis*). The morphology of prepared nanocrystal from parenchyma cellulose was cleaner and smoother than preparation from vascular bundle. The TEM images also demonstrated that parenchyma cellulose nanocrystals indicated a higher length and diameter than vascular bundle cellulose nanocrystals. Moreover, parenchyma cellulose nanocrystals provided better thermal stability than vascular bundle cellulose nanocrystals as well.

The TEM micrographs of cellulose nanocrystals of parenchyma and vascular bundle of oil palm trunk are presented in Figure 2.15.

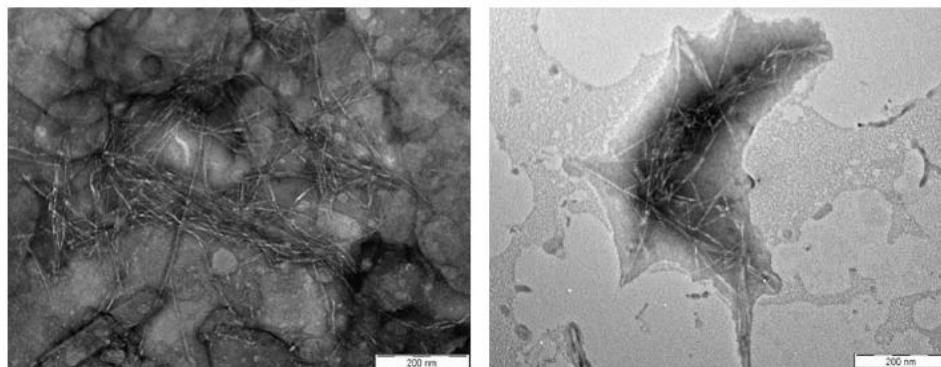


Figure 2.15 The TEM micrographs of cellulose nanocrystals from a) parenchyma and b) vascular bundle

2.4.2 Microcrystalline cellulose (MCC)

Microcrystalline cellulose (MCC) is a purified cellulose which is prepared from hydrolysis of cellulose. MCC can be synthesized by using acid hydrolysis or enzyme. Appearance of MCC is a white, odourless, tasteless, crystalline powder composed of porous particles [38]. Thus, preparation of MCC can be summarized as Figure 2.16. The popular method for producing MCC is acid hydrolysis using hydrochloric or sulfuric acid. It can be explained that glycosidic linkage is broken by acid solution. The properties of MCC depends on sources and region of cellulose affect to different properties of the prepared microcrystalline cellulose such as crystallinity, molecular weight, moisture content, surface area, and porous structure. MCC can be applied in many applications such as pharmaceutical, food cosmetic, paint, polymer composites and other industries. Moreover, MCC can be used as a starting material for the preparation of valuable cellulose derivatives [39].

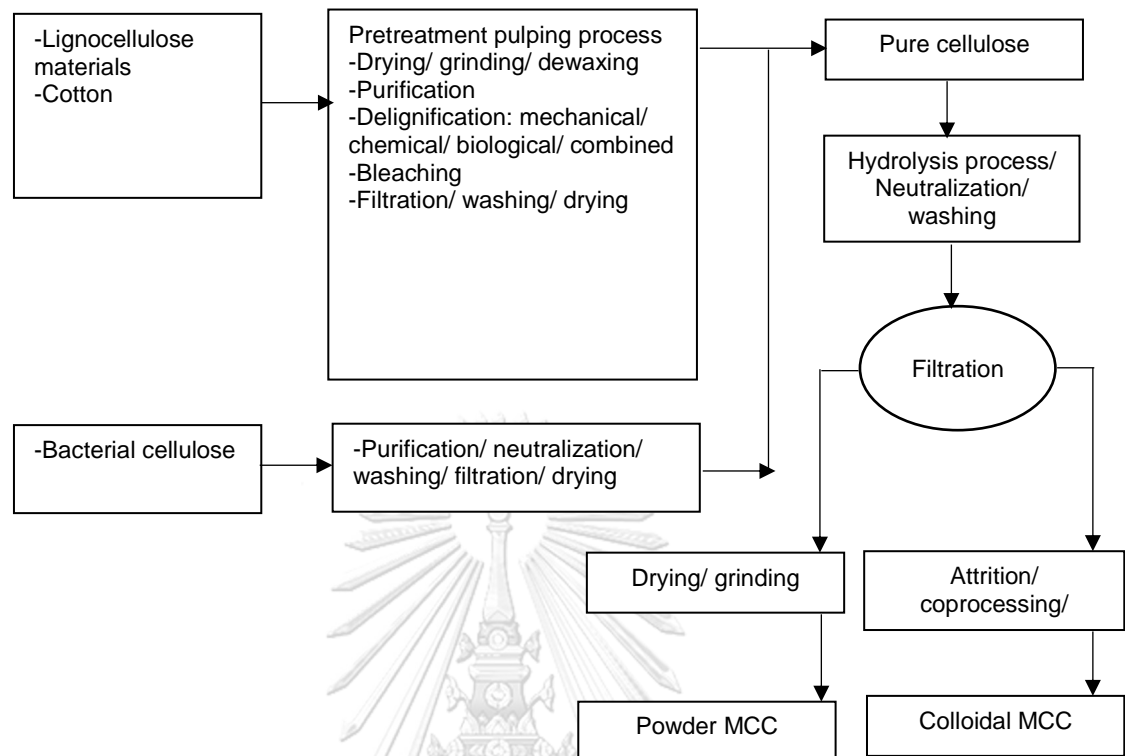


Figure 2.16 Preparation MCC steps from cellulose materials [40]

Life cycle of MCC is presented in Figure 2.17. MCC provides eco-friendly benefit and can be applied to many applications especially in composite materials. In addition, MCC as reinforcing agent is very interesting and gains a lot of attention because of its potential advantages such as renewability, biodegradability and high surface area for bonding with polymer resins [40]. Thus, there are many studies using MCC as a reinforcing material in polymer matrix such as polyethylene, poly (lactic acid), polypropylene, and poly (vinyl chloride).

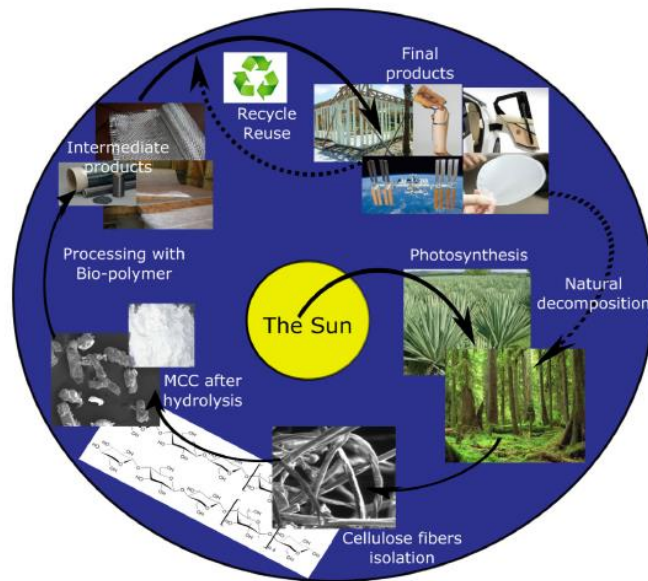


Figure 2.17 Life cycle of MCC – based polymer biocomposites [40]

2.5 Literature review of microcrystalline cellulose preparation

El-Sakhawy and Hassan [41] prepared MCC from bagasse, rice straw, and cotton stalks bleached pulps. MCC was obtained from acid hydrolysis using hydrochloric acid or sulfuric acid to investigate the effect of acid types. The obtained MCC demonstrated cellulose I with crystallinity index about 75-78. It was observed that using of sulfuric acid gave lower degree of polymerization and thermal stability than using of hydrochloric acid according to introduction of sulfate group to obtained MCC. However, all of obtained MCC indicated degree of polymerization lower than 350. SEM micrograph presented that all of MCC revealed rod-shaped form.

Ejikeme [42] investigated MCC from orange mesocarp. The hydrolysis of orange mesocarp was carried out using 2.5 N hydrochloric acid at 105°C for 15 min. The obtained MCC was white in appearance, odorless, tasteless, and crystalline. The water absorption of obtained orange mesocarp-MCC was about 300% higher than orange mesocarp. The bulk density of orange mesocarp-MCC was higher than commercial MCC (Avicel PH102). However, SEM micrographs of orange mesocarp-MCC exhibited a spherical in shape and still remaining of discrete particles.

Das et al. [43] prepared MCC from cotton silver using different sulfuric acid concentration (20, 30, 35, 40, 47, and 64 wt%) at 45°C for 30 min. It was found that

using acid concentration provided different MCC properties. The results indicated that acid concentration had effect on particle size of product and thermal stability. The finest particle size of MCC was obtained by using acid concentration at 35 and 47%. Moreover, thermal stability of MCC was better than cotton silver itself. Thus, acid concentration played a key factor on MCC properties.

Wang et al. [44] hydrolyzed three kind of pulp which were bleached kenaf bast, bleached kenaf core, and wood pulp. These pulps were hydrolyzed by using hydrochloric acid at 105°C for 60 min. The ratio of hydrochloric to pulp was 20. The obtained MCC exhibited XRD pattern of cellulose I with high crystallinity. MCC from bleached kenaf bast and wood pulp gave crystallinity index (Crl) of 77.7 and 76.4, respectively. While, MCC from bleached kenaf core provided the lowest Crl at 68.8. The morphology of obtained MCC were different. MCC with high crystallinity revealed the rod-like shaped morphology. In contrast, MCC from bleached kenaf core presented from of cluster due to more amorphous part than others. In addition, MCC form bleached bast kenaf gave the highest bulk density followed by MCC from wood pulp and MCC from bleached core kenaf.

Kashk and Haija [45] prepared MCC from *Gluconacetobacter xylinus* and kenaf by using new method which was acid hydrolysis and precipitation in ethanol. Initially, *Gluconacetobacter xylinus* and kenaf was hydrolyzed by using hydrochloric acid. Then, the obtained products were treated with 10% sodium hydroxide to form homogenous gel and precipitated in ethanol to obtain MCC product. The results showed that *Gluconacetobacter xylinus*-MCC presented cellulose I with high crystallinity with particle size 1-5 μm while kenaf-MCC exhibited cellulose II with high crystallinity with particle size 5-20 μm . Moreover, thermal stability of *Gluconacetobacter xylinus*-MCC was higher than kenaf-MCC. In addition, *Gluconacetobacter xylinus*-MCC had physical properties similar to commercial MCC named Avicel[®] PH101.

Zhao et al. [46] produced MCC from Oolong tea waste by acid hydrolysis method. The optimum hydrolysis condition was carried out using 1.5 M hydrochloric acid with ratio acid to pulp at 20 for 90 min at 65°C. The obtained MCC had product yield at 86.7% and degree of polymerization was 145. The XRD pattern exhibited

cellulose I and functional group from Fourier transform-infrared spectroscopy (FT-IR) presented cellulosic structure. The morphology of MCC showed shorter fiber with rough surface containing some holes. Moreover, the prepared MCC indicated good thermal stability.

2.6 Literature review of microcrystalline cellulose composites

Petersson and Oksman [47] compared the mechanical, thermal properties and barrier properties of two type biopolymer composites. The polymer matrix was polylactic acid (PLA). The reinforcement materials were MCC and bentonite using at 5 wt% loading of each composite. The composites were prepared by solution casting. The bentonite composites presented significantly improved tensile strength and tensile modulus. On the other hand, MCC composites indicated only an improvement in yield strength. It was noticed that MCC exhibited more satisfactory elongation at break compared to bentonite composites. The dynamic mechanical thermal analysis (DMTA) presented an increment of storage modulus and $\tan \delta$ were shifted to higher temperature for both of composites. Oxygen permeability testing results indicated that bentonite composites showed the reduction of oxygen permeability while MCC composites did not show this behavior.

Ashori and Nourbakhsh [4] prepared polypropylene (PP)/microcrystalline cellulose (MCC)/wood flour composites. Polypropylene-graft-maleic anhydride (PP-g-MA) was used as compatibilizer for enhancing interfacial adhesion between fibers and PP matrix. The composites contained the ratio of cellulosic materials to PP matrix at 40:60 by weight. The results exhibited that the composites with addition of MCC gave an improvement of tensile strength, flexural strength, and impact strength. The morphology of composites containing compatibilizer demonstrated better fiber-matrix adhesion. Moreover, thermal stability of composites made with compatibilizer was increased when using 5% compatibilizer.

Chuayjuljit et al. [48] investigated MCC/poly(vinyl chloride) composites for film application. MCC was hydrolyzed from cotton fabric waste by using 2.5 N HCl at 100°C for 30 min. The prepared MCC had average size of 40 μm and showed XRD pattern of

cellulose I. The composites were produced with MCC content 5-30 parts per hundred of resin. The film composites were fabricated by a two-roll mill. The results indicated that increasing of MCC content led to enhanced tensile strength and Young's modulus. In addition, moisture absorption and biodegradability were improved as the amount of MCC increased. Thus, MCC could be a reinforcing materials and a biodegradability promoter of PVC films.

Haafiz et al. [14] studied the composites made from polylactic acid (PLA) filled with MCC from oil palm biomass. The composites were prepared by solution casting. The data exhibited that addition of MCC did not affect the chemical structure of PLA. The decomposition temperature of composites at $T_{d50\%}$ was increased when adding of MCC. Moreover, composites with MCC provided a high amount of char residue compared to pure PLA. This results referred that MCC had potential as a flame retardant. Tensile modulus of composites were enhanced by about 30% while the tensile strength and elongation at break were reduced with incorporation of MCC. The SEM image of composites fracture surface revealed an aggregation of MCC in polymer matrix resulting in poor tensile strength and elongation at break.

Zulkifli et al. [49] investigated the properties of MCC composites using recycled polypropylene (rPP) as polymer matrix. Maleic anhydride grafted-polypropylene (MAPP) was used as a coupling agent. The composites were compounded by extruder and then specimen fabricated by injection molding machine. It was observed that composites without coupling agent showed reduction of tensile strength with increasing amount of MCC. In addition, the impact strength of composites were higher than rPP. Moreover, the composites with adding of coupling agent exhibited better mechanical properties due to good interfacial adhesion between MCC and rPP. However, fracture analysis presented ductile and quasi-brittle behavior in both composites with or without coupling agent. Thus, the fracture behavior of composites was affected by the interfacial adhesion strength and fibers content.

2.7 Purification of natural fibers

Lignocellulose is a complex of cellulose, hemicellulose, and lignin. It contains amorphous and crystalline domains. In order to obtain only cellulose, chemical treatment is required. However, chemical treatment process should focus on preservation of cellulose structure, must be cost effective and minimize use of toxic or hazardous chemicals.

2.7.1 Alkaline treatment

Alkaline treatment or mercerization is applied for removing lignin, wax, and oil from fiber cell walls. Commonly, chemical for alkaline treatment is sodium hydroxide (NaOH). Alkaline treatment is performed at mild condition (below 140°C). Alkaline reacts with natural fibers in amorphous part to promote the ionization of the hydroxyl group to the alkoxide and remove from fiber structure.



In addition, the fiber obtained from alkaline treatment is rough and clean surface due to extraction of hemicellulose and lignin [50].

2.7.2. Oxidation agent treatment

Oxidation agent treatment is applied to treat fibers by using such as hydrogen peroxide, ozone, oxygen, and air. This step is called bleaching or decolorization process. An oxidizing agent attacks and cleavages lignin ring structure. Aromatic part of lignin and hemicellulose are oxidized to carboxylic acid compounds. Thus, this treatment is specified for elimination of lignin and part of hemicellulose [13]. After bleaching process, the obtained fibers are called pulp with is white in appearance.

2.8 Surface modification of natural fibers

Due to hydroxyl group of cellulose causes poor adhesion between natural fibers and polymer matrix, surface modification of natural fiber to become more hydrophobic is required. There are many approaches to modify the surface of cellulose such as application of coupling agents, acetylation, benzylation, acylation, silanization, grafting, and corona/plasma discharge.

2.8.1 Physical modification

Physical modification uses an instrument for modifying cellulose surface. The methods involve stretching, thermotreatment, calendaring, and the production of hybrid yarn. Physical modification does not interfere in chemical structure of natural fibers [51].

2.8.1.1 Corona treatment

Corona treatment is one of most popular methods for surface oxidation activation. This method concerns about the surface energy of natural fibers. This energy discharge onto cellulose surface enhances the interfacial adhesion between hydrophilic fibers and hydrophobic polymer matrix [21].

2.8.1.2 Plasma treatment

Plasma treatment is method similar to corona treatment. Plasma technique is to induce changes on the surface of natural fibers. Plasma treatment causes chemical implantation, polymerization, etching, crystallization, and free radical formation leading to physical changes such as surface roughness. These changing causes an improvement of compatibility between natural fibers and polymer matrix [51].

2.8.2 Chemical modification

2.8.2.1 Acetylation

Acetylation is a method to introduce an acetyl functional group into cellulose and leads to more hydrophobic cellulose. One of well-known acetylation of cellulose is esterification method which causes plasticization of cellulosic fibers. Acetyl group (CH_3CO) reacts with hydroxyl group (OH) leading to decrease of hydrophilic nature of cellulose and improve water resistance of cellulose [52]. Acetylation is applied to modify the cellulose surface for using in fiber-reinforced composites [53]. The acetylation reaction of cellulose with acetic anhydride is presented in Figure 2.18.

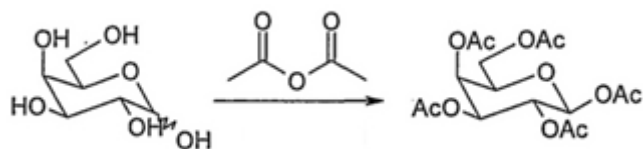


Figure 2.18 Acetylation reaction of cellulose with acetic anhydride [53]

Çetin et al. [54] modified cellulose nanowhiskers via acetylation reaction with vinyl acetate. Cellulose nanowhiskers were prepared from cotton linters. Potassium carbonate was used as catalyst for acetylation reaction. The results showed that reaction time was a major factor to control the levels of acetylation. Longer reaction time led to enhanced degree of substitution of hydroxyl by acetyl group in cellulose. XRD pattern of modified cellulose nanowhiskers was cellulose I which did not change at reaction time 1 hour. The changing of XRD pattern occurred with prolonged reaction time by decreasing intensity at $2\theta = 22.8^\circ$ implying that the inner crystalline parts were increasingly modified during reaction time. In order to enhance acetylation reaction, a solvent of low polarity such as tetrahydrofuran (THF) was required.

2.8.2.2 Acylation

Acylation is applied to enhance interfacial adhesion between the fibers and hydrophobic polymer matrix. Hydroxyl group of cellulose are treated with acid chloride. The acid bonds via ester linkage with the hydroxyl group by esterification and grafts onto cellulose backbone. During esterification, the reactive molecule of alkyl acid are penetrating inside the cellulose structure to react with hydroxyl group of cellulose. The esterified cellulose decreases hydrophilic hydroxyl group from the fiber structure leading to improve moisture resistance and compatibility between modified fibers and polymer matrix. The acylation reaction of cellulose with acid chloride is presented in Figure 2.19.

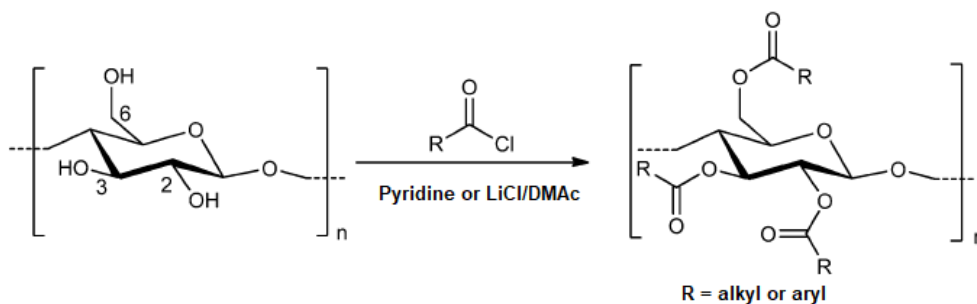


Figure 2.19 Acylation reaction of cellulose with acid chloride [55]

Corrales et al. [56] treated jute fibers with oleoyl chloride to enhance compatibility between jute fibers with polymer matrix. Dichloromethane was used as non-swelling solvent while pyridine was applied as swelling solvent for modification. 4-dimethylaminopyridine (DMAP) was used as catalyst. The acylation of cellulose by using swelling solvent (pyridine) increased ability of oleoyl chloride to react deeply in cellulose structure resulting in higher degree of substitution than non-swelling solvent. When using non-swelling solvent, the reaction proceeded only at surface of cellulose. The esterification occurred between hydroxyl groups of jute fibers and oleoyl chloride. The infrared spectrum of modified jute fibers exhibited new peak at 1737 cm^{-1} assigned to C=O stretching of carbonyl group. In addition, the modified jute fibers with pyridine solvent provided a high intensity carbonyl peak. It was noticed that the reaction with pyridine solvent did not depend on presence of catalyst. The using of catalyst with dichloromethane was significantly affected the acylation leading to enhanced reaction. The treated jute fibers indicated the changing of fiber surface. Higher surface roughness of jute fibers was observed after modification with oleoyl chloride using pyridine as swelling solvent.

Ratanakamnuan et al. [57] esterified waste cotton fabric with fatty acid chloride such as butyryl chloride (C4), capryloyl chloride (C8), and lauroyl chloride (C12) in a N,N-dimethylacetamide/lithium chloride solvent system. N,N-dimethyl 1-4-aminopyridine was used as catalyst. The esterification reaction was performed under conventional and microwave heating. The esterification by microwave activation was carried out at 2.45 GHz. The optimum condition for esterified cotton cellulose with C4, C8, and C12 were at 360W for 60 s, 270W for 60 s, and 150W for 150 s, respectively. While, esterification under convention at heating required longer reaction time which

optimum condition were at 100°C for 2 h, 80°C for 12 h, and 60°C for 12 h with C4, C8, and C12, respectively. The FTIR spectra of the esterified cotton cellulose demonstrated the evidence of esterification by presenting functional group of carbonyl at 1740 cm⁻¹ and strong intensity of methyl and methylene peak at 2800-2900cm⁻¹. The thermal stability of esterified cellulose cottons were decreased according to reduction of crystallinity after esterification. Moreover, the obtained cellulose cottons provided single weight loss step, confirming that the modified cellulose cotton became more hydrophobic than the cotton cellulose before modification. Moreover, the chain length of fatty acid chloride affected to thermal degradation such that increment chain length of fatty acid chloride caused reduction of thermal stability.

Labafzadeh et al. [55] modified cellulose with various of acid chlorides in hot pyridine solvent. Aliphatic and aromatic acid chlorides such as acetyl, decanoyl, palmitoyl, hexanoyl, 4-nitrobenzoyl, and 4-methoxybenzoyl chloride were used as coupling agents. The ratio between acyl chloride to cellulose was 5. The reaction was carried out at 90°C for 3 hour. The obtained products were washed with deionized water then filtrated and dried in vacuum-oven. The treated cellulose was purified by dissolving in chloroform and precipitated by methanol. The results exhibited that acylation in pyridine solvent was effective for long chain and aromatic acid chloride. While, short chain acid chlorides (C<6) failed resulting in a dark black solution after reaction. This process led to highly substituted cellulose ester within 3 hour. The degree of substitution (DS) of esterified cellulose was closed to 3 when using decanoyl and palmitoyl chloride. Thermal stability of esterified cellulose was increased after modification.

2.8.2.3 Benzoylation

Benzoylation is the reaction to modify cellulose with benzoyl group using benzoyl chloride as reagent. Introduction of benzoyl group to cellulose resulting in reduction of hydrophilic nature and enhance interfacial adhesion between cellulose and non-polar polymer matrix. The benzoylation reaction of cellulose with benzoyl chloride is shown in Figure 2.20. The hydroxyl groups (OH) of cellulose are reacted

with benzoyl chloride resulting in replacement of hydroxyl group by benzoyl group [12].

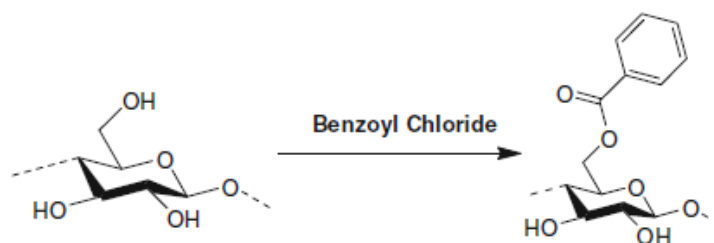


Figure 2.20 Benzoylation reaction of cellulose with benzoyl chloride [58]

Zhang et al. [58] synthesized cellulose benzoate via acylation reaction using benzoyl chloride without catalyst. The ionic liquid 1-allyl-3-methylimidazolium chloride (AmimCl) was applied as a reaction medium for dissolving cellulose. Microcrystalline cellulose (MCC) was used as starting material for acylation. The degree of substitution with benzoate was in range from 1 to 3 depended on reaction condition. Cellulose benzoate with high degree of substitution were from increasing of the molar ratio of benzoyl chloride/anhydroglucose unit (AGU) in cellulose. FTIR spectra of cellulose benzoate showed several new peaks such as at 1718 cm^{-1} for carbonyl group and 3067 cm^{-1} for benzene ring C-H stretching, confirming that benzoylation had occurred.

Yuan et al. [59] modified wood fibers with benzoyl chloride under homogenous condition and used ionic liquid 1-butyl-3-methylimidazolium chloride as solvent to enhance compatibility and photostability. Moreover, triethylamine was applied as a neutralizer. The modified wood fibers had the weight percentage gain (WPG) from 29.6 to 118.1%. The molecular structure of modified wood fibers was investigated by FT-IR and ^{13}C NMR. The results confirmed that benzoylation had successfully occurred. Thermal stability of modified wood fibers increased and hydrophilic nature of wood fibers decreased. Moreover, the weight percentage gain related to photodegradation properties implying that high weight gain led to improved photodegradation stability of wood fibers.

2.8.2.4 Silanization

Silane is a well-known multifunctional molecule to use as a coupling agent to treat natural fibers surface. The silane molecule should contain bifunctional group to form a siloxane bridge between natural fibers and polymer matrix. The generic chemical structure of silane coupling agents are $R(4-n)\text{-Si}(\text{R}'\text{X})_n$ ($n = 1,2$) where R is alkoxy, X is referred to an organofunctionality, and R' is assigned to alkyl bridge (or alkyl spacer) connecting the silicon atom and the organofunctionality [60].

Functionality of silane is a main factor for improving compatibility between silane treated natural fibers and polymer. It is explained that the ability of the silane functional group to bond covalently with the polymer matrix leads to increasing interfacial adhesion between fibers and polymer matrix such that non-polar polymer matrix is compatible with a non-reactive alkyl group of the silane [61]. Thus, it can be summarized the use of silane type with target polymer as presented in Table 2.4. Commonly, the silane treatment is performed with a silane water-alcohol solution in concentration range of 0.5-2.0% by weight. Silane treatment undergoes several steps of hydrolysis, condensation, and bond formation with fibers. Initially, silane is hydrolyzed by moisture to obtain silanols group, R-OH. Then, one end of silanol groups undergo a further condensation reaction with hydroxyl group of fibers and other end bonds with polymer matrix. Moreover, self-condensation of silane occurs to form a polysiloxane network on the fibers surface during condensation stage [61]. The chemical reaction of silanization of alkoxy silane with cellulose is presented in Figure 2.21.

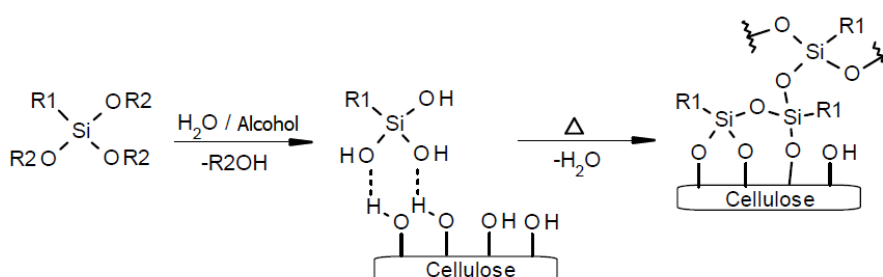


Figure 2.21 The chemical reaction of silanization of alkoxy silane with cellulose [62]

Table 2.4 Silane type and applied target polymer matrix [60]

Structure	Functionality	Abbreviation	Matrix
$(RO)_3Si-(CH_2)_3-NH_2^a$	Amino	APS	Epoxy, Polyethylene Butyl rubber Polyacrylate, PVC
$(RO)_3Si-CH=CH_2$	Vinyl	VTS	Polyethylene Polypropylene Polyacrylate
$(RO)_3Si-(CH_2)_3-OOC(CH_3)C=CH_2$	Methacryl	MPS	Polyethylene, Polyester
$(RO)_3Si-(CH_2)_3-SH$	Mercapto	MRPS	Natural rubber, PVC
$(RO)_3Si-(CH_2)_3-O-CH_2CHCH_2O$	Glycidoxy	GPS	Epoxy, Butyl rubber Polysulfide
$R_2-Si-Cl_2$	Chlorine	DSC	Polyethylene, PVC
VTS grafted plastic	Vinyl	VSPP	Polypropylene
$(RO)_3-Si-R''-N_3^b$	Azide	ATS	Polyethylene Polypropylene Polystyrene
$(RO)_3Si-(CH_2)_{15}CH_3$	Alkyl	HDS	Polyethylene Natural rubber

^a R = -methyl or ethyl

^b R = -C₆H₄-SO₂-

Valadez-Gonzalez et al. [63] treated short henequen fibers with vinyltris(2-methoxy-ethoxy) silane, (Silane A-172) at various concentrations. Dicumyl peroxide (DCP) was used as initiator. Fibers were treated with alkali to remove lignin and hemicellulose before silanization for increasing the adsorption of silane coupling agents. The results showed that silane bonding to henequen fibers was reduction when the silane concentration was higher than 0.01, indicating the formation of polysiloxanes.

Abdelmouleh et al. [64] modified surface of microcrystalline cellulose using organofunctional silane coupling agents in aqueous solution of ethanol/water. The coupling agents were γ -aminopropyltriethoxysilane (APS), γ -methacryloxypropyltrimethoxysilane (MPS), hexadecyltrimethoxysilane, and γ -mercaptopropyltrimethoxysilane (MRPS). Moreover, heat treatment was performed after prehydrolysed silanes onto cellulose surface. FTIR spectra of modified cellulose indicated functional group of Si-O-Cellulose and Si-O-Si bond on cellulose surface implying that the silane coupling agents was successfully reacted with cellulose surface. Contact angles and inverse gas chromatographic (IGC) results showed the reduction of hydrophilic nature of cellulose after silane treatment.

Zhou et al. [65] modified sisal fibers with silane coupling agent which was amino silane; N-(2-aminoethyl)-3-aminopropyltrimethoxysilane (AAPTS) and 3-aminopropyltriethoxysilane (APS) using aqueous mixture of ethano/water at room temperature for 72 h. The SEM images of treated sisal fibers revealed a smooth layer of silane on fibers surface. Moreover, they found the degradation temperature at around 180°C was due to removal of the residue from self-condensation reaction and decomposition of oligomer.

2.8.2.5 Maleated coupling agents

Maleated coupling agents gives an effective interaction with the functional surface of the natural fiber and polymer matrix. It has been widely used to strengthen composites containing fillers and fiber reinforcements. During grafting, hydroxyl group of fibers in amorphous region are reacted by maleic anhydride resulting in removal of

hydroxyl group from the fiber surface. This covalent bonding provides balanced properties to produce bridge interface for efficient interlocking [66]. This modification obtains long chain polymer coating on fibers and decrease hydrophilic tendency. Consequently, carbon-carbon bond is formed between maleated coupler and the polymer chain [12]. An interaction of maleated-graft-polypropylene with natural fiber is exhibited in Figure 2.22.

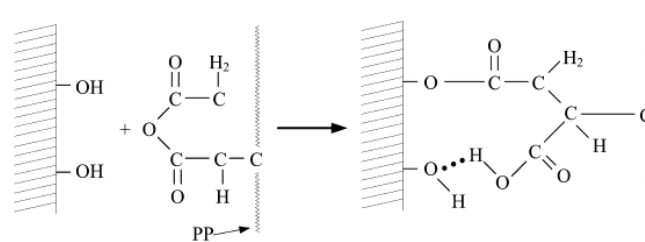


Figure 2.22 An interaction of maleated-graft-polypropylene with natural fiber [67]

2.9 Literature review of modified fiber polymer composites

Spolijaric et al. [1] studied the effect of modified MCC with various chemical treatment to apply in polypropylene containing 5% maleic anhydride graft polypropylene (PP-g-MA). MCC was modified with silicone oil, stearic acid, and alkyltitanate coupling agents to enhance matrix-filler dispersion. They suggested that addition of MCC to PP may lead to increased thermal stability of composites. However, the treated MCC did not affect to degradation temperature of composites. MCC treated with alkyltitanate/PP composite showed the highest improvement of tensile moduli suggesting that MCC was effective as reinforcing materials. Moreover, an increment of MCC treated with alkyltitanate content in PP composite led to increase of permanent deformation and storage modulus.

Conzatti et al. [68] prepared polypropylene composites using wool fibers as reinforcing material. Wool fibers were treated with hydrogen peroxide then modified with 10% of silane coupling agent. The coupling agent was [3-(methacryloyloxy)propyl]trimethoxysilane (MPTS). The composites contained 20wt% reinforcing wool fiber. The results exhibited that modified wool fiber enhanced yield stress of composites due to increased polymer-fiber adhesion. The morphology of

fragile fracture surface of unmodified wood fiber composite showed fiber pull-out, void, and cavities related to poor polymer-fiber adhesion while modified wool fiber composites showed fewer voids and cavities around the fiber implying increased fiber/matrix adhesion.

Zahari et al. [69] investigated mechanical properties of ljuk/polypropylene composites. ljuk fiber was pretreated by alkali before modification with vinyltrimethoxy silane by immersion method. Composites with fiber content at 10wt%, 20wt%, and 30wt% were compounded using roll-mill mixer at 190°C. The tensile strength of modified ljuk/PP composites showed higher strength than neat PP and unmodified ljuk/PP composites according to improvement of interfacial adhesion between fiber and PP. When increasing content of fiber, tensile strength remained the same while tensile modulus were significantly increased. Young's modulus of modified ljuk/PP composites was surprisingly much increased even with fiber content at 10wt%. However, water absorption of both composites exhibited similar behavior.

Aht-Ong and Puttane [70] modified newspaper pulp with dodecanoyl chloride for using as reinforcing material in polypropylene (PP) matrix and compared the mechanical properties with newspaper pulp/PP composite containing 10% maleic anhydride graft polypropylene (MAPP) as compatibilizer. They reported that newspaper pulp/PP composite with 10% MAPP provided higher mechanical properties than esterified newspaper pulp/PP composite. However, esterified newspaper pulp increased interfacial adhesion between newspaper pulp and PP resulting in improved elongation at break and flexibility of composites.

Suchaiya and Aht-Ong [71] studied the compatibilizer from esterified banana leaf sheath (BS) for biocomposite film. Poly(lactic acid) (PLA) was used as polymer matrix. BS microcrystalline cellulose (BS MCC) was esterified with 2 types of acid chloride which were butyryl chloride and lauroyl chloride under microwave activation to obtain cellulose butyrate and cellulose laurate using LiCl/DMac as co-solvent. The optimum condition for preparing cellulose butyrate was 180 sec of reaction time and microwave power at 80 watt while the proper condition for producing cellulose laurate was 150 sec of reaction time and microwave power at 160 watt. It was noticed that

cellulose laurate had lower thermal stability than cellulose butyrate according to reduction of crystalline structure of cellulose. Biocomposite films were prepared from 40% of BS MCC and 60% of PLA using cellulose ester as compatibilizer. They found that addition of cellulose ester to biocomposite films enhanced the elongation at break but reduced of Young's modulus and degradation temperature. The suitable amount of cellulose ester was 5 wt%. Moreover, cellulose butyrate had better compatibility with PLA and BS MCC than cellulose laurate.

2.10 Mechanochemistry

Mechanochemistry or mechanochemical process is mechanical activation or stress-induced reaction. It is an interdisciplinary science based on mechanics and chemistry. Applying mechanical force such as mechanical milling or shearing leads to size reduction of solid and increase of its specific surface area. This is accompanied by chemical bonding distortion and bond length extending according to the imposed stress, and when the imposed stress is beyond the chemical bonding energy, bond rupture occurs. This produces radicals and activates functional groups which may react with other reagents [72]. Mechanochemistry approach is eco-friendly according to reduction of energy and harmful organic solvents. In addition, it can be performed simultaneously in the ball milling process [73]. Mechanochemistry method can be applied in many applications as presented in Figure 2.23.

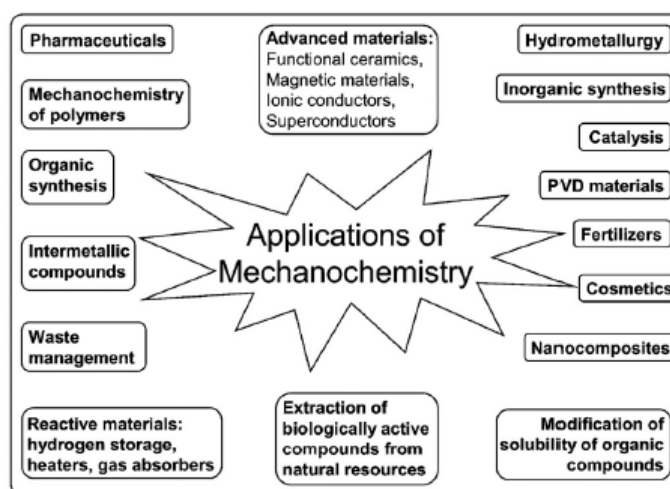


Figure 2.23 Various applications of mechanochemistry [74]

Mechanical disruption of cellulose is an interesting method for producing highly accessible surface area cellulose without the loss of molar mass compositions. A conventional ball milling process is a popular approach to prepare powder cellulose by impaction and mechanical shear stress. The crystallinity of cellulose was decreased after ball milling. The degree of cellulose structure disruption depends on the condition applied during process such as the size of balls, milling time, and rotation speed of milling [75].

2.10.1 Ball mill

Ball milling is a type of grinder applied to grind and blend materials for use in many application such as paints, ceramics, mineral, and selective laser sintering. Ball milling process is widely and popular method to use in mechanochemistry due to its inexpensive and environmentally friendly nature. Ball mill is top-down process to reduce macro to nano scale [76].

A ball mill consists of a hollow cylindrical chamber rotating about its axis. The axis of the chamber may be either horizontal or at a small angle to the horizontal. The cylindrical jar or chamber of ball mill is made of stainless steel, steel (chrome steel), or ceramics. The grinder media is the balls that are from the same materials as chamber. The inner surface of the cylindrical chamber is usually lined with an abrasion-resistant material.

Planetary ball mill is one of ball mill technique that provides high energy densities and effective particle breakage accompanied by high reliability and easy handling which makes it a widespread and successful tool. A planetary ball mill is assembled with a rotating sun disc, on which one up to four grinding chambers are located. The grinding chambers themselves rotate at higher speeds, normally in opposite direction to the sun disc to ensure high forces and a highly random motion and collision pattern of grinding media as presented in Figure 2.24 [77].

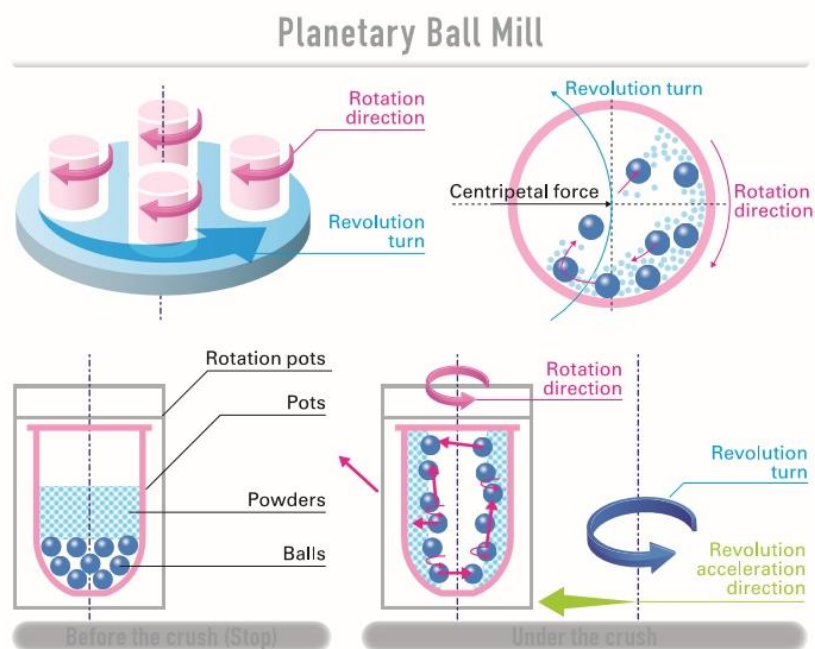


Figure 2.24 Planetary ball mill with four grinding chambers rotating in opposite direction to sun disc [78]

Zhang et al. [79] prepared surface-acetylated cellulose powder (SACP) by using pan-milling in solid-state at ambient temperature. They successfully modified surface by using mechanochemical process. The addition of SACP to natural rubber provided better scorch safety and processability. They suggested the mechanism of acetylation under mechanochemical process as presented in Figure 2.25.

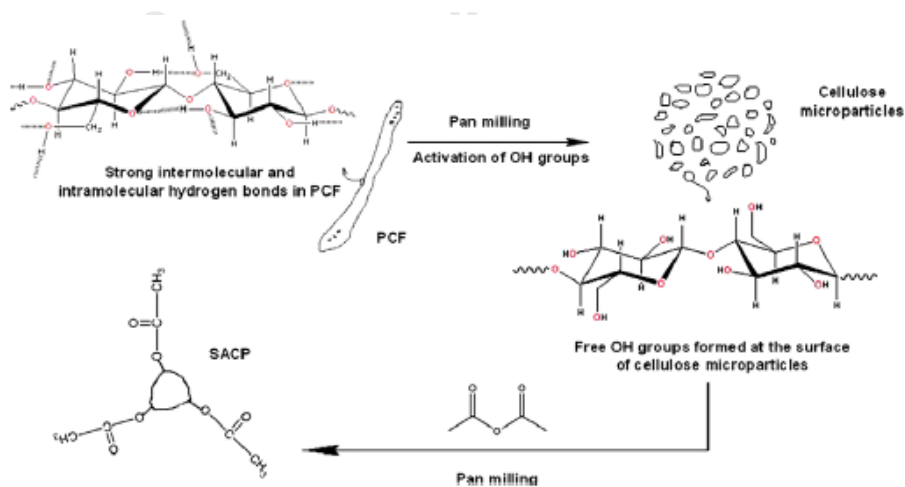


Figure 2.25 Mechanism of acetylation via pan-milling method [79]

Avolio et al. [80] investigated the effect of ball milling on cellulose properties and structure. The results indicated that crystallinity index and particle size of cellulose was decreased after ball milling suggesting that amorphous fraction was increased leading to reduction of thermal stability and increase of moisture absorption. They also found that cellulose fibers changed to particulate shape. The thermal stability of milled cellulose was reduced with increasing ball milling time.

Zhang et al. [81] prepared the composites made from cassava stillage residue (CSR) as reinforcement and poly(vinyl chloride) (PVC) as polymer matrix. CSR was surface modified by coupling agent (CA), mechanical activation (MA), and MA-assisted CA (MACA), respectively. Among these treatments, MACA method or Mechanochemistry gave the best improvement of interfacial adhesion implying to better mechanical properties, dimension stability, and water resistance. MACA treatment was effective and green process for enhancing reinforcement efficiency of plant fibers and the properties of composites.

Niu et al. [72] studied the dispersion and the degree of crosslinking between cellulose fiber and poly(vinyl alcohol) (PVA) under mechanochemical method to produce biocomposites without using solvent and catalyst. Succinic anhydride (SA) was used as crosslinker. They reported that during a pan-milling process, hydrogen bonds of cellulose and PVA were broken and then reacted with SA to form covalent bond among them. The morphology of composites fracture surface displayed better dispersion and firmly embedment in PVA after pan-milling method. Moreover, tensile strength, elongation at break and thermal stability was improved after modification.

CHAPTER III EXPERIMENTAL

3.1 Materials

3.1.1 Polypropylene (PP)

Polypropylene block copolymer resin (PP), grade 2500PC, for injection application with melt flow index of 16 g/10 min was provided by IRPC Public Company Limited, Thailand. The PP was used as a matrix for microcrystalline cellulose plastic composites.

3.1.2 Parawood sawdust

Parawood sawdust (PW) was a waste from local furniture factory in Thailand. PW was used as raw material for preparing microcrystalline cellulose (MCC).

3.1.3 Chemicals for preparation of PW-MCC

Chemicals used in parawood sawdust microcrystalline cellulose preparation were shown as Table 3.1.

Table 3.1 Chemical and supplier used in PW-MCC preparation

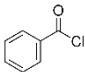
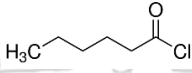
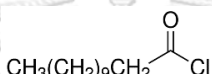
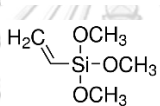
Chemicals	Purpose	Suppliers
Avicel® PH101	Reference MCC	Sigma Aldrich, USA
Hydrochloric acid	Hydrolysis agent	RCI Labscan, Thailand
Sodium hydroxide	Chemical treatment	RCI Labscan, Thailand
Sodium hypochlorite	Bleaching reagent	Sigma Aldrich, USA
Sulfuric acid	Hydrolysis agent	RCI Labscan, Thailand

3.1.4. Chemical for surface modification

3.1.4.1 Modifying agents

Modifying agents used in modification of parawood sawdust microcrystalline cellulose surface were presented in Table 3.2.

Table 3.2 Modifying agents and suppliers

Modifying agents	Structure	Suppliers
Benzoyl chloride		Sigma Aldrich, USA
Hexanoyl chloride		Sigma Aldrich, USA
Lauroyl chloride		Sigma Aldrich, USA
Vinyltrimethoxy silane		Momentive, USA

3.1.4.2 Chemicals and solvents

Chemicals and solvents used in modification of parawood sawdust microcrystalline cellulose surface were displayed in Table 3.3.

Table 3.3 Chemical and supplier used in surface modification PW-MCC

Chemicals	Purpose	Suppliers
Chloroform	Purified solvent	RCI Labscan, Thailand
Dicumyl peroxide	Catalyst	Sigma Aldrich, USA
Methanol	Solvent	Phu-taley, Thailand
Pyridine	Solvent & catalyst	Merck, Germany
Toluene	Solvent	IRPC, Thailand

3.1.5 Polypropylene grafted maleic anhydride (PP-g-MA)

Maleic anhydride modified homopolymer polypropylene (PP-g-MA) or Polybond[®] 3200 was applied as a coupling agent in order to improve interfacial adhesion between parawood sawdust microcrystalline cellulose and PP matrix. Polybond[®] 3200 with a melt flow index of 115 g/10 min and the maleic anhydride content of 1wt% was supplied by Addivant, USA.

3.2 Equipment and Instruments

All equipment and instrument being used in this study are summarized in Table 3.4, 3.5 and 3.6. The list of equipment was categorized based on experimental procedure.

Table 3.4 Equipment and instruments used to characterize PW-MCC and esterified PW-MCC

Instrument	Model/Manufacturer	City/Country
Fourier transform infrared spectroscopy (FTIR)	Vertex 70/Bruker	Ettlingen/Germany
Proton Nuclear magnetic resonance spectroscopy (¹ H-NMR)	Varian Inova 500 MHz NMR system/Varian	California/USA
Particle size analyzer	1180L/Cilas	Wisconsin/USA
Thermogravimetric analyzer (TGA)	TGA/DSC1/Mettler Toledo	Greifensee/Switzerland
Scanning electron microscopy (SEM)	LEO1450VP/LEO	Oberkochen, Germany
X-ray photoelectron spectroscopy (XPS)	AXIS Ultra DLD/Shimadzu	Manchester/United Kingdom
X-ray diffraction (XRD)	PW3710/ Phillips	Almelo/Netherlands

Table 3.5 Equipment and instruments used to prepare modified PW-MCC and composites

Instrument	Model/Manufacturer	City/Country
Planetary ball mill	QM-BP/NANJING	Jiangsu/China
Internal mixer	Lab Station/Barbender,	Duisburg/Germany
Mini injection	HAAKE MiniJet II/ ThermoScientific	Karlsruhe/Germany

Table 3.6 Equipment and instruments used to characterize composites

Instrument	Model/Manufacturer	City/Country
Density balance	201/Mettler Toledo	Greifensee/Switzerland
Dynamic mechanical analyzer (DMA)	EPLEXOR/GABO	AhlDen/Germany
Impact tester	IMPACTOR II/CEAST	Pianezza /Italy
Melt flow indexer (MFI)	CEAST MF50/ Instron,	Illinois/ USA
Thermogravimetric analyzer (TGA)	TGA/DSC1/Mettler Toledo	Greifensee/Switzerland
Thermomechanical analyzer (TMA)	TMA/SDTA841 ^e /Mettler Toledo	Greifensee/Switzerland
Universal testing machine (Tensile and Flexural)	Instron 5566/Instron,	Illinois/ USA
Scanning electron microscopy (SEM)	LEO1450VP/LEO	Oberkochen/Germany

3.3 Experimental procedure

3.3.1 Preparation of PW pulp

Parawood sawdust (PW) was dried at 80°C for 2 hours before chemical treatment. The dried PW was treated with 0.5 M NaOH at temperature 80°C for 2 h. The ratio of pulp to NaOH was 1:10. After completed the reaction time, the PW fibers were thoroughly washed with deionized water until the solution obtained pH 7. The obtained PW fibers were dried in a hot air oven at 80°C overnight. The dried PW fibers were bleached by using 5% sodium hypochlorite at room temperature for 2 hours. The liquor ratio of 1:10 was used. The bleaching procedure was repeated 3 times. The bleached fibers were thoroughly washed with deionized water until the solution became neutral and dried at 70°C overnight. The bleached fibers was obtained as white pulp.

3.3.2 Preparation of parawood microcrystalline cellulose (PW-MCC)

PW-MCC was prepared from hydrolyzed PW pulp using acid hydrolysis method in glass reactor with agitation speed 180 rpm. The reaction conditions were presented in Table 3.7.

Table 3.7 Reaction condition for preparation of PW-MCC

Parameters	Unit	Conditions
Acid type		HCl, H ₂ SO ₄
Acid concentration	N	2
Acid : pulp ratio	-	1:10 and 1:15
Temperature	°C	80 and 105
Time	h	2 and 4

After acid hydrolysis reaction, the hydrolyzed pulp was filtered and washed with deionized water several times until it was free from acid. The hydrolyzed pulp was dried in a hot air oven at 80°C until the constant weight was achieved. The

obtained PW-MCC was ground into a fine powder by using grinding pulverizer. Finally, the prepared PW-MCC from acid hydrolysis method was snowy-white in appearance. Table 3.8 shows the designated name of prepared PW-MCC.

Table 3.8 List of prepared parawood sawdust microcrystalline cellulose

Formula	Acid type	Acid : pulp ratio	Temperature (°C)	Time (h)
PW-MCC-H01	HCl	1:10	80	2
PW-MCC-H02		1:10	80	4
PW-MCC-H03		1:10	105	2
PW-MCC-H04		1:10	105	4
PW-MCC-H05		1:15	80	2
PW-MCC-H06		1:15	80	4
PW-MCC-H07		1:15	105	2
PW-MCC-H08		1:15	105	4
PW-MCC-S01	H ₂ SO ₄	1:10	80	2
PW-MCC-S02		1:10	80	4
PW-MCC-S03		1:10	105	2
PW-MCC-S04		1:10	105	4
PW-MCC-S05		1:15	80	2
PW-MCC-S06		1:15	80	4
PW-MCC-S07		1:15	105	2
PW-MCC-S08		1:15	105	4

3.3.3 Surface modification of PW-MCC

3.3.3.1 Surface modification of PW-MCC using organosilane

Initially, the dried PW-MCC was mixed with dicumyl peroxide (DCP) 50 wt% of organosilane. Then, vinyltrimethoxysilane was added to the mixture. The content of vinyltrimethoxysilane was varied at 10, 20, and 30wt%. The mixture was milled in the planetary ball mill (QM-BP, NANJING, Jiangsu, China) at rotating speed 400 rpm for 60-240 min. After that, silane treated PW-MCC was obtained and was dried at 80°C overnight. Figure 3.1 presents planetary ball mill with ceramic chamber and balls.



Figure 3.1 Planetary ball mill with ceramic chamber and balls (QM-BP, NANJING, Jiangsu, China)

3.3.3.2 Surface modification of PW-MCC using acid chloride

In order to modify the surface of PW-MCC via esterification reaction using acid chloride such as benzoyl chloride, hexanoyl chloride, and lauroyl chloride. The dried PW-MCC was stirred in pyridine at 60°C for 1 hour before esterification. In case of using benzoyl chloride as a modifying agent, mixed pyridine and benzoyl chloride (pyridine:acid chloride in 2:1 ratio) was added to the PW-MCC. For hexanoyl chloride

and lauroyl chloride, toluene was used as co-solvent in mixture between pyridine and modifying agent (hexanoyl chloride and lauroyl chloride). The ratio between PW-MCC to toluene was 1:10. After that, the mixture was milled in the planetary ball mill (Figure 3.1) using rotation speed at 400 rpm. The molar ratio of benzoyl chloride /anhydroglucose unit (AGU) was varied from 3 to 6. The mixture was milled in the planetary ball mill for 60-180 min. After ball milling, esterified PW-MCC was washed with methanol and filtrated for several times. The esterified PW-MCC (cellulose ester) was dried at room temperature for 24 hours. The obtained product was purified by dissolving in chloroform and was then precipitated in methanol. The purified cellulose ester was obtained after filtered and dried at room temperature. The modified PW-MCC with benzoyl chloride, hexanoyl chloride, and lauroyl chloride were name as cellulose benzoate, cellulose hexanoate, and cellulose laurate, respectively.

3.3.4 Preparation of PP composites

Unmodified PW-MCC and modified PW-MCC were dried at 80°C overnight before using. Dried PW-MCC and modified PW-MCC were compounded with PP by using internal mixer (Lab Station, Barbender, Duisburg, Germany) as shown in Figure 3.2 at 180°C with a mixing speed of 60 rpm for 6 min.



Figure 3.2 Internal mixer (Lab Station, Barbender, Duisburg, Germany)

The recipes of PP composites using unmodified PW-MCC and coupling agent are listed in Table 3.9 In case of modified PW-MCC/PP composites, the recipes are presented in Table 3.10.

Table 3.9 PP composites using unmodified PW-MCC

Formula	Raw materials		
	PP (wt%)	PP-g-MA* (wt% of MCC)	PW-MCC (wt%)
PMCC5	95	-	5
PMCC10	90	-	10
PMCC20	80	-	20
PMCC30	70	-	30
PMCC5MA	95	2	5
PMCC10MA	90	2	10
PMCC20MA	80	2	20
PMCC30MA	70	2	30

Table 3.10 PP composites using modified PW-MCC

Formula	PP (wt%)	Modified PW-MCC (wt%)			
		organosilane	benzoate	hexanoate	laurate
PMCC5S	95	5	-	-	-
PMCC10S	10	10	-	-	-
PMCC20S	20	20	-	-	-
PMCC30S	30	30	-	-	-
PMCC5B	95	-	5	-	-
PMCC10B	90	-	10	-	-
PMCC20B	80	-	20	-	-
PMCC30B	70	-	30	-	-
PMCC5H	95	-	-	5	-
PMCC10H	90	-	-	10	-
PMCC20H	80	-	-	20	-
PMCC30H	70	-	-	30	-
PMCC5L	95	-	-	-	5
PMCC10L	10	-	-	-	10
PMCC20L	20	-	-	-	20
PMCC30L	30	-	-	-	30

3.3.5 Injection of composite specimens

After compounding, the compounded samples were dried at 80°C for 4 hours before injection testing specimens. The dried compounded composites were injected by using minijet injection machine (HAAKE MiniJet II, Thermo, Scientific, Karlsruhe, Germany) as shown in Figure 3.3 at temperature of 210°C with injection pressure 650

bar using injection time 15 second. The dimension of tensile specimens was according to ASTM D638 type 5. The dimension of flexural specimens were 87.0 × 6.43 × 3.02 mm (length × width × thickness) While, impact specimens were 63.5 × 12.7 × 4.0 mm.



Figure 3.3 Minijet injection machine (HAAKE MiniJet II, Thermo, Scientific, Karlsruhe, Germany)

3.4 Characterization of PW-MCC and modified PW-MCC

3.4.1 Bulk density

Bulk density of prepared PW-MCC was measured according to ASTM D1895B. The dried PW-MCC was poured in 25 ml cylinder and sliced of the sample at the top of cylinder. After that, the containing cylinder was weighted and the bulk density was calculated following the equation (3.1):

$$\text{Bulk density} = (w_{\text{sample}} - w_{\text{cylinder}}) / v_{\text{cylinder}} \quad 3.1$$

Where w_{sample} is weigh of sample and cylinder, w_{cylinder} is weight of cylinder only and v_{cylinder} is volume of cylinder. The unit of bulk density is g/cm^3 .

3.4.2 Chemical constituent analysis

The chemical composition of parawood sawdust, PW pulp, and PW-MCC were investigated according to TAPPI T204-OM-97, TAPPI T264-OM-97, and TAPPI T207-OM-93, respectively. At the first step, the samples were extracted using alcohol-benzene, alcohol, and hot water. Then, the remained compositions such as cellulose,

hemicellulose and lignin (as A fraction) were treated with 24% KOH in order to remove hemicellulose (as B fraction). After that B fraction was treated with 72% H₂SO₄ and refluxed with 5% H₂SO₄ to eliminate cellulose (as C fraction). The remaining composition in fibers was lignin as C fraction. Thus, chemical composition can be calculated as followed [82]

- Cellulose content = B fraction – C fraction
- Hemicellulose content = A fraction – B fraction
- Lignin content = C fraction

3.4.3 Crystallinity

X-ray diffraction (XRD) was used to investigate the crystallinity of prepared PW-MCC with CuK α in a sealed tube operated at 40 kV and 30 mA. The diffraction pattern was performed between $2\theta = 10-40^\circ$. The crystallinity of the samples was calculated based on the reflected intensity data following the method of Segal et al. [83]. The crystallinity-to-amorphous ratio of materials was calculated using the following equation:

$$CrI(\%) = \frac{(I_{002} - I_{am})}{I_{002}} \times 100 \quad 3.2$$

where CrI is the crystallinity index, I_{002} is the peak intensity corresponding to both the amorphous and crystalline fraction of cellulose I at about $2\theta = 22.5^\circ$ and I_{am} is the lowest intensity donating to the amorphous fraction at 2θ value near 18.5° . The X-ray diffraction machine is presented in Figure 3.4.



Figure 3.4 X-ray diffraction (XRD) (PW3710, Phillips, Almelo, Netherlands)

3.4.4 Degree of polymerization

The degree of polymerization (DP) was determined by viscosity measurement of the samples dissolved in a cupriethylenediamine (CED) solution using Cannon-Frenske viscometer according to ASTM D1795. Each experiment was measured in triplicate. This determination used CED solution which was sensitive to air. Thus, it was necessary to perform under nitrogen atmosphere. 0.75 g of dried sample was placed into 100 ml high density polyethylene (HDPE) bottle with cap. 25 ml CED solution and 25 ml deionized water were added to sample in HDPE bottle. After that, the mixture was shaken until sample completely dissolved in solution. Cannon-Frenske viscometer was placed in water bath at 25°C and was flushed with nitrogen gas before adding sample solution. Then, 7 ml sample solution was pipetted to Cannon-Frenske viscometer and hold at least 5 minute for sample solution to reach bath temperature. The sample solution was sucked into the top of bulb and measured the time (t) used to pass from top to lower bulb. The viscosity was calculated using follow equation:

$$\eta_{rel} = t/t_0 \quad 3.3$$

where η_{rel} is relative viscosity, t is flow time of sample solution and t_0 is flow time of blank solution. The relative viscosity to intrinsic viscosity was determined by using intrinsic viscosity table from ASTM D1795. The degree of polymerization (DP) is calculated by multiplying intrinsic viscosity by 190.

3.4.5 Degree of substitution

The degree of substitution (DS) of esterified products was characterized by using proton nuclear magnetic resonance spectroscopy ($^1\text{H-NMR}$) (Varian Inova 500 MHz NMR system, Varian Inc., PaloAlto, CA) as shown in Figure 3.5. Esterified products were dissolved in deuterium solvent. The cellulose benzoate (PW-MCC modified using benzoyl chloride as a modifying agent) was dissolved in acetone ($\text{C}_3\text{D}_6\text{O}$). On the other hand, cellulose hexanoate and laurate (the modified PW-MCC using hexanoyl chloride and lauroyl chloride) were dissolved in chloroform (CDCl_3). The degree of substitution (DS) of esterified PW-MCC using benzoyl chloride as the modifying agent was calculated according to Goodlett and co-workers [84] by using the following equation:

$$\text{DS} = \frac{7I_{\text{phenyl}}}{5I_{\text{AGU}}} \quad 3.4$$

where I_{phenyl} is phenyl proton integration and I_{AGU} is anhydroglucose unit integration. In order to determine the degree of substitution (DS) of esterified PW-MCC using hexanoyl chloride and lauroyl chloride as modifying agent, the DS values were calculated according to Satgé and coworkers [85] by using the following formula;

$$\text{DS} = \frac{10 \times I_{\text{CH}_3}}{3 \times I_{\text{C}} + I_{\text{CH}_3}} \quad 3.5$$

where I_{CH_3} is methyl proton integration and I_{C} is carbohydrate proton integration.



Figure 3.5 Proton nuclear magnetic resonance spectroscopy ($^1\text{H-NMR}$) (Varian Inova 500 MHz NMR system, Varian Inc., PaloAlto, CA)

3.4.6 Functional group

Functional group of samples (raw materials, PW-MCC and modified PW-MCC) was determined by using Fourier transform infrared spectroscopy (FTIR) (Vertex 70, Bruker, Ettlingen, Deutschland) as presented in Figure 3.6 with KBr method. The samples were scanned at a resolution of 2 cm^{-1} with 64 scans in range of $4000\text{-}500\text{ cm}^{-1}$. The dried samples were mixed with KBr powder using ratio sample to KBr 1:100. Then, the mixture of KBr and sample was compressed into film for further testing.

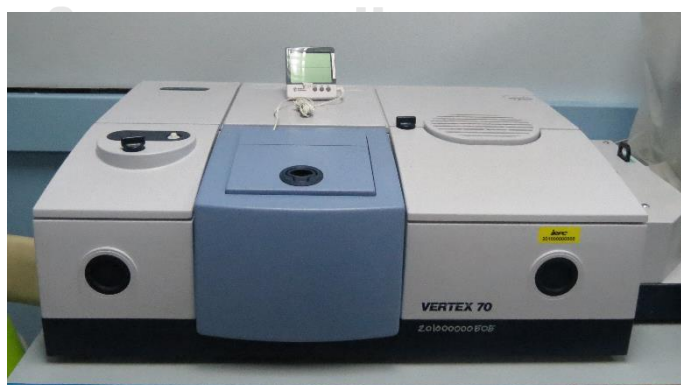


Figure 3.6 Fourier transform infrared spectroscopy (Vertex 70, Bruker, Ettlingen, Deutschland)

3.4.7 Morphology

The morphology of prepared PW-MCC and modified PW-MCC samples was investigated by scanning electron microscopy (SEM) (LEO1450VP, LEO, Oberkochen, Germany) as shown in Figure 3.7. The samples were coated with gold for 10 minutes before investigation using accelerating voltage of 15 kV.



Figure 3.7 Scanning electron microscopy (LEO1450VP, LEO, Oberkochen, Germany)

3.4.8 Particle size analysis

Particle size of prepared PW-MCC was measured by particle size analyzer (1180L, Cilas, Wisconsin, United State) as presented in Figure 3.8. This particle size analyzer uses the technique of laser diffraction to determine the size of particle. Deionized water was used as a media for measurement. The dried sample of PW-MCC was measured by using stirring cell (volume 10 ml) containing water.



Figure 3.8 Particle size analyzer (1180L, Cilas, Wisconsin, United State)

3.4.9 Surface composition

X-ray photoelectron spectroscopy (XPS) is a technique for determining the surface composition of materials. XPS is an analytical technique that an atom or molecule absorbs an X-ray photon then electron is ejected called photoelectron to electron energy analyzer. X-rays penetrate the specimen surface to a depth of a few micrometers but only the electrons near the surface can be emitted without losing energy due to collisions with other atoms as presented in Figure 3.9 (a). Surface composition of PW-MCC and silane treated PW-MCC was investigated by X-ray photoelectron spectroscopy (XPS) (AXIS Ultra DLD, Shimadzu, Manchester, United Kingdom) using $MgK\alpha_{1,2}$ source. A survey spectrum was from 0 to 1200 eV binding energy. Figure 3.9 (b) presents X-ray photoelectron spectroscopy machine.

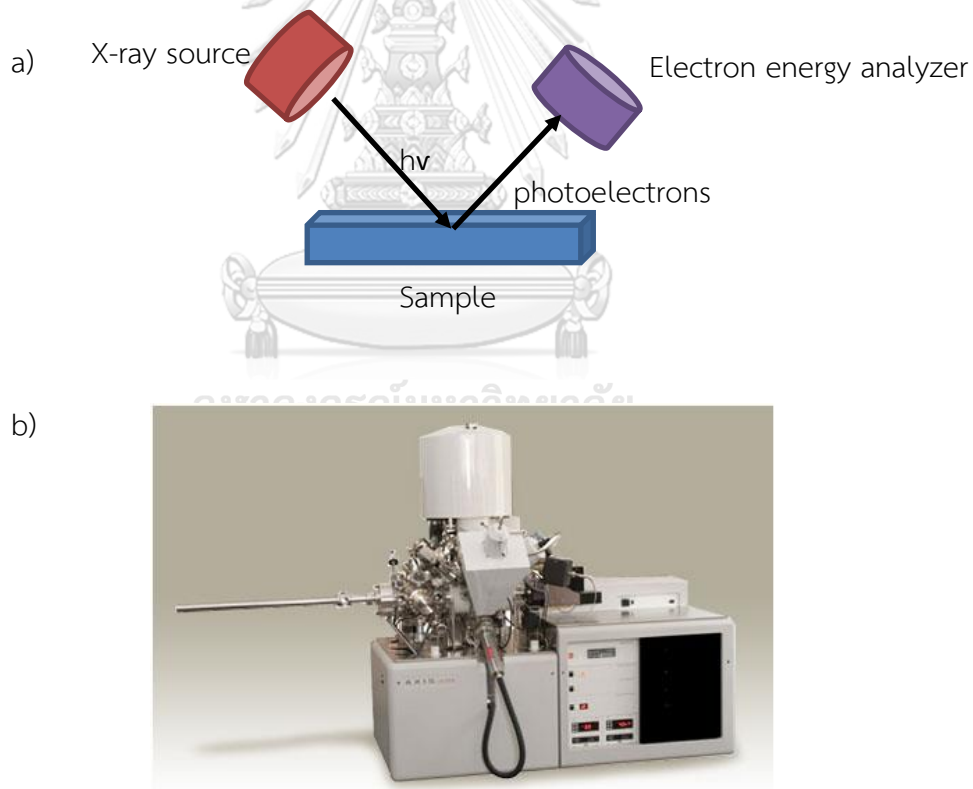


Figure 3.9 a) Principle of XPS technique and b) X-ray photoelectron spectroscopy (AXIS Ultra DLD, Shimadzu, Manchester, United Kingdom)

3.4.10 Thermogravimetric analysis

Thermal stability of raw material and obtained product was analyzed with thermogravimetric analyzer (TGA) (TGA/DSC1, Mettler Toledo, Greifensee, Switzerland). Approximately 20 mg of each sample was heated from 30°C up to 900°C at a heating rate of 20°C/min under nitrogen atmosphere. The onset of thermal degradation temperature ($T_{d_{onset}}$), percent of weight loss, and thermal degradation behavior were investigated from the TGA thermogram. Figure 3.10 displays thermogravimetric analyzer used in this research.



Figure 3.10 Thermogravimetric analyzer (TGA) (TGA/DSC1, Mettler Toledo, Greifensee, Switzerland)

3.5 Characterization and testing of PP composites

3.5.1 Mechanical properties

3.5.1.1 Tensile properties

Tensile properties were evaluated using universal testing machine (Instron 5566, Instron, Illinois/ United State). The testing method was performed according to the ASTM D638 by using load cell of 500 N at a crosshead speed of 10 mm/min at 23°C. The tensile specimens were prepared following the ASTM D638 type 5, dumb-bell shaped as shown in Figure 3.11 (a). Five specimens were tested and the averaged values for each composite specimen were reported. The obtained properties were

tensile strength, Young's modulus, and elongation at break. The universal testing machine is presented in Figure 3.11 (b).

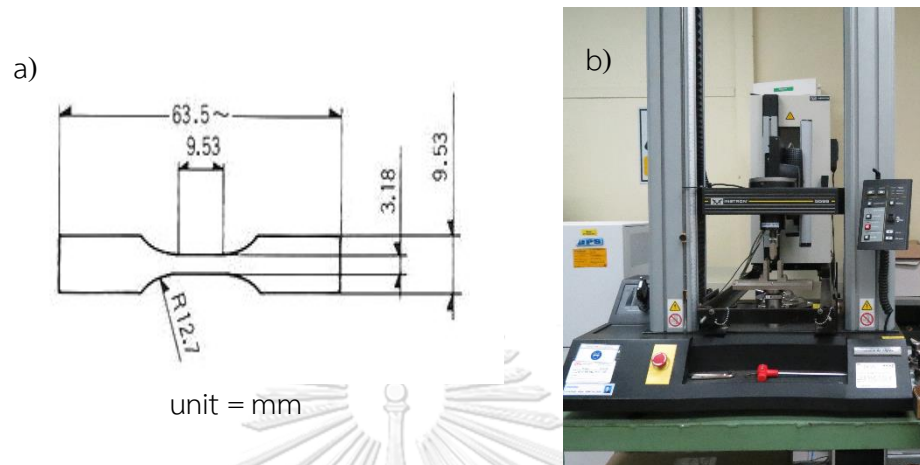


Figure 3.11 a) Tensile specimen dumb-bell shaped following ASTM D638-V and b) universal testing machine (Instron 5566, Instron, Illinois/ United State)

3.5.1.2 Flexural properties

Flexural properties were measured using universal testing machine as shown in Figure 3.12 (b). The flexural testing was carried out following the ASTM D790. The dimension of specimens are demonstrated in Figure 3.12 (a).

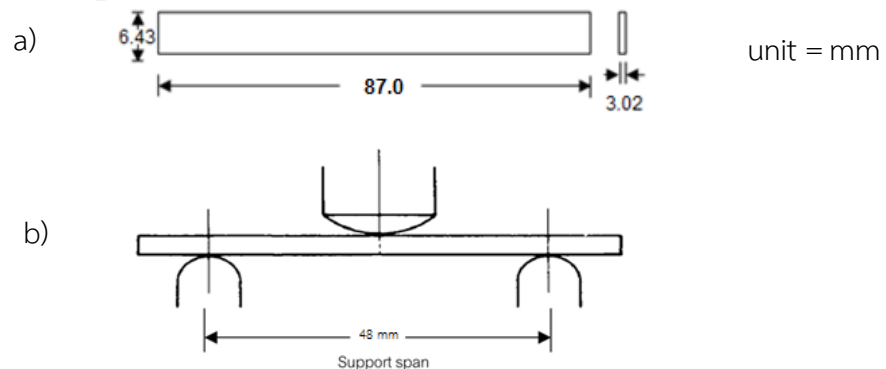


Figure 3.12 a) Dimension of flexural tested specimen and b) three point bending mode testing

Load cell of 500 N was used with three point bending mode with a crosshead speed of 1.23 mm/min using a span length of 48 mm at 23°C. Five specimens were measured and averaged. The results were reported as flexural modulus and flexural strength.

3.5.1.3 Impact strength

The notched izod impact strength of specimens was determined according to ASTM D256 Figure 3.13 (a) presents the dimension of specimens using impact testing machine (IMPACTOR II, CEAST, Pianezza, Italy) as shown in Figure 3.13 (b). The pendulum of 1.0 J was used to test with speed 3.5 m/sec at 23°C. The impact strength was averaged from five specimens testing.

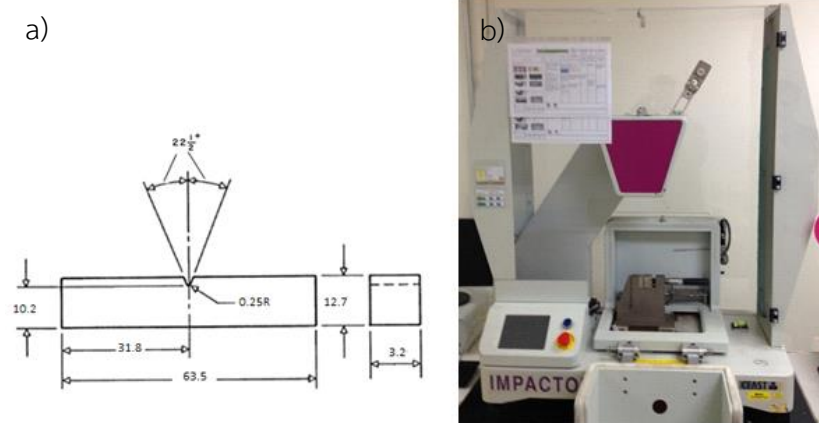


Figure 3.13 a) Dimension of impact tested specimen and b) impact testing machine (IMPACTOR II, CEAST, Pianezza, Italy)

3.5.2 Dynamic mechanical properties

Dynamic mechanical properties were characterized by dynamic mechanical analyzer (DMA) (EPLEXOR, GABO, Ahlden, Germany) as shown in Figure 3.14. The prepared composites were compressed into 1 mm thick and cut into the dimension of 1 cm x 3.5 cm. The prepared specimens were measured using three point bending mode at a frequency of 1 Hz and static force of 0.01 N. The temperature was set from -100 to 130°C with a heating rate of 5°C/min. The obtain results were storage modulus, loss modulus, $\tan \delta$, and glass transition temperature of composites.



Figure 3.14 Dynamic mechanical analyzer (DMA) (EPLEXOR, GABO, Ahlden, Germany)

3.5.3 Physical properties

3.5.3.1 Density

The density (ρ) of prepared composites (g/cm³) was measured by the density balance (201, Mettler Toledo, Greifensee, Switzerland) as shown in Figure 3.15 with a kit measurement of the density based on Archimedes's principle. The prepared composites were weighed in air and known-density liquid, high purity water. The density was measured at room temperature by the buoyancy system and the density value was calculated following the equation (3.6):

จุฬาลงกรณ์มหาวิทยาลัย
CHULALONGKORN UNIVERSITY

$$\rho_{\text{polymer}} = \frac{w_0}{w_0 - w_1} \rho_{\text{liquid}} \quad 3.6$$

Where w_0 is weight of composite in air and w_1 is weight of composite in water [86].



Figure 3.15 Density balance (201, Mettler Toledo, Greifensee, Switzerland)

3.5.3.2 Melt flow index

The melt flow index (MFI) was used to evaluate the ability of thermoplastic to flow into the mold. MFI is defined as weight of melt polymer flowing through a die in ten minutes. MFI was measured by melt flow indexer machine (CEAST MF50, Instron, Illinois, United State) shown in Figure 3.16. The MFI of prepared PP composites was evaluated according to ASTM D1238 using temperature 230°C with an applied load 2.16 kg. The L/D ratio of die was 8 mm/2.095 mm.



Figure 3.16 Melt flow indexer machine (CEAST MF50, Instron, Illinois, United State)

3.5.3.3 Morphology

The fracture surface of specimen was used to observe morphology by using scanning electron microscopy (SEM) (LEO1450VP, LEO, Oberkochen, Germany) as shown in Figure 3.7. The fracture surface of specimen was sputter-coated with gold for 10 minutes before determination using accelerating voltage of 15 kV.

3.5.3.4 Water uptake isotherm

The tensile specimens shaped according to ASTM D638 type V (Figure 3.11 (a)) was applied for water uptake isotherm experiment. The specimens were dried in an oven at 105°C for 24 hours before using. After that, specimens were placed in a desiccator using silica gel and weighed when they cooled down. After weighing, sample specimens were immersed in deionized water as a function of time following ASTM D570 for different periods (0, 7, 14, 21 and 28 days). The weight gained by the immersed sample was applied to evaluate the water uptake by the samples. After immersion, the samples were wiped by soft cloth to remove water on specimen surface. The percent weight increase (%WI) of the prepared composite specimens was calculated using the following equation:

$$\%WI = \frac{W - W_i}{W_i} \times 100 \quad 3.7$$

3.5.4 Thermal properties

3.5.4.1 Thermogravimetric analysis (TGA)

The thermal stability of prepared composites was evaluated by thermogravimetric analyzer (TGA) (TGA/DSC1, Mettler Toledo, Greifensee, Switzerland) as shown in Figure 3.10. The measurement was performed using approximately 10 mg of composites. TGA instrument was heated from 50 to 900°C at a heating rate of 10°C/min under nitrogen atmosphere. Thermal degradation and stability were determined in terms of the onset of degradation temperature and percentage of weight loss.

3.5.4.2 Differential scanning calorimetry (DSC)

The thermal properties of obtained PP composites carried out by differential scanning calorimetry (DSC) (DSC 204 F1, NETZSCH, Selb, Germany) as presented in Figure 3.17. The approximate 10 mg of sample was scanned from 25 to 200 °C a heating rate of 10°C/min and then cooled at the same rate under a nitrogen atmosphere with gas flow rate 50 ml/min. The samples were first heated to 200°C and held for 3 min to eliminate the thermal history of samples and then cooled to 25°C with a rate of heating at 10°C/min, after that the samples were subsequently heated to 200°C at the same rate for the second run. Melting temperature (T_m) were measured from the second scan. The degree of crystallinity (X_c) was calculated according to the following equation:

$$X_c = \frac{\Delta H_f \times 100}{\Delta H_f^0 w} \quad 3.8$$

Where ΔH_f is the heat of fusion of the PP composites, ΔH_f the heat of fusion for 100% crystalline PP ($\Delta H_{100} = 190 \text{ J/g}$) and w is the mass fraction for PP in the composites [87].



Figure 3.17 Differential scanning calorimetry (DSC) (DSC 204 F1, NETZSCH, Selb, Germany)

3.5.4.3 Thermo mechanical analysis

The dimension stability was investigated by thermomechanical analyzer (TMA) (TMA/SDTA841e, Mettler Toledo, Greifensee, Switzerland) as presented in Figure 3.18 in order to obtain coefficient of thermal expansion (CTE). The specimens were cut into the dimension 5 mm x 5 mm with 3 mm thickness. The tests were determined using a expansion probe with a 3 mm ball-point probe. The temperature was scanned from 20 to 160°C with a scanning rate of 5°C/min and the static load at 0.05 N was applied on the top of ball probe.



Figure 3.18 Thermomechanical analyzer (TMA/SDTA841^e, Mettler Toledo, Greifensee, Switzerland) [88]

CHAPTER IV

RESULTS

4.1 Characterization of parawood sawdust (PW)

4.1.1 Chemical composition

The percentage of cellulose, hemicellulose, lignin, extractives, and ash of raw PW is shown in Table 4.1. It could be seen that raw PW had a small amount of cellulose. In order to increase the amount of cellulose, parawood sawdust needed to be chemically processed to decrease other components such as hemicellulose, lignin, and extractives.

Table 4.1 Chemical composition of parawood sawdust

%Cellulose	%Hemicellulose	%Lignin	%extractives
37.75	25.20	15.17	21.88

4.2 Preparation of parawood microcrystalline cellulose (PW-MCC)

4.2.1 Chemical composition of PW-MCC

The chemical compositions of raw PW and PW-MCC are shown in Table 4.2. The results showed that the percentage of cellulose was gradually increased after chemical treatment PW with alkaline. Therefore, the content of cellulose was increased from 37.75% to 55.96% after delignification using NaOH. Since the delignified PW was subjected to bleaching with sodium hypochlorite for pulping fibers. The content of cellulose was also increased from 55.96% to 76.75% while hemicellulose, lignin, and extractives were significantly decreased. Using an alkaline treatment could remove lignin, hemicellulose and extractives that containing in the raw PW [53]. In addition, PW pulp was hydrolyzed with hydrochloric acid and sulfuric acid to obtain PW-MCC-H and PW-MCC-S, respectively. The results presented that the cellulose content of PW-MCCs was similar to that of pulp PW.

Table 4.2 Chemical composition of PW and PW-MCC

Sample	%Cellulose	%Hemicellulose	%Lignin	%Extractives
Raw PW	37.75	25.20	15.17	21.88
De-lignin PW	55.96	18.90	19.87	5.27
PW pulp	76.75	8.85	6.19	7.29
PW-MCC-H	77.67	8.80	6.93	6.60
PW-MCC-S	76.89	8.35	5.24	9.52

4.2.2 Product yield

Product yield of all acid hydrolysis conditions is presented in Table.4.3. The product yield was found to be different depending on the hydrolysis conditions.

Table 4.3 Product yield of PW-MCC from acid hydrolysis

Pulp to acid ratio	Temperature (°C)	Time (h)	Product yield (%)			
			HCl		H ₂ SO ₄	
1:10	80	2	44.48	<	48.30	
		4	39.93	>	26.30	
	105	2	35.40	~	36.43	
		4	28.91	<	34.53	
	1:15	80	2	41.66	<	47.43
			4	37.80	~	38.90
105		2	29.33	<	39.87	
		4	15.08	<	30.43	

It can be noticed that using hydrolysis temperature at 105°C gave lower product yield. This result could be because the higher temperature gave fast acid hydrolysis resulting in reduction in degree of polymerization and generating a small particle of PW-MCC [89]. Moreover, hydrolysis time at 4 h provided lower product yield than the one hydrolyzed at 2 h as well. In addition, using different types of acid also gave different amount of product yield. It could be observed that using sulfuric acid gave higher of product yield than using hydrochloric acid. Beside, increasing pulp to acid ratio from 1:10 to 1:15 showed a reduction of product yield. This results suggested that higher hydrolysis temperature, longer hydrolysis time and higher pulp to acid ratio could be too much hydrolyzed on PW-pulp resulting to lower product yield.

4.2.3 Bulk density of prepared PW-MCC

Bulk density of the prepared PW-MCC is presented in Table 4.4. The results showed that hydrolysis condition and acid type resulted in the different in its bulk density. However, both of acid type, higher temperature or at 105°C provided higher bulk density than at 80°C. It could be explained that hydrolysis reaction performed at higher temperature produced a small particle and fibers became dense while the product yield was reduced. However, it could be observed that using sulfuric acid gave slightly higher bulk density than using hydrochloric because sulfuric acid is dibasic acid. Besides, sulfuric acid is fully dissociated in water and the H⁺ ion concentration of sulfuric acid is slightly greater than that of hydrochloric acid of same concentration because sulfuric acid almost entirely exists as H⁺ and HSO₄⁻ ions in aqueous. Therefore, using different of hydrolysis time and increasing of pulp to acid ratio did not significant affect to bulk density.

Table 4.4 Bulk density of prepared PW-MCC

Pulp to acid ratio	Temperature (°C)	Time (h)	Bulk density (g/cm ³)	
			HCl	H ₂ SO ₄
1:10	80	2	0.1531	0.1268
		4	0.1523	0.1461
	105	2	0.1968	0.1875
		4	0.1875	0.2085
1:15	80	2	0.1583	0.1836
		4	0.1595	0.2124
	105	2	0.1658	0.1968
		4	0.2245	0.2125

4.2.4 Particle size of PW-MCC

The particle size of prepared PW-MCC from all conditions was measured by particle size analyzer using water as media. In fact, the microparticle of MCC were agglomerated led to lump particle during drying step of the prepared MCC. Hence, they were pulverized to obtain PW-MCC powder. The particle size of PW-MCC is displayed in Table 4.5. Nevertheless, the different condition of acid hydrolysis did not caused much different in particle size of PW-MCC. The results presented that the obtained PW-MCC had particle size within the range of 27 – 33 μm .

Table 4.5 Particle size of PW-MCC

Pulp to acid ratio	Temperature (°C)	Time (h)	Particle size (µm)	
			HCl	H ₂ SO ₄
1:10	80	2	28.73	31.16
		4	32.54	30.27
	105	2	29.06	29.97
		4	30.96	27.15
1:15	80	2	30.56	30.97
		4	30.02	28.31
	105	2	29.61	29.86
		4	30.50	30.78

4.2.5 Functional group of prepared PW-MCC

The functional group of prepared MCCs was characterized by FTIR technique. The comparison between FTIR spectra of PW-pulp and PW-MCC is displayed in Figure 4.1. All spectra exhibited broad absorption band in the 2800-3600 cm⁻¹ region which was referred to O-H stretching vibration, the main component of cellulose molecule. In addition, there was a peak at 1641 cm⁻¹ which was attributed to the H-O-H bending of absorbed water molecule [57]. The other main functional group of cellulose was C-H stretching of cellulose [90] which showed the peak in the region of 2900-2940 cm⁻¹. The spectrum of raw PW showed the dominant peak of the C=O stretching in the acetyl and uronic ester groups of hemicellulose or the carboxylic ester group of the ferulic and p-coumaric unit of lignin at peak 1740 cm⁻¹ [91]. This peak was related to chemical composition of fiber that was a composite consisting of cellulose, hemicellulose, and lignin in its structure. After chemical treatment with alkali solution, this peak was decreased intensity. Moreover, the peak at 1504 cm⁻¹ which was assigned to lignin aromatic ring [92] was also absence in bleached PW and PW-MCC. This was a

significant evidence that lignin and hemicellulose were removed during chemical treatment. Both peaks did not show in ref-MCC spectrum either. Furthermore, it can be observed the peak at 1429 cm^{-1} and 1330 cm^{-1} in all spectra sample which were attributed to the saturated C-H bending and wagging vibration, respectively [93]. The absorption band at 1163 cm^{-1} was referred to C-O-C stretching, and the peak at 897 cm^{-1} was assigned to C-H rocking vibration of cellulose [90].

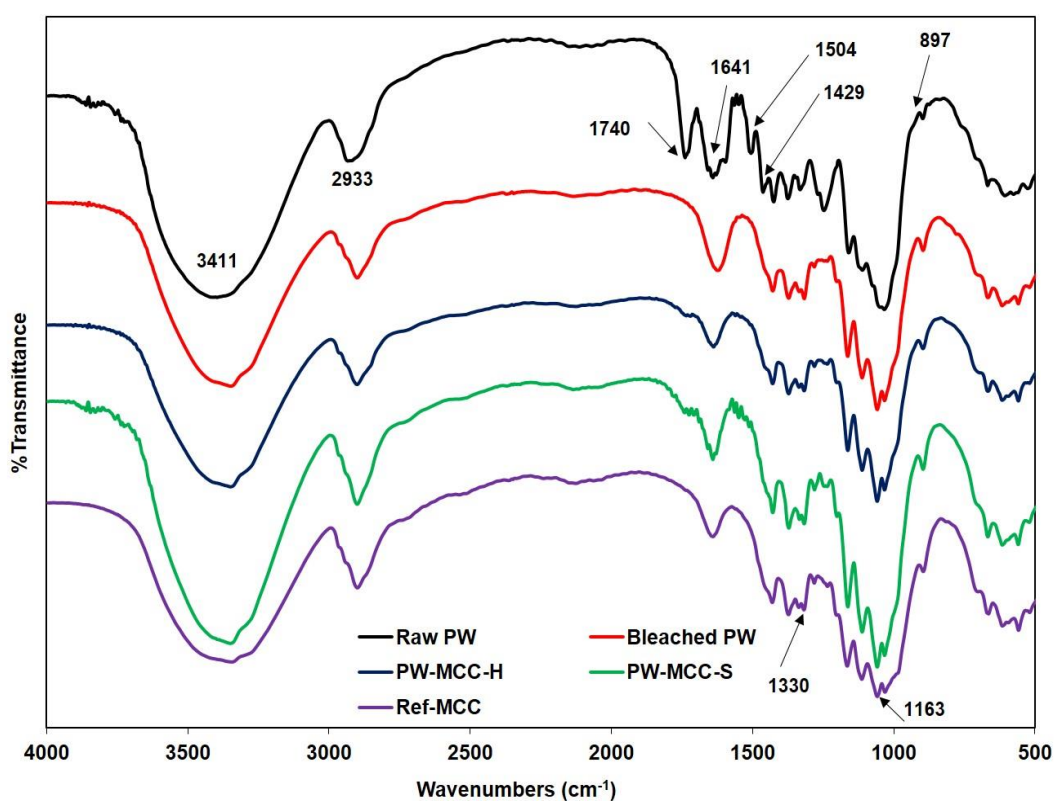


Figure 4.1 FTIR spectra of raw-PW, bleached PW, PW-MCC, and ref-MCC

Using different acid types for hydrolysis PW pulp did not affect the chemical structure of cellulose. Both of acid type, either hydrochloric acid or sulfuric acid gave the similar FT-IR spectra to comparing to ref-MCC. In addition, the different of acid hydrolysis condition such as acid types, reaction temperature (80°C and 105°C), reaction time (2 h and 4 h), and pulp to acid ratio (1:10 and 1:15) did not alter the function group of cellulose. The FTIR spectra of PW-MCC hydrolyzed at different acid hydrolysis conditions are presented in Figure 4.2.

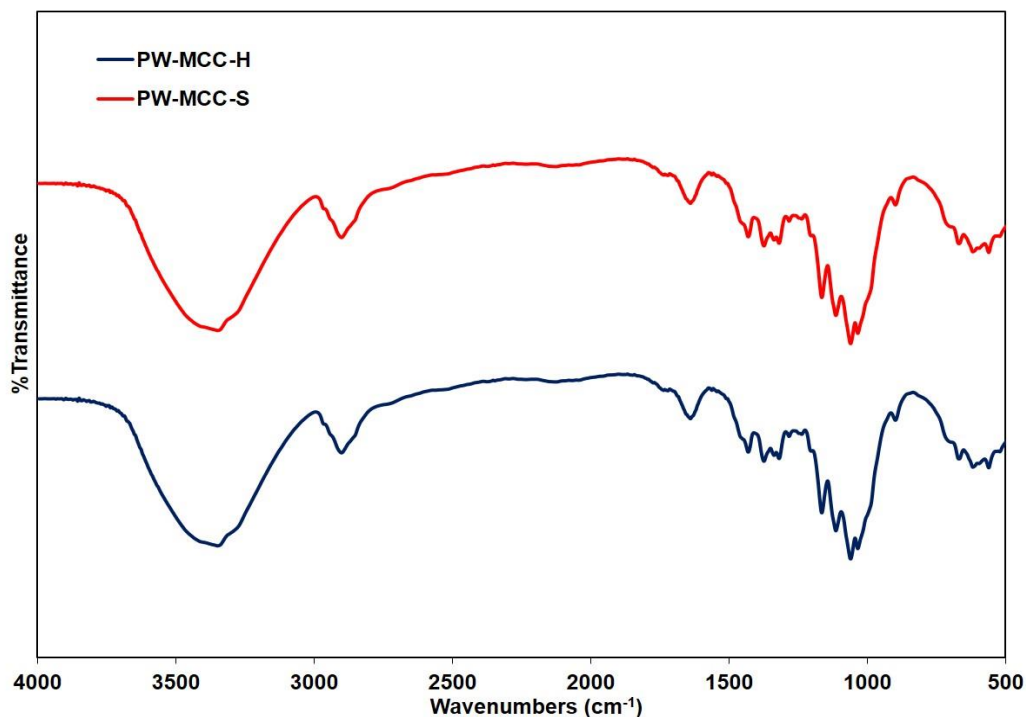


Figure 4.2 FTIR spectra of PW-MCC using HCl hydrolysis and H₂SO₄ hydrolysis at temperature 80°C

4.2.6 Degree of polymerization of PW-MCC

The effect of different acid hydrolysis conditions (i.e., acid type, reaction time, reaction temperature, and pulp to acid ratio) on the degree of polymerization (DP) of the prepared microcrystalline cellulose was investigated. The DP values of PW-MCC prepared from different acid hydrolysis conditions are presented in Table 4.6. Before acid hydrolysis, DP value of raw PW was 850. After acid hydrolysis, DP values of PW-MCC decreased according to the degradation of the glycosidic bond of cellulose chain which was catalyzed by the H⁺ ions of dilute acid solution [44].

Table 4.6 Degree of polymerization of PW-MCC

Pulp to acid ratio	Temperature (°C)	Time (h)	DP	
			HCl	H ₂ SO ₄
1:10	80	2	437	355
		4	425	307
	105	2	365	306
		4	330	287
1:15	80	2	375	287
		4	369	279
	105	2	350	267
		4	293	232

It was found that DP values of PW-MCC hydrolyzed using hydrochloric acid were higher than in the case of using sulfuric acid. These results were obtained from all hydrolysis conditions. Theoretically, using different acid types should give similar DP value. However, this effect from using sulfuric acid could come from an esterification reaction of cellulose and then an introduction of sulfate groups into the cellulose molecule [38]. These sulfate groups on MCC will be ionized in solution and caused repulsion between chains leading to easier flow or shorter flow time than PW-MCC prepared using hydrochloric acid during viscosity measurement [41]. Therefore, PW-MCC prepared using sulfuric acid having shorter flow time and thus smaller viscosity value exhibited lower DP values.

Furthermore, the results exhibited that increasing pulp to acid ratio from 1:10 to 1:15 caused reduction of DP values. This phenomenon could be explained that higher acid to cellulose ratio can induce the rate of hydrolysis [94] attributing to fast depolymerization of cellulose. When the reaction time was increased from 2 h to 4 h, the DP values were continuously decreased because acid hydrolysis still carried on

but with slow degradation rate. At the initial time, the hydrolysis of cellulose occurred with the fast degradation rate followed by slow degradation rate. These results agreed well with previous research [95]. Moreover, an increase of reaction temperature from 80°C to 105°C could also catalyze the hydrolysis reaction resulting in the reduction of DP value. This result could be from progressive increase of temperature and hydrolyzing time caused an increasing the diffusion of acids into the amorphous part of cellulose. At longer contact time would alter physical swelling of MCC. Therefore, the surface area of the fiber would increase led to higher hydrolysis efficiency [96]. This progressive hydrolysis caused a decreasing of DP value.

4.2.7 Crystallinity of PW-MC

As known that cellulose consists of both crystalline and amorphous regions [97]. The acid hydrolysis is a protonation of glycosidic oxygen by H⁺ resulting in breaking of β -1,4-glycosidic bond of cellulose polymer by the water addition [36]. X-ray diffraction was used to investigate effect of hydrolysis on crystallinity of PW-MCC. The XPD pattern of PW-MCC samples are displayed in Figure 4.3.

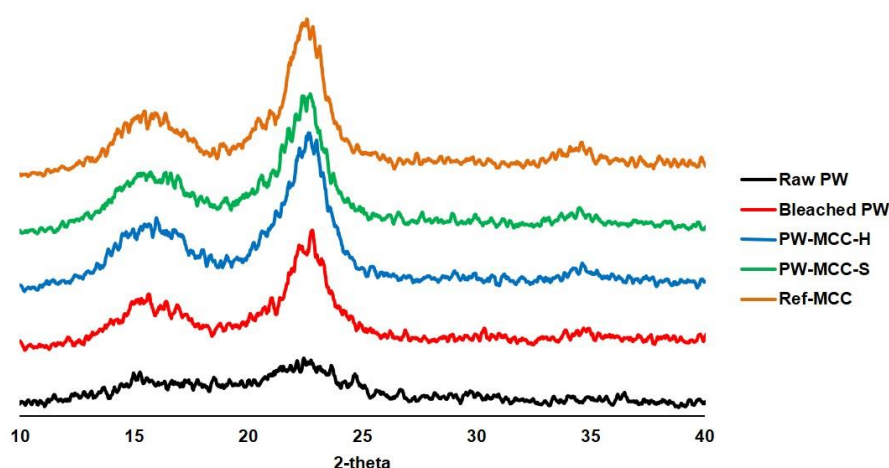


Figure 4.3 X-ray diffraction pattern of raw-PW, PW pulp, and PW-MCC

It can be seen that there were three main reflections presented in all samples at $2\theta = 15.2^\circ$, 16.4° , and 22.7° . These XRD patterns exhibited that all samples had a typical crystal form of cellulose I and having highest scattering intensity at 22.7° [98].

Nevertheless, using different hydrolysis condition to prepare PW-MCC indicated similar XRD pattern but with slightly difference in its intensity. The crystalline index (CrI) of samples calculated from X-ray diffraction pattern is presented in Table 4.7. Initially, the CrI of raw PW was only 33%. After removing lignin and hemicellulose during chemical treatment, the CrI of bleached PWS was increased to 60%. However, as shown in Table 4.7 the obtained PW-MCC also had CrI value around 60% which was similar to that of bleached PW. These results indicated that acid hydrolysis condition in this study did not affect or destroy to crystalline structure of PW pulp.

Table 4.7 CrI values of PW-MCC prepared from different acid hydrolysis conditions

Pulp to acid ratio	Temperature (°C)	Time (h)	CrI (%)	
			HCl	H ₂ SO ₄
1:10	80	2	62	60
		4	61	57
	105	2	66	61
		4	59	60
1:15	80	2	60	58
		4	62	57
	105	2	61	65
		4	62	62

4.2.8 Thermogravimetric analysis

One of important of reinforcing materials for processing and utilization is thermal stability. In this research, TGA was used to evaluate the thermal degradation of obtained PW-MCC. The TGA curves of PW, bleached PW, and PW-MCC are displayed in Figure 4.4. It can be clearly observed from TGA curves that all samples exhibited minor mass loss at the temperature below 100°C, which indicated the desorption of

water molecule from the polysaccharide structure [99]. After that, comparatively, raw PW started to decompose at the temperature lower than PW-MCC. The decomposition temperature of raw PW was 282°C while that of bleached PW was 326°C. This lower thermal stability could be due to the thermal decomposition of hemicellulose [100]. The raw PW consisted of hemicellulose, lignin, and other non-cellulosic constituents which had low thermal stability. Thus, these compositions caused raw PW began early thermal decomposition than PW-MCC. In fact, the thermal degradation of natural fiber materials begins with decomposition of lignin and hemicellulose followed by decomposition of cellulose [101].

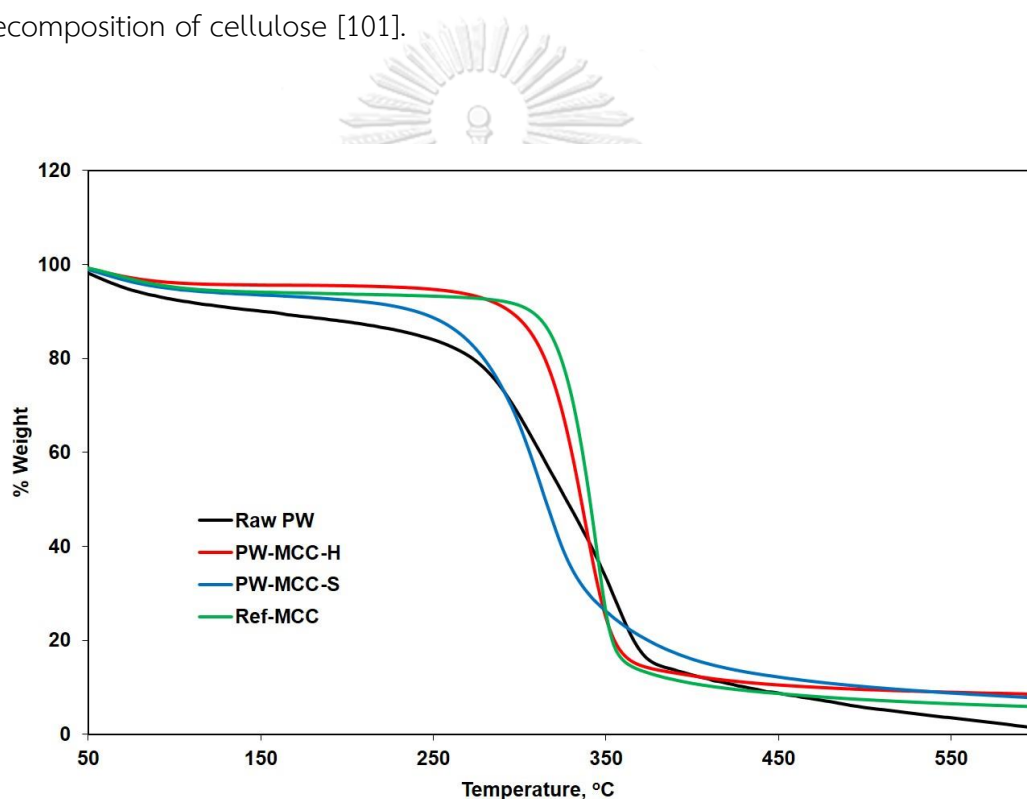


Figure 4.4 TGA thermograms of PW-MCC prepared using pulp to acid ratio 1:10 at 80°C for 2 h

In addition, the thermal stability of bleached PW was improved because of the removal of non-cellulosic materials during alkali treatment. Furthermore, cellulose became dense and compact that could increase the onset of thermal degradation temperature.

For hydrolysis conditions, using different acid types affected differently to thermal stability of the obtained PW-MCC is presented in Table 4.8.

Table 4.8 Thermal stability of PW-MCC prepared from different acid hydrolysis conditions

Pulp to acid ratio	Temperature (°C)	Time (h)	Td (°C)	
			HCl	H ₂ SO ₄
1:10	80	2	311	298
		4	306	279
	105	2	311	294
		4	308	278
1:15	80	2	311	293
		4	309	284
	105	2	306	272
		4	309	251

As shown in Table 4.8, using sulfuric acid hydrolysis provided PW-MCC with lower thermal stability than using hydrochloric acid. This was because of an introduction of sulfate groups on cellulose chains during acid hydrolysis. These sulfate groups catalyzed the thermal degradation of cellulose [102], resulting in lower Td of PW-MCC hydrolyzed with sulfuric acid. Moreover, as explained earlier, using sulfuric acid yield lower degree of polymerization (DP) than using hydrochloric acid as shown in Table 4.5, affecting to the lower in thermal stability of PW-MCC prepared using sulfuric acid. In fact, the thermal decomposition behavior of cellulose has 2 steps which are depolymerization anhydrosugars and char formation step. The depolymerized anhydrosugars is at between 290°C and 320°C. When, DP of PW-MCC decreased led to lower depolymerization anhydrosugars temperature [103]. The

degradation temperature data are showed in Table 4.8. This result is in agreement with other researchers [41, 43, 104, 105].

In addition, it can be observed from the results that using different reaction times or pulp to acid ratios slightly affected thermal stability of the obtained PW-MCC. When the hydrolysis was prolonged to 4 h, thermal degradation temperature was decreased due to the reduction of DP value as indicated in Table 4.5.

4.2.9 Morphological analysis

The SEM micrographs of raw PW and PW pulp are presented in Figure 4.5. The SEM micrograph of raw PW revealed the rough surface containing short fiber and some small particles. This roughness could be implied to the presence of wax or other impurities on the surface resulting in the fibers with a protective layer [106]. After alkali treatment and bleaching to remove non-cellulosic materials, the PW pulp became fibrillated and smoother surface can be observed. The morphology of raw PW and PW pulp was related to the chemical composition results.

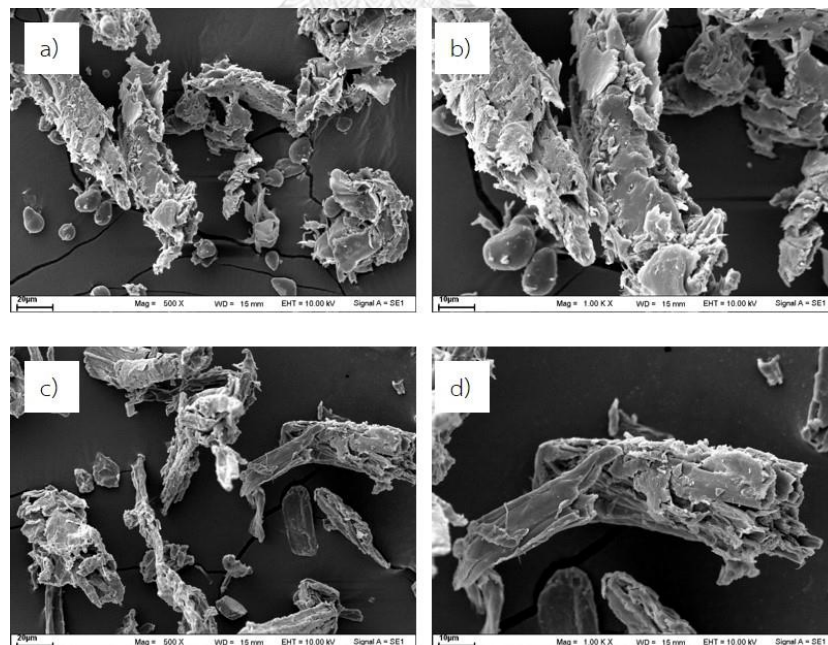


Figure 4.5 SEM micrographs of a) raw PW at 500x, b) raw PW at 1000x, c) PW pulp at 500x, and d) PW pulp at 1000x

Moreover, the SEM micrograph of the ref-MCC (Avicel[®] PH101) is presented in Figure 4.6 It could be observed the rod-like structure and smooth surface. The particle size of ref-MCC was 27 μm .

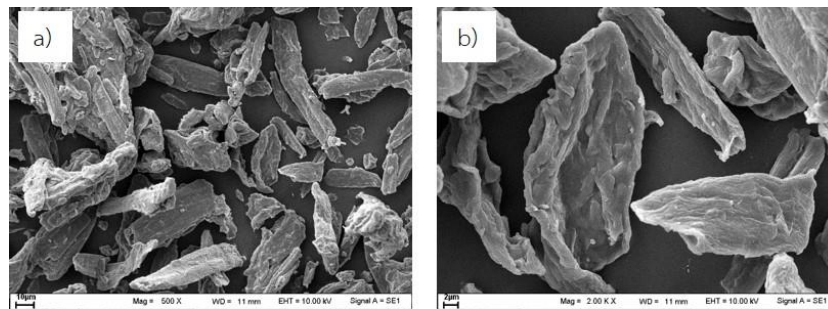


Figure 4.6 SEM micrographs of the ref-MCC at a) 500x and b) 1000x

The effects of hydrolysis conditions on the morphology of PW-MCC were displayed in Figure 4.7-4.10. It was observed that PW-MCC exhibited rod-like structure and smooth surface after acid hydrolysis which was similar morphology and particle size to ref-MCC. Moreover, the clear smooth surface can be observed when using higher pulp to acid ratio. Both acids gave the same morphology of PW-MCC.

There was no significant difference observed of the obtained PW-MCC from different of hydrolysis time and temperature. Thus, it could be concluded that hydrolysis condition slightly affected to morphology of prepared PW-MCC.

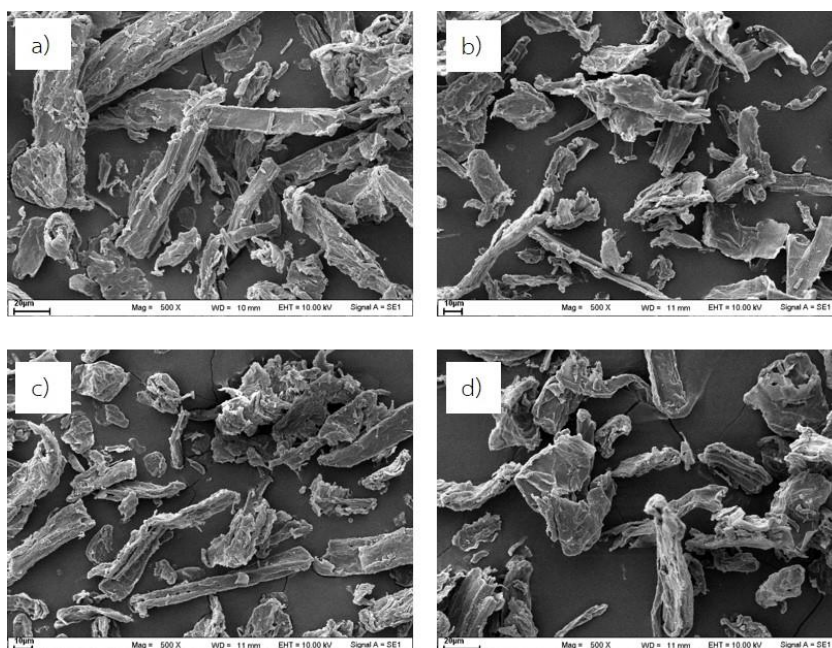


Figure 4.7 SEM micrographs of PW-MCC prepared using pulp to HCl ratio 1:10 at a) 80°C/2h b) 80°C/4h, c) 105°C/2h and e) 105°C/4h

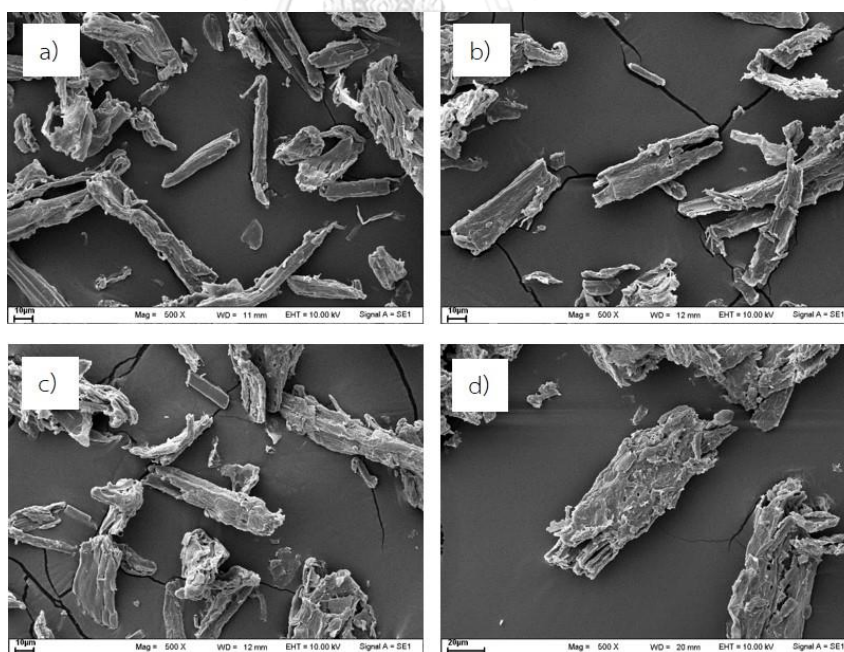


Figure 4.8 SEM micrographs of PW-MCC prepared using pulp to HCl ratio 1:15 at a) 80°C/2h b) 80°C/4h, c) 105°C/2h, and e) 105°C/4h

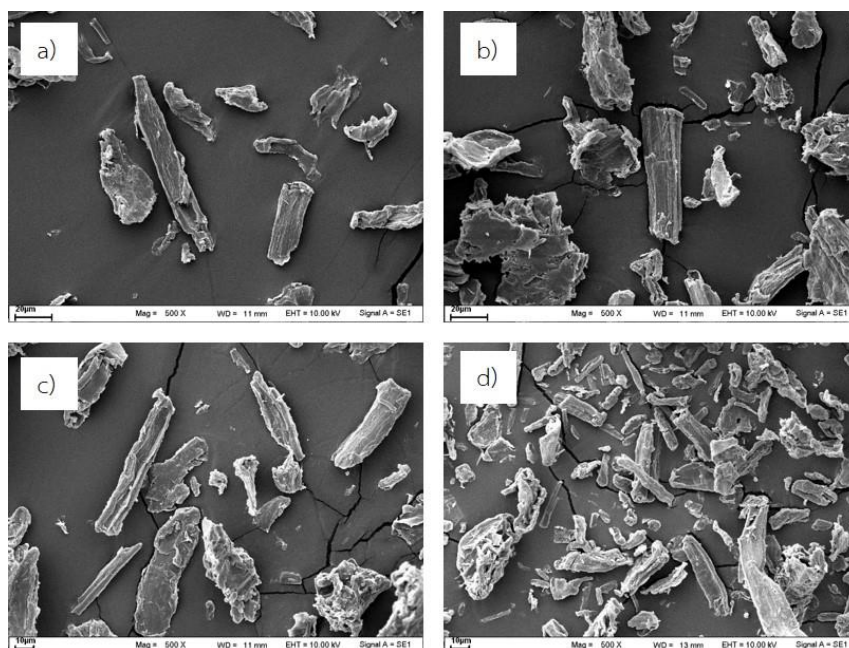


Figure 4.9 SEM micrographs of PW-MCC prepared using pulp to H_2SO_4 acid ratio 1:10 at a) $80^\circ\text{C}/2\text{h}$ b) $80^\circ\text{C}/4\text{h}$, c) $105^\circ\text{C}/2\text{h}$, and e) $105^\circ\text{C}/4\text{h}$

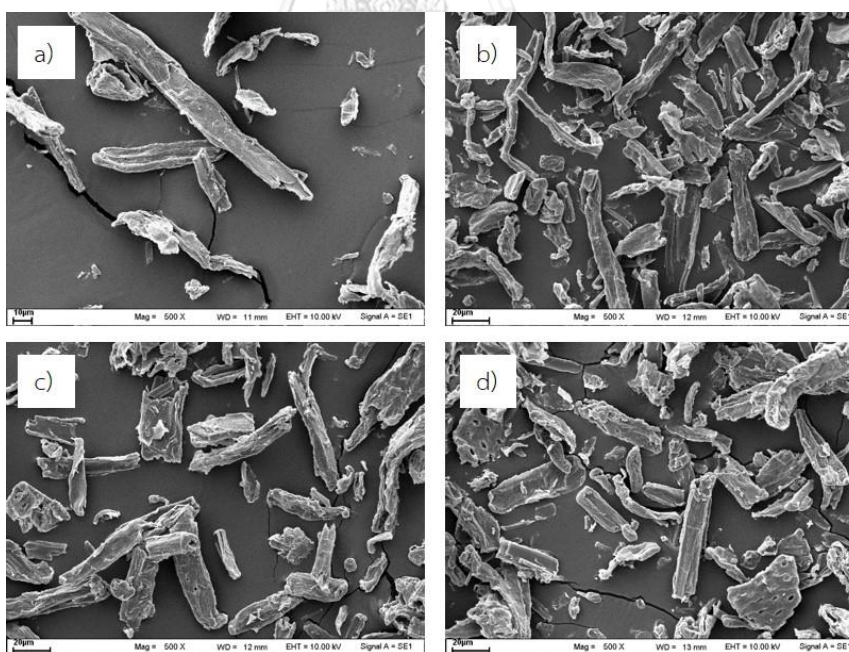


Figure 4.10 SEM micrographs of PW-MCC prepared using pulp to H_2SO_4 acid ratio 1:15 at a) $80^\circ\text{C}/2\text{h}$ b) $80^\circ\text{C}/4\text{h}$, c) $105^\circ\text{C}/2\text{h}$, and e) $105^\circ\text{C}/4\text{h}$

Therefore, PW-MCC was successfully prepared from parawood sawdust (PW). The characterized results exhibited that acid hydrolysis affected to the obtained PW-MCC. The FTIR spectra and XRD pattern confirmed that the obtained PW-MCC was cellulose structure with cellulose type I. However, different of hydrolysis condition provided the different of thermal stability and DP of PW-MCC. Using hydrochloric acid gave better stability than that using of sulfuric acid. Moreover, longer hydrolysis time and higher temperature caused degradation of PW-MCC during hydrolysis. Thus, the suitable condition for further study step was using hydrochloric acid with pulp to acid ratio 1:15 at 80°C for 2 h.

4.3 Surface modification of PW-MCC

In this section, PW-MCC was modified with various coupling agents such as vinyltrimethoxysilane, benzoyl chloride, hexanoyl chloride, and lauroyl chloride mechanochemical method using planetary ball mill. During ball milling process, relative motion between milling media and samples generates collision friction, impact, and shear forces resulting in changing physicochemical properties and crystalline structure of PW-MCC. Besides, the particle size is reduced and the specific area and surface energy is increased contributing to enhancing chemical reactivity [107]. Therefore, one factor that affected ball milling activation is ball milling speed.

4.3.1 Effect of ball milling speed on crystallinity and structure of PW-MCC

Ball milling speed was also an important factor for stress-induced structural change of crystallinity of cellulose and chemical reaction. In order to investigate the effect of ball milling on crystallinity of PW-MCC, XRD diffraction was performed and the crystallinity index (Cri) of sample was calculated according to the method of Segal et al. [83]. Thus, the various speeds of planetary ball mill was studied without coupling agents. Figure 4.11 displays the crystallinity of PW-MCC after ball milling at different speed at 60 min.

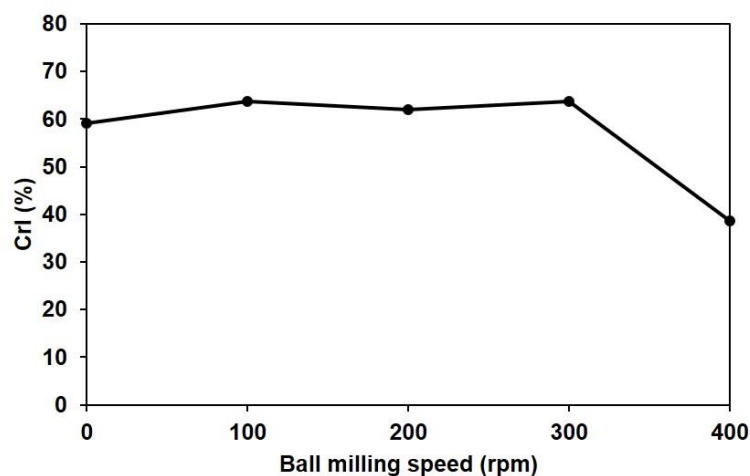


Figure 4.11 The CrI (%) of PW-MCC with different ball milling speed at 60 min

It could be seen that ball milling speed at 400 rpm caused the reduction in the crystallinity of PW-MCC. The reduction of CrI of PW-MCC from 60 to 38 after ball milling suggesting that the crystalline structure of cellulose was significant damaged by mechanical force [107]. X-ray diffraction pattern of milled PW-MCC at a rotation speed 400 rpm is presented in Figure 4.12.

After ball milling, the intensity peak at $2\theta = 22.7^\circ$ was decreased and broader which referred to the destruction of crystallinity of cellulose from mechanical action. Increment of amorphous part of cellulose is expected to enhance the active of cellulose in chemical modification [79]. However, ball milling speed at 100 to 300 rpm did not affect to the crystallinity of the cellulose.

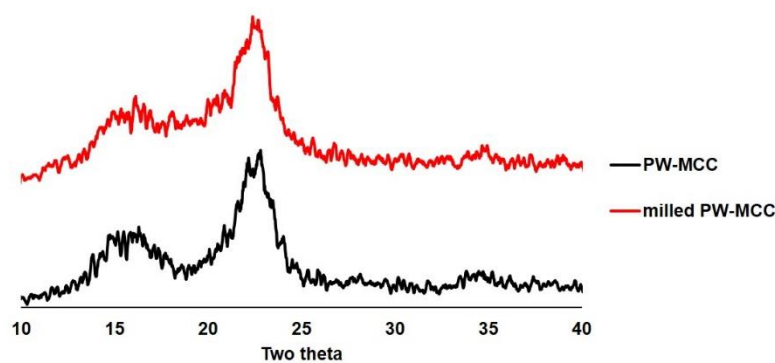


Figure 4.12 XRD patterns of PW-MCC and milled PW-MCC at rotation speed 400 rpm for 60 min

4.3.2 Effect of ball milling speed on morphology

Since ball milling is a top-down method to obtain micro or nano scale of materials. The morphology of the obtained PW-MCC from various ball milling speeds was investigated and display in Figure 4.13. SEM micrographs of milled PW-MCC at different ball milling speeds revealed that size and morphology of milled PW-MCC at 100, 200, and 300 rpm did not significantly change from un-milled PW-MCC (Figure 4.8(a)). However, ball milling speed at 400 rpm gave the reduction in size and morphology of milled PW-MCC. Before milling, the particle size of un-milled PW-MCC size was approximately 50-80 μm . After milling, particle size of milled PW-MCC was reduced to 10-30 μm due to mechanical force of the planetary ball mill. In addition, the morphology of PW-MCC was changed from short fiber to mixed of particle, flake and shorter fiber. This result was in agreement with CrI value that rotation speed at 400 rpm was damaged crystallinity of cellulose. Thus, ball mill speed at 400 rpm was selected for modifying PW-MCC in further step.

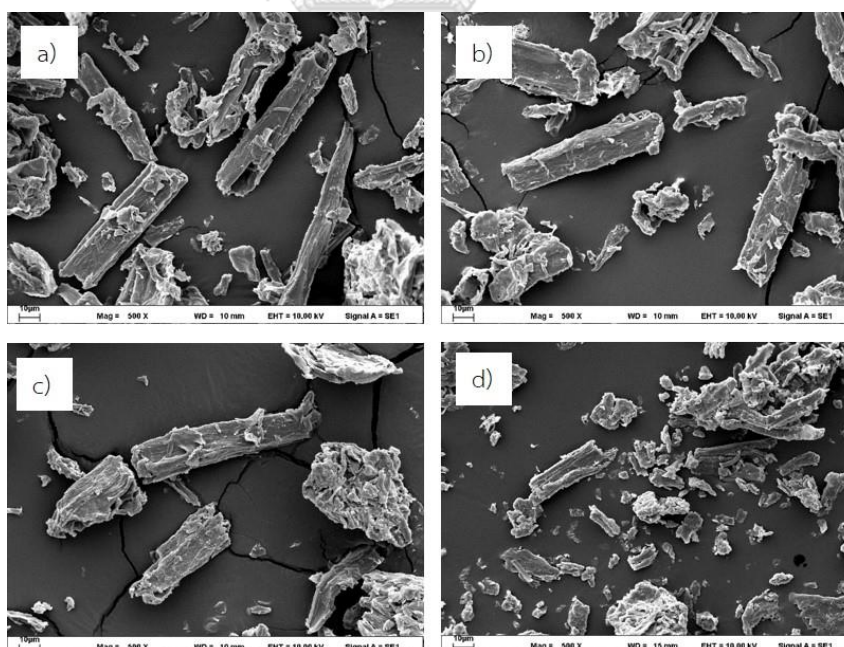


Figure 4.13 XRD patterns of milled PW-MCC at a) 100 rpm, b) 200 rpm, c) 300 rpm, and d) 400 rpm

4.3.3 Surface modification of PW-MCC using organosilane

In this part, PW-MCC was modified with vinyltrimethoxysilane at milling speed 400 rpm to obtain silane treated PW-MCC. In addition, silane content and ball milling time were studied and characterized the properties.

4.3.3.1 Functional group of silane treated PW-MCC

Generally, the mechanism of condensation reaction of organosilane and PW-MCC begins with hydrolyzation of organosilane to obtain silanols group. After that, silanols react with hydroxyl group of cellulose molecule to form covalent bond (Si-O-C) and generate by product which is water. Thus, the chemical reaction between PW-MCC and vinyltrimethoxysilane is presented in Figure 4.14.

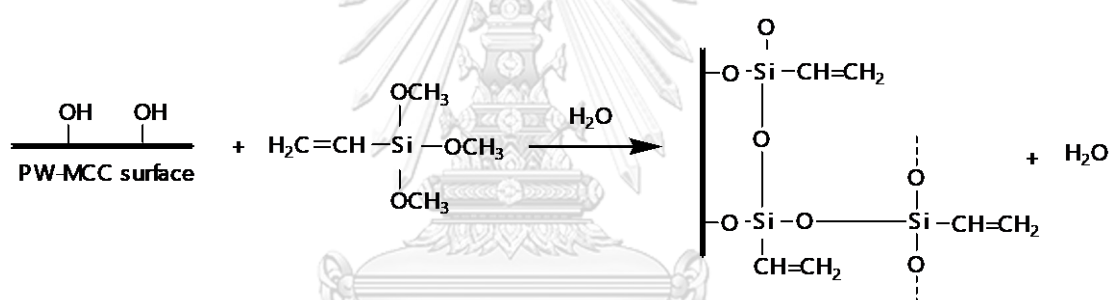


Figure 4.14 Silanization reaction of silane treated PW-MCC

However, in this study, the addition of water into the system was not necessary since there was moisture from PW-MCC due to hydrophilic nature of cellulose. When the mechanical force from ball mill was applied to system, the structure of cellulose was destroyed resulting in size reduction and elimination of moisture from the system. Thus, this moisture hydrolyzed organosilane to obtain silanols group. The functional group of silane treated PW-MCC was investigated by FTIR spectroscopy in order to confirm chemical the reaction between PW-MCC and vinyltrimethoxysilane. The FTIR spectra of PW-MCC and silane treated PW-MCC are displayed in Figure 4.15.

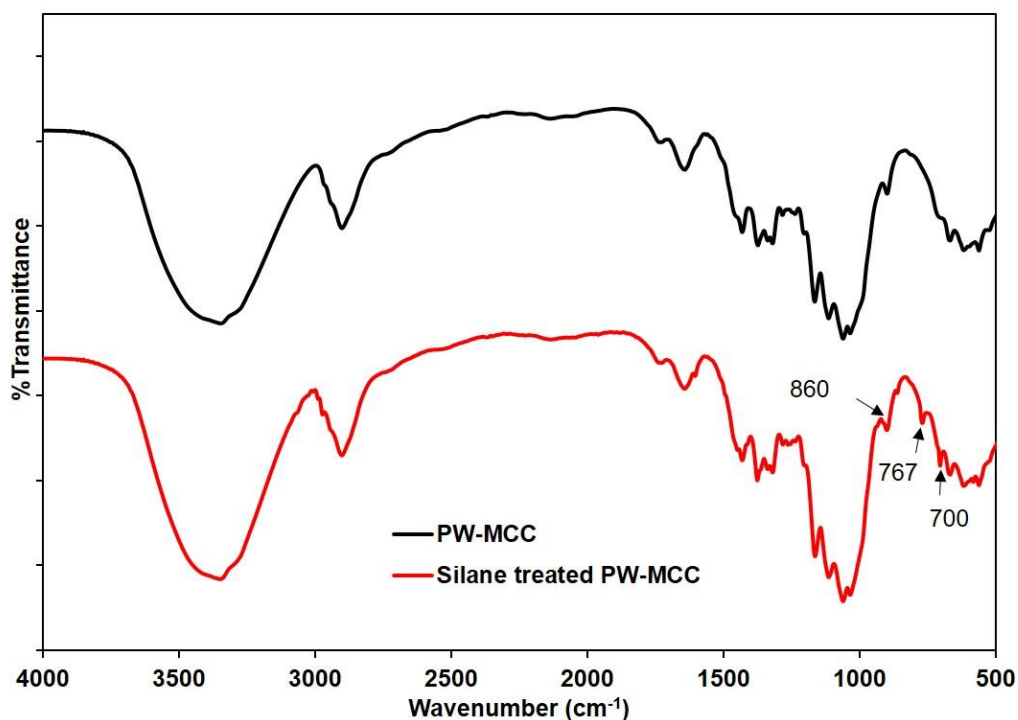


Figure 4.15 FTIR spectra of PW-MCC and silane treated PW-MCC

Comparing to PW-MCC, several new peaks from the spectra of silane treated PW-MCC could be observed. The peaks at 860 and 767cm^{-1} were referred to the $-\text{Si-C}$ symmetric stretching while the peak at 700cm^{-1} was assigned to the $-\text{Si-O-Si}$ symmetric stretching. Since an observation from FTIR spectra was difficult to notice $-\text{Si-O-C}$ bond in region $1150\text{-}950\text{cm}^{-1}$ because the finger print of FTIR spectrum of cellulose was overlapped with $-\text{Si-O-C}$ bond region [108]. Therefore, using other technique to confirm the reaction between organosilane and PW-MCC was reasonable. Thus, XPS technique was performed to determine the surface composition and the chemical environment including bonding of surface

4.3.3.2 Surface composition of silane treated PW-MCC

XPS technique was performed to determine the surface composition and the chemical environment including bonding of surface. The XPS photoelectron spectra of electron intensity at low resolution of PW-MCC and silane treated PW-MCC are presented in Figure 4.16. As PW-MCC is a purified cellulosic material so the dominant peak at 531 and 284eV which were assigned to O_{1s} and C_{1s} , respectively, could be

observed [63]. After surface modification of PW-MCC with organosilane, two new peaks were found at 154 eV which was referred to Si_{2s} and at 102 eV which was assigned to Si_{2p} atom emission. These two new peaks were corresponding to the existence of silicon atom on the surface of treated PW-MCC [109]. The results confirmed that silane group was successfully deposited on PW-MCC surface. In addition, the high-resolution of XPS patterns to carbons peak of PW-MCC before and after silane treatment are presented in Figure 4.17. For PW-MCC, it can be observed that there were 4 peaks at 287.7, 286.4, 285.0, and 283.3 eV, respectively and binding energies used to identify of bond type of carbon as displayed in Table 4.9. It could be confirmed that there were many bond types of carbon on PW-MCC surface [110].

Table 4.9 Binding energy and bond type for high-resolution XPS scan of C1s [111]

Carbon group	Binding energy (eV)	Bond type
C ₁	283.3	C-H/C-C
C ₂	285.0	C-O-H
C ₃	286.4	O-C-O
C ₄	287.7	O-C=O

After the surface of PW-MCC was treated with organosilane, the carbon peaks of silane treated PW-MCC sample were changed. It can be seen that the intensity of peak at 285.0 eV decreased because hydroxyl group was grafted with organosilane led to more hydrophobicity of silane treated PW-MCC [112]. Moreover, there was a new peak at 288.3 eV which can be referred to the emission of C-O-Si bond on PW-MCC surface [63]. These results indicated that there was polysiloxanes deposited on PW-MCC surface and the condensation reaction between organosilane and PW-MCC was successfully occurred. Thus, the FTIR and XPS spectra confirmed that using a mechanical activation from ball milling gave an achievement of chemical reaction between organosilane and PW-MCC.

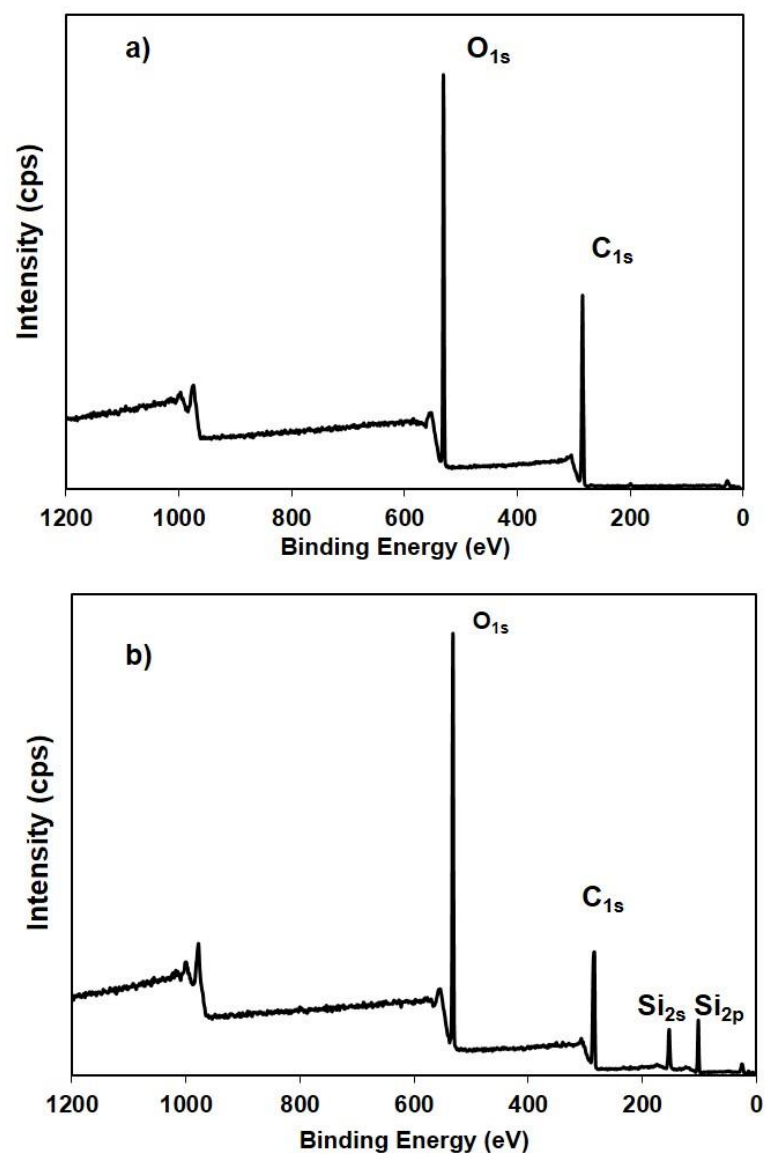


Figure 4.16 XPS survey spectra of a) PW-MCC and b) silane treated PW-MCC

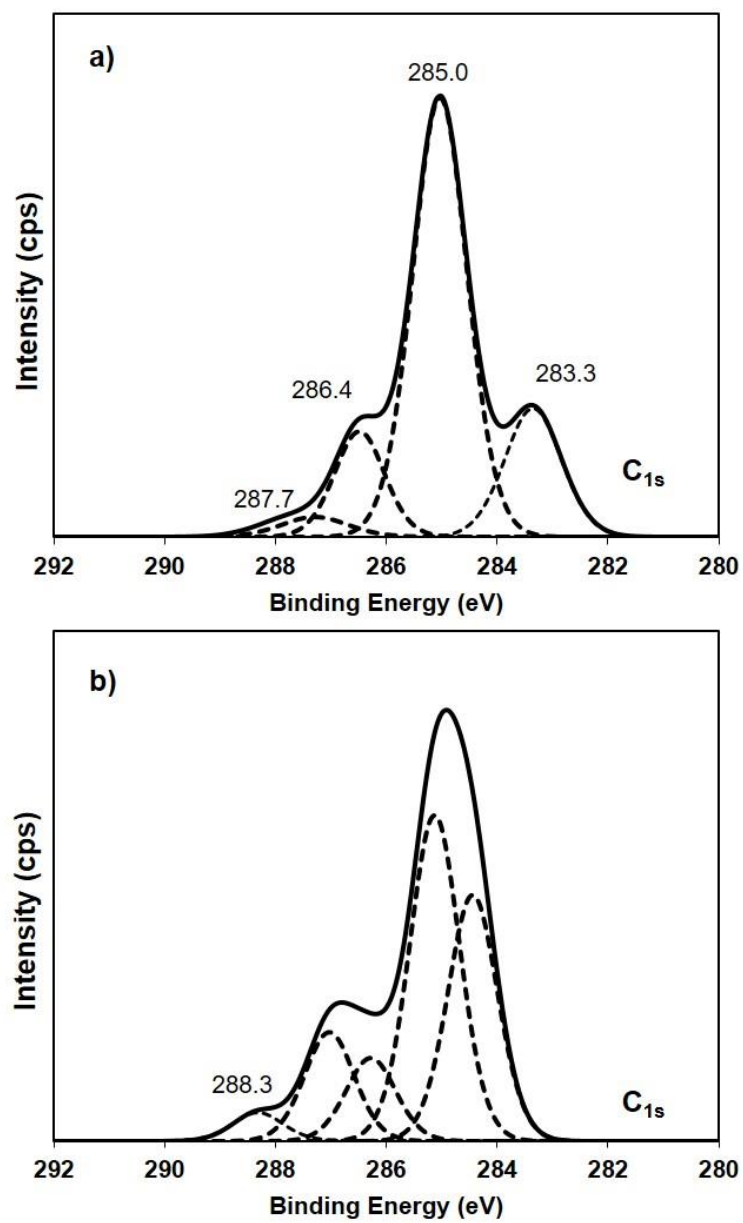


Figure 4.17 XPS patterns of carbon peak for a) PW-MCC and b) silane treated PW-MCC

In order to optimize the ball milling condition, ball milling time was studied from 60 to 240 min at 10wt% silane content. The percentage of elemental composition of silane treated PW-MCC at different ball milling times was determined by XPS and presented in Table 4.10. The results showed that an increment of ball milling time resulted in the reduction of percentage of silicon. This result can be explained that longer ball milling time could be destroyed Si-O-C bond on PW-MCC surface due to progressive of mechanical activation of ball milling [107] led to decreasing of silicon. The highest percentage of silicon was obtained at 60 min. Thus, the effective of ball milling time was 60 min.

Table 4.10 Elemental composition of silane treated PW-MCC evaluated by low – resolution XPS scan using 10% vinyltrimethoxy silane at different ball milling times

Silane (wt%)	Time (min)	Elemental composition (%)		
		O	C	Si
-	-	41.54	58.46	-
10	60	36.98	42.57	20.45
10	120	37.47	45.70	16.83
10	180	38.26	45.43	16.30
10	240	37.18	44.45	18.38

Besides the ball milling time, another important factor for silanisation reaction as silane content was investigated at 10, 20, and 30 wt% by fixing the ball milling time at 60 min. The percentage of elemental composition of silane treated PW-MCC is presented in Table 4.11.

Table 4.11 Elemental composition of silane treated PW-MCC evaluated by low – resolution XPS scan

Silane (wt%)	Elemental composition (%)		
	O	C	Si
-	41.54	58.46	-
10	36.98	42.57	20.45
20	35.53	34.19	29.47
30	34.65	37.15	28.19

As expected, an increase in silane content contributed to an increment of percentage of silicon on treated PW-MCC surface. However, using silane at 20 and 30 wt% provided similar percentage of silicon because the condensation reaction between silanol group of vinyltrimethoxysilane and hydroxyl group of cellulose molecule reached an equilibrium state. Thus, the optimum condition for treating PW-MCC with organosilane under ball milling process was 20 wt% vinyltrimethoxysilane at 60 min.

4.3.3.3 Thermal stability of silane treated PW-MCC

Thermal stability of reinforced fiber is an important factor for applying them in application. Thus, thermal stability of silane treated PW-MCC was investigated by TGA and the TGA thermograms of the untreated and silane treated PW-MCC are presented in Figure 4.18. The results exhibited that all samples showed weight loss below 100°C due to an evaporation of absorbed moisture in cellulose. PW-MCC showed two steps of weight loss. The first step was under 100°C and, while the second one started to decompose at 306°C which was corresponding to the decomposition of cellulose structure [99]. In case of silane treated PW-MCC, three steps of weight loss can be observed. After the first degradation step due to the moisture evaporation at approximately 100°C, there was a new or second degradation step at 165-175°C

according to the evaporation of water from the self-condensation reactions of the residual Si-OH groups or partially removal of uncrosslinked oligomers [65].

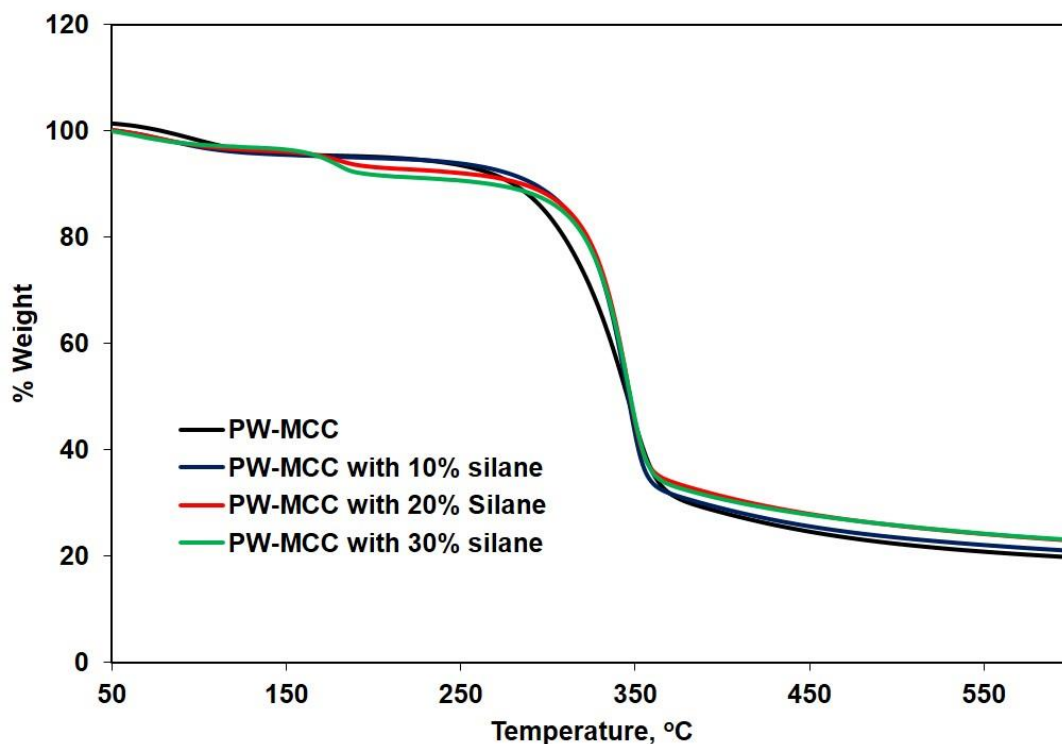


Figure 4.18 TGA thermogram of PW-MCC and silane treated PW-MCC

Thus, the results implied that there was an existence of silane group on PW-MCC after treatment under ball milling process. When silane content was increased, this peak at 165-175°C was much clearly observed. In addition, silane treated PW-MCC samples started to show the decomposition of cellulose at 323-324°C which was higher than that of the untreated PW-MCC. This results was in agreement with previous report [65, 113]. The thermal decomposition temperatures of untreated PW-MCC and silane treated PW-MCC are showed in Table 4.12.

Table 4.12 The thermal decomposition temperature of silane treated PW-MCC

Silane (wt%)	T _{d1}	T _{d2}	T _{d3}	T _{d at 50%} (°C)
0	93	-	306	345
10	94	172	323	345
20	94	172	323	347
30	94	172	324	347

4.3.3.4 Morphological studies of silane treated PW-MCC

The surface morphology of PW-MCC and silane treated MCC was investigated by SEM. It was found that PW-MCC has a rod-like shape with smooth surface as shown in Figure 4.7 – 4.10. While Silane treated MCC at different of ball milling times is presented in Figure 4.19. It can be observed that after treated with organosilane, surface of PW-MCC became rougher implying that silane was successfully coated of PW-MCC surface [113]. In addition, the size of silane treated PW-MCC was decreased due to mechanical force of ball milling process. SEM micrograph also presented that an increase of ball milling time led to an increment of small particles.

Moreover, the morphology of silane treated PW-MCC with different silane content was also observed as shown in Figure 4.20. It can be noticed that the surface of silane treated PW-MCC also exhibited the rough surface. SEM micrograph also presented that using different content of silane did not significantly affect to the morphology.

The optimized condition for modifying PW-MCC with organosilane was by using 20%wt vinyltrimethoxysilane and DCP as a catalyst at a ball milling speed of 400 rpm for 60 min which provided the highest percentage of silicon on PW-MCC surface.

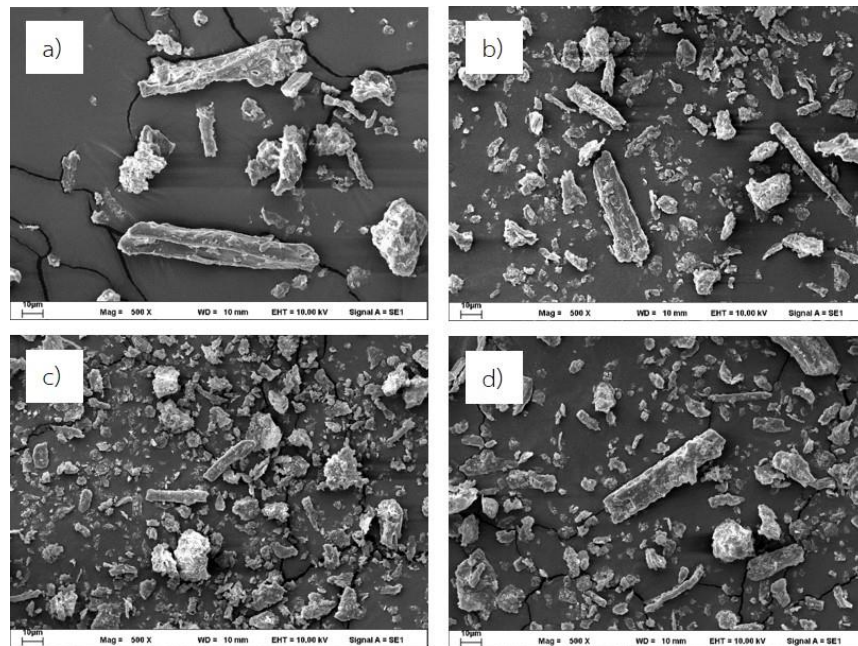


Figure 4.19 SEM micrographs of silane treated PW-MCC at different ball milling times
a) 60 min, b) 120 min, c) 180 min, and d) 240 min

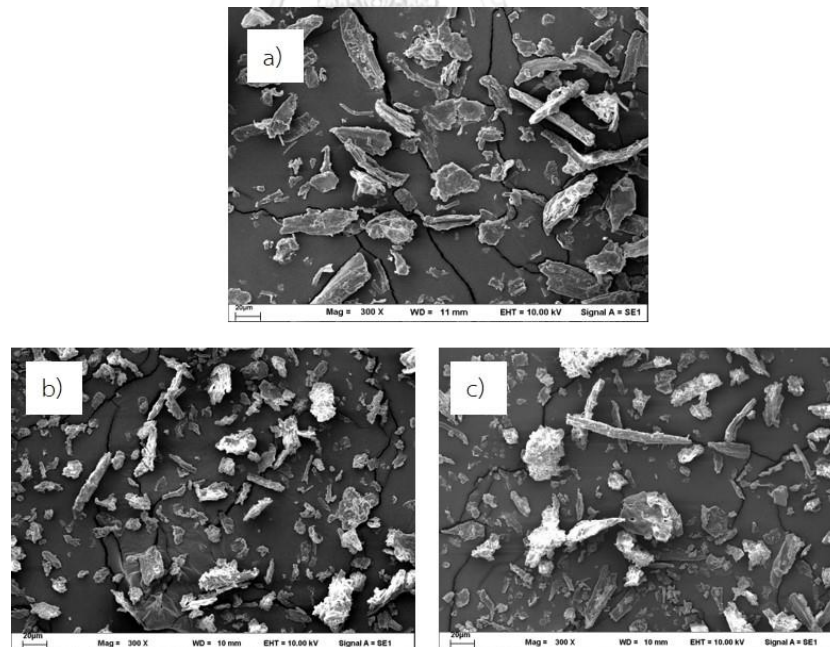


Figure 4.20 SEM micrographs of silane treated PW-MCC at 60 min using silane content
at a) 10 wt%, b) 20 wt%, and c) 30 wt%

4.3.4 Surface modification of PW-MCC using benzoyl chloride

4.3.4.1 Chemical structure of cellulose benzoate

In this section, surface of PW-MCC was modified by using benzoyl chloride under ball milling process via esterification reaction. The chemical reaction of cellulose benzoate (esterified PW-MCC) via acylation process is displayed in Figure 4.21.

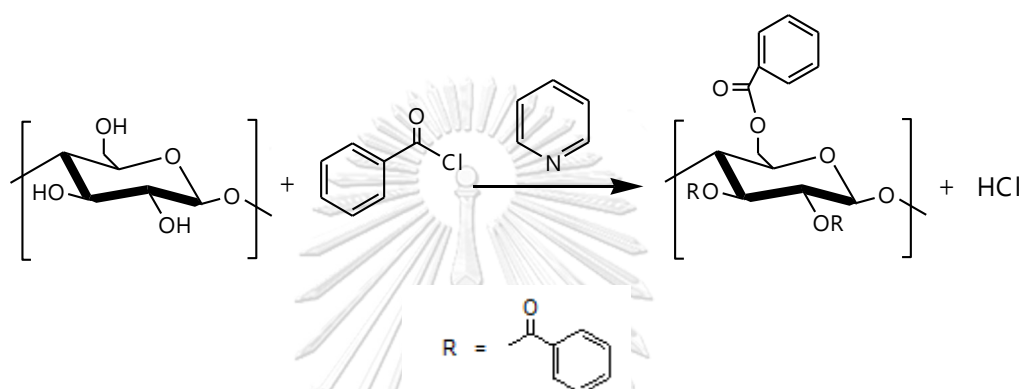


Figure 4.21 Acylation reaction of cellulose benzoate

Pyridine was added to the system and used as a cellulose-swelling organic compound that enhanced the reactivity of cellulose, while benzoyl chloride acted as modifying and solvent in the system [55].

$^1\text{H-NMR}$ technique was used to confirm the acylation reaction and analyze the chemical structure and degree of substitution and of esterified PW-MCC. The $^1\text{H-NMR}$ spectrum of cellulose benzoate is presented in Figure 4.22. It can be observed that cellulose benzoate revealed peaks around 3.10-5.60 ppm which were attributed to the protons of cellulose backbone, while the signal peaks around 6.80-8.20 ppm were corresponding to phenyl protons [114].

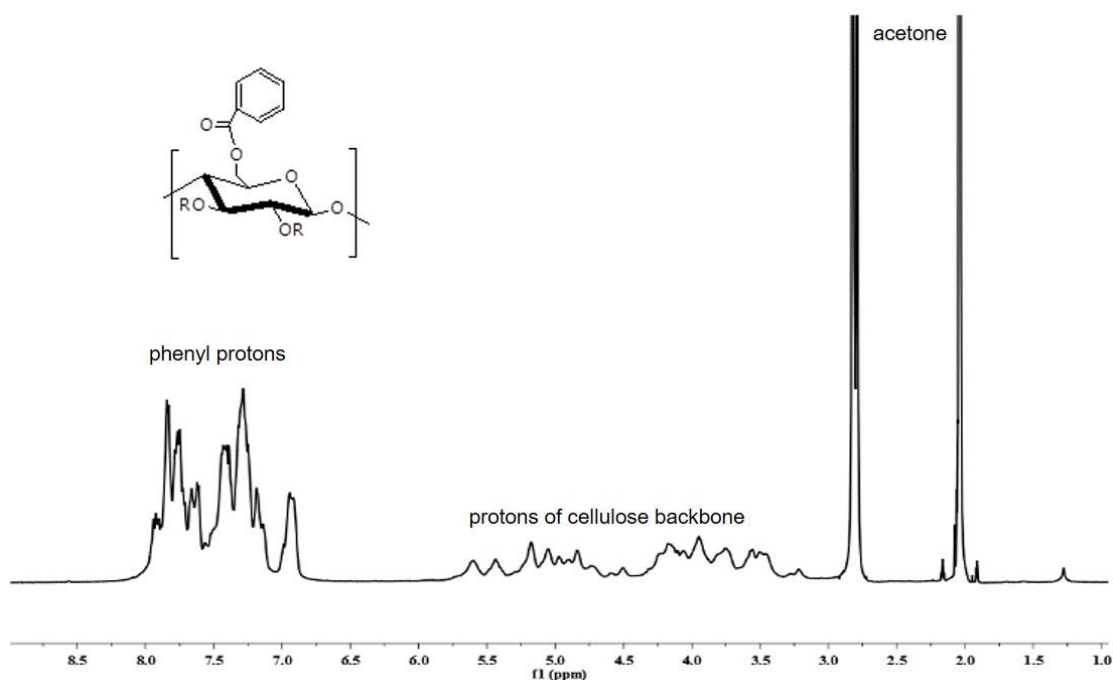


Figure 4.22 ¹H-NMR spectrum of cellulose benzoate

4.3.4.2 Functional group of cellulose benzoate

The functional groups of cellulose benzoate were characterized by FTIR. The FTIR spectra of PW-MCC and cellulose benzoate are compared in Figure 4.23. It can be seen that both of FTIR spectra exhibited a dominant broad band at 3400-3600 cm^{-1} which is referred to O-H stretching of hydroxyl group and sharp peak at 2900 cm^{-1} corresponding to C-H stretching of methyl and methylene group [57]. In addition, cellulose benzoate presented the new peaks from benzylation; i.e., the peaks at 1741 cm^{-1} which is assigned to C=O stretching of carbonyl group on ester chain and the strong absorption band at 1265 cm^{-1} which is attributed to the stretching of (O) C–O of ester. Moreover, it can be observed the new peak at 3064 cm^{-1} which is assigned to the C-H stretching of benzene ring and the two peaks at 1450 and 1602 cm^{-1} corresponding to aromatic C=C stretching [58, 115]. Moreover, there was a peak at 713 cm^{-1} which is contributed to the out of plan C-H bending of the monosubstituted benzene [116]. After esterification, the intensity of O-H stretching vibration at 3400-3600 cm^{-1} and C-H stretching at 2900 cm^{-1} were reduced. These results confirmed that the esterification reaction was successfully occurred.

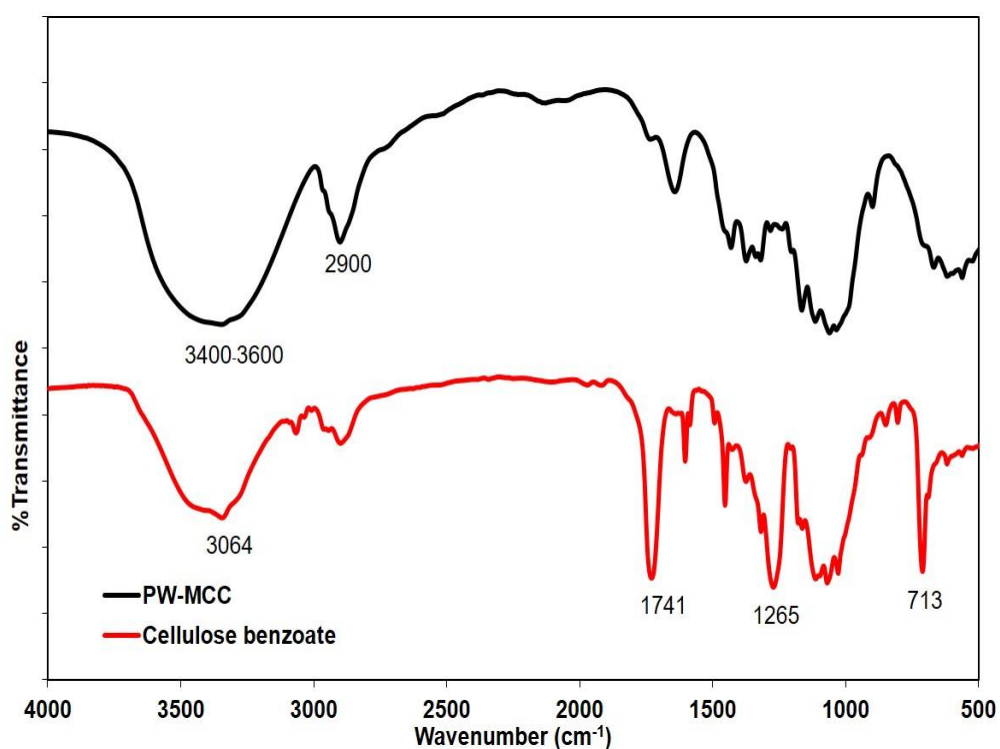


Figure 4.23 FTIR spectra of PW-MCC and cellulose benzoate

The optimum condition for the esterification reaction of PW-MCC was investigated in terms of molar ratio of benzoyl chloride /AGU and reaction time. Table 4.13 displays the effect of molar ratio of benzoyl chloride /AGU on percentage of weight increase (%WI) and DS values. The ball milling time was fixed at 60 minute.

Table 4.13 Degree of substitution and %WI for cellulose benzoate at 60 min

Benzoyl chloride/AGU	DS	%WI
unmodified	0	0
3	2.42	10.42
4	2.68	18.93
5	3.00	49.50
6	3.00	53.11

The results present that an increment of molar ratio of benzoyl chloride /AGU leading to an increase in esterification reaction, resulting in an increasing of %WI and DS values. It can be noticed that cellulose benzoate reached the maximum degree of substitution at 3.00 when benzoyl chloride /AGU molar ratio was raised to 5. The DS value was increased along with increase in weight. Although at higher 6 molar ratio weight increase value was slightly increase, the DS value remained constant. This result indicated that the esterification reaction of cellulose had already been to an equilibrium state. Thus, the optimum molar ratio of benzoyl chloride /AGU for esterification of PW-MCC was 5.

FTIR spectra of the esterified PW-MCC obtained with different molar ratio of benzoyl chloride /AGU is displayed in Figure 4.24. It can be observed from FTIR spectra that the intensity of O-H stretching vibration at 3400-3600 cm^{-1} was reduced upon increasing the benzoyl chloride/AGU molar ratio [58]. In addition, the intensity of C-H bending of the benzene at 713 cm^{-1} was increased. This evidence was related to %WI and DS values that and increment of benzoyl chloride/AGU molar ratio enhanced the esterification reaction.

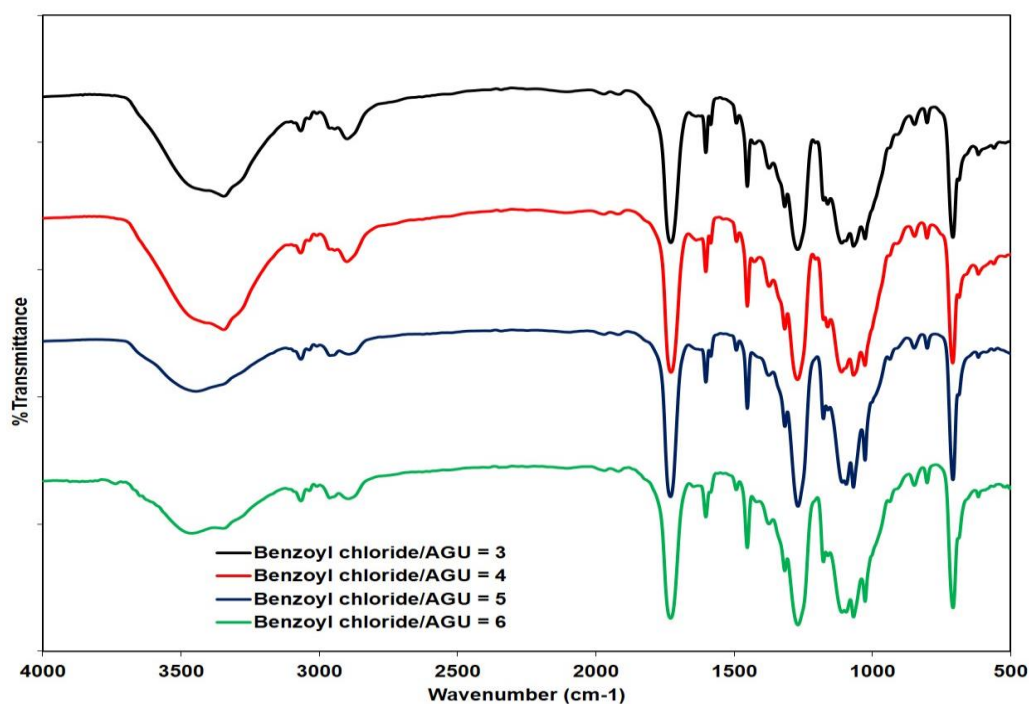


Figure 4.24 FTIR spectra of cellulose benzoate at benzoyl chloride/AGU ratio 3 to 6.

In term of reaction time, from 60 to 180 min the functional group of cellulose benzoate at different reaction times is shown in Figure 4.25 and the DS and %WI values are presented in Table 4.14. The FTIR spectra presented that an increment of reaction time led to broader O-H stretching peak at 3400-3600 cm^{-1} , which is in accordance with the decrement of the DS and %WI values was. It can be explained that the degradation of cellulose was occurred at longer reaction time. Comparatively, the esterification reaction occurred relatively fast at shorter reaction time. However, when the reaction was prolonged, by-product from the esterification reaction such as hydrochloric acid could cause the degradation of the cellulose. This results is in agreement of Yamashita and Endo [117] who studied deterioration behavior of cellulose acetate films hydrochloric acid.

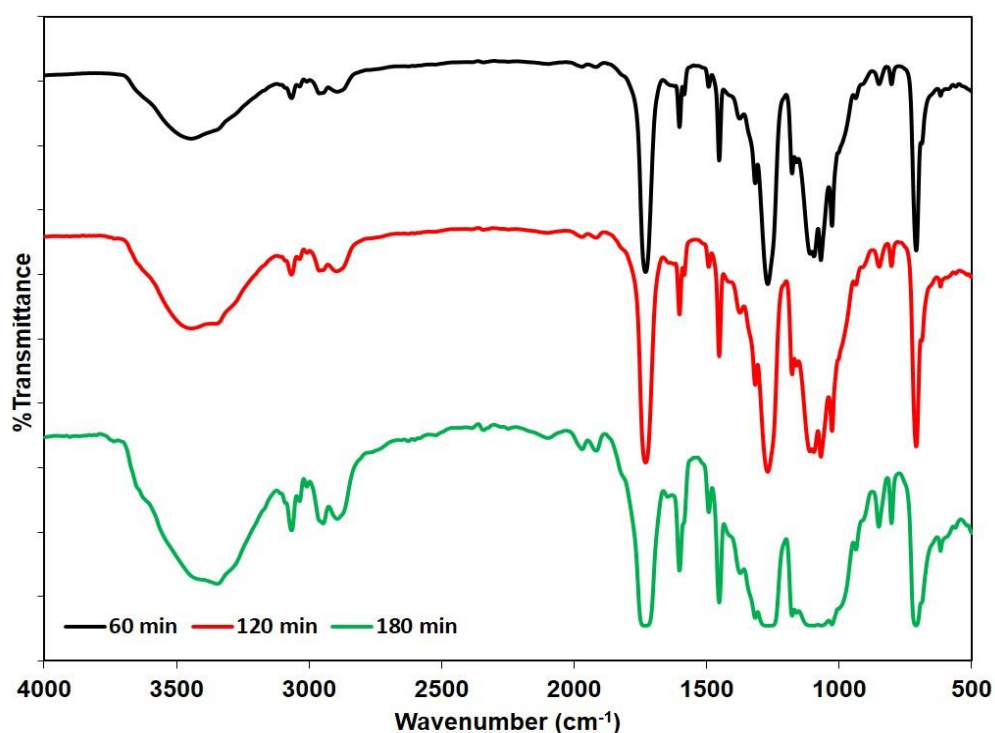


Figure 4.25 FTIR spectra of cellulose benzoate at benzoyl chloride/AGU ratio at 5 with reaction time 60 min, 120 min, and 180 min

Table 4.14 Degree of substitution and %WI for esterified PW-MCC at benzoyl chloride/AGU ratio at 5 with different reaction time

Reaction time (min)	DS	%WI
60	3.00	49.50
120	2.61	19.98
180	2.44	15.15

Therefore, based on the scope of this work the optimum condition for esterification of PW-MCC with benzoyl chloride using ball milling process which yielded the highest DS value was to perform the reaction using benzoyl chloride /AGU molar ratio at 5 and reaction time at 60 min.

4.3.4.3 Thermal stability of cellulose benzoate

Thermogravimetric curves of PW-MCC and cellulose benzoate are shown in Figure 4.26. Cellulose benzoate did not show the degradation below 100°C which implying that the esterified samples were more hydrophobic than the unmodified PW-MCC. Cellulose benzoate showed single-step degradation similar to PW-MCC. The main degradation at 50% weight loss or at higher temperature in the range of 360-380°C was contributed to the degradation of cellulose molecule. It can be observed that the degradation temperature of cellulose benzoate was shifted to higher temperature comparing to that of unmodified PW-MCC.

The thermal decomposition temperatures of PW-MCC and cellulose benzoate are presented in Table 4.15. The results exhibited that increasing of DS values resulted in slightly an enhancement of thermal stability of cellulose benzoate. The improvement in the thermal stability of cellulose benzoate was due to the reduction of the hydroxyl group after esterification [118]. In addition, introduction of benzoyl group to PW-MCC enhanced of thermal stability because cellulose benzoate required high energy to cleavage of ester bond. This result is similar to Agustin et al. 2018 [119] who studied on improving the thermal stability of wood-based cellulose by

esterification. Beside, char residue to cellulose ester was higher than PW-MCC particular cellulose benzoate using benzoyl chloride/AGU ratio molar at 5. The higher of char residue was due to the resistant by-product of decomposition [120]. However, it was surprisingly observed that char residue of cellulose ester was different and did not depend on DS values.

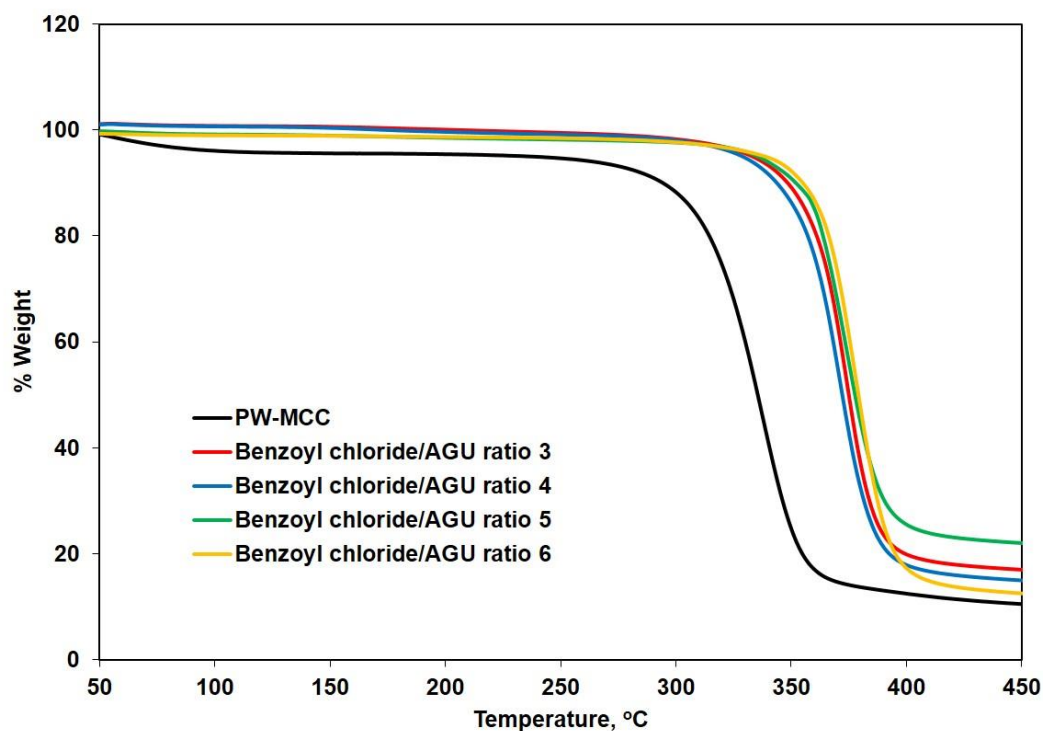


Figure 4.26 TGA curves of PW-MCC and cellulose benzoate

Table 4.15 The decomposition temperature of cellulose benzoate

Benzoyl chloride/AGU	DS	T _d (onset) (°C)	T _d at 50% (°C)	%Char at 450°C
unmodified	0	311	352	10.45
3	2.42	353	374	16.95
4	2.68	351	372	14.94
5	3.00	354	377	21.99
6	3.00	354	379	12.49

4.3.4.4 Morphological properties of cellulose benzoate

SEM images of cellulose benzoate with various benzoyl chloride/AGU ratios are presented in Figure 4.27. After benzylation under ball milling process, cellulose benzoate presented rough surface and there was an aggregation of benzoyl substituent on PW-MCC surface.

The difference in the DS value or benzoyl chloride/AGU ratio also affected to the morphology of cellulose benzoate. An increment of DS value was clearly related to an aggregation of benzoyl substituent on PW-MCC. Obviously, there were a mixture of fibrous structure and small particle after ball milling [80]. In addition, the particle size of cellulose benzoate was decreased due to mechanical force from ball milling process. It is a known that ball mill is a top-down process which produces micro or nano particle size of materials [76]. Cellulose benzoate had particle size around 10-40 μm .

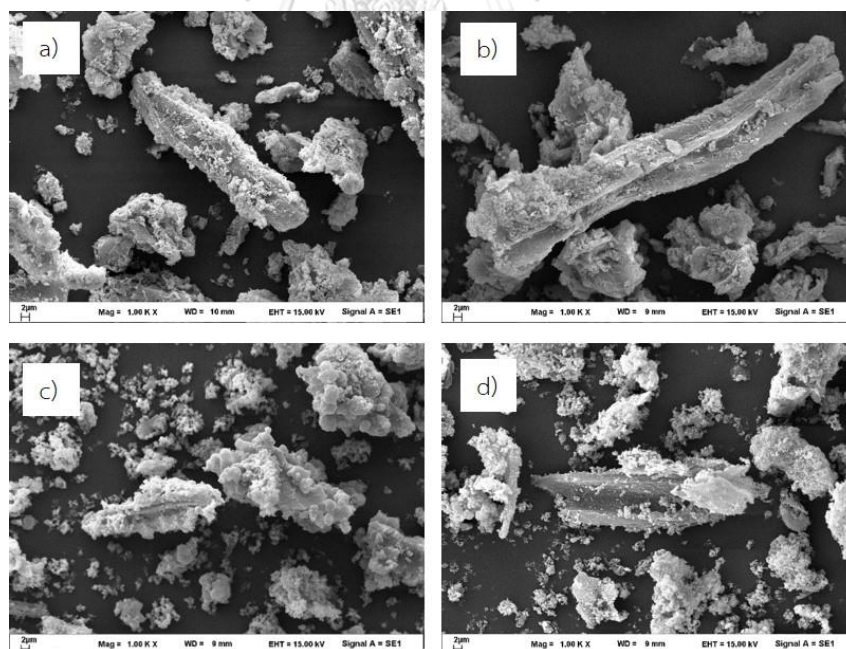


Figure 4.27 SEM micrographs of cellulose benzoate at ball milling 60 min with benzoyl chloride/AGU ratio a) 3, b) 4, c) 5 and d) 6

4.3.5 Surface modification of PW-MCC using hexanoyl chloride

4.3.5.1 Chemical structure of cellulose hexanoate

In this part, surface of PW-MCC was esterified by using hexanoyl chloride which was an alkyl chain with 6 carbon atoms under ball milling process via acetylation reaction. Moreover, toluene was used as co-solvent to enhance reaction activity. The chemical reaction is presented in Figure 4.28.

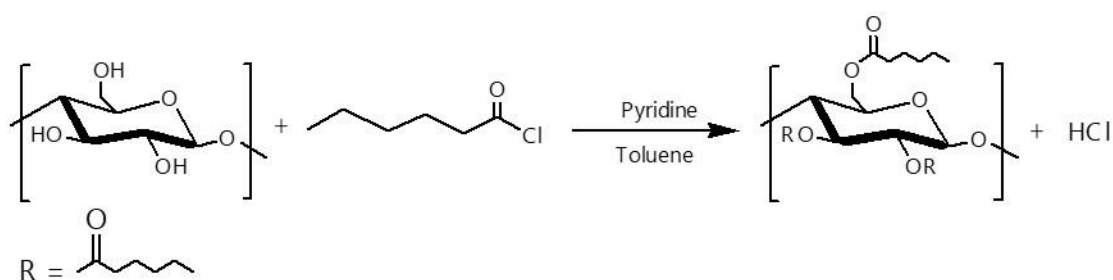


Figure 4.28 Acylation reaction of cellulose hexanoate

The $^1\text{H-NMR}$ spectrum was also used to confirm the success of esterification reaction of PW-MCC using hexanoyl chloride as shown in Figure 4.29.

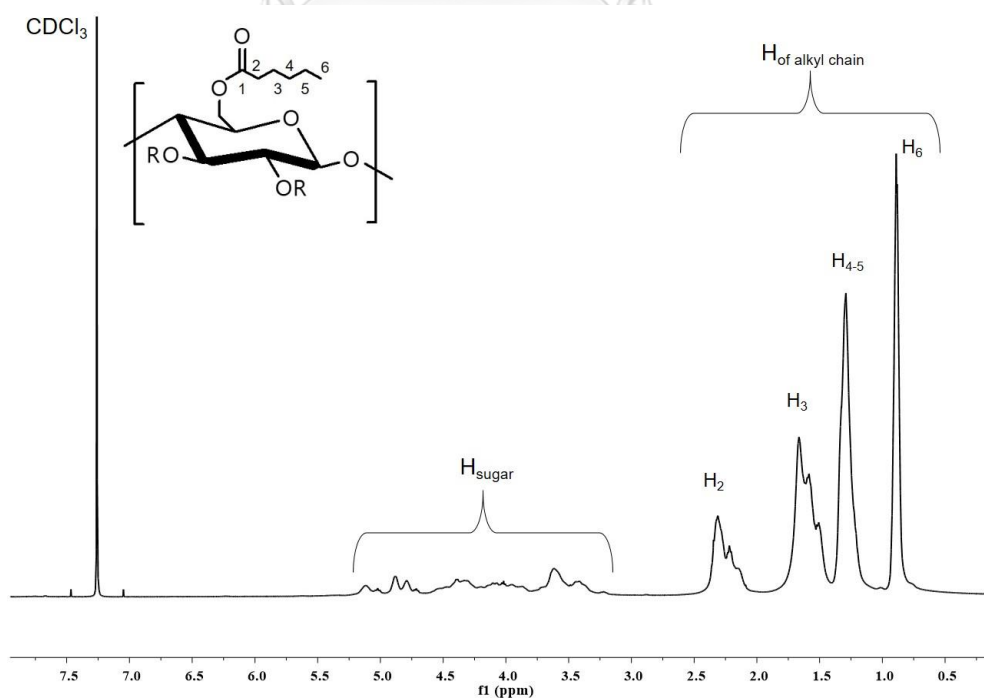


Figure 4.29 $^1\text{H-NMR}$ spectrum of cellulose hexanoate

It can be seen that cellulose hexanoate presented a few peak around 5.20-3.20 ppm which were corresponded to anhydroglucose unit of cellulose skeleton, whereas the signal peaks around 2.40-0.85 ppm were corresponding to protons signal on alkyl chain [121].

4.3.5.2 Functional group of cellulose hexanoate

The FTIR spectrum of cellulose hexanoate was investigated and compared with that of unmodified PW-MCC as presented in Figure 4.30. There were several new peaks appeared after esterification with hexanoyl chloride. It can be clearly observed the characteristic peak of ester carbonyl stretching at 1749 cm^{-1} along with the other peaks such as a peak at 1246 cm^{-1} which was contributed to the stretching vibrations of C-O bond in ester group and the peaks at 2960 and 2870 cm^{-1} which were assigned to C-H stretching of alkyl chain of cellulose ester [122]. Besides all these new peaks, the O-H stretching vibration at $3400\text{-}3500\text{ cm}^{-1}$ was still observed in cellulose hexanoate but the intensity of O-H stretching was significantly decreased. Hence, this difference in hydroxyl group intensity suggesting that a large amount of hydroxyl group (-OH) was successfully substituted.

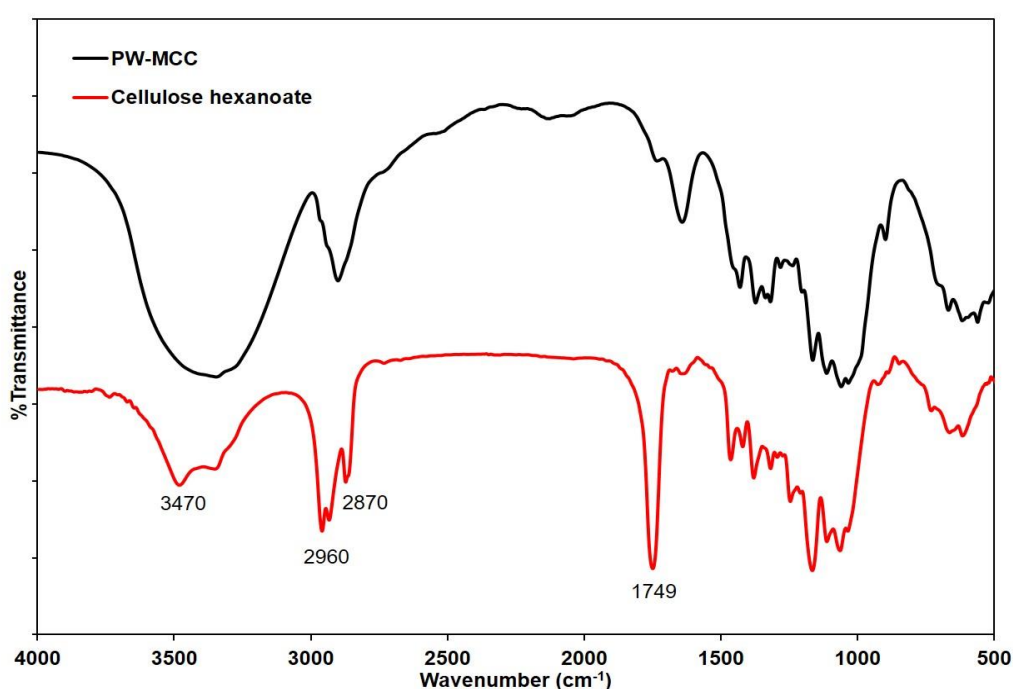


Figure 4.30 FTIR spectra of PW-MCC and cellulose hexanoate

Thus, it could be concluded from $^1\text{H-NMR}$ and FTIR data that PW-MCC was successfully esterified with hexanoyl chloride to obtain cellulose hexanoate under heterogeneous condition.

The DS value of cellulose hexanoate was around 2.1-2.2 which was lower than that of cellulose benzoate when using only pyridine in the system. It could be explained that pyridine was used as a catalyst, neutralizing agent, and swelling solvent. Pyridine can swell cellulose increasing the accessibility of hydroxyl groups to react with modified molecule leading to the esterification reaction of hydroxyl group in both external and internal layers [56]. Moreover, pyridine was a neutralizing agent that can neutralize hydrochloric acid which was a by-product from the reaction. In order to enhance the DS value, co-solvent such as toluene was used. Toluene was applied as dispersing agent to disperse PW-MCC in the media to improve accessibility of reaction to cellulose [123]. The comparison between the DS values of esterified samples is presented in Table 4.16. It can be noticed that adding toluene into the esterification reaction increased DS value approximately 26%.

Table 4.16 Comparison between the DS values of cellulose hexanoate with and without toluene

Hexanoyl chloride/AGU	DS	
	Without toluene	With toluene
unmodified	0	0
3	2.18	2.66
4	2.19	2.63
5	2.28	2.73
6	2.14	2.69

The FTIR spectra of esterified PW-MCC by hexanoyl chloride with toluene and without toluene are presented in Figure 4.31. It can be noticed that cellulose hexanoate using toluene as dispersion medium provided an increasing of intensity peak of the carbonyl group at 1749 cm^{-1} and reduction of the O-H stretching vibration intensity at $3400\text{-}3500\text{ cm}^{-1}$. Thus, it was an evidence that using toluene as dispersion medium attributing to an improvement in the esterification reaction between PW-MCC and hexanoyl chloride. The FTIR spectra were evidently related to the DS values results.

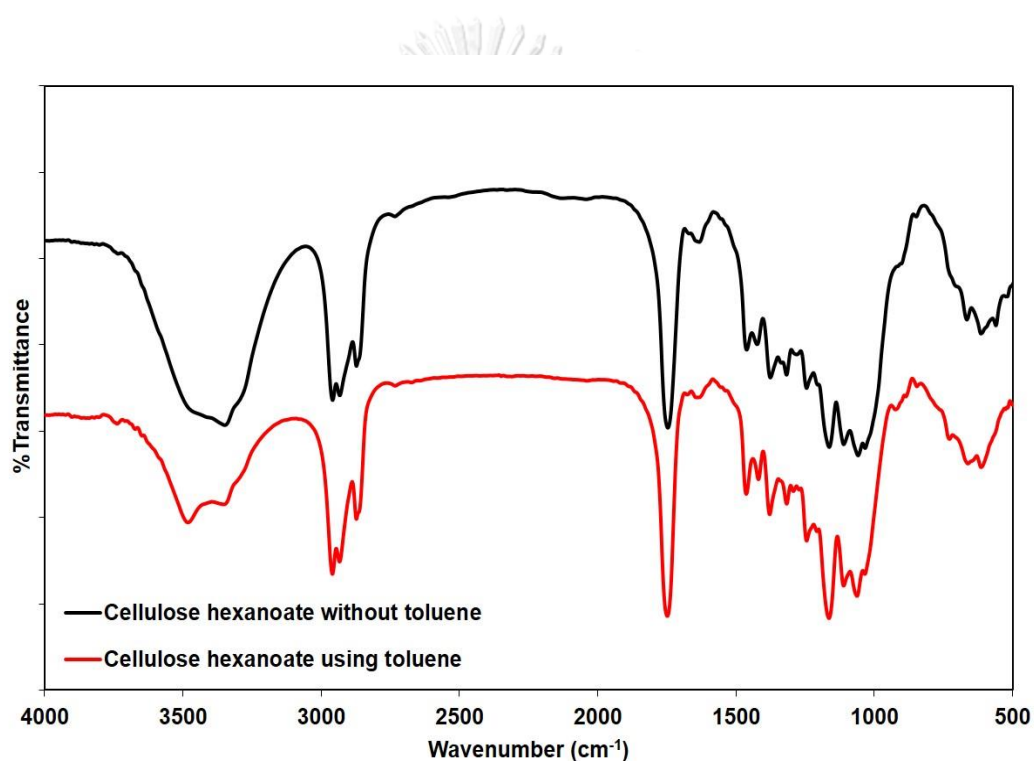


Figure 4.31 FTIR spectra of cellulose hexanoate with and without toluene

The optimum condition for the esterification reaction of PW-MCC with hexanoyl chloride was studied in terms of molar ratio of hexanoyl chloride/AGU and reaction time. Table 4.17 presents the effect of molar ration of hexanoyl chloride /AGU on percentage of weight increase (%WI) and DS values. The ball milling time was set at 60 minute.

Table 4.17 Degree of substitution and %WI for cellulose hexanoate at 60 min

Hexanoyl chloride/AGU	DS	%WI
unmodified	0	0
3	2.66	54.82
4	2.63	59.64
5	2.73	83.85
6	2.69	69.43

It can be seen that DS value and %WI were increased when using higher molar ratio of hexanoyl chloride/AGU. The maximum DS value was 2.73 when using hexanoyl chloride/AGU molar ratio at 5. However, at higher molar ratio, the DS value and %WI were slightly decreased. It can be assumed that esterification reaction of cellulose with hexanoyl chloride went to the maximum substitution at ratio 5. Thus, optimum the molar ratio of hexanoyl chloride/AGU ratio for producing cellulose hexanoate was 5.

FTIR spectra of the cellulose hexanoate from different molar ratios of hexanoyl chloride/AGU are shown in Figure 4.32. It can be seen that the intensity of O-H stretching vibration at $3400\text{-}3600\text{ cm}^{-1}$ was decreased while the carbonyl peak intensity was increased with an increment of hexanoyl chloride/AGU molar ratio. This result was correlated to %WI and DS values that an increment of hexanoyl chloride/AGU molar ratio led to an improvement of esterification reaction.

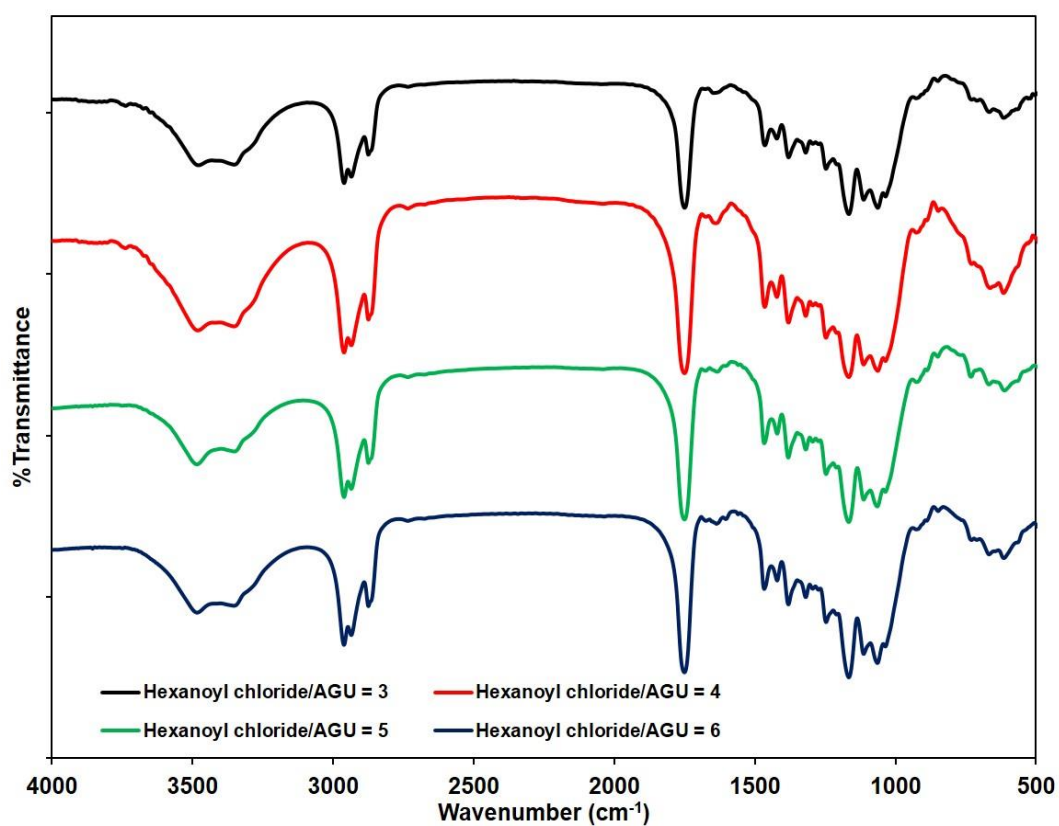


Figure 4.32 FTIR spectra of cellulose hexanoate at hexanoyl chloride/AGU ratio 3 to 6

The effect of reaction time was studied at 60, 120, and 180 min using hexanoyl chloride/AGU molar ratio at 5. DS and %WI were also investigated, and the results are demonstrated in Table 4.18.

CHULALONGKORN UNIVERSITY

Table 4.18 DS and %WI for cellulose hexanoate using hexanoyl chloride/AGU ratio at 5 with different reaction times

Reaction time (min)	DS	%WI
60	2.73	83.85
120	2.70	73.35
180	2.59	63.21

The FTIR spectra of cellulose hexanoate at different of milling times are exhibited in Figure 4.33. The spectra from showed that increment of reaction time resulting in slightly a decrease of the intensity of C=O stretching of carbonyl group. The results is correlated well with reduction of DS and %WI values along with the increasing of milling time as well. The reduction of DS could be explained by the partial hydrolysis of ester group or dissolution of cellulose hexanoate from by-product which was hydrochloric acid. This result was agree with Leszczyńska et al. [124] who esterified microfibrillated cellulose (MFC) by acid chlorides.

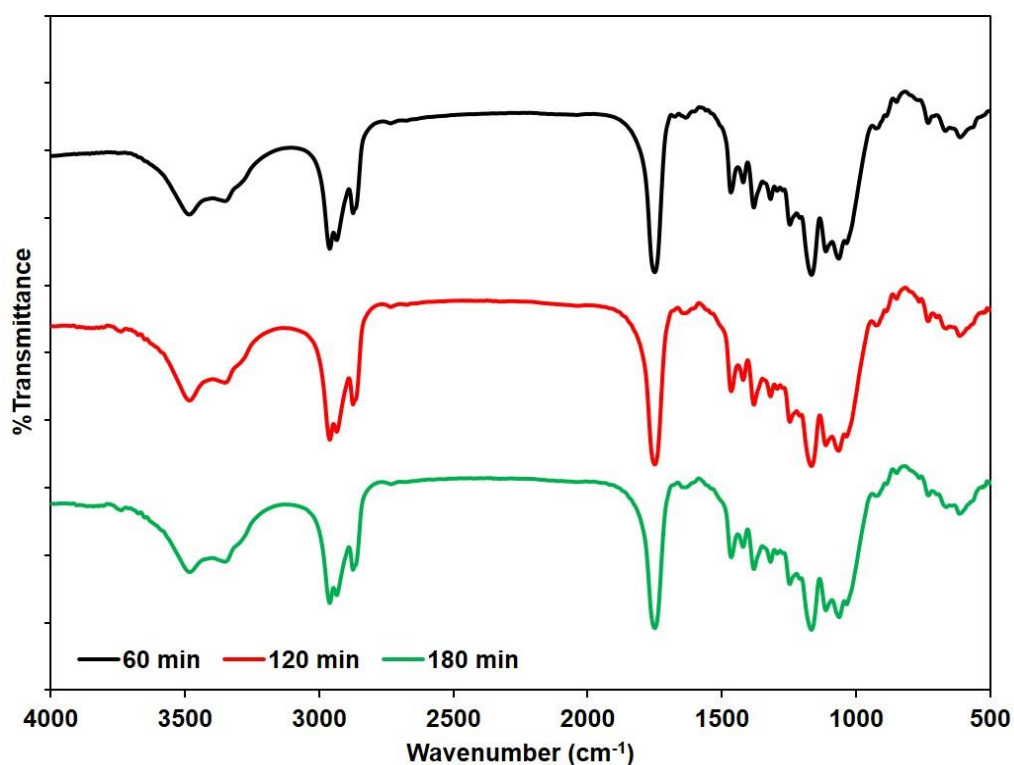


Figure 4.33 FTIR spectra of cellulose hexanoate using hexanoyl chloride/AGU ratio at 5 with reaction time 60 min, 120 min, and 180 min

Thus, based on the scope of this experimental the optimum condition for esterification of PW-MCC with hexanoyl chloride using ball milling process was to carry out the reaction using hexanoyl chloride /AGU molar ratio at 5 for 60 min in order to obtain the highest DS value (2.73).

4.3.5.3 Thermal stability of cellulose hexanoate

TGA thermograms of PW-MCC and cellulose hexanoate are presented in Figure 4.34. After esterification with hexanoyl chloride, the decomposition below 100°C was disappeared from TGA curves due to more hydrophobic nature of cellulose hexanoate. However, using hexanoyl chloride/AGU molar ratio at 3 and 4 (DS = 2.63 and 2.66, respectively) presented the similar $T_{d(\text{onset})}$ to PW-MCC. It could be assumed that at these hexanoyl chloride/AGU molar ratio did not affect to thermal stability of PW-MCC.

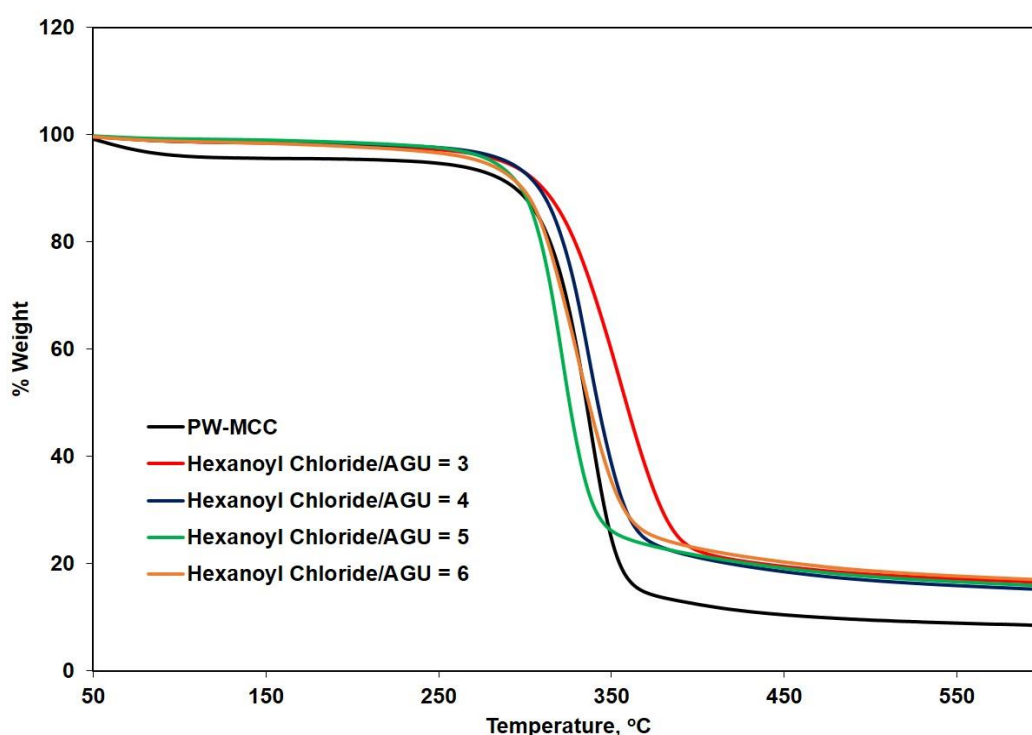


Figure 4.34 TGA curve of PW-MCC and cellulose hexanoate

However, the thermal stability of cellulose hexanoate from hexanoyl chloride/AGU ratio (5 and 6) which had DS value of 2.73 and 2.69, respectively, showed reduction of thermal stability. The reduction of thermal stability of cellulose hexanoate at higher DS values because the substitution of the alkyl chain (C6) in the cellulose structure interfered the crystallinity of cellulose [125]. It might be explained that at higher DS value led to reduction crystallinity of cellulose which was affected to reduce thermal stability of cellulose hexanoate [126]. Moreover, char residue of cellulose hexanoate was higher than PW-MCC due to hexanoic chain substituted on

hydroxyl group of cellulose. Besides char residue of cellulose hexanoate gave slightly increased upon with DS value [127]. The thermal decomposition temperature of PW-MCC and cellulose hexanoate are shown in Table 4.19.

Table 4.19 The decomposition temperature of cellulose hexanoate

Hexanoyl chloride/AGU	DS	T _{d(onset)} (°C)	T _{d at 50%} (°C)	%Char at 450°C
unmodified	0	311	352	10.45
3	2.63	312	358	18.52
4	2.66	311	354	19.48
5	2.73	302	325	19.17
6	2.69	305	349	20.32

4.3.5.4 Morphological properties of cellulose benzoate

SEM images of cellulose hexanoate with various hexanoyl chloride/AGU ratios are shown in Figure 4.35. The SEM images illustrated an aggregation of hexanoyl substituent groups on PW-MCC surface after esterification with hexanoyl chloride. In addition, the roughness of cellulose hexanoate resulted from the large amount of hexanoyl chloride substitution on PW-MCC surface. Surprisingly, cellulose hexanoate revealed the higher diameter and particle size in flake and particle shape which were different from PW-MCC morphology. Besides, their average particle size of cellulose hexanoate was slightly increased when increasing DS value. It was observed that its size was increase according to low DS to high DS value, approximately from 40-80 μm to 80-160 μm .

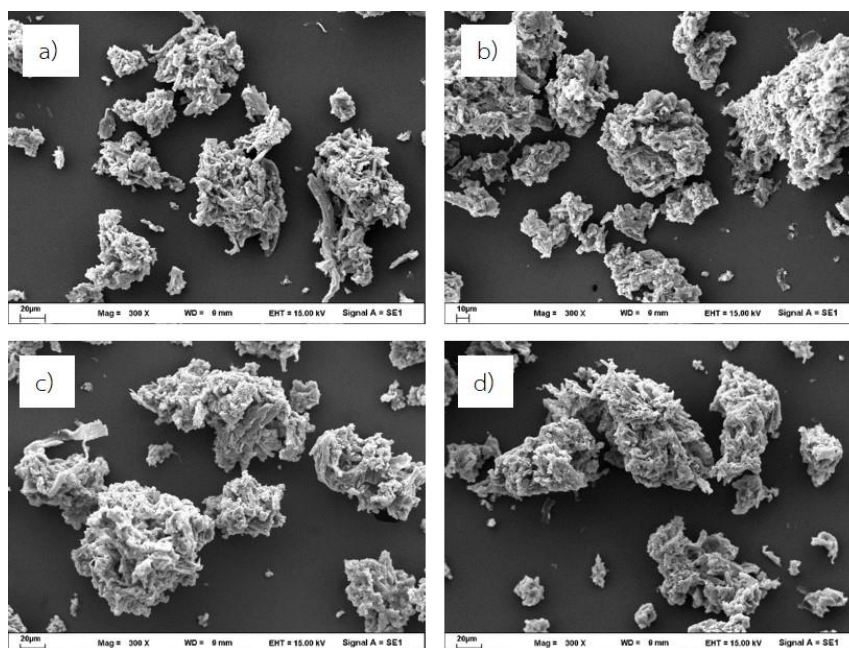


Figure 4.35 SEM micrographs of cellulose hexanoate at ball milling 60 min with hexanoyl chloride/AGU ratio a) 3, b) 4, c) 5 and d) 6

4.3.6 Surface modification of PW-MCC using lauroyl chloride

4.3.6.1 Chemical structure of cellulose laurate

In this section, surface of PW-MCC was esterified by lauroyl chloride which was an alkyl chain with 12 carbons under ball milling process via acetylation reaction. Toluene was used as a dispersing medium to increase esterification reaction activity. The chemical reaction is shown in Figure 4.36.

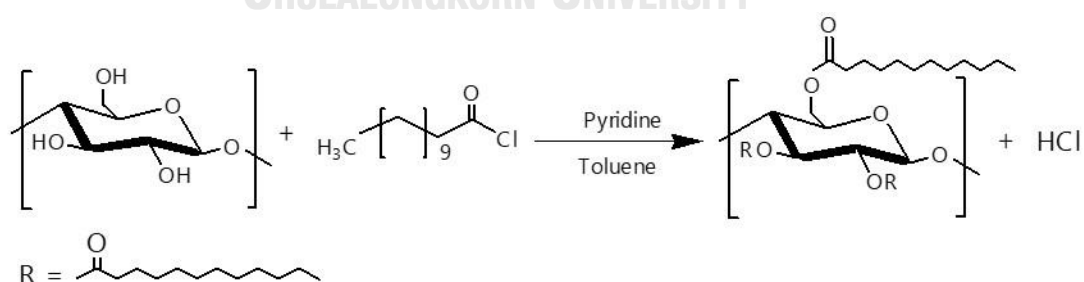


Figure 4.36 Acylation reaction of cellulose laurate

The $^1\text{H-NMR}$ spectrum of cellulose laurate is presented in Figure 4.36. It can be observed that cellulose laurate showed the proton signal from 5.20-3.10 ppm which

was assigned to AGU in cellulose backbone, while the signal at 2.45-0.75 ppm was attributed to methylene proton of alkyl chain [57, 128].

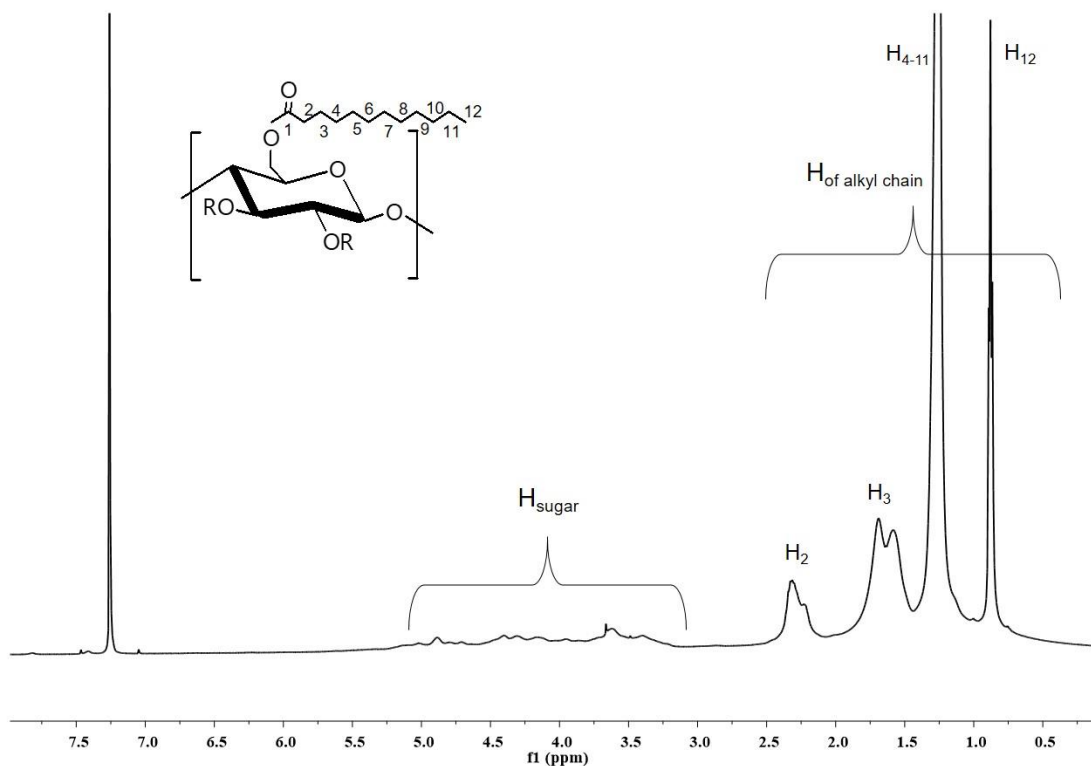


Figure 4.37 $^1\text{H-NMR}$ spectrum of cellulose laurate

4.3.6.2 Functional group of cellulose laurate

Figure 4.38 depicted a comparison of PW-MCC and cellulose laurate FTIR spectra. The FTIR spectrum of cellulose laurate presented the reduction in the intensity of O-H stretching at $3400\text{--}3500\text{ cm}^{-1}$ implying that hydroxyl groups were substituted by fatty acid chains. Moreover, there were several new peaks were distinctly appeared. For example, the peak at 1747 cm^{-1} was attributed to the stretching of carbonyl ester group, while the others peaks at $2800\text{--}2900\text{ cm}^{-1}$ was designated as C-H stretching of fatty acid chain [129]. Thus, these were an evidence that PW-MCC was successfully esterified with alkyl chains.

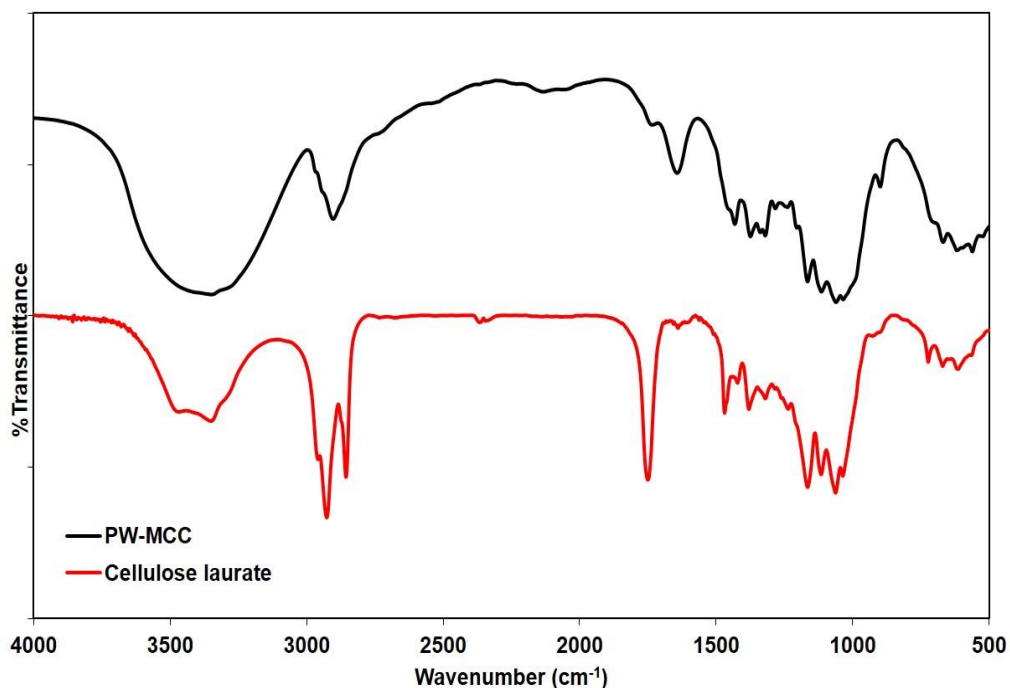


Figure 4.38 FTIR spectra of PW-MCC and cellulose laurate

The effect of lauroyl chloride/AGU ratio was investigated at milling time 60 min. The FTIR spectra of cellulose laurate with various lauroyl chloride/AGU ratios are presented in Figure 4.39. In order to compare the esterification activity, DS value of cellulose laurate was evaluated by $^1\text{H-NMR}$ as presented in Table 4.20.

It could be noticed that using lauroyl chloride/AGU ratio at 3 gave the lowest DS value while an increasing the lauroyl chloride/AGU ratio to 4 provided an increase of DS value. However, using lauroyl chloride/AGU ratio at 5 caused the reduction of DS value because an increasing of lauroyl chloride/AGU ratio to 5 led to an increase in the viscosity of reaction which then diminished the reaction between PW-MCC and reagents [130]. This results could be assumed that the maximum DS value was obtained when using lauroyl chloride/AGU ratio at 4. Comparatively, the esterification with the long carbon chain length (i.e., lauroyl chloride) had low activity than using aromatic ring and short carbon chain length (i.e., benzyl and hexanoyl, respectively) according to the steric hindrance of long alkyl chain [131].

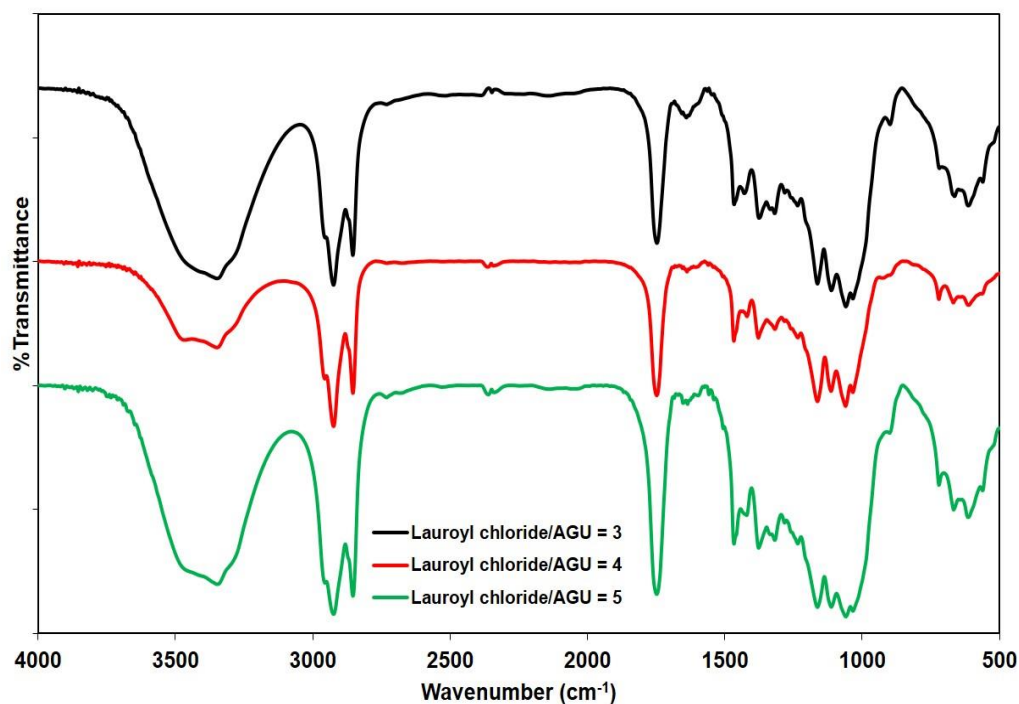


Figure 4.39 FTIR spectra of cellulose laurate at lauroyl chloride/AGU ratio 3 to 5

Table 4.20 Degree of substitution and %WI for cellulose laurate at 60 min

Lauroyl chloride/AGU	DS	%WI
unmodified	0	0
3	1.95	51.23
4	2.27	95.12
5	2.06	75.37

The milling time was also studied at 60, 120, and 180 min by using lauroyl chloride/AGU ratio at 4. The FTIR spectra of cellulose laurate with varying milling time are shown in Figure. 4.40. It could be seen that an increment of milling time resulting to an increase of O-H stretching intensity and a decrease in DS value as presented in Table 4.21. Similar to cellulose benzoate and cellulose hexanoate, as discussed earlier,

decreasing of DS value could be due to the partial hydrolysis of ester group during milling at longer time [124].

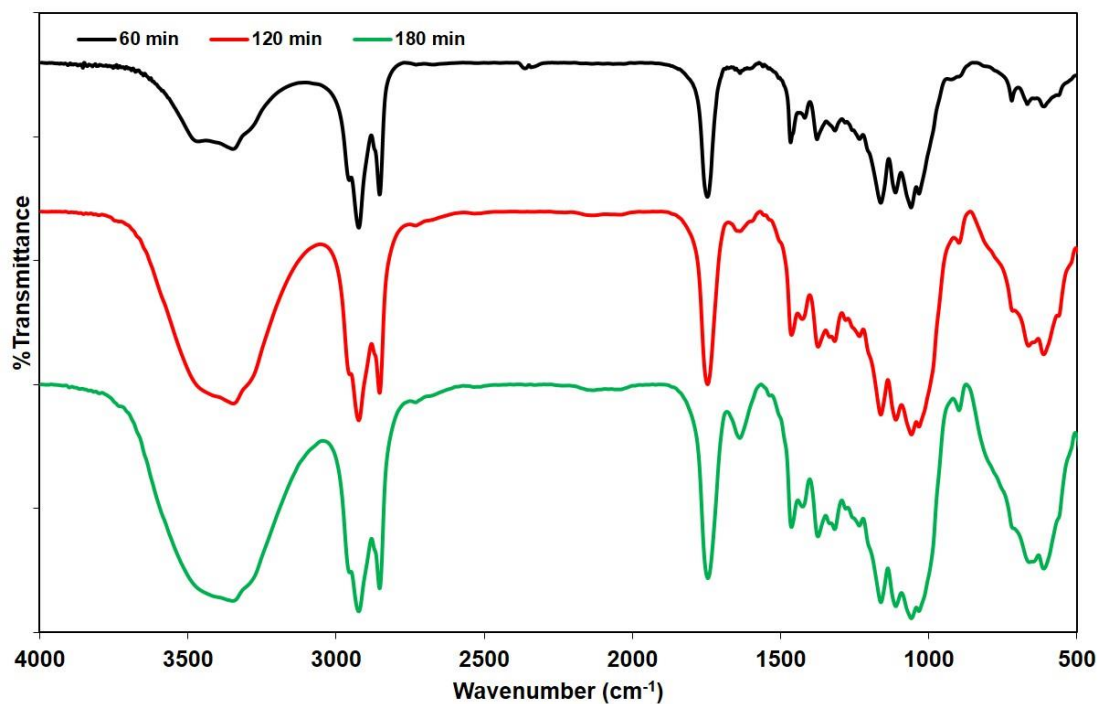


Figure 4.40 FTIR spectra of cellulose laurate at lauroyl chloride/AGU ratio at 4 with reaction time 60 min, 120 min, and 180 min

Table 4.21 DS and %WI for cellulose laurate at lauroyl chloride/AGU ratio at 4 with different reaction time

Reaction time (min)	DS	%WI
60	2.27	95.12
120	2.02	58.55
180	2.01	51.23

Hence, the optimum condition for esterification of PW-MCC with lauroyl chloride using ball milling process was using lauroyl chloride /AGU molar ratio at 4 and reaction time at 60 min.

4.3.6.3 Thermal stability of cellulose laurate

The comparison of thermogravimetric curves of PW-MCC and cellulose laurate is presented in Figure 4.41. It could be seen that there was a thermal decomposition below 100°C from cellulose laurate with lauroyl chloride/AGU ratio 3 (DS = 1.95) which was referred to an elimination of moisture. This result confirmed that lower DS provided higher hydrophilic nature than DS at 2.06 and 2.27. Meanwhile, this moisture decomposition did not show on cellulose laurate at higher lauroyl chloride/AGU ratio or higher DS value. Table 4.22 presented the decomposition temperature of cellulose laurate.

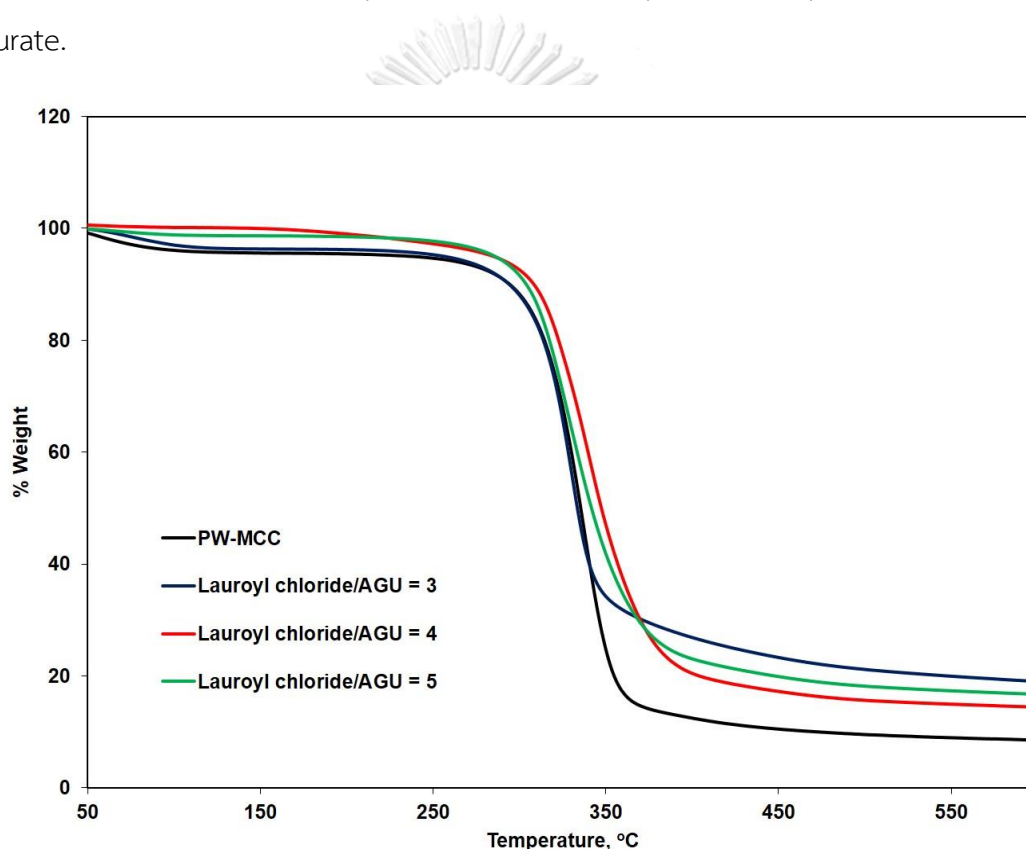


Figure 4.41 TGA curve of PW-MCC and cellulose laurate

It was also noticed that cellulose laurate from lauroyl chloride/AGU ratio 4 with DS value at 2.27 exhibited a slight decomposition at 210-220°C which was assigned to the decomposition of esterified fraction on cellulose structure. At higher temperature approximately 300-320°C, the thermal decomposition of unesterified cellulose molecule occurred. In addition, introduction of long alkyl chain to cellulose

caused an increased in thermal stability according to a regular arrangement and form a new ordered structure [126]. This results was in agreement with the report from Wen et al; [128] they also found an increase of thermal stability. Thus, thermal stability of cellulose laurate was improved after esterification. The char residue of cellulose laurate was higher than PW-MCC was attributed to the lauric chain substituted on the hydroxyl group of cellulose. Surprisingly, char residue was related to DS value. It could be observed that higher of DS indicated the reduction of char residue.

Table 4.22 The decomposition temperature of cellulose laurate

Lauroyl chloride/AGU	DS	T _{d(onset)} (°C)	T _{d at 50%} (°C)	%Char at 450°C
unmodified	0	311	352	10.45
3	1.95	312	350	23.28
4	2.27	314	363	17.21
5	2.06	317	358	19.86

4.3.6.4 Morphological properties of cellulose laurate

The SEM images revealed that morphology of PW-MCC was changed after esterification with lauroyl chloride as Figure 4.42. SEM images displayed an aggregation of lauroyl substituent groups on PW-MCC surface leading to rough surface. However, using different lauroyl chloride/AGU ratios did not affect to the morphology of cellulose laurate.

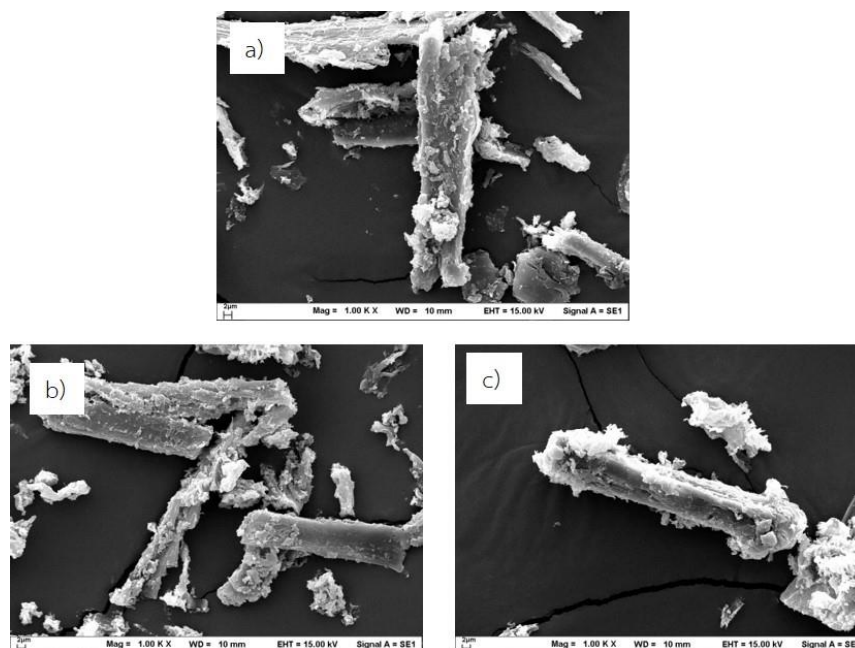


Figure 4.42 SEM micrographs of cellulose laurate at ball milling 60 min with lauoyl chloride/AGU ratio a) 3, b) 4 and c) 5

4.3.7 Comparison of cellulose ester

In this part, cellulose ester with different substitution type was compared to clarify the effect of substitution type on cellulose ester properties.

The FTIR spectra of PW-MCC before and after acylation of different types of fatty acid chloride are presented in Figure 4.43. All the IR spectra of cellulose ester indicated the reduction of O-H vibration of hydroxyl group. Moreover, the spectra of cellulose ester clearly showed the peak of carbonyl group (C=O) at 1740 cm^{-1} confirming that the esterification was occurred between PW-MCC and fatty acid chloride. However, the different of acid chloride chain length or type provided the different in their FTIR spectra. Cellulose benzoate contained benzene group which was an aromatic ring resulting in an appearance of monosubstituted benzene ring peak at 713 cm^{-1} . The FTIR spectra of fatty acid alkyl chain depicted some differences between short carbon chain (C6) and long carbon chain (C12). The intensity of C-H stretching of methyl and methylene at $2800\text{-}2900\text{ cm}^{-1}$ of long alkyl chain (C12) showed more intense than short alkyl chain (C6). This result are in good agreement with the previous works reported by Ratanakamnuan et al. [57] and Suchaiya et al. [71].

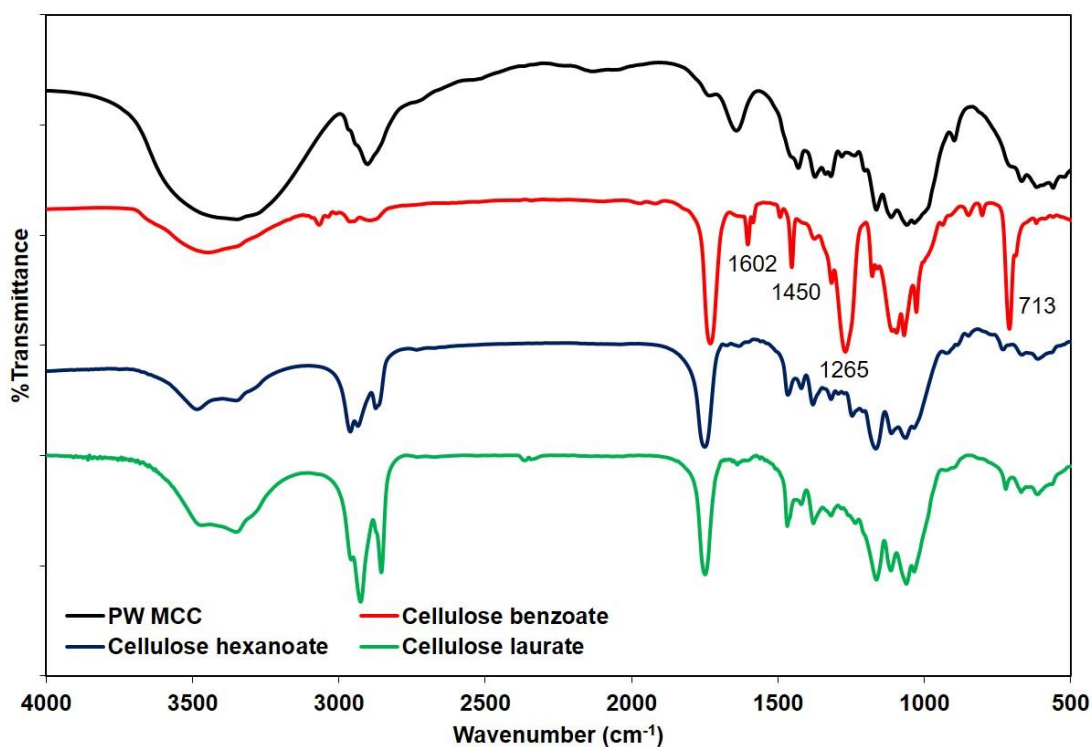


Figure 4.43 FTIR spectra of PW-MCC and cellulose ester

In addition, different fatty acid chloride type provided difference in esterification activity. It could be noted that benzoyl chloride resulted in the best esterification reactivity since the reaction could reach the maximum DS value without using a dispersing media. This could be according to lower of steric hindrance of the benzene ring when substituted on cellulose [132]. For hexanoyl chloride and lauroyl chloride, the reaction needed to use a dispersion media to enhance the esterification reactivity. However, the difference of carbon chain length also affected to the substitution ability. The DS value was decreased with an increasing of alkyl chain length. A longer fatty acid chloride caused the steric hindrance and a bulkier fatty acylium ion resulting to the reduction of esterification activity [123]. The comparison of DS value and thermal decomposition temperature from different cellulose ester is shown in Table 4.23.

Table 4.23 DS and thermal decomposition temperature of cellulose ester

Cellulose ester	DS	T _{d(onset)} (°C)	T _{d at 50%} (°C)	%Char at 450°C
PW-MCC	0	311	352	10.45
Cellulose benzoate	3.00	354	377	21.99
Cellulose hexanoate	2.73	302	325	19.17
Cellulose laurate	2.27	317	358	17.21

Thermal stability of cellulose ester with different substitution groups was compared and shown in Figure 4.44. It could be observed that introduction of benzoyl group improved thermal stability of cellulose because the thermal decomposition temperature of an aromatic ester of benzoyl directly cleavage of ester bond, while the thermal decomposition temperature of alkyl chain of either hexanoyl or lauroyl was due to producing symmetrical ketones through a condensation reaction between two ester group which used less energy than directly cleavage [133]. Thus, the benzoylation provided an enhancement of thermal stability of esterified cellulose [119]; while, grafting with hexanoyl chain resulted in a reduction of thermal stability due to the decreased the crystalline order after esterification. Nevertheless, using longer carbon chain length (lauroyl) exhibited higher thermal degradation temperature than using shorter carbon chain length (hexanoyl). This could be due to the formation a new ordered structure in substituted part of side chain so called side-chain crystallization which could be occurred when the carbon chain length was equaled to or greater than 12 [126]. In addition, the char residue of esterified cellulose was higher than that of PW-MCC confirming that the char residue was absolutely associated with the benzene ring or aliphatic chain substitution on the hydroxyl group of cellulose.

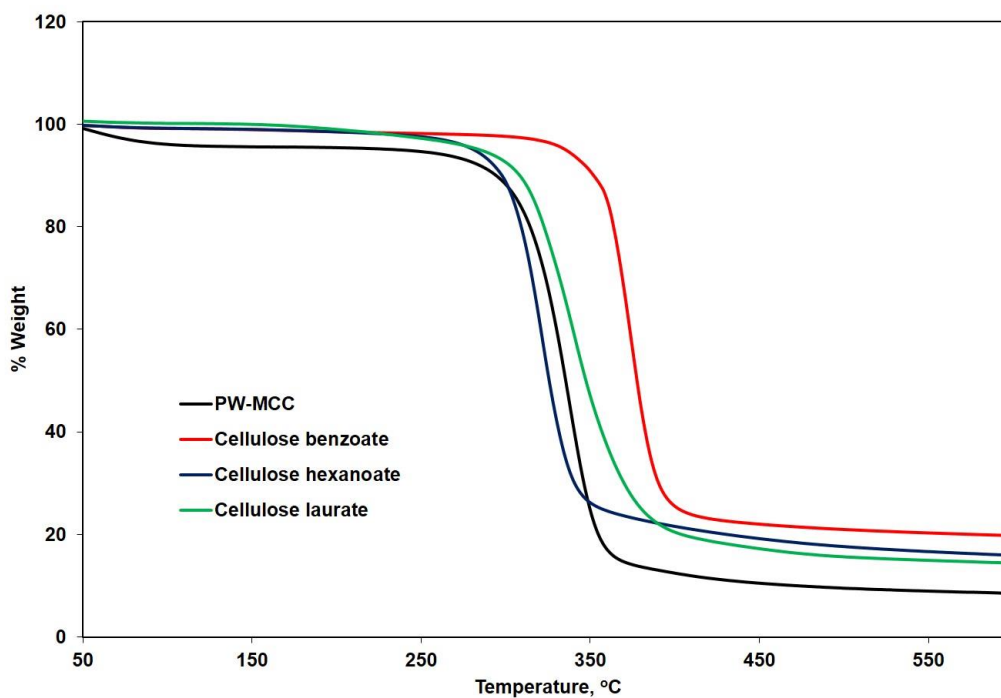


Figure 4.44 TGA curves of PW-MCC and cellulose ester

The morphology of cellulose ester is shown in Figure 4.45. The morphology of cellulose ester displayed rougher surface than that of PW-MCC according to the substitution of acyl group on their surface. It could be observed that after esterification under ball milling process, the morphology of PW-MCC changed from fiber to mixture of flake and particle. Cellulose benzoate revealed the most roughness among them while cellulose laurate presented the less of roughness surface. The particle size of cellulose benzoate and cellulose laurate were decreased due to mechanical force from ball mill process. Whereas cellulose hexanoate showed large of aggregation after esterification reaction and particle size of cellulose hexanoate was increased approximately from 40-80 μm to 80-160 μm .

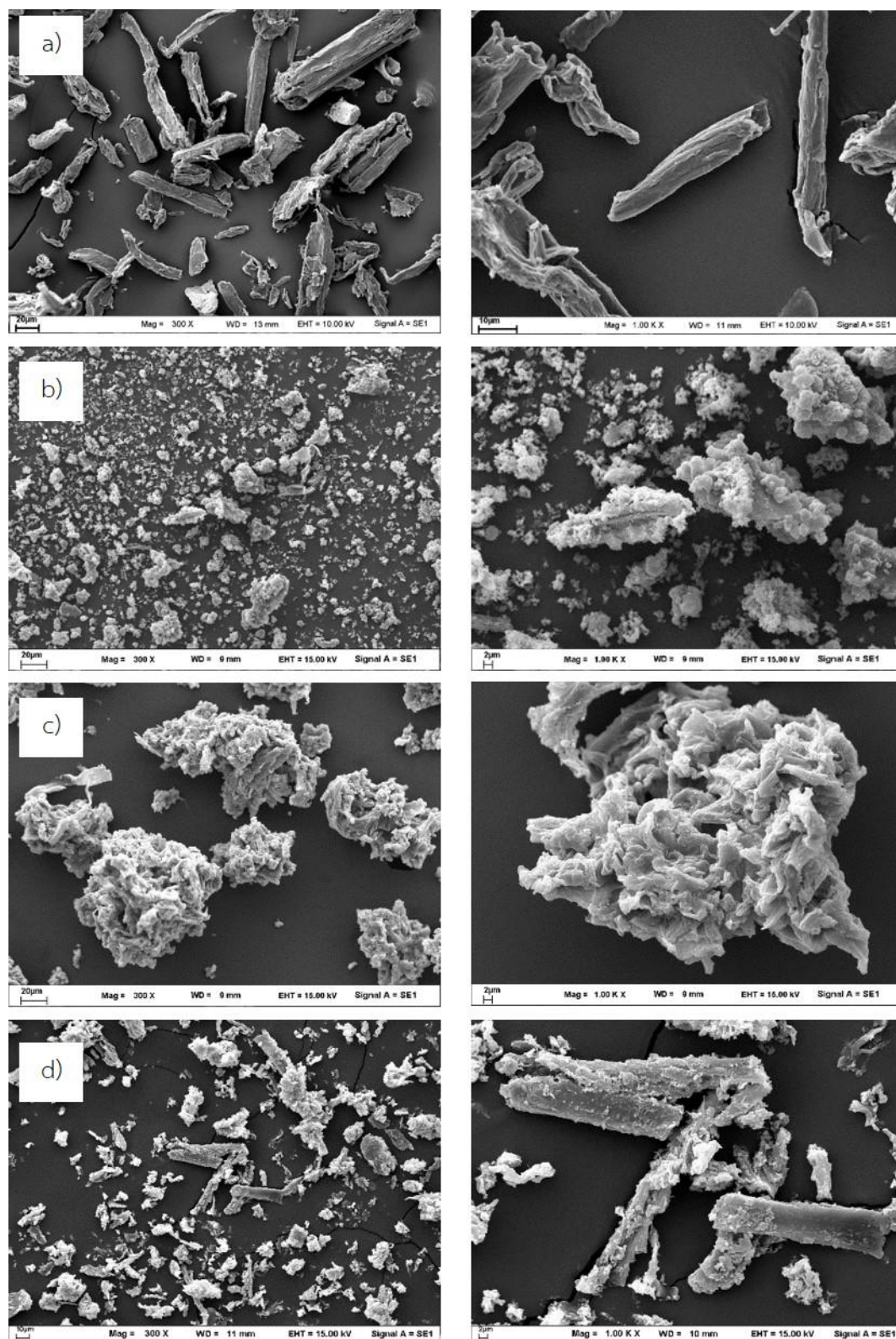


Figure 4.45 SEM micrographs at 300x and 1000x of a) PW-MCC, b) cellulose benzoate, c) cellulose hexanoate, and d) cellulose laurate

4.4 Mechanical properties of the composites

4.4.1 Tensile properties

The composites were prepared from PW-MCC and modified PW-MCC with 5-30wt% MCC loading. The tensile strength, elongation at break, and Young's modulus of the obtained PP composites were measured according to ASTM D638 and the data are shown in Figure 4.46. Moreover, Figure 4.50 and Figure 4.51.

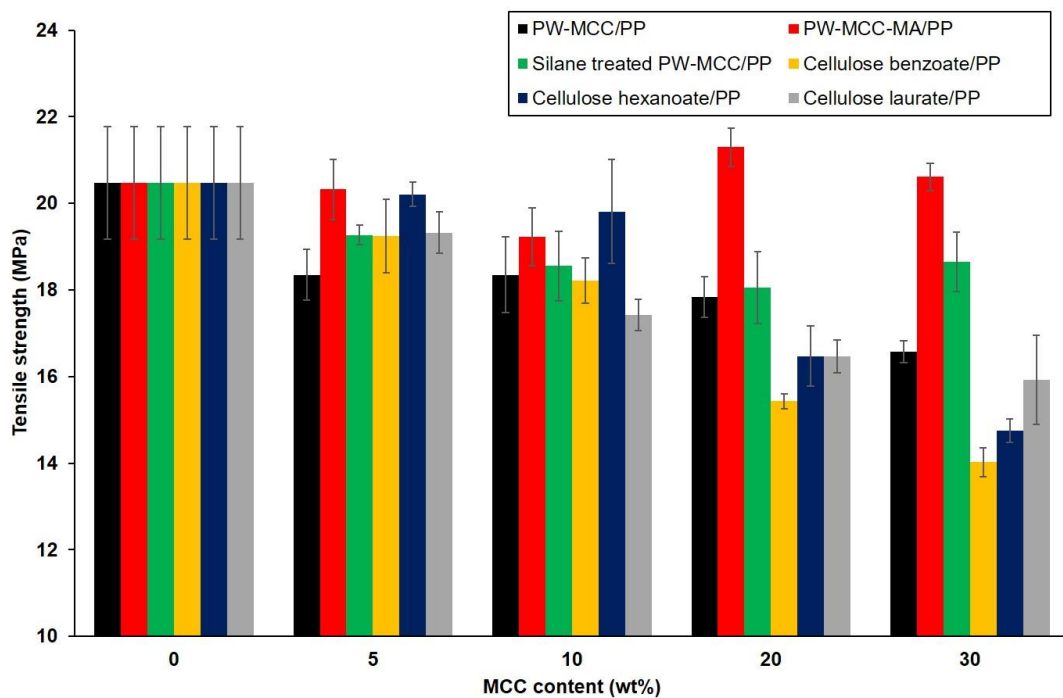


Figure 4.46 Tensile strength of obtained PP composites

When PW-MCC or modified PW-MCC were added into the PP matrix, reduction of tensile strength as compared to neat PP was occurred except for the composites using maleic-graft-anhydride polypropylene (PW-MCC-MA/PP) at 20 and 30wt% MCC. The reduction of tensile strength was according to poor compatibility between PP and PW-MCC [1]. In addition, an increment of PW-MCC content to PP led to a reduction of tensile strength due to an aggregation of PW-MCC [134]. Higher amount of PW-MCC could generate agglomeration leading to a deterioration of tensile strength between PW-MCC and PP matrix. Hence, the composites with high amount of PW-MCC became more brittle behavior [135].

For the effect of modifying agent, PW-MCC-MA/PP composites gave higher tensile strength than any other composites in every MCC loading. This improvement is because maleic-graft-anhydride enhanced the adhesion between PW-MCC and PP matrix (non-polar) through the interaction between hydroxyl group of cellulose and carboxyl group of maleic anhydride (MAPP). Moreover, PP chains of maleic-graft-anhydride polypropylene also diffused into PP matrix resulting in the physical entanglement of PP molecule [136]. Hypothetical chemical structure of MAPP between MCC and PP matrix is presented in Figure 4.47. However, an increment of PW-MCC-MA/PP composite up to 30 wt% still showed higher tensile strength than other modified PW-MCC/PP composites. The highest tensile strength was found at 20 wt% MCC content then tensile strength at 30wt% MCC content was decreased due to fiber agglomeration.

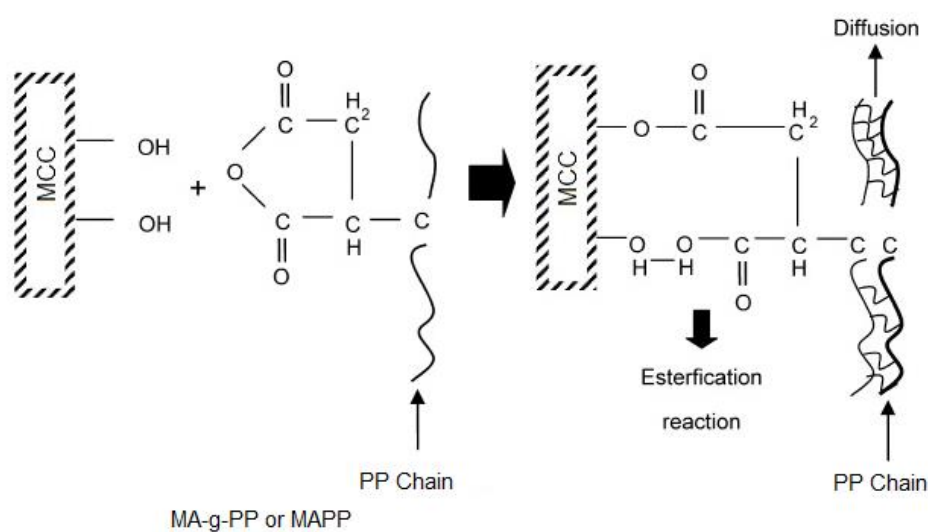


Figure 4.47 Hypothetical chemical structure of MAPP between MCC and PP matrix [137]

In term of MCC loading, it could be observed that at 5 wt% loading, the tensile strength of modified PW-MCC/PP composite was higher than that of unmodified PW-MCC/PP composite, especially PW-MCC-MA/PP and cellulose hexanoate/PP composites. These results confirmed that modified PW-MCC with chemical treatment increased compatibility between cellulose and PP matrix although with different capability depending on the chemical structure of each modifying agent. At 10 wt%

MCC content, cellulose benzoate/PP and cellulose laurate/PP composites demonstrated slight decrease of tensile strength comparing to unmodified PW-MCC/PP composites; while the tensile strength of the other modified cellulose/PP composites was comparable to or better than that of the unmodified PW-MCC/PP composite. However, at higher MCC loading (20-30 wt%), all cellulose ester/PP composites showed a dramatic decrease in the tensile strength according to an overridden by the internal plasticizing effect of the benzoyl, hexanoyl, and lauroyl chains of fatty acid ester grafted on PW-MCC [70, 138]. Plasticizers can increase the free volume between the polymer chains leading to a greater chain mobility. Meanwhile, polymer with plasticizer provides lower strength than the one without the plasticizer [139]. Among them, benzoyl group exhibited the lowest tensile strength because high amount of benzoyl group reduced the surface energy of the filler to matrix resulting in a decrease in the strength of interaction. This behavior was similar to previous work reported by Dányádi et al. [134]. Nevertheless, the tensile strength of PW-MCC-MA/PP composites was much greater than that of the unmodified composites. Similarly, silane treated PW-MCC could also provide better tensile strength than the unmodified and esterified PW-MCC composites. In addition, hypothetical chemical structure of esterified cellulose and PP matrix is displayed in Figure 4.48. The substituent group was hydrophobic chain which was similar to PP matrix resulting in good adhesion interfacial by Van der Waals force leading to the entanglement of PP molecule.

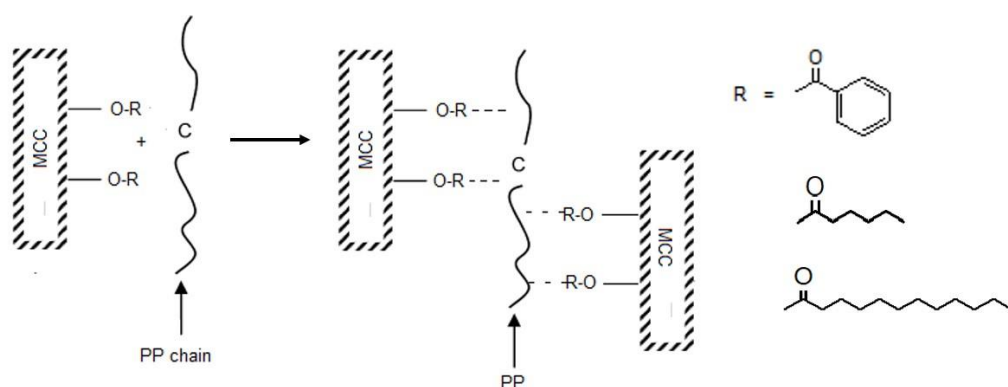


Figure 4.48 Hypothetical chemical structure of esterified cellulose and PP matrix [140]

The elongation at break of prepared composites were significantly decreased in all cases. This result indicated that the presence of PW-MCC or modified PW-MCC in PP matrix reduced the ability of the composite to deform by restricting the mobility of the PP chain [141]. Comparing among the modified agents, the results showed that the esterified PW-MCC with alkyl chains/PP composites indicated higher elongation at break than the ones using MAPP, silanization, and benzoylation as a modifying process. It could be assumed that esterified PW-MCC with alkyl chain provided more adhesion to PP matrix.

In the case of silane treated PW-MCC composites, the results (Figure 4.46) showed better tensile strength than PW-MCC/PP composites owing to an increase of interfacial adhesion after silanization. However, the tensile strength values of PP composites were found to be similar in all samples implying that cellulose content had no significant effect on the tensile strength values of the composites. Although the tensile strength of silane treated PW-MCC/PP was improved but the elongation at break was dramatically decreased and lower than PW-MCC/PP composites. The reduction could be resulted from crosslinking network between silane treated PW-MCC and PP matrix [142]. Hypothetical chemical structure of silane treated PW-MCC and PP matrix is presented in Figure 4.49.

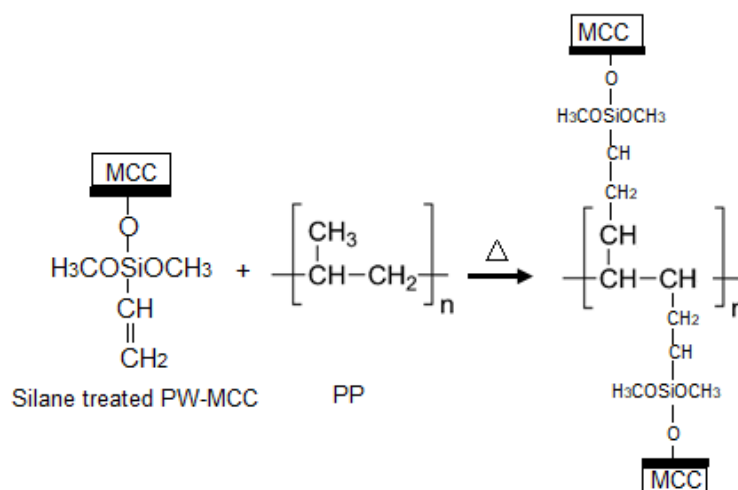


Figure 4.49 Hypothetical chemical structure of silane treated PW-MCC and PP matrix [142]

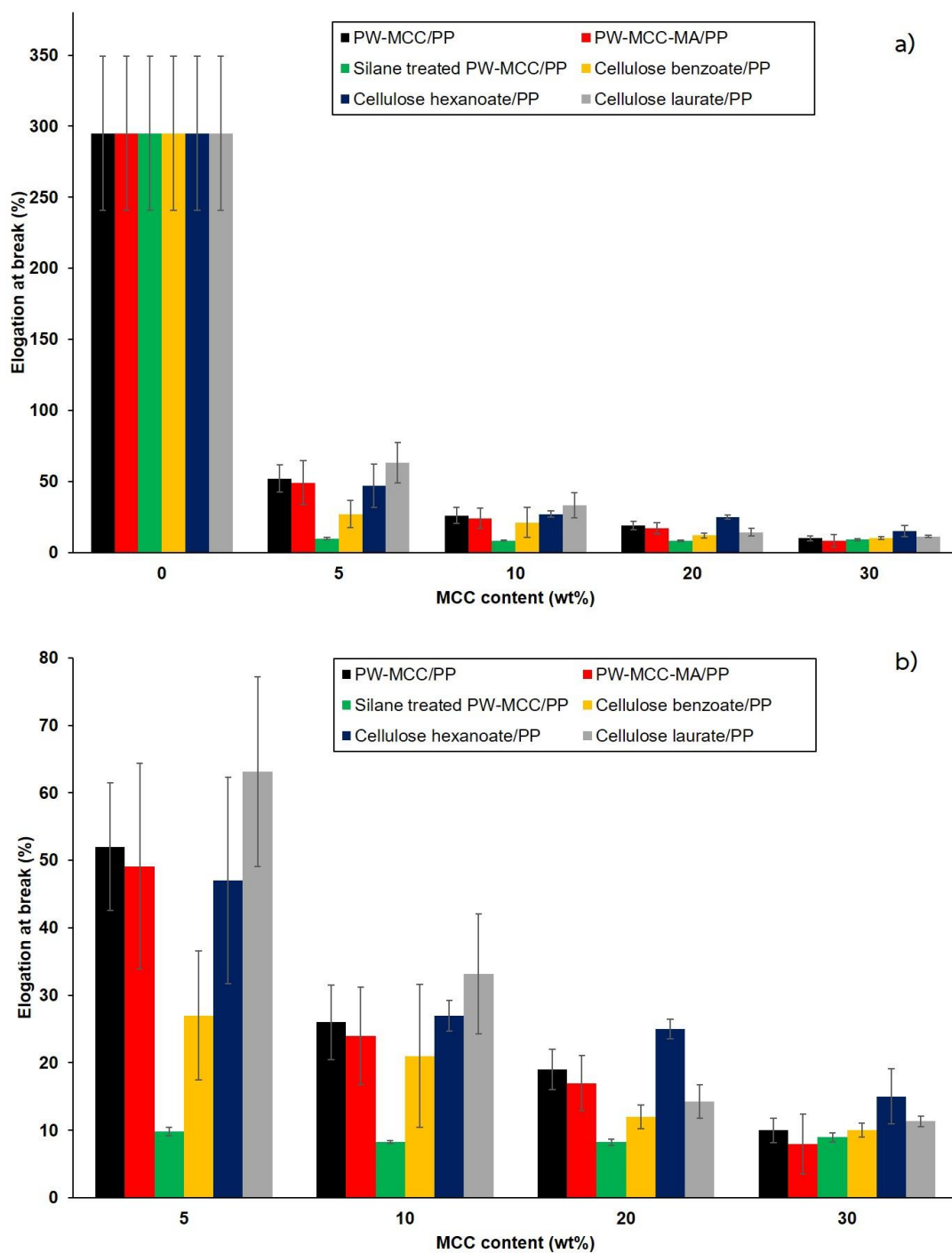


Figure 4.50 Elongation at break of a) PP and obtained PP composites and b) obtained PP composites

The Young's modulus of PW-MCC/PP and PW-MCC-MA/PP composites showed an increase upon increasing PW-MCC content, as shown in Figure 4.51. This increasing

was due to the higher Young's modulus of natural fibers than pure thermoplastic. The modulus of parawood is 9.07 GPa [143] while PP is 1.00 GPa. It is well known that the loading of hard filler into thermoplastic matrix increases the stiffness of the composites [144]. Meanwhile, the Young's modulus of modified PW-MCC composites indicated an improvement with an increment of cellulose content but with lower magnitude than PW-MCC/PP and PW-MCC-MA/PP composites. The slightly increased of Young's modulus was due to plasticizer effect from substituent grafted on PW-MCC [70]. It was noticed that at 5wt% MCC loading, esterified PW-MCC/PP composite exhibited higher Young's modulus than PW-MCC/PP, PW-MCC-MA/PP, and silane treated PW-MCC/PP composites. After that, the Young's modulus values of silane treated PW-MCC/PP composites seemed to be constant; whereas the unmodified and MA treated MCC/PP composites revealed a distinct increment of their Young's modulus values.

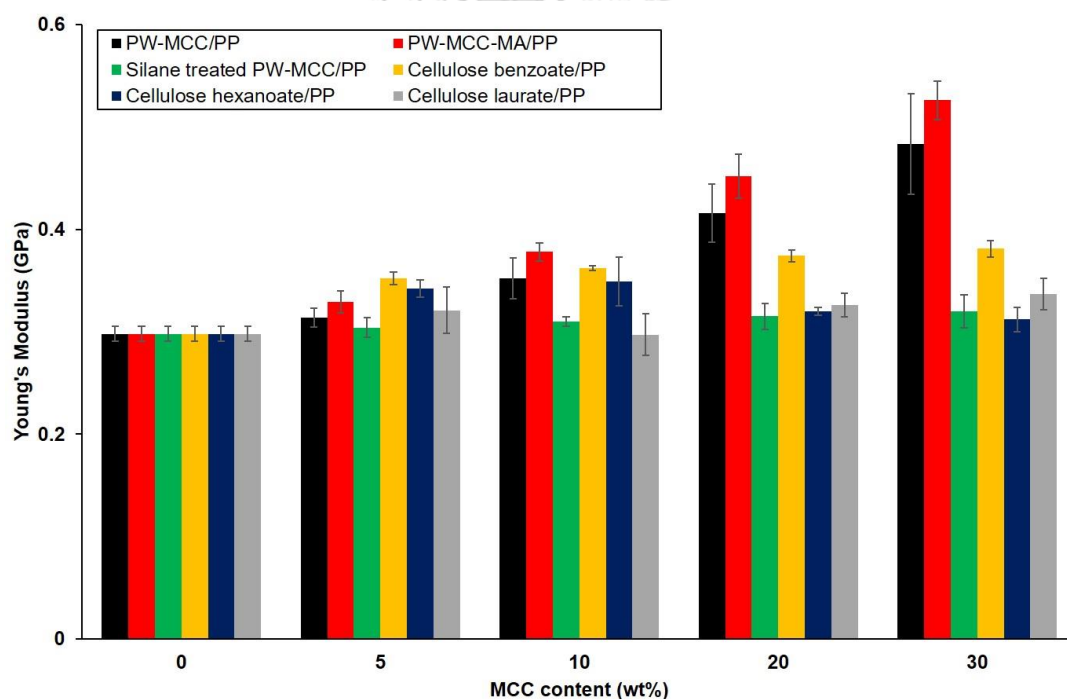


Figure 4.51 Young's modulus of obtained PP composites

4.4.2 Flexural properties

Flexural properties of unmodified and modified PW-MCC/PP composites with varying amount of cellulose are presented in Figure 4.52. Flexural modulus of PP composites were higher than that of neat PP. It was known that the addition of hard fillers to thermoplastics resulting to an increase in the stiffness of the composites [144]. The increase of flexural modulus suggested that the composite became more rigid. Similar to the Young's modulus discuss earlier, PW-MCC filled composites and PW-MCC with maleic anhydride grafted PP composite showed significant increase of flexural modulus upon increasing PW-MCC content. It could be observed that PW-MCC with maleic anhydride grafted PP composites had highest flexural modulus values among all. The addition of maleic anhydride grafted PP (MAPP) caused an increment in flexural modulus because MAPP improved dispersion of the PW-MCC in the polypropylene matrix [145].

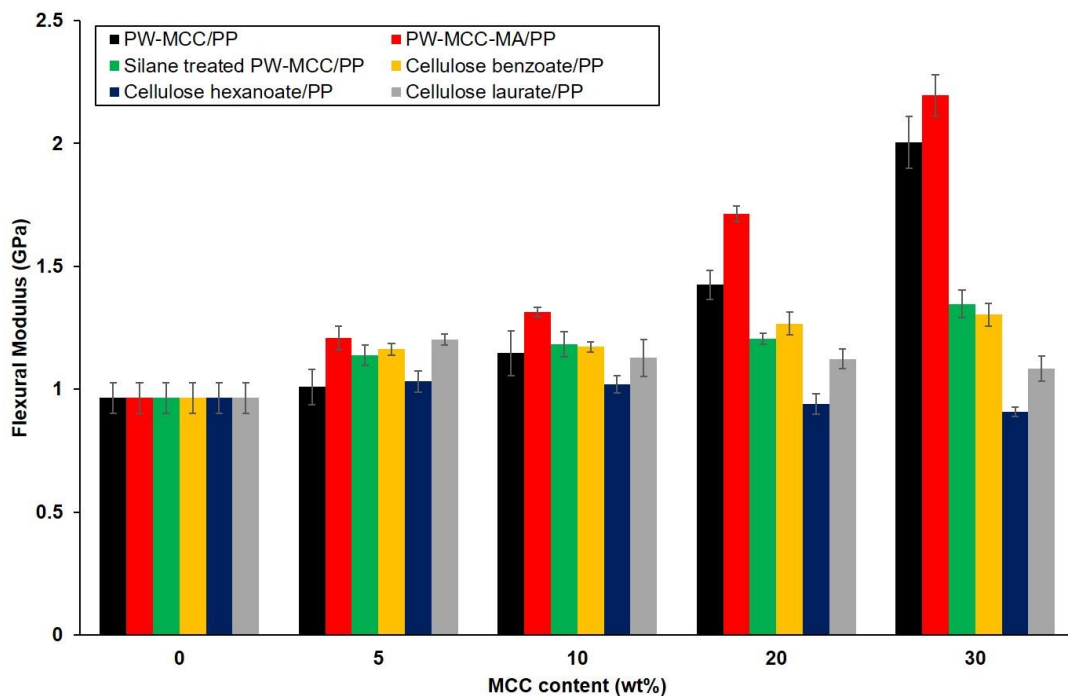


Figure 4.52 Flexural modulus of obtained PP composites

On the other hand, silane treated PW-MCC/PP composites provided small increment on flexural modulus comparing to their counterparts. However, using silane treated PW-MCC at 5 and 10 wt% gave higher flexural modulus of the composites than those PW-MCC/PP composites implying that surface treatment improved dispersion between PW-MCC and PP matrix. Nevertheless, silane treated PW-MCC/PP composites with silane treated PW-MCC at 20 and 30 wt% showed slight increase of flexural modulus but lower than those PW-MCC/PP and PW-MCC-MA/PP composites at the same loading.

For esterified PW-MCC/PP composites, the composite containing 5 wt% esterified PW-MCC gave higher of flexural modulus compared to the PW-MCC/PP composites. Nevertheless, an increment of esterified PW-MCC content into PP did not give an increasing of flexural modulus. These results were similar to the Young's modulus properties. These results might due to plasticizing effect from substituent on attached to the PW-MCC. It could be observed that esterified cellulose with alkyl chain particularly cellulose hexanoate/PP composites showed the lowest of flexural modulus and a decrease flexural modulus upon cellulose hexanoate content. Even so, the flexural modulus of cellulose benzoate/PP composites was higher than that of cellulose hexanoate/PP and cellulose laurate/PP composites. These results were due to better dispersion of cellulose benzoate into PP matrix while cellulose hexanoate itself had an aggregation as evidenced by the SEM analysis (Figure 4.35 & Figure 4.62), which then became big particle leading to a decrease the flexural modulus [145].

The effects of PW-MCC and modified PW-MCC on the flexural strength at maximum of the composites are shown in Figure 4.53. The flexural strength of PW-MCC/PP and PW-MCC-MA/PP composites exhibited in the same trend as neat PP. While, silane treated PW-MCC/PP composites showed a decrease flexural strength and found to be similar in all loading. This reduction was because the residue of silanol group might be formed a polysiloxane network by self-condensation [61]. On the other hand, the addition of esterified PW-MCC reduced the flexural strength with an increasing of cellulose content. These results were owing to the plasticizing effect of benzoyl or alkyl chain fatty acid ester [70]. It might be described that introduction of benzyl group

or alkyl chain attaching to cellulose improved the interfacial adhesion between cellulose and PP matrix but there was a limitation of usage content according to plasticizing effect. It could be noticed that cellulose laurate/PP composites at 5wt% loading exhibited the highest flexural strength among silane treated PW-MCC and esterified PW-MCC/PP composites.

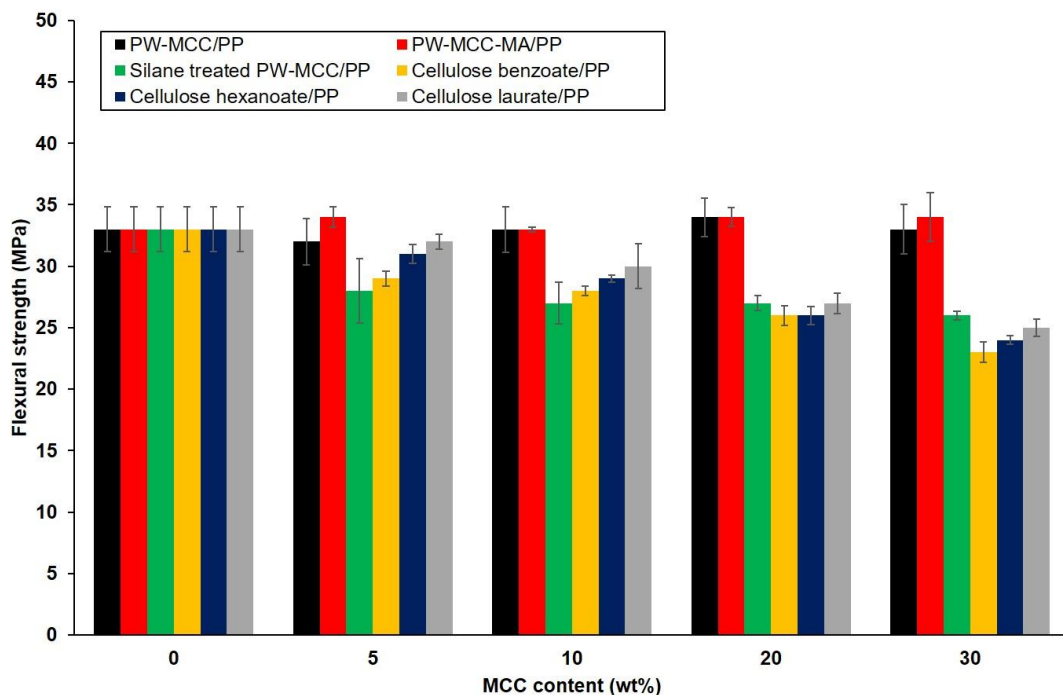


Figure 4.53 Flexural strength of obtained PP composites

4.4.3 Izod impact properties

The Izod impact strength of notched samples was evaluated in accordance with ASTM D257 as presented in Figure 4.54. Normally, the impact strength is implied to the toughness of materials. It was noted that neat PP exhibited an average impact strength at 93 J/m, while the impact strength of obtained PP composites were dramatically lower than that of neat PP matrix. It could be explained that the stiffer cellulose fibers play as stress concentrator in the polymer matrix leading to a decrease in the crack initiation energy and consequently the impact strength of the composites [145]. Therefore, an increasing of cellulose content resulted in the reduction of impact

strength. Both elongation at break and impact strength of the obtained PP composites were dropped because the higher content of cellulose enhanced a probability of cellulose agglomeration and generated void in the composites [136]. Thus, the brittleness of composites at higher amount of cellulose was connected with a reduction of free space and chain mobility [130].

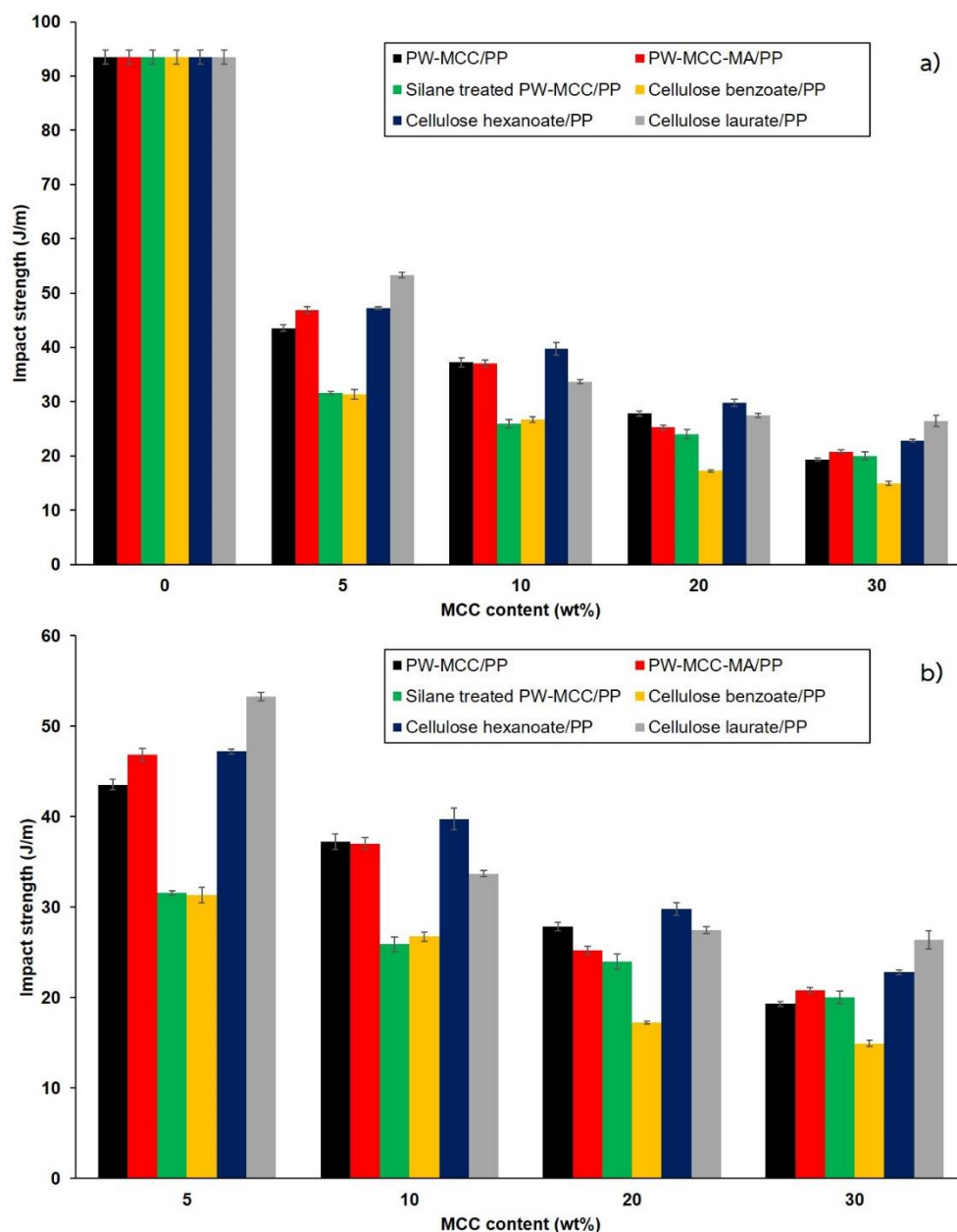


Figure 4.54 Izod notched impact strength of a) PP and obtained PP composites and b) obtained PP composites

When comparing among the obtained PP composites, the results showed that cellulose ester with alkyl chain gave better impact strength than cellulose modified with MAPP, silanisation, and benzylation. These results were similar to elongation at break value as well. It could be indicated that substitution of the hydroxyl group with alkyl chain fatty acid increased compatibility between cellulose and PP matrix resulting in the increase of impact strength, while Young's modulus or stiffness was decreased [71]. Besides, silane treated PW-MCC/PP obviously indicated the decrease of impact strength upon increasing cellulose content. Using silane treatment, the formation of silanol from hydrolysis and siloxane from condensation reaction were formed resulting in the formation of hydrogen bond with hydroxyl groups that are on surface of PW-MCC or it might be from self-crosslink of siloxane resulting in reduction the toughness of the composites [146].

Conclusively, the mechanical properties of the obtained PP composites indicated that modified PW-MCC with MAPP promoted an increasing of tensile strength and stiffness of the composite when compared to neat PP and PW-MCC/PP composite at every PW-MCC content but toughness of the PP composites with MAPP were quite similar to PW-MCC/PP composites. On the other hand, silane treated PW-MCC did not show significant change of the mechanical properties when increasing content of PW-MCC, except for the elongation at break which was lower than the other PP composites. Finally, PP composites made from cellulose ester exhibited higher mechanical properties than the others, particularly at 5-10wt% esterified PW-MCC loading. Moreover, it could be noted that silane treated PW-MCC/PP and cellulose benzoate/PP composites indicated the brittleness behavior as evidenced by their lower of elongation at break and impact strength values.

4.5 Physical properties of the composites

4.5.1 Density

The density of the composites is affected by content of fibers and fiber types which loaded into the composites system. PW-MCC or modified PW-MCC and PP matrix were main components of the PP composites. Hence, the amount of PW-MCC in

composites performed a major parameter to composites density. The density of the obtained PP composites is presented in Figure 4.55. Obviously, the density of the PP composites was higher than that of neat PP and all PP composites revealed similar trend that an increment of PW-MCC content increased the density of the composites. Eventhough, PW-MCC has lower density than PP but since injection molding was used to fabrication the specimens; thus, the high pressure from injection molding machine caused the collapsed cell of PW-MCC or modified PW-MCC leading to a reduction in the volume cell [42]. As a result, the density of the composites were increased upon increasing the MCC content. Furthermore, the density of PP composites with PW-MCC-MA gave the highest density, while cellulose ester/PP composites had the lower density than PW-MCC/PP composite. This reduction was due to branching of fatty acid group grafted on cellulose structure [147].

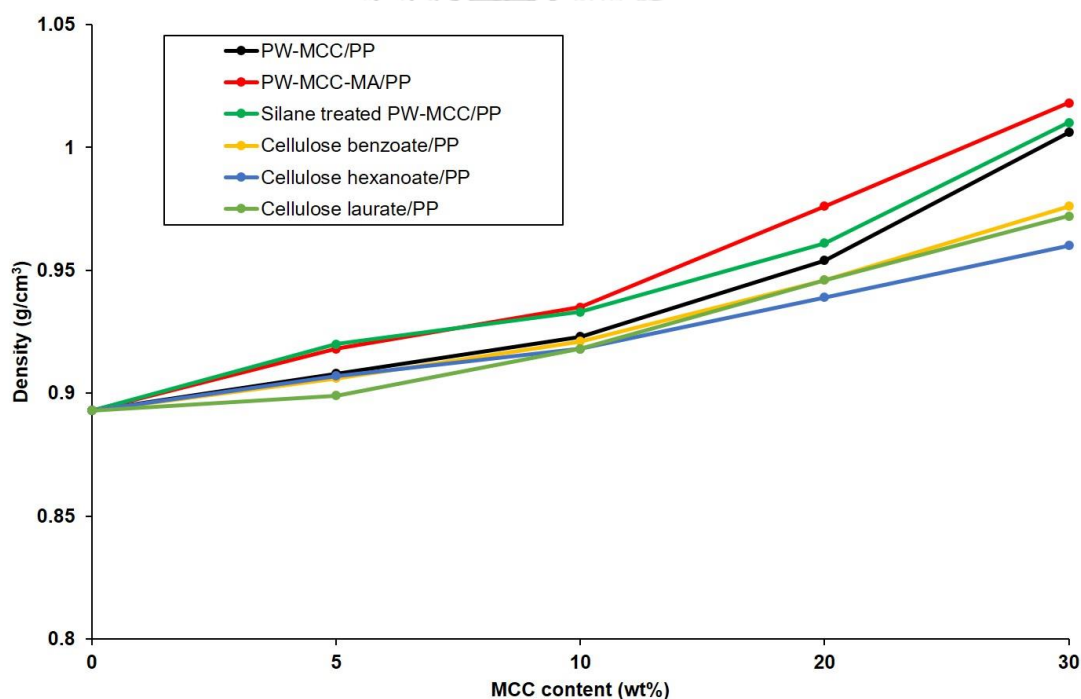


Figure 4.55 Density of obtained PP composites

4.5.2 Melt flow index

The flow properties of prepared PP composites were investigated by using melt flow indexer. It is known that addition of filler or reinforced materials to polymer leads to a decrease in the viscosity particularly with high content of filler. The melt flow index (MFI) of the obtained PP composites is demonstrated in Figure 4.56. The addition of PW-MCC to in PP composites resulted in the reduction of MFI upon increasing PW-MCC content. It can be explained that the movement of polypropylene molecules are obstructed by PW-MCC. So, an increasing of PW-MCC content caused high viscosity of the melt composites. In case of PP composites with MAPP, their MFI was slightly higher than that of PW-MCC composites due to an improvement of the compatibility between PW-MCC and PP matrix. The better of interfacial adhesion of PW-MCC and PP matrix resulting in increase of viscosity of composite. For silane treated PW-MCC/PP composites, the result revealed an increase of MFI because it could be assumed that silane treated PW-MCC significant increased liquidity processing of composite. This high liquidity led to reducing the flow resistance and friction of composite [148].

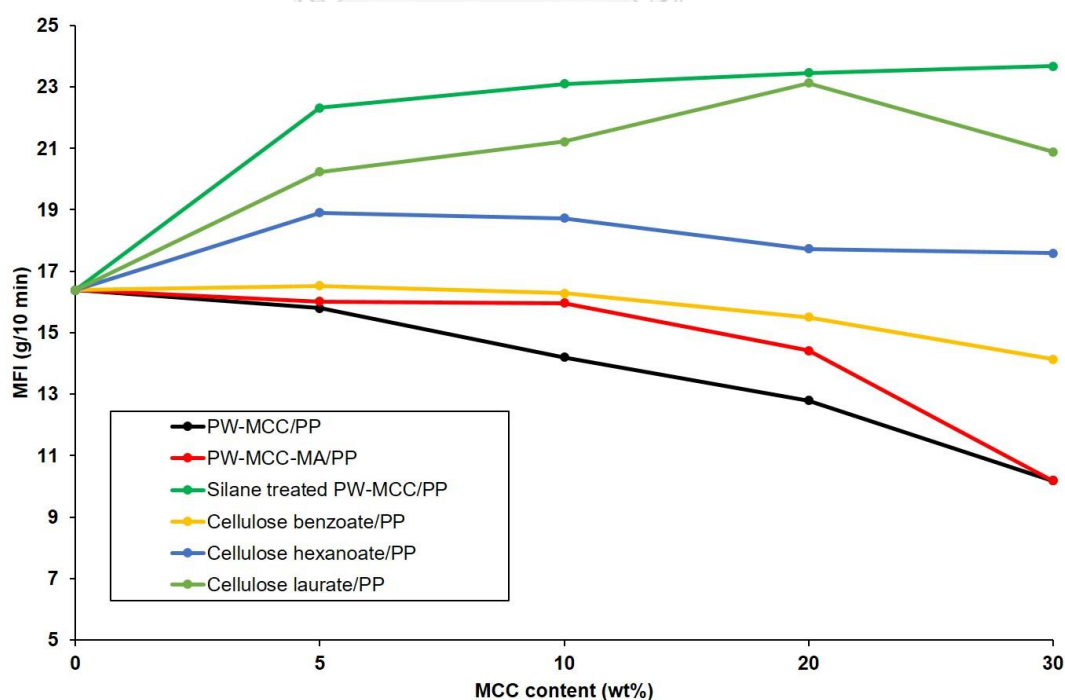


Figure 4.56 Melt flow index (MFI) of obtained PP composites

In the case of cellulose ester/PP composites, the opposite results among cellulose ester/PP composites were obtained. The MFI values of cellulose benzoate/PP composites were slightly decreased when increasing amount of cellulose content, while cellulose hexanoate/PP and cellulose laurate/PP composites had higher of MFI values than neat PP. This phenomenon was due to an internal plasticization from an alkyl chain grafted on PW-MCC. In addition, cellulose ester with alkyl chain could act as a lubricant to the composite system [149]. Therefore, an increasing of MFI value was attributed to an improvement of interfacial adhesion, so this result confirmed that esterified PW-MCC with alkyl chain had better compatibility between cellulose ester and PP matrix than cellulose ester with benzoyl group.

4.5.3 Morphology of PP composites

SEM images of the fracture morphologies of neat PP is shown in Figure 4.57 while those of the obtained PP composites are presented in Figure 4.58-4.63. The neat PP revealed smooth surface; whereas, the fracture surface of PW-MCC/PP composites presented rough surface with the gaps between PW-MCC and PP interfaces. When increasing PW-MCC loading, the rough surface, fiber aggregation, and many holes were clearly observed. Fiber pulled out was also noticed from SEM micrographs. This gap and hole were contributed to low compatibility and low interfacial adhesion between PW-MCC and PP [150]. Besides, PP is a hydrophobic polymer, while PW-MCC is a hydrophilic fiber which they were incompatible with each other.

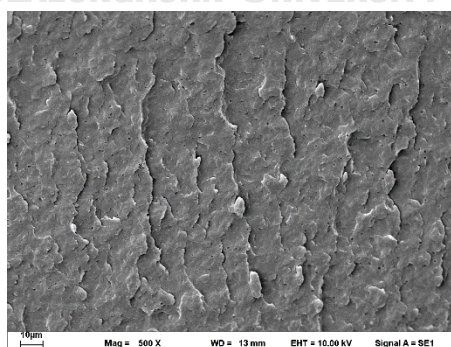


Figure 4.57 SEM micrograph at 500 magnification of neat PP

In case of PW-MCC-MA/PP composites, a better polymer-filler adhesion and an improved dispersion after an addition of maleic anhydride grafted PP could be

observed. As discussed earlier in mechanical properties section, the mechanical properties of PW-MCC/PP composites with maleic anhydride grafted PP provided a positive effect on mechanical properties.

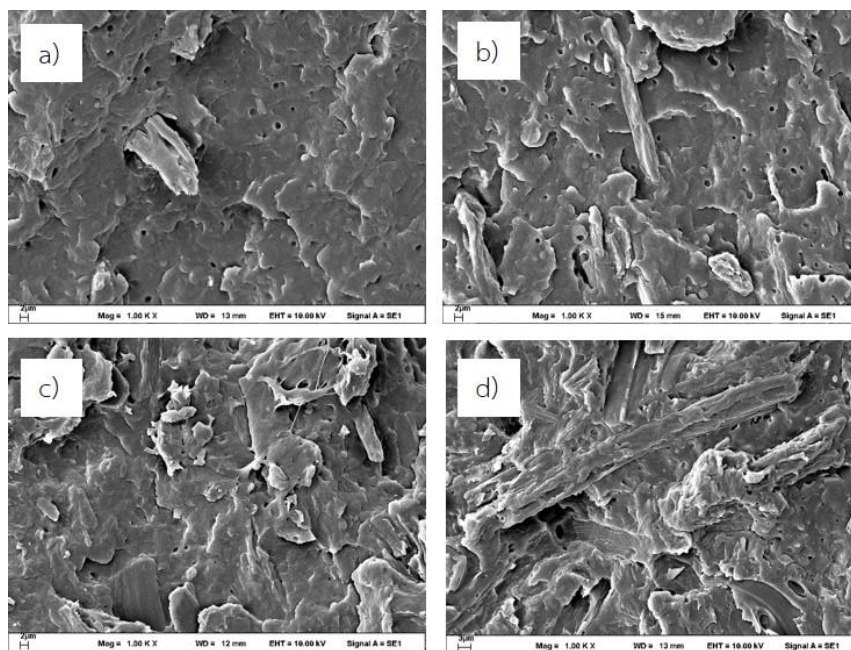


Figure 4.58 SEM micrographs at 1000 magnification of PW-MCC/PP composites at a) 5 wt%, b) 10 wt%, c) 20 wt%, and d) 30 wt%

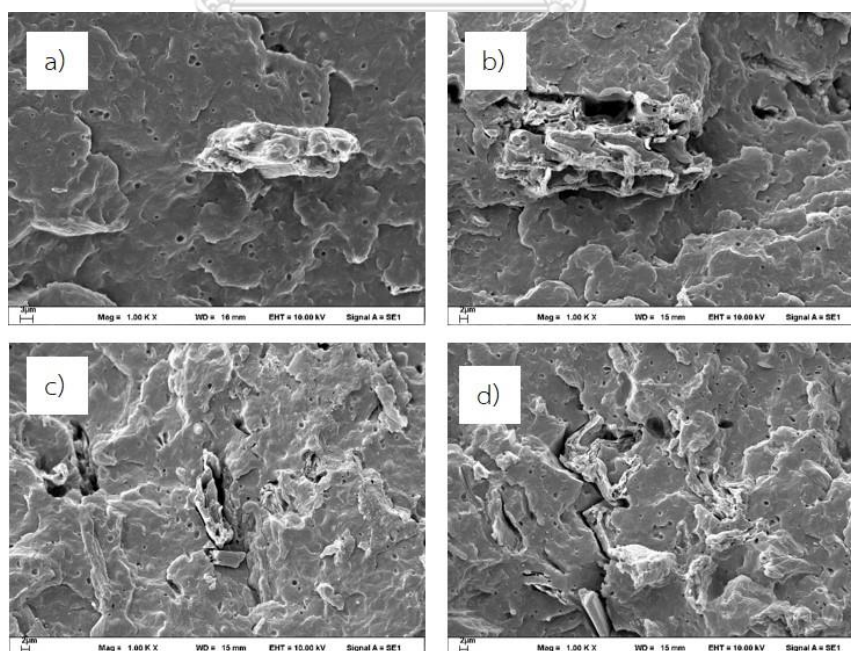


Figure 4.59 SEM micrographs at 1000 magnification of PW-MCC-MA/PP composites at a) 5 wt%, b) 10 wt%, c) 20 wt%, and d) 30%

SEM micrographs of the fracture surface of silane treated PW-MCC/PP composites displayed smoother and had less holes than the PW-MCC/PP composites. A significant improvement in the interaction between silane treated PW-MCC and PP matrix can be noticed easily. However, it could be noticed that at high MCC loading some gaps and rough surface occurred indicating the agglomeration of silane treated PW-MCC.

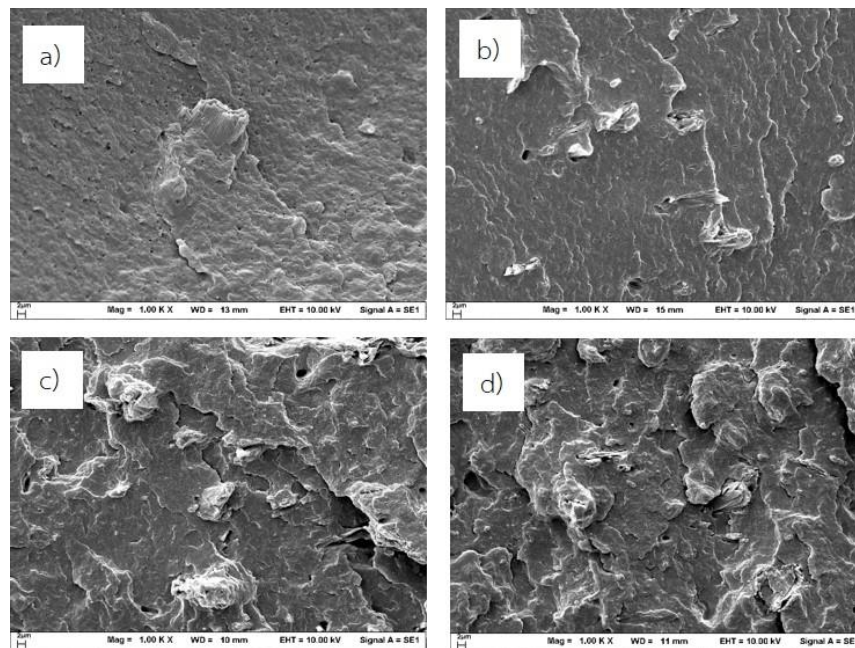


Figure 4.60 SEM micrographs at 1000 magnification of silane treated PW-MCC/PP composites at a) 5 wt%, b) 10 wt%, c) 20 wt%, and d) 30 wt%

On the other hand, the esterified PW-MCC/PP composites revealed a good dispersion of esterified PW-MCC in PP matrix. Moreover, large holes were disappeared in the esterified PW-MCC composites. The absence of gap and hole in fracture surface of esterified PW-MCC/PP composites implying that there was an improvement of interfacial adhesion and compatibility between PP and PW-MCC because the ester chain grafted on cellulose structure was a hydrophobic ester chain which was compatible with hydrophobic PP [135]. Comparing among esterified PW-MCC/PP composites, rough surface and gap between cellulose laurate and PP on the fracture surface of cellulose laurate/PP composites can be observed at high MCC loading (20 and 30wt%).

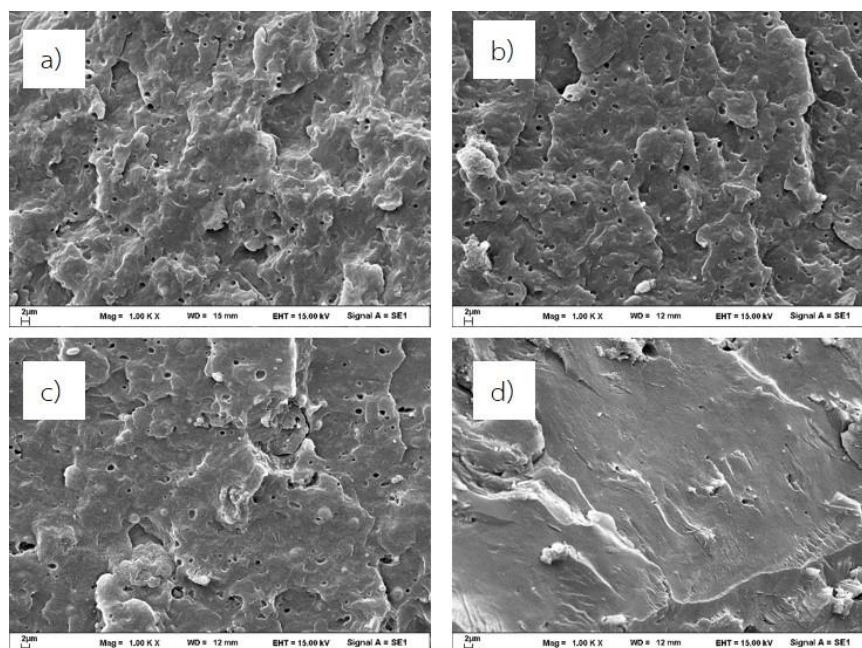


Figure 4.61 SEM micrographs at 1000 magnification of cellulose benzoate/PP composites at a) 5 wt%, b) 10 wt%, c) 20 wt%, and d) 30 wt%

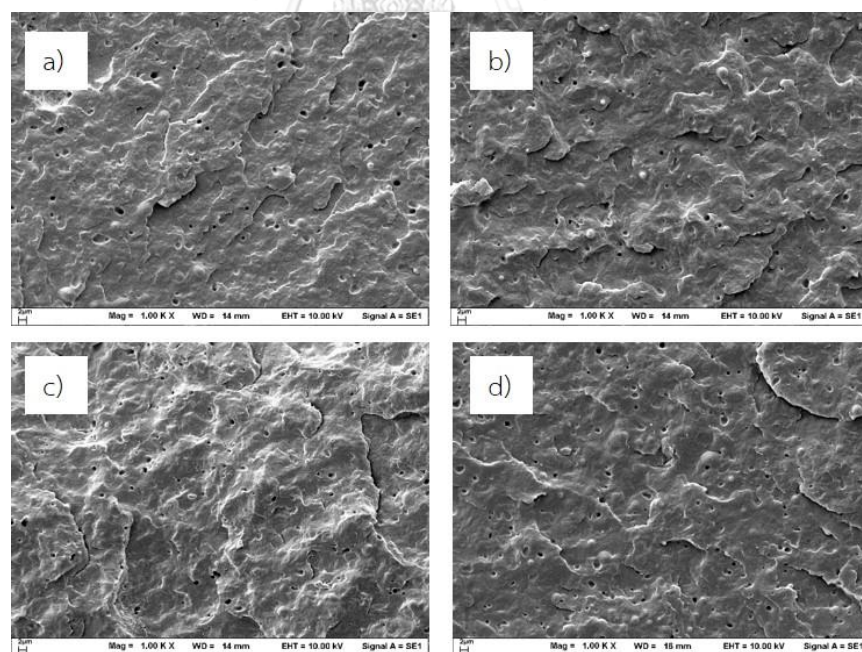


Figure 4.62 SEM micrographs at 1000 magnification of cellulose hexanoate/PP composites at a) 5 wt%, b) 10 wt%, c) 20 wt%, and d) 30 wt%

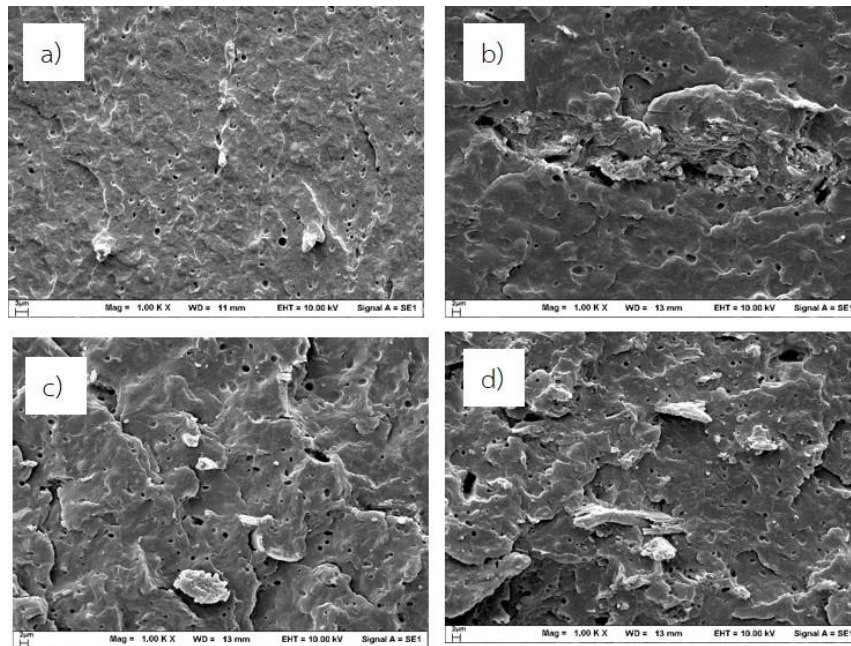


Figure 4.63 SEM micrographs at 1000 magnification of cellulose laurate/PP composites at a) 5 wt%, b) 10 wt%, c) 20 wt%, and d) 30 wt%

4.5.4 Water absorption of composites

The most serious drawback of using natural fiber as reinforcing material in polymer composites is the hydrophilic nature of cellulose, of which it is sensitive to water. The absorption of water of the composites causes many problems such as poor mechanical properties and dimension instability [151]. Therefore, water absorption of natural fiber reinforced composites should be evaluated. The improvement of water resistance of the composite also provides many benefits such as longer life time and maintaining properties of the product. Actually, surface treatment of cellulose could decrease the number of free hydroxyl groups on the cellulose surface, resulting in the more hydrophobic characteristic of cellulose, the relationship between percentage of water absorption and immersion time of PP and the obtained PP composites at various of PW-MCC contents is displayed in Figure 4.64. The results indicated that there was no significant change on water absorption of the PP matrix even at longer immersion time. Meanwhile, it was observed that obtained PP composites from PW-MCC and modified PW-MCC exhibited an increase in water absorption with an increment of PW-MCC content and immersion time. The obtained PP composites showed higher water

absorption than the neat PP due to hydrophilic character of PW-MCC resulting in high water absorption. The composites with 30wt% of PW-MCC gave the highest percentage of water absorption.

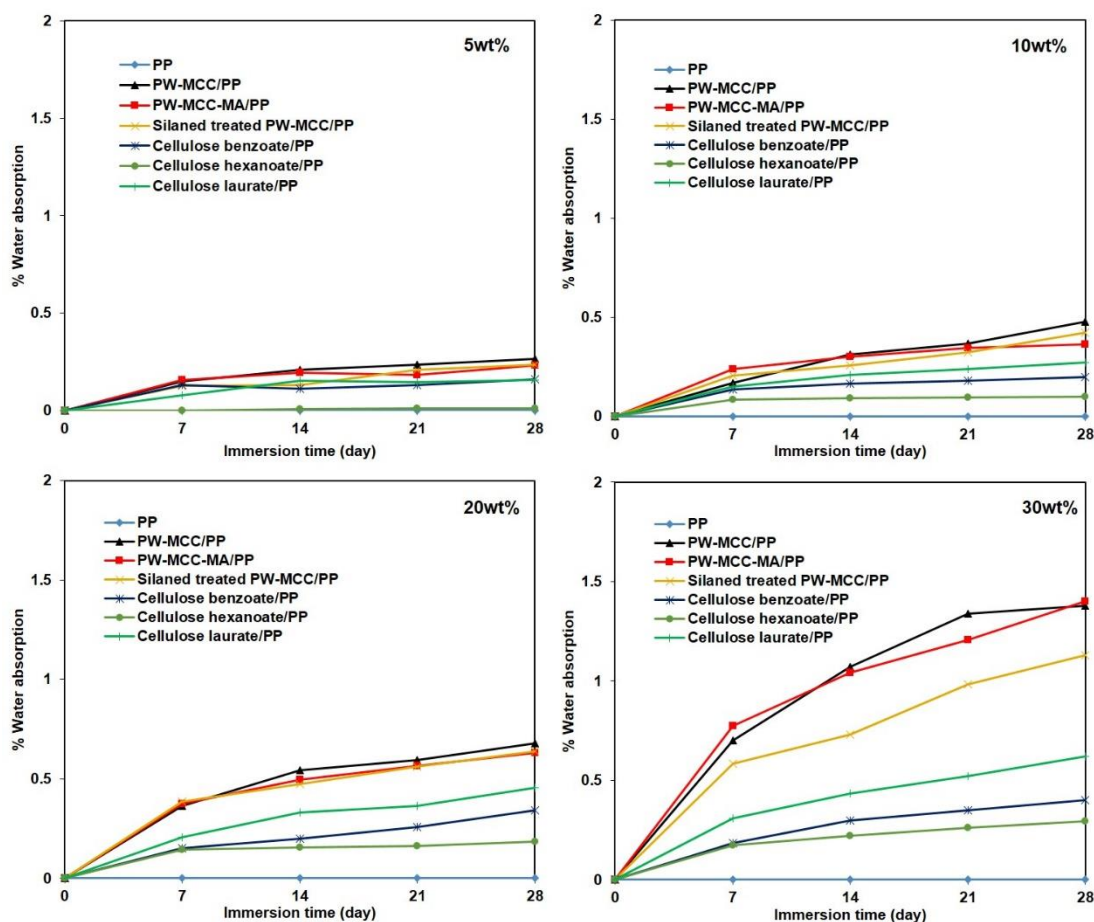


Figure 4.64 Water absorption of PP and obtained PP composites

On the other hand, treatment of PW-MCC with different methods provided a difference in water absorption behavior. Comparing to the untreated PW-MCC/PP composites, the PW-MCC/PP composites with addition of MAPP showed a slight decrease of water absorption due to the improvement of surface adhesion. Moreover, the hydroxyl group of cellulose was blocked by the coupling effect [4]. Nevertheless, long period of immersion time led to the degradation of bondings between PW-MCC and MAPP which caused the penetration of water through to interface [22]. Meanwhile, silane treated PW-MCC composites exhibited lower water absorption than PW-MCC/PP

composites with MAPP. Hence, using silane for fiber surface treatment was also an effective method to limit water penetration into the composites.

For esterified PW-MCC/PP composites, it was an interesting to note that esterification reaction of PW-MCC with fatty acid chloride provided dramatical reduction of water absorption, especially when using hexanoyl chloride. For the composites containing 30 wt% of PW-MCC, the water uptake continued increasing upon increasing immersion time, whereas the water absorption of cellulose hexanoate/PP composites seemed to be constant after 14 days, implying the better water resistance of the cellulose hexanoate/PP composites. The efficiency to increase the water resistance to PP composites could be ordered from low to high water absorption among esterified PW-MCC as cellulose hexanoate, cellulose benzoate, and cellulose laurate. As a result, cellulose laurate showed higher water absorption than cellulose benzoate and cellulose hexanoate, probably because of its the lowest degree of substitution of hydrophobic group [147]. Thus, it can be concluded that surface modification had a beneficial effect on water resistance. These results indicated that surface modification of PW-MCC via esterification reaction was an effective method to prevent the water absorption of the composites.

4.6 Dynamic mechanical properties of the composites

The dynamic mechanical properties of PP and the obtained PP composites were evaluated by DMA. The storage modulus (E') indicates the relationship between components of the remaining stress and strain. Figure. 4.65 illustrates the storage modulus of PP composites at different PW-MCC contents. It can be observed that the obtained composites gave higher storage modulus than neat PP. Moreover, storage modulus was increased along with an increment of PW-MCC content. This result indicated that PW-MCC could improve stiffness of the composites [1]. In addition, the storage modulus continuously reduced along with an increasing of the temperature which is contributed to the transition from glassy to the rubbery stage [152].

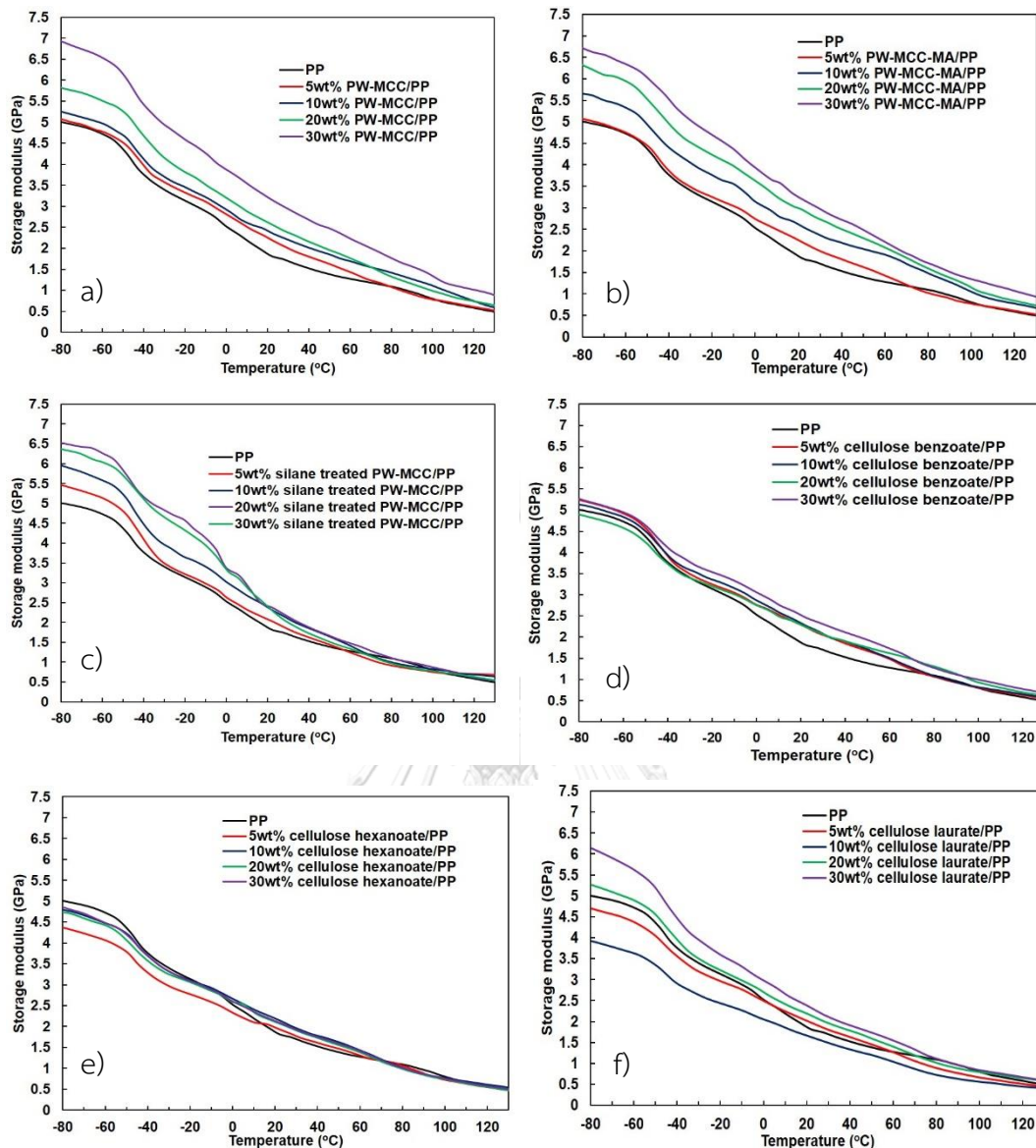


Figure 4.65 Storage modulus of a) PW-MCC/PP, b) PW-MCC-MA/PP, c) silane treated PW-MCC/PP, d) cellulose benzoate/PP, e) cellulose hexanoate/PP, and f) cellulose laurate/PP composites

PW-MCC/PP composites and PW-MCC/PP composites with MAPP (Figure 4.65(a) and (b)) gave similar storage modulus value when comparing to the other modified PW-MCC/PP composites. Moreover, an increasing of PW-MCC amount led to a significant increase of storage modulus for both PP composites. The stiffness of composites depend on crystallinity of filler so PW-MCC without any modification under ball milling process maintained high crystallinity of cellulose [22]. It might be the

reason for greater stiffness of PP composites in the rubbery stage. The best improvement in storage modulus was found in PW-MCC/PP composite at 30 wt% loading. These results correlates well with the flexural modulus test.

From Figure 4.65 (c), the addition of silane treated PW-MCC at 5-20 wt% into PP matrix indicated higher storage modulus of PP composites than PW-MCC. However, it was surprisingly noticed that the PP composite with 30wt% silane treated PW-MCC had similar storage modulus value similar to the 20wt% silane treated PW-MCC/PP composites. This might be due to the agglomeration of silane treated PW-MCC within the matrix.

In the case of esterified PW-MCC/PP composites, the results presented the different trend of storage modulus depending on fatty acid type grafted on cellulose structure. When comparing to neat PP, cellulose benzoate/PP composites (Figure 4.65 (d)) showed slight increase of storage modulus, while cellulose hexanoate/PP composites provided a deterioration of storage modulus. Nevertheless, cellulose laurate/PP composites exhibited an increasing of storage modulus at 20 and 30 wt% PW-MCC loading but at lower PW-MCC loading the storage modulus was lower than that of the neat PP. The possible reason could be from plasticization effect by benzoyl and alkyl chain from substituent [124]. In this work, plasticization effect was clearly observed from esterified cellulose with acid chloride. However, it was difficult to conclude the effect of cellulose laurate to PP composites. It can be observed that 10wt% cellulose laurate/PP composite had the lowest storage modulus when comparing among PP composites. Nevertheless, the decrease in storage modulus of these composites at higher temperature was contributed to viscoelastic deformation behavior of the polymer which made the PW-MCC to debond from the matrix phase [49].

The damping peak takes place in the region of glass transition temperature which is expressed as $\tan \delta$, where the polymer changes from rigid to a more elastic state. This region corresponds to the movement of molecular chain within the polymer matrix. $\tan \delta$ demonstrates the glass transition temperature (T_g) of the composites, which is displayed in Figure 4.66. It was found that the neat PP and the obtained PP

composites indicated two transitions on the DMA thermogram. The first transition at 17°C was attributed to the glass transition temperature of PP which did not alter after increasing PW-MCC content or changing surface modification. The other distinct transition found at -42°C was referred to the transition temperature of the ethylene-propylene (EP) phase of the block copolymer used as a matrix [116].

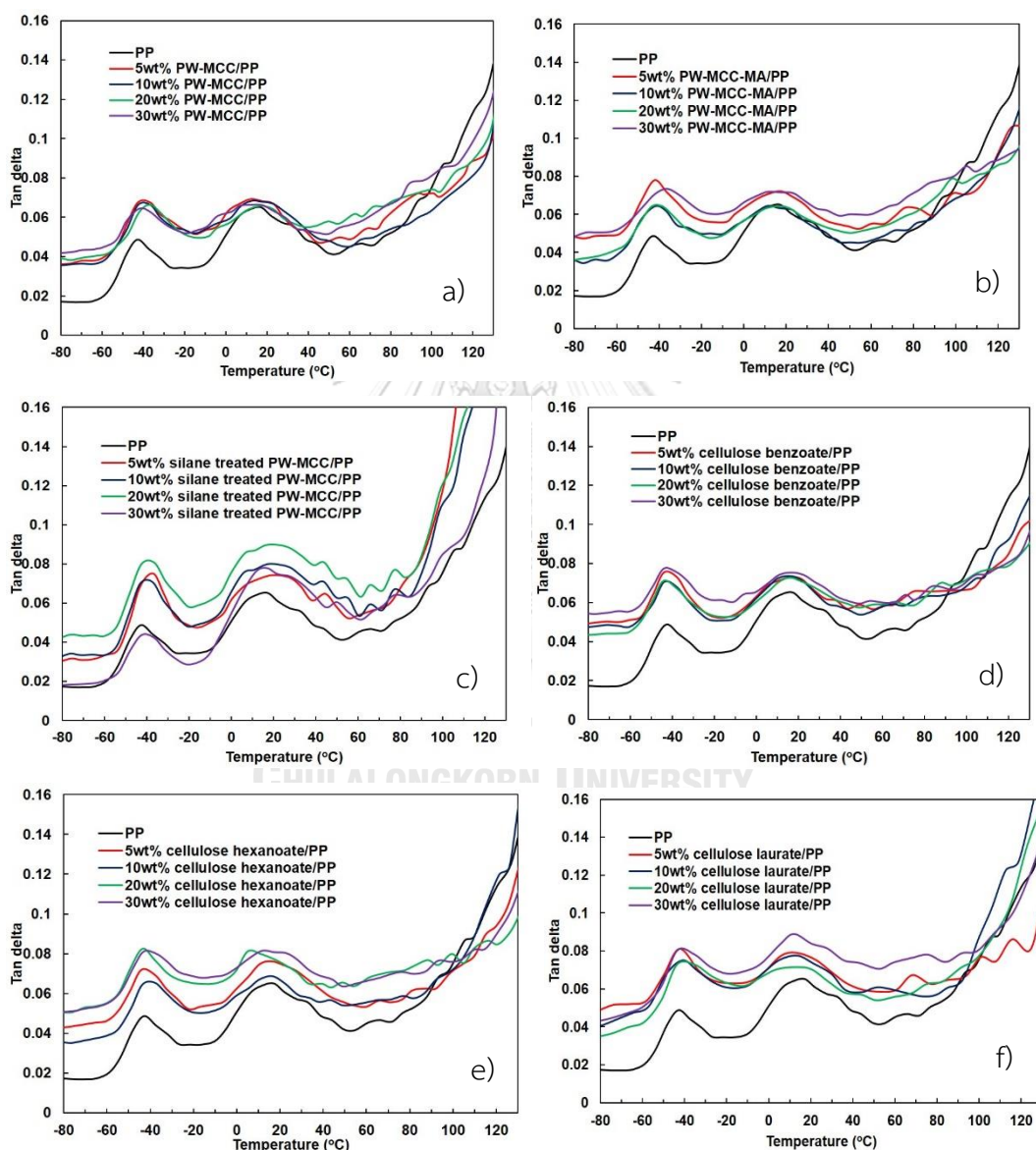


Figure 4.66 Tan δ of a) PW-MCC/PP, b) PW-MCC-MA/PP, c) silane treated PW-MCC/PP, d) cellulose benzoate/PP, e) cellulose hexanoate/PP, and f) cellulose laurate/PP composites

It could be observed that T_g of the composites shifted to the higher temperature after adding PW-MCC to the PP matrix compared to the $\tan \delta$ peak of PP. The shifted of $\tan \delta$ was due to the reduction of molecular motion of polymer matrix [47]. This shifting of $\tan \delta$ was found in PW-MCC/PP with MAPP (Figure 4.66 (b)) and silane treated PW-MCC/PP composite (Figure 4.66 (c)). However, the T_g of esterified PW-MCC/PP composites did not change. This result suggested that the addition of esterified PW-MCC did not influence to the T_g value of the composites. In other words, esterified PW-MCC did not interfere or restrict the molecular motion of PP matrix. In addition, the width of $\tan \delta$ became broader than PP matrix. This behavior suggested that there were molecular relaxation in the composite. The molecular motions at the interfacial region was mainly assigned to the damping of the material apart from those of the constituents [153]. Thus, the width of the $\tan \delta$ was related to the increasing volume of the interface [154]. This phenomenon was generally found in higher loading of PW-MCC to PP matrix.

4.7 Thermal properties of the composites

4.7.1 Thermal stability of composites

In order to investigate the thermal stability of PP and its composites, thermogravimetric analysis (TGA) was used. TGA thermograms of 20 wt% PW-MCC and modified PW-MCC/PP composites are illustrated in Figure 4.67 along with their onset of thermal degradation temperatures which are summarized in Table 4.24. As seen, thermal degradation of neat PP exhibited one degradation step around 420°C. The obtained PP composites indicated two steps of weight loss, the first step was the degradation of PW-MCC at temperature below 350°C, after that the second step of degradation was contributed to the decomposition of PP which was occurred at higher temperature. Obviously, the obtained PP composites started to decompose at lower T_d than neat PP according to the lower thermal stability of PW-MCC [155]. As the amount of fiber content increased in the composites, a reduction in thermal stability occurred.

For PW-MCC/PP composites with MAPP, the $T_{d\text{ at }50\%}$ were shifted towards higher temperature, compared to the PW-MCC composites. The improvement was due to the addition of MAPP which can enhance the interaction between PW-MCC and PP [156]. The char residue of PW-MCC-MA/PP composites gave seemed to be higher than that of PW-MCC/PP composites.

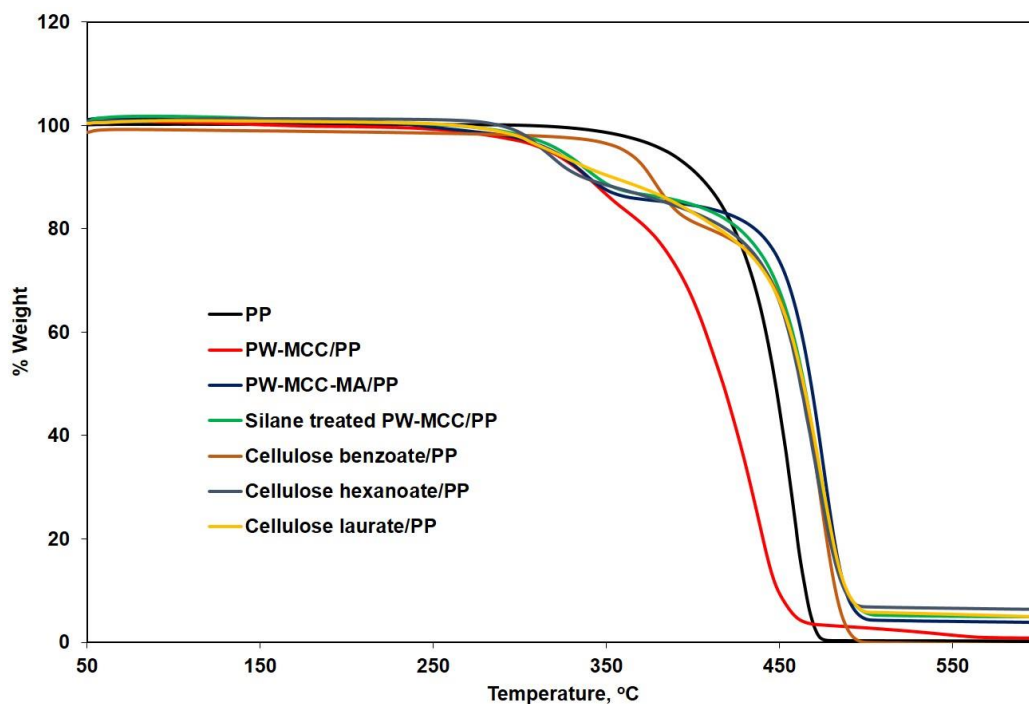


Figure 4.67 TGA thermograms of PP and PP composites at 20 wt% PW-MCC content

Table 4.24 The thermal decomposition temperature of PP and PP composites

Sample	MCC (wt%)	$T_{d(\text{onset})}$ (°C)	$T_{d\text{ at }50\%}$ (°C)	%Char at 550°C
PP	0	420	447	0.26
PW-MCC/PP	5	317	431	0.76
	10	317	420	1.32
	20	316	417	1.38
	30	312	411	2.30

Table 4.24 The thermal decomposition temperature of PP and PP composites (continued)

Sample	MCC (wt%)	T _{d(onset)} (°C)	T _{d at 50%} (°C)	%Char at 550°C
PW-MCC-MA/PP	5	317	467	1.26
	10	317	468	2.36
	20	317	468	4.04
	30	313	411	2.30
Silane treated PW-MCC/PP	5	319	465	1.83
	10	319	465	3.77
	20	319	464	5.02
	30	316	462	6.53
Cellulose benzoate/PP	5	364	465	0
	10	359	465	0
	20	358	463	0
	30	356	461	0
Cellulose hexanoate/PP	5	295	462	5.84
	10	298	462	5.89
	20	296	462	6.57
	30	295	461	7.34
Cellulose laurate/PP	5	290	462	4.23
	10	290	454	5.59
	20	289	463	5.41
	30	289	464	6.75

Similarly, silane treated PW-MCC/PP composites showed higher thermal stability than the PW-MCC/PP composites. The reason could be due to bond formation during silane treatment [157]. As shown in Figure 4.14 that silanol molecule reacted with hydroxyl group of cellulose to form strong covalent bond with cellulose surface. Moreover, the free silanol could react to each other forming -Si-O-Si bond as well. The vinyl group of silane molecule coupled with PP matrix to enhance the compatibility resulting in better thermal stability of PP composites having silane treated PW-MCC. Evidently, $T_{d\text{ at }50\%}$ decomposition of silane treated PW-MCC/PP composites exhibited higher degradation temperature than that of neat PP and PW-MCC/PP composites which suggested that silane treated PW-MCC could act as heat stabilizer for polypropylene. Nevertheless, varying amount of silane treated PW-MCC showed no significant effect on the $T_{d\text{ at }50\%}$ decomposition. Moreover, higher char residue can be observed from silane treated PW-MCC/PP composites indicating flame retardancy properties as well [158].

For esterified PW-MCC/PP composite, it was surprisingly to found that the TGA thermogram did not show any weight loss at temperature below 200°C which was referred the degradation of ester bond of esterified PW-MCC. It was remarkable that the decomposition temperature of PP was shifted to higher temperature, implying that the presence of esterified PW-MCC had an effect on the thermal stability of the PP matrix due to an improvement of adhesion between esterified PW-MCC and PP [4]. Therefore, cellulose benzoate/PP composites had higher thermal stability than cellulose hexanoate and cellulose laurate/PP composite because cellulose benzoate also had higher thermal decomposition temperature than esterified PW-MCC with alkyl chain. The decomposition temperature of cellulose benzoate did not concern on α -hydrogens as discussed in section 4.37 and results was similar to the literature [119]. In contrast, T_d of cellulose hexanoate/PP and cellulose laurate/PP composites was shifted towards lower temperature than the others. This reduction could be due to the alkyl chain group grafted on cellulose structure which contributed to the decreasing in the thermal stability of composites. Nevertheless, effect of alkyl chain length also affected in thermal decomposition temperature. As seen that cellulose

laurate/PP composites started to decompose at lower temperature than cellulose hexanoate/PP composites. The amount of char residue of esterified PW-MCC/PP composites was higher than that of PW-MCC/PP composite, implying that esterified cellulose could act as flame retardancy to polypropylene as well. Nevertheless, when the PW-MCC or modified PW-MCC content was increased, the $T_{d_{onset}}$ of the composites was shifted to lower temperature.

4.7.2 Differential scanning calorimetry of composites

Thermal properties in term of melting temperature (T_m), crystallization temperature (T_c), and degree of crystallinity (% X_c) were evaluated by differential scanning calorimetry (DSC). The DSC thermograms of cooling and second heating scans of PP and the obtained composite are presented in Figure 4.68 and the data are summarized in Table 4.25. It could be observed a single melting peak for all sample suggesting that only α (monoclinic) crystalline polymorph of PP is formed [159]. From Table 4.25, neat PP indicated T_m at 168.1°C while T_c was 125.6°C with crystallinity at 42.8%. The addition of PW-MCC and esterified PW-MCC did not significantly affect to the T_m of PP composites, except for silane treated PW-MCC/PP composites. In addition, an introduction of PW-MCC and PW-MCC with MAPP to PP matrix did not change the T_m and degree of crystallinity of PP.

In case of the silane treated PW-MCC/PP composites, the results displayed the reduction of T_m , T_c and degree crystallinity of PP upon increasing silane treated PW-MCC content. This reduction was due to a silane crosslink network in PP chain. The crosslink network altered the PP chain resulting in the reduction in the crystalline component implying an increase in the amorphous region [160].

Regarding to the esterified PW-MCC, the results revealed that the addition of this filler did not influence on the T_m and degree of crystallinity. However, it was surprisingly found that addition of cellulose laurate caused a dramatic reduction of T_c . This reduction was due to the hindered mobility of long alkyl chain attributing to the decrement in crystallization rate of PP [161]. Besides, the addition of cellulose benzoate and cellulose hexanoate at higher content also caused a decrease in the

crystallinity of PP because PP chain was obstructed by PW-MCC molecule particularly at 20 and 30wt% [162].

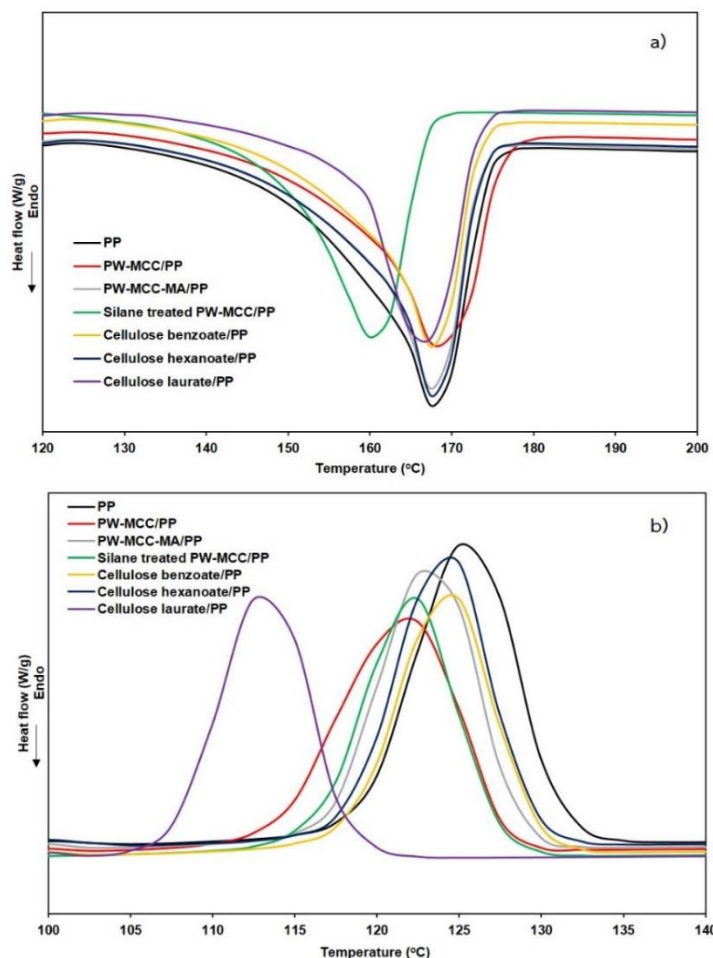


Figure 4.68 DSC thermograms of PP and PP composite at 10wt% a) second endothermic curve and b) first exothermic curve

Table 4.25 Melting and crystallization properties of PP and PP composites

Sample	MCC (wt%)	T _m (°C)	T _c (°C)	ΔH _f (J/m)	%X _c
PP	-	168.1	125.6	81.4	42.8
PW-MCC/PP	5	168.2	119.5	67.7	37.5
	10	168.0	122.1	70.4	41.2
	20	167.6	123.8	65.9	43.4
	30	167.7	124.6	56.4	42.4

Table 4.25 Melting and crystallization properties of PP and PP composites (continued)

Sample	MCC (wt%)	T _m (°C)	T _c (°C)	ΔH _f (J/m)	%X _c
PW-MCC-MCC/PP	5	167.7	124.0	73.8	40.9
	10	167.4	123.4	71.8	42.0
	20	167.0	124.5	63.9	42.0
	30	166.4	124.4	56.9	42.8
Silane treated PW-MCC/PP	5	163.4	123.4	77.2	42.8
	10	160.5	122.1	64.1	37.5
	20	156.5	119.2	57.3	37.7
	30	153.1	117.5	42.8	31.7
Cellulose benzoate/PP	5	167.7	125.0	79.9	44.2
	10	167.7	124.3	66.1	38.6
	20	168.0	123.2	65.1	42.8
	30	167.6	121.7	51.6	38.8
Cellulose hexanoate	5	167.6	124.3	73.9	41.0
	10	168.1	124.3	71.9	42.1
	20	167.1	124.1	59.3	39.1
	30	167.0	123.2	46.7	35.1
Cellulose laurate/PP	5	166.6	115.7	71.4	39.6
	10	166.5	113.4	60.4	35.3
	20	168.2	114.8	57.8	38.1
	30	166.9	116.2	56.1	42.2

4.7.3 Thermal expansion of composites

Thermal expansion is an important property in polymer composites for various applications. Thus, the relationship between PW-MCC content and coefficient of thermal expansion was evaluated and the results are displayed in Figure 4.69. As seen, comparing to neat PP matrix, a dramatic decrease of CTE values for PW-MCC/PP and PW-MCC-MA/PP composites could be observed. The addition of PW-MCC clearly presented the reduction of CTE value with increasing of PW-MCC content. The reduction of CTE value was assigned to the higher modulus of cellulosic fibers. In addition, cellulose has low CTE value around $0.1 (\mu\text{m}/\text{m})/^{\circ}\text{C}$ which could lead to lower CTE value of PP composites [163]. However, the CTE value of silane treated PW-MCC/PP composites gave a reverse trend to the aforementioned composites. An increment of silane treated PW-MCC content resulted in an increasing of CTE value. Obviously, based on the scope of this work, the highest CTE value was reached at 30wt% silane treated PW-MCC. This unexpected result difficult to discuss and needed to be further investigated. It might be due to low degree crystallinity of silane treated PW-MCC/PP composites. An increasing amorphous region was attributed to increase chain mobility of composite.

In the case of esterified PW-MCC/PP composites, the CTE value depended on the substituent grafted on PW-MCC surface. It could be explained that thermal expansion esterified cellulose was related to alkyl chain length. Normally, thermal expansion coefficient increased with an increasing alkyl chain length [164]. In addition, thermal expansion of hexanoate was higher than that of laureate [165]. At 5 and 10wt% esterified PW-MCC loading, all esterified cellulose/PP composites exhibited a continuous decrease of CTE than neat PP. This reduction of CTE values was because a good interfacial adhesion and dispersion of esterified cellulose in PP matrix resulting in a strong interaction restricted the mobility of the polymer chain [166]. Then, the CTE value was increased upon increasing the esterified PE-MCC content to 20 and 30 wt%. This phenomenon might be thermal expansion behavior of the substituent when using at higher content of cellulose ester.

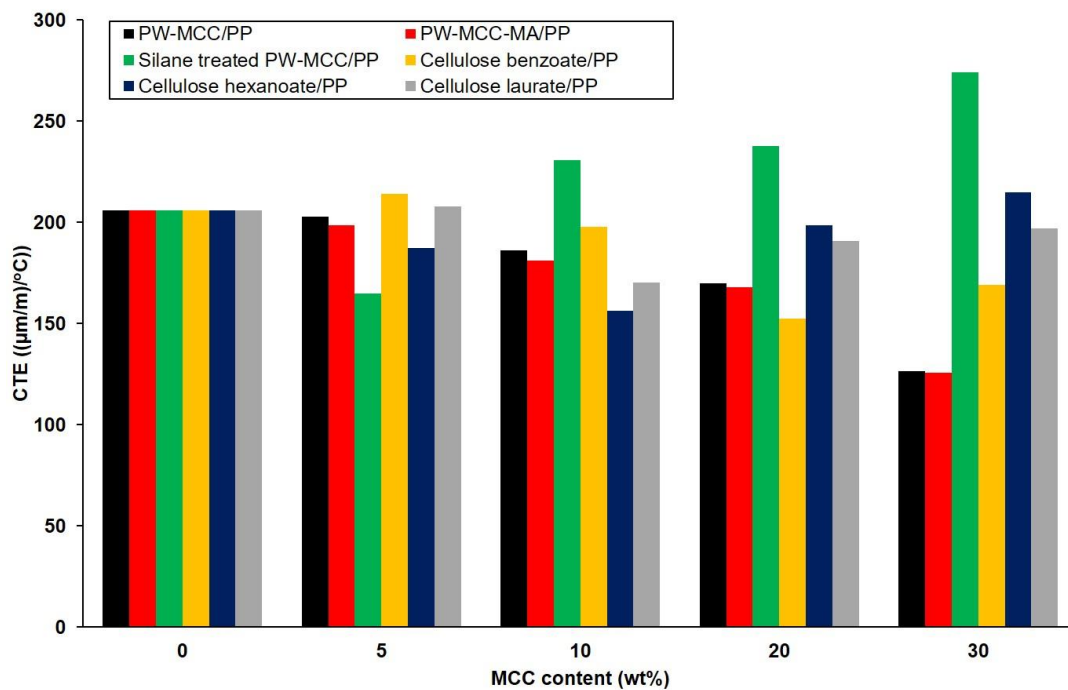


Figure 4.69 The coefficient of thermal expansion (CTE) of PP and PP composites



CHAPTER V

CONCLUSIONS

Microcrystalline cellulose was successfully prepared from parawood sawdust to obtain parawood microcrystalline cellulose (PW-MCC). Surface modification of PW-MCC was performed to enhance compatibility between PW-MCC and hydrophobic polymer matrix which was polypropylene (PP). The different chemical treatment methods on PW-MCC were performed such as using maleic anhydride grafted polypropylene (MA-G-PP), silanization, and esterification with 3 types of acid chloride. The properties of modified PW-MCC was evaluated. The different content of modified PW-MCC was added into PP matrix by an internal mixer and then fabricated into specimens by an injection molding. The properties of the obtained PP composites were characterized. The obtained results from each research part can be concluded as follows:

Part I: Preparation of PW-MCC

Microcrystalline cellulose was successfully prepared from parawood sawdust (PW) which was a waste from furniture factory via acid hydrolysis method. The results from FTIR analysis indicated that PW-MCC still had cellulose structure, while hemicellulose and lignin were removed during chemical treatment. The DP value of PW-MCC was lower when using sulfuric acid; meanwhile, increasing pulp to acid ratio from 1:10 to 1:15 and increasing temperature from 80 to 105°C also caused the reduction in the DP values as well. However, using higher temperature and longer reaction time led to the degradation of PW-MCC during acid hydrolysis. The optimum condition for hydrolysis parawood sawdust to obtain PW-MCC was using hydrochloric acid with pulp to acid ratio 1:15 at 80°C for 2 h. From the XRD patterns, PW-MCC exhibited cellulose type I with crystallinity index about 60%. This evidence also confirmed that acid hydrolysis did not change the cellulose structure. TGA analysis indicated that PW-MCC had better thermal stability than raw PW although using sulfuric acid yielded MCC with lower thermal stability due to the introduction of sulfate group

on cellulose chains. SEM micrographs revealed that PW-MCC was rod-like structure similar to the reference or commercial MCC

Part II: Surface modification of PW-MCC

Silane treatment on PW-MCC was successfully achieved by using mechanochemical process. The condition for modifying PW-MCC with organosilane was by using 20%wt vinyltrimethoxysilane and DCP as a catalyst at a ball milling speed of 400 rpm for 60 min which provided the highest percentage of silicon on PW-MCC surface. FTIR and XPS also confirmed the achievement of surface treatment. After silane treatment under mechanochemical process, the size of PW-MCC was decreased and its morphology was changed from smooth to rough surface.

Acylation of PW-MCC with acid chloride such as benzoyl chloride, hexanoyl chloride, and lauroyl chloride was successfully prepared. However, each of acid chloride provided the different degree of substitution and property of cellulose ester.

In the case of benzoyl chloride, the esterification reaction required only pyridine as a solvent. ¹H-NMR and FTIR techniques were used to confirm the success of esterified cellulose (cellulose benzoate). The optimum condition for esterifying PW-MCC was using benzoyl chloride/AGU ratio at 5 for 60 min which provided the maximum degree of substitution at 3.00. Moreover, using the longer milling time caused a reduction of DS value. The morphology of cellulose benzoate revealed rough surface and there was an aggregation of benzoyl substituent on PW-MCC surface. In addition, cellulose benzoate had higher thermal stability than unmodified PW-MCC

Cellulose hexanoate was obtained from esterification of PW-MCC with hexanoyl chloride at hexanoyl chloride/AGU ratio at 5 for 60 min under ball milling process. The maximum DS of cellulose hexanoate was 2.73. Nevertheless, the esterification of PW-MCC and hexanoyl chloride required dispersion media such as toluene to enhance reaction activity. Thermal stability of cellulose hexanoate was lower than PW-MCC. The morphology of cellulose hexanoate revealed an increase particle size after modification.

Cellulose laurate was prepared from esterification of PW-MCC with lauroyl chloride at lauroyl chloride/AGU ratio at 4 with toluene as dispersion media for 60 min under ball milling process. Cellulose laurate exhibited the lowest DS among esterified PW-MCC at 2.27 due to its steric hindrance. Cellulose laurate indicated slightly lower of thermal stability compared to PW-MCC. Nevertheless, the morphology of cellulose hexanoate displayed rough surface and there was an aggregation of lauroyl substituent on PW-MCC surface

Accordingly, the thermal stability of esterified cellulose could be ordered from high to low as cellulose benzoate, cellulose laurate, and cellulose hexanoate. Among them, using benzoyl chloride was the easiest esterification reaction that required no dispersion solvent while, the modification by hexanoyl chloride and lauroyl chloride needed to use toluene as a dispersion media to improve the esterification reaction. In addition, the difference in carbon chain length caused the difference in substitution ability. The DS value was reduced with an increasing of alkyl chain length.

Obviously, esterification of cellulose under ball milling process was an effective method which used less energy and solvent compared to conventional method. Mechanical force from ball milling process destroyed the structure providing the accessibility of cellulose structure to react with silane or acid chloride.

Part III: The properties of the composites

PW-MCC/PP and modified PW-MCC/PP composites were compounded at various PW-MCC contents of 5-30 wt%. The characterized properties can be listed as follows:

- The mechanical properties

PW-MCC was an effective reinforcing material for polypropylene. The stiffness of PW-MCC/PP composites was increased with increasing PW-MCC content. The addition MAPP into composite system resulting to an enhanced of the tensile and flexural properties. Tensile strength and flexural modulus of PW-MCC-MA composites at 30wt% PW-MCC loading was increased 24% and 10%, respectively. However, at high content

(30wt%) of PW-MCC showed an aggregation of PW-MCC in PP matrix. On the other hand, the tensile strength of silane treated PW-MCC at every loading gave the similar value which was increased upto 12%. However, silane treated PW-MCC/PP composites gave the lower elongation at break value compared to the others. Nevertheless, PP composite made from cellulose ester exhibited higher mechanical properties of when loading esterified PW-MCC at low content (at 5-10%). Tensile strength at 5wt% of cellulose benzoate/PP, cellulose hexanoate/PP, and cellulose laurate/PP composite were 5, 10, and 5%, respectively. Meanwhile, elongation at break of cellulose laurate/PP composite was significantly improved upto 21%. Moreover, the toughness of cellulose laurate/PP composite was increase 23%. In addition, using long chain fatty grafted on PW-MCC exhibited a plasticizing effect to composites resulting to the reduction of modulus of the composites. It could be noted that silane treated PW-MCC/PP and cellulose benzoate/PP composites exhibited the brittleness behavior due to lower elongation at break and impact strength.

- The physical properties

All PP composites had higher density than neat PP due to an incorporation of PW-MCC into PP matrix. Among them, cellulose ester/PP composites had the lower density than PW-MCC/PP composite. This reduction was due to the branching of fatty acid group grafted on cellulose structure. The addition of PW-MCC to in PP composites resulted in the reduction of MFI upon increasing PW-MCC content. The lowest of melt flow index was PW-MCC/PP composite while silane treated PW-MCC/PP composite exhibited the highest of melt flow index. In the case of cellulose ester/PP composites, the opposite results among cellulose ester/PP composites were obtained. The MFI values of cellulose benzoate/PP composites were slightly decreased when increasing amount of cellulose content, while cellulose hexanoate/PP and cellulose laurate/PP composites had higher of MFI values than neat PP. The SEM micrograph of modified PW-MCC/PP

composites displayed an improvement of interfacial adhesion and dispersion as evidenced by the decreased in gap and the increasing of rough surface. The water resistance of modified PW-MCC/PP composites were significantly increased when using cellulose ester/PP composites. The water resistance of cellulose cellulose benzoate/PP, cellulose hexanate/PP, and cellulose laurate/PP composite were increased approximately 68, 237, and 80%, respectively. Whereas, PW-MCC-MA/PP composites was increased approximately 17% which was similar to silane treated PW-MCC/PP composites. It can be concluded that surface modification had a beneficial effect on water resistance.

- Dynamic properties of the composites

Addition of PW-MCC to PP resulted to an increasing in the storage modulus of the PP composites. The greater enhancement of storage modulus belonged to PW-MCC/PP and PW-MCC-MA/PP composites because high crystallinity of PW-MCC was preserved. On the other hand, the modified PW-MCC under ball milling destroyed the crystallinity of PW-MCC leading to a slight increase of storage modulus. Nevertheless, plasticizing effect from fatty acid chain grafted on PW-MCC was affected as well. The $\tan \delta$ of PW-MCC/PP and PW-MCC-MA/PP composites was shifted towards higher temperature whereas the other modified PW-MCC presented that the $\tan \delta$ was similar to neat PP.

- Thermal properties of composites

Thermal properties of composites were improved when using modified PW-MCC. It could be concluded that enhancing of an interfacial adhesion between PW-MCC and PP attributed to the improvement in thermal stability. The addition of PW-MCC and esterified PW-MCC did not significantly affect to the T_m of PP composites, except for silane treated PW-MCC/PP composites. In addition, an introduction of PW-MCC and PW-MCC with MAPP to PP matrix did not change the T_c and degree of

crystallinity of PP. In case of the silane treated PW-MCC/PP composites, the results displayed the reduction of T_m , T_c and degree crystallinity of PP upon increasing silane treated PW-MCC content. However, it was surprisingly found that addition of cellulose laurate caused a dramatic reduction of T_c . The coefficient of thermal expansion dramatically decreased when adding PW-MCC and PW-MCC with MAPP to PP matrix according to the higher modulus of cellulosic fibers. However, the CTE value of silane treated PW-MCC/PP composites gave a reverse trend to the aforementioned composites. An increment of silane treated PW-MCC content resulted in an increasing of CTE value. At 5 and 10wt% esterified PW-MCC loading, all esterified cellulose/PP composites exhibited a continuous decrease of CTE than neat PP. Then, the CTE value was increased upon increasing the esterified PE-MCC content to 20 and 30 wt%.

REFERENCES

1. Spoljaric, S., Genovese, A. and Shanks, R.A., *Polypropylene–microcrystalline cellulose composites with enhanced compatibility and properties*. Composites Part A: Applied Science and Manufacturing, 2009. **40**(6): p. 791-799.
2. Sobczak, L., Lang, R.W. and Haider, A., *Polypropylene composites with natural fibers and wood – General mechanical property profiles*. Composites Science and Technology, 2012. **72**(5): p. 550-557.
3. Lu, T., Jiang, M., Jiang, Z., Hui, D., Wang, Z. and Zhou, Z., *Effect of surface modification of bamboo cellulose fibers on mechanical properties of cellulose/epoxy composites*. Composites Part B: Engineering, 2013. **51**: p. 28-34.
4. Ashori, A. and Nourbakhsh, A., *Performance properties of microcrystalline cellulose as a reinforcing agent in wood plastic composites*. Composites Part B: Engineering, 2010. **41**(7): p. 578-581.
5. Ghosh, P., *Polymer Science and Technology: Plastics, Rubbers, Blends and Composites*, . Third ed. 2011, New York: McGraw-Hill Education.
6. Zihlif, A.M. and Ragosta, G., *Mechanical properties of talc-polypropylene composites*. Materials Letters, 1991. **11**(10): p. 368-372.
7. Qiu, F., Wang, M., Hao, Y. and Guo, S., *The effect of talc orientation and transcrystallization on mechanical properties and thermal stability of the polypropylene/talc composites*. Composites Part A: Applied Science and Manufacturing, 2014. **58**: p. 7-15.
8. Hufenbach, W.A., Stelmakh, A., Kunze, K., Böhm, R. and Kupfer, R., *Tribomechanical properties of glass fibre reinforced polypropylene composites*. Tribology International, 2012. **49**: p. 8-16.
9. Billmeyer, F.W., *Textbook of Polymer Science*. Third ed. 1984, New York: John Wiley & Sons.
10. Maddah, H.A., *Polypropylene as a Promising Plastic: A Review*. American Journal of Polymer Science, 2016. **6**(1): p. 1-11.

11. *Type of polypropylene.* [cited 2018 April 6]; Available from: http://www.sangir.in/pro_pp_pipes.html.
12. Kabir, M.M., Wang, H., Lau, K.T. and Cardona, F., *Chemical treatments on plant-based natural fibre reinforced polymer composites: An overview.* Composites Part B: Engineering, 2012. **43**(7): p. 2883-2892.
13. Lee, K.-Y., Aitomäki, Y., Berglund, L.A., Oksman, K. and Bismarck, A., *On the use of nanocellulose as reinforcement in polymer matrix composites.* Composites Science and Technology, 2014. **105**: p. 15-27.
14. Haafiz, M.K.M., Hassan, A., Zakaria, Z., Inuwa, I.M., Islam, M.S. and Jawaid, M., *Properties of polylactic acid composites reinforced with oil palm biomass microcrystalline cellulose.* Carbohydrate Polymers, 2013. **98**(1): p. 139-145.
15. Mwaikambo, L.Y. and Ansell, M.P., *Chemical modification of hemp, sisal, jute, and kapok fibers by alkalization.* Journal of Applied Polymer Science 2002. **84**(12): p. 2222-2234.
16. Credou, J. and Berthelot, T., *Cellulose: from biocompatible to bioactive material.* Journal of Materials Chemistry B, 2014. **2**(30): p. 4767-4788.
17. Oudiani, A.E., Chaabouni, Y., Msahli, S. and Sakli, F., *Crystal transition from cellulose I to cellulose II in NaOH treated Agave americana L. fibre.* Carbohydrate Polymers, 2011. **86**(3): p. 1221-1229.
18. Bledzki, A.K. and Gassan, J., *Composites reinforced with cellulose based fibres.* Progress in Polymer Science, 1999. **24**(2): p. 221-274.
19. Morán, J.I., Alvarez, V.A., Cyras, V.P. and Vázquez, A., *Extraction of cellulose and preparation of nanocellulose from sisal fibers.* Cellulose, 2008. **15**(1): p. 149-159.
20. *Pectin structure.* [cited 2018 14 May]; Available from: <http://www1.lsbu.ac.uk/water/pectin.html>
21. Faruk, O., Bledzki, A.K., Fink, H.-P. and Sain, M., *Biocomposites reinforced with natural fibers: 2000–2010.* Progress in Polymer Science, 2012. **37**(11): p. 1552-1596.

22. Hosseinaei, O., Wang, S., Enayati, A.A. and Rials, T.G., *Effects of hemicellulose extraction on properties of wood flour and wood-plastic composites*. Composites Part A: Applied Science and Manufacturing, 2012. **43**(4): p. 686-694.
23. Wambua, P., Ivens, J. and Verpoest, I., *Natural fibres: can they replace glass in fibre reinforced plastics?* Composites Science and Technology, 2003. **63**(9): p. 1259-1264.
24. Doan, T.-T.-L., Brodowsky, H. and Mäder, E., *Jute fibre/polypropylene composites II. Thermal, hydrothermal and dynamic mechanical behaviour*. Composites Science and Technology, 2007. **67**(13): p. 2707-2714.
25. Yang, H.-S., Kim, H.-J., Park, H.-J., Lee, B.-J. and Hwang, T.-S., *Effect of compatibilizing agents on rice-husk flour reinforced polypropylene composites*. Composite Structures, 2007. **77**(1): p. 45-55.
26. Kuo, P.-Y., Wang, S.-Y., Chen, J.-H., Hsueh, H.-C. and Tsai, M.-J., *Effects of material compositions on the mechanical properties of wood-plastic composites manufactured by injection molding*. Materials & Design, 2009. **30**(9): p. 3489-3496.
27. Singh, S., Deepak, D., Aggarwal, L. and Gupta, V.K., *Tensile and Flexural Behavior of Hemp Fiber Reinforced Virgin-recycled HDPE Matrix Composites*. Procedia Materials Science, 2014. **6**: p. 1696-1702.
28. Kurdthongmee, W., *Colour classification of rubberwood boards for fingerjoint manufacturing using a SOM neural network and image processing*. Computers and Electronics in Agriculture, 2008. **64**(2): p. 85-92.
29. Hengniran, P., *Future potential of Forest and Agriculture Residues for the energy production in Thailand – Strategies for a better utilization*, in *Faculty of Mathematics, Informatics and Natural Sciences*. 2010, University of Hamburg.
30. Boerhendy, H.I., Agustina, D.S. and Suryaningtyas, H. *Basic Characteristics of Rubber Wood for Some Recommended Clones in Indonesia*. in *IRRDB Annual Meeting and International Rubber Conference 2010*. 2010. Hainan.
31. Prachasaree, W., Limkatanyu, S. and Hawa, A., *Parawood particle cement composite boards under accelerated wet/dry cycling and natural aging*. Journal of Sustainable Cement-Based Materials, 2013. **2**(3-4): p. 227-237.

32. Rimdusit, S., Kampangsaeree, N., Tanthapanichakoon, W., Takeichi, T. and Suppakarn, N., *Development of wood-substituted composites from highly filled polybenzoxazine-phenolic novolac alloys*. Polymer Engineering and Science 2007. **47**(2): p. 140-149.
33. Abdul Khalil, H.P.S., Davoudpour, Y., Islam, M.N., Mustapha, A., Sudesh, K., Dungani, R. and Jawaid, M., *Production and modification of nanofibrillated cellulose using various mechanical processes: A review*. Carbohydrate Polymers, 2014. **99**: p. 649-665.
34. Rosa, M.F., Medeiros, E.S., Malmonge, J.A., Gregorski, K.S., Wood, D.F., Mattoso, L.H.C., Glenn, G., Orts, W.J. and Imam, S.H., *Cellulose nanowhiskers from coconut husk fibers: Effect of preparation conditions on their thermal and morphological behavior*. Carbohydrate Polymers, 2010. **81**(1): p. 83-92.
35. Ferreira, F.V., Pinheiro, I.F., Gouveia, R.F., Thim, G.P. and L.M.F., L., *Functionalized cellulose nanocrystals as reinforcement in biodegradable polymer nanocomposites*. Polymer Composites 2017. **39**(51): p. 1-21.
36. Mendes, C.A.d.C., Ferreira, N.M.S., Furtado, C.R.G. and de Sousa, A.M.F., *Isolation and characterization of nanocrystalline cellulose from corn husk*. Materials Letters, 2015. **148**: p. 26-29.
37. Lamaming, J., Hashim, R., Leh, C.P., Sulaiman, O., Sugimoto, T. and Nasir, M., *Isolation and characterization of cellulose nanocrystals from parenchyma and vascular bundle of oil palm trunk (*Elaeis guineensis*)*. Carbohydrate Polymers, 2015. **134**: p. 534-540.
38. Adel, A.M., Abd El-Wahab, Z.H., Ibrahim, A.A. and Al-Shemy, M.T., *Characterization of microcrystalline cellulose prepared from lignocellulosic materials. Part II: Physicochemical properties*. Carbohydrate Polymers, 2011. **83**(2): p. 676-687.
39. Parakilar, K.M. and Bhatawdekar, S.P., *Microcrystalline cellulose from Bagasse pulp*. Biological Wastes, 1988. **24**(1): p. 75-77.
40. Trache, D., Hussin, M.H., Hui Chuin, C.T., Sabar, S., Fazita, M.R.N., Taiwo, O.F.A., Hassan, T.M. and Haafiz, M.K.M., *Microcrystalline cellulose: Isolation,*

- characterization and bio-composites application—A review*. International Journal of Biological Macromolecules, 2016. **93**: p. 789-804.
41. El-Sakhawy, M. and Hassan, M.L., *Physical and mechanical properties of microcrystalline cellulose prepared from agricultural residues*. Carbohydrate Polymers, 2007. **67**(1): p. 1-10.
 42. Ejikeme, P.M., *Investigation of the physicochemical properties of microcrystalline cellulose from agricultural wastes I: orange mesocarp*. Cellulose, 2008. **15**(1): p. 141-147.
 43. Das, K., Ray, D., Bandyopadhyay, N.R., Ghosh, T., Mohanty, A.K. and Misra, M., *A study of the mechanical, thermal and morphological properties of microcrystalline cellulose particles prepared from cotton slivers using different acid concentrations*. Cellulose, 2009. **16**(5): p. 783-793.
 44. Wang, D., Shang, S.-b., Song, Z.-q. and Lee, M.-K., *Evaluation of microcrystalline cellulose prepared from kenaf fibers*. Journal of Industrial and Engineering Chemistry, 2010. **16**(1): p. 152-156.
 45. Keshk, S.M.A.S. and Haija, M.A., *A new method for producing microcrystalline cellulose from Gluconacetobacter xylinus and kenaf*. Carbohydrate Polymers, 2011. **84**(4): p. 1301-1305.
 46. Zhao, T., Chen, Z., Lin, X., Ren, Z., Li, B. and Zhang, Y., *Preparation and characterization of microcrystalline cellulose (MCC) from tea waste*. Carbohydrate Polymers, 2018. **184**: p. 164-170.
 47. Petersson, L. and Oksman, K., *Biopolymer based nanocomposites: Comparing layered silicates and microcrystalline cellulose as nanoreinforcement*. Composites Science and Technology, 2006. **66**(13): p. 2187-2196.
 48. Chuayjuljit, S., Su-uthai, S. and Charuchinda, S., *Poly(vinyl chloride) film filled with microcrystalline cellulose prepared from cotton fabric waste: properties and biodegradability study*. Waste Management & Research, 2009. **28**(2): p. 109-117.
 49. Izzati Zulkifli, N., Samat, N., Anuar, H. and Zainuddin, N., *Mechanical properties and failure modes of recycled polypropylene/microcrystalline cellulose composites*. Materials & Design, 2015. **69**: p. 114-123.

50. Sepe, R., Bollino, F., Boccarusso, L. and Caputo, F., *Influence of chemical treatments on mechanical properties of hemp fiber reinforced composites*. Composites Part B: Engineering, 2018. **133**: p. 210-217.
51. Hodzic, A. and Shanks, R., *Natural Fibre Composites Materials, Processes and Properties*. 2013.
52. Fang, J.M., Sun, R.C., Tomkinson, J. and Fowler, P., *Acetylation of wheat straw hemicellulose B in a new non-aqueous swelling system*. Carbohydrate Polymers, 2000. **41**(4): p. 379-387.
53. Li, X., Tabil, L.G. and Panigrahi, S., *Chemical Treatments of Natural Fiber for Use in Natural Fiber-Reinforced Composites: A Review*. Journal of Polymers and the Environment, 2007. **15**(1): p. 25-33.
54. Çetin, N.S., Tingaut, P., Özmen, N., Henry, N., Harper, D., Dadmun, M. and Sèbe, G., *Acetylation of Cellulose Nanowhiskers with Vinyl Acetate under Moderate Conditions*. Macromolecular Bioscience, 2009. **9**(10): p. 997-1003.
55. Labafzadeh, S.R., Kavakka, J.S., Sievänen, K., Asikkala, J. and Kilpeläinen, I., *Reactive dissolution of cellulose and pulp through acylation in pyridine*. Cellulose, 2012. **19**(4): p. 1295-1304.
56. Corrales, F., Vilaseca, F., Llop, M., Gironès, J., Méndez, J.A. and Mutjè, P., *Chemical modification of jute fibers for the production of green-composites*. Journal of Hazardous Materials, 2007. **144**(3): p. 730-735.
57. Ratanakamnuan, U., Atong, D. and Aht-Ong, D., *Cellulose esters from waste cotton fabric via conventional and microwave heating*. Carbohydrate Polymers, 2012. **87**(1): p. 84-94.
58. Zhang, J., Wu, J., Cao, Y., Sang, S., Zhang, J. and He, J., *Synthesis of cellulose benzoates under homogeneous conditions in an ionic liquid*. Cellulose, 2009. **16**(2): p. 299-308.
59. Yuan, T.-Q., Zhang, L.-M., Xu, F. and Sun, R.-C., *Enhanced photostability and thermal stability of wood by benzylation in an ionic liquid system*. Industrial Crops and Products, 2013. **45**: p. 36-43.

60. Xie, Y., Hill, C.A.S., Xiao, Z., Militz, H. and Mai, C., *Silane coupling agents used for natural fiber/polymer composites: A review*. Composites Part A: Applied Science and Manufacturing, 2010. **41**(7): p. 806-819.
61. Brochier Salon, M.-C., Abdelmouleh, M., Boufi, S., Belgacem, M.N. and Gandini, A., *Silane adsorption onto cellulose fibers: Hydrolysis and condensation reactions*. Journal of Colloid and Interface Science, 2005. **289**(1): p. 249-261.
62. Loof, D., Hiller, M., Oschkinat, H. and Koschek, K., *Quantitative and qualitative analysis of surface modified cellulose utilizing TGA-MS*. Materials, 2016. **9**(6): p. 415-429.
63. Valadez-Gonzalez, A., Cervantes-Uc, J.M., Olayo, R. and Herrera-Franco, P.J., *Chemical modification of henequén fibers with an organosilane coupling agent*. Composites Part B: Engineering, 1999. **30**(3): p. 321-331.
64. Abdelmouleh, M., Boufi, S., Belgacem, M.N., Duarte, A.P., Ben Salah, A. and Gandini, A., *Modification of cellulosic fibres with functionalised silanes: development of surface properties*. International Journal of Adhesion and Adhesives, 2004. **24**(1): p. 43-54.
65. Zhou, F., Cheng, G. and Jiang, B., *Effect of silane treatment on microstructure of sisal fibers*. Applied Surface Science, 2014. **292**: p. 806-812.
66. Keener, T.J., Stuart, R.K. and Brown, T.K., *Maleated coupling agents for natural fibre composites*. Composites Part A: Applied Science and Manufacturing, 2004. **35**(3): p. 357-362.
67. Pickering, K.L., Efendy, M.G.A. and Le, T.M., *A review of recent developments in natural fibre composites and their mechanical performance*. Composites Part A: Applied Science and Manufacturing, 2016. **83**: p. 98-112.
68. Conzatti, L., Giunco, F., Stagnaro, P., Patrucco, A., Tonin, C., Marano, C., Rink, M. and Marsano, E., *Wool fibres functionalised with a silane-based coupling agent for reinforced polypropylene composites*. Composites Part A: Applied Science and Manufacturing, 2014. **61**: p. 51-59.
69. Zahari, W.Z.W., Badri, R.N.R.L., Ardyananta, H., Kurniawan, D. and Nor, F.M., *Mechanical Properties and Water Absorption Behavior of Polypropylene / Ijuk*

- Fiber Composite by Using Silane Treatment*. Procedia Manufacturing, 2015. **2**: p. 573-578.
70. Aht-Ong, D. and Puttana, T., *Effects of surface modifications on mechanical properties of polypropylene/newspaper pulp composites*. Journal of scientific research, Chulalongkorn University, 2002. **27**(1): p. 25-42.
71. Suchaiya, V. and Aht-Ong, D., *Microwave-assisted modification of cellulose as a compatibilizer for PLA and MCC biocomposite film: Effects of side chain length and content on mechanical and thermal Properties*. Polymers & Polymer Composites 2014. **22**(7): p. 613-624.
72. Niu, Y., Zhang, X., He, X., Zhao, J., Zhang, W. and Lu, C., *Effective dispersion and crosslinking in PVA/cellulose fiber biocomposites via solid-state mechanochemistry*. International Journal of Biological Macromolecules, 2015. **72**: p. 855-861.
73. Baláž, M., *Ball milling of eggshell waste as a green and sustainable approach: A review*. Advances in Colloid and Interface Science, 2018. **256**: p. 256-275.
74. Boldyreva, E., *Mechanochemistry of inorganic and organic systems: what is similar, what is different?* Chemical Society Reviews, 2013. **42**(18): p. 7719-7738.
75. Lin, Z., Huang, H., Zhang, H., Zhang, L., Yan, L. and Chen, J., *Ball Milling Pretreatment of Corn Stover for Enhancing the Efficiency of Enzymatic Hydrolysis*. Applied Biochemistry and Biotechnology, 2010. **162**(7): p. 1872-1880.
76. Lu, Q., Lin, W., Tang, L., Wang, S., Chen, X. and Huang, B., *A mechanochemical approach to manufacturing bamboo cellulose nanocrystals*. Journal of Materials Science, 2015. **50**(2): p. 611-619.
77. Burmeister, C., Titscher, L., Breitung-Faes, S. and Kwade, A., *Dry grinding in planetary ball mills: Evaluation of a stressing model*. Advanced Powder Technology, 2018. **29**(1): p. 191-201.
78. *Planetary ball mill* [cited 2018 April 24]; Available from: <http://www4.plala.or.jp/nagaosystem/planetbrochureE.html>.
79. Zhang, W., Zhang, X., Liang, M. and Lu, C., *Mechanochemical preparation of surface-acetylated cellulose powder to enhance mechanical properties of*

- cellulose-filler-reinforced NR vulcanizates*. Composites Science and Technology, 2008. **68**(12): p. 2479-2484.
80. Avolio, R., Bonadies, I., Capitani, D., Errico, M.E., Gentile, G. and Avella, M., *A multitechnique approach to assess the effect of ball milling on cellulose*. Carbohydrate Polymers, 2012. **87**(1): p. 265-273.
81. Zhang, Y., Gan, T., Li, Q., Su, J., Lin, Y., Wei, Y., Huang, Z. and Yang, M., *Mechanical and interfacial properties of poly(vinyl chloride) based composites reinforced by cassava stillage residue with different surface treatments*. Applied Surface Science, 2014. **314**: p. 603-609.
82. Brindha, D., Vinodhini, S. and Alarmelumangai, K., *Fiber dimension and chemical content of fiber from PASSIFLORA FOETIDA, L. and their suitability in paper production*. Science Research Reporter, 2012. **2**(3): p. 210-219
83. Segal, L., Creely, J.J., Martin, A.E. and Conrad, C.M., *An Empirical Method for Estimating the Degree of Crystallinity of Native Cellulose Using the X-Ray Diffractometer*. Textile Research Journal, 1959. **29**(10): p. 786-794.
84. Goodlett, V.W., Dougherty, J.T. and Patton, H.W., *Characterization of cellulose acetates by nuclear magnetic resonance*. Journal of Polymer Science Part A: Polymer Chemistry 1971. **9**(1): p. Pages 155-161.
85. Satgé, C., Granet, R., Verneuil, B., Branland, P. and Krausz, P., *Synthesis and properties of biodegradable plastic films obtained by microwave-assisted cellulose acylation in homogeneous phase*. Comptes Rendus Chimie, 2004. **7**(2): p. 135-142.
86. Keenan, M.J., Hegsted, M., Jones, K.L., Delany, J.P., Kime, J.C., Melancon, L.E., Tulley, R.T. and Hong, K.D., *Comparison of bone density measurement techniques: DXA and Archimedes' principle*. Journal of bone and Mineral Research 1997. **12**(1): p. 1903-1907.
87. Roy, S.B., Ramaraj, B., Shit, S.C. and Nayak, S.K., *Polypropylene and potato starch biocomposites: Physicomechanical and thermal properties*. Journal of Applied Polymer Science, 2011. **120**(5): p. 3078-3086.

88. *Thermomechanical analyzer (TMA)*. [cited 2017 March 6]; Available from: <http://www.labwrench.com/?equipment.view/equipmentNo/7523/METTLER-TOLEDO/TMA-SDTA841e/>.
89. Vanhatalo, K.M. and Dahl, O.P., *Effect of mild acid hydrolysis parameters on properties of microcrystalline cellulose*. *Bioresource Technology* 2014. **9**(3): p. 4729-4740.
90. Mohamad Haafiz, M.K., Eichhorn, S.J., Hassan, A. and Jawaid, M., *Isolation and characterization of microcrystalline cellulose from oil palm biomass residue*. *Carbohydrate Polymers*, 2013. **93**(2): p. 628-634.
91. Alemdar, A. and Sain, M., *Isolation and characterization of nanofibers from agricultural residues – Wheat straw and soy hulls*. *Bioresource Technology*, 2008. **99**(6): p. 1664-1671.
92. Ibrahim, M.M., Agblevor, F.A. and El-Zawawy, W.K., *ISOLATION AND CHARACTERIZATION OF CELLULOSE AND LIGNIN FROM STEAM-EXPLODED LIGNOCELLULOSIC BIOMASS*. *BioResources*; Vol 5, No 1 (2010), 2010.
93. Li, J., Qiang, D., Zhang, M., Xiu, H. and Zhang, X., *Joint action of ultrasonic and Fe³⁺ to improve selectivity of acid hydrolysis for microcrystalline cellulose*. *Carbohydrate Polymers*, 2015. **129**: p. 44-49.
94. Camacho, F., González-Tello, P., Jurado, E. and Robles, A., *Microcrystalline - cellulose hydrolysis with concentrated sulphuric acid*. *Journal of Chemical Technology & Biotechnology* 1996. **67**(4): p. 350-356.
95. Håkansson, H. and Ahlgren, P., *Acid hydrolysis of some industrial pulps: effect of hydrolysis conditions and raw material*. *Cellulose*, 2005. **12**(2): p. 177-183.
96. Karim, M.Z., Chowdhury, Z.Z., Hamid, S.B.A. and Ali, M.E., *Statistical optimization for acid hydrolysis of microcrystalline cellulose and its physiochemical characterization by using metal ion catalyst*. *Materials*, 2014. **13**(7): p. 6982-6999.
97. Sonia, A. and Priya Dasan, K., *Chemical, morphology and thermal evaluation of cellulose microfibrils obtained from Hibiscus sabdariffa*. *Carbohydrate Polymers*, 2013. **92**(1): p. 668-674.

98. Cherian, B.M., Leão, A.L., de Souza, S.F., Thomas, S., Pothan, L.A. and Kottaisamy, M., *Isolation of nanocellulose from pineapple leaf fibres by steam explosion*. Carbohydrate Polymers, 2010. **81**(3): p. 720-725.
99. Jeske, H., Schirp, A. and Cornelius, F., *Development of a thermogravimetric analysis (TGA) method for quantitative analysis of wood flour and polypropylene in wood plastic composites (WPC)*. Thermochemica Acta, 2012. **543**: p. 165-171.
100. Abraham, E., Deepa, B., Pothan, L.A., Jacob, M., Thomas, S., Cvelbar, U. and Anandjiwala, R., *Extraction of nanocellulose fibrils from lignocellulosic fibres: A novel approach*. Carbohydrate Polymers, 2011. **86**(4): p. 1468-1475.
101. Jakab, E., Várhegyi, G. and Faix, O., *Thermal decomposition of polypropylene in the presence of wood-derived materials*. Journal of Analytical and Applied Pyrolysis, 2000. **56**(2): p. 273-285.
102. Xiong, R., Zhang, X., Tian, D., Zhou, Z. and Lu, C., *Comparing microcrystalline with spherical nanocrystalline cellulose from waste cotton fabrics*. Cellulose, 2012. **19**(4): p. 1189-1198.
103. Bouchard, J., Abatzoglou, N., Chornet, E. and Overend, R.P., *Characterization of depolymerized cellulosic residues*. Wood Science and Technology, 1989. **23**(4): p. 343-355.
104. Jahan, M.S., Saeed, A., He, Z. and Ni, Y., *Jute as raw material for the preparation of microcrystalline cellulose*. Cellulose, 2011. **18**(2): p. 451-459.
105. Mandal, A. and Chakrabarty, D., *Isolation of nanocellulose from waste sugarcane bagasse (SCB) and its characterization*. Carbohydrate Polymers, 2011. **86**(3): p. 1291-1299.
106. Jonoobi, M., Khazaeian, A., Tahir, P.M., Azry, S.S. and Oksman, K., *Characteristics of cellulose nanofibers isolated from rubberwood and empty fruit bunches of oil palm using chemo-mechanical process*. Cellulose, 2011. **18**(4): p. 1085-1095.
107. Yuan, X., Liu, S., Feng, G., Liu, Y., Li, Y., Lu, H. and Liang, B., *Effects of ball milling on structural changes and hydrolysis of lignocellulosic biomass in liquid hot-*

- water compressed carbon dioxide*. Korean Journal of Chemical Engineering, 2016. **33**(7): p. 2134-2141.
108. Jandas, P.J., Mohanty, S. and Nayak, S.K., *Surface treated banana fiber reinforced poly (lactic acid) nanocomposites for disposable applications*. Journal of Cleaner Production, 2013. **52**: p. 392-401.
109. Fang, L., Chang, L., Guo, W.-j., Chen, Y. and Wang, Z., *Influence of silane surface modification of veneer on interfacial adhesion of wood-plastic plywood*. Applied Surface Science, 2014. **288**: p. 682-689.
110. Stark, N.M. and Matuana, L.M., *Characterization of weathered wood-plastic composite surfaces using FTIR spectroscopy, contact angle, and XPS*. Polymer Degradation and Stability, 2007. **92**(10): p. 1883-1890.
111. Ly, B., Belgacem, M.N., Bras, J. and Brochier Salon, M.C., *Grafting of cellulose by fluorine-bearing silane coupling agents*. Materials Science and Engineering: C, 2010. **30**(3): p. 343-347.
112. Chen, J., Wu, D., Tam, K.C., Pan, K. and Zheng, Z., *Effect of surface modification of cellulose nanocrystal on nonisothermal crystallization of poly(β -hydroxybutyrate) composites*. Carbohydrate Polymers, 2017. **157**: p. 1821-1829.
113. Thakur, M.K., Gupta, R.K. and Thakur, V.K., *Surface modification of cellulose using silane coupling agent*. Carbohydrate Polymers, 2014. **111**: p. 849-855.
114. Acemoglu, M., Küsters, E., Baumann, J., Hernandez, I. and Mak, C.P., *Synthesis of regioselectively substituted cellulose derivatives and applications in chiral chromatography*. Chirality, 1998. **10**(4): p. 294-306.
115. Prakash, G.K. and Mahadevan, K.M., *Enhancing the properties of wood through chemical modification with palmitoyl chloride*. Applied Surface Science, 2008. **254**(6): p. 1751-1756.
116. Dominkovics, Z., Dányádi, L. and Pukánszky, B., *Surface modification of wood flour and its effect on the properties of PP/wood composites*. Composites Part A: Applied Science and Manufacturing, 2007. **38**(8): p. 1893-1901.
117. Yamashita, Y. and Endo, T., *Deterioration behavior of cellulose acetate films in acidic or basic aqueous solutions*. Journal of Applied Polymer Science, 2004. **91**(5): p. 3354-3361.

118. Pinheiro, I.F., Ferreira, F.V., Souza, D.H.S., Gouveia, R.F., Lona, L.M.F., Morales, A.R. and Mei, L.H.I., *Mechanical, rheological and degradation properties of PBAT nanocomposites reinforced by functionalized cellulose nanocrystals*. European Polymer Journal, 2017. **97**: p. 356-365.
119. Agustin, M.B., Nakatsubo, F. and Yano, H., *Improving the thermal stability of wood-based cellulose by esterification*. Carbohydrate Polymers, 2018. **192**: p. 28-36.
120. Fundador, N.G.V., Enomoto-Rogers, Y., Takemura, A. and Iwata, T., *Syntheses and characterization of xylan esters*. Polymer, 2012. **53**(18): p. 3885-3893.
121. Samaranayake, G. and Glasser, W.G., *Cellulose derivatives with low DS. II. Analysis of alkanoates*. Carbohydrate Polymers, 1993. **22**(2): p. 79-86.
122. Wei, Y., Cheng, F. and Hou, G., *Synthesis and properties of fatty acid esters of cellulose*. Journal of Scientific & Industrial Research, 2007. **66**: p. 1019-1024.
123. Vaca-Garcia, C. and Borredon, M.E., *Solvent-free fatty acylation of cellulose and lignocellulosic wastes. Part 2: reactions with fatty acids* The first paper of this series is: Thiebaud, S., Borredon, M.E., 1995. *Solvent-free wood esterification with fatty acid chlorides*. Bioresour. Technol., 52, 169-173.1. Bioresource Technology, 1999. **70**(2): p. 135-142.
124. Leszczyńska, A., Stafin, K., Pagacz, J., Mičušík, M., Omastova, M., Hebda, E., Pielichowski, J., Borschneck, D., Rose, J. and Pielichowski, K., *The effect of surface modification of microfibrillated cellulose (MFC) by acid chlorides on the structural and thermomechanical properties of biopolyamide 4.10 nanocomposites*. Industrial Crops and Products, 2018. **116**: p. 97-108.
125. Freire, C.S.R., Silvestre, A.J.D., Neto, C.P., Belgacem, M.N. and Gandini, A., *Controlled heterogeneous modification of cellulose fibers with fatty acids: Effect of reaction conditions on the extent of esterification and fiber properties*. Journal of Applied Polymer Science, 2006. **100**(2): p. 1093-1102.
126. Jandura, P., Riedl, B. and Kokta, B.V., *Thermal degradation behavior of cellulose fibers partially esterified with some long chain organic acids*. Polymer Degradation and Stability, 2000. **70**(3): p. 387-394.

127. Uschanov, P., Johansson, L.-S., Maunu, S.L. and Laine, J., *Heterogeneous modification of various celluloses with fatty acids*. Cellulose, 2011. **18**(2): p. 393-404.
128. Wen, X., Wang, H., Wei, Y., Wang, X. and Liu, C., *Preparation and characterization of cellulose laurate ester by catalyzed transesterification*. Carbohydrate Polymers, 2017. **168**: p. 247-254.
129. Winkler, H., Vorwerg, W. and Wetzel, H., *Synthesis and properties of fatty acid starch esters*. Carbohydrate Polymers, 2013. **98**(1): p. 208-216.
130. Almasi, H., Ghanbarzadeh, B., Dehghannia, J., Pirsá, S. and Zandi, M., *Heterogeneous modification of softwoods cellulose nanofibers with oleic acid: Effect of reaction time and oleic acid concentration*. Fibers and Polymers, 2015. **16**(8): p. 1715-1722.
131. Vanmarcke, A., Leroy, L., Stoclet, G., Duchatel-Crépy, L., Lefebvre, J.-M., Joly, N. and Gaucher, V., *Influence of fatty chain length and starch composition on structure and properties of fully substituted fatty acid starch esters*. Carbohydrate Polymers, 2017. **164**: p. 249-257.
132. Vuoti, S., Talja, R., Johansson, L.-S., Heikkinen, H. and Tammelin, T., *Solvent impact on esterification and film formation ability of nanofibrillated cellulose*. Cellulose, 2013. **20**(5): p. 2359-2370.
133. Agustin, M.B., Nakatsubo, F. and Yano, H., *Products of low-temperature pyrolysis of nanocellulose esters and implications for the mechanism of thermal stabilization*. Cellulose, 2016. **23**(5): p. 2887-2903.
134. Dányádi, L., Janecska, T., Szabó, Z., Nagy, G., Móczó, J. and Pukánszky, B., *Wood flour filled PP composites: Compatibilization and adhesion*. Composites Science and Technology, 2007. **67**(13): p. 2838-2846.
135. Robles, E., Urruzola, I., Labidi, J. and Serrano, L., *Surface-modified nano-cellulose as reinforcement in poly(lactic acid) to conform new composites*. Industrial Crops and Products, 2015. **71**: p. 44-53.
136. Kaewkuk, S., Sutapun, W. and Jarukumjorn, K., *Effects of interfacial modification and fiber content on physical properties of sisal fiber/polypropylene composites*. Composites Part B: Engineering, 2013. **45**(1): p. 544-549.

137. Kim, H.-S., Kim, S., Kim, H.-J. and Yang, H.-S., *Thermal properties of bio-flour-filled polyolefin composites with different compatibilizing agent type and content*. *Thermochimica Acta*, 2006. **451**(1): p. 181-188.
138. Chauvelon, G., Gergaud, N., Saulnier, L., Lourdin, D., Buléon, A., Thibault, J.F. and Krausz, P., *Esterification of cellulose-enriched agricultural by-products and characterization of mechanical properties of cellulosic films*. *Carbohydrate Polymers*, 2000. **42**(4): p. 385-392.
139. Lim, H. and Hoag, S.W., *Plasticizer Effects on Physical–Mechanical Properties of Solvent Cast Soluplus® Films*. *AAPS PharmSciTech*, 2013. **14**(3): p. 903-910.
140. Joseph, K., Thomas, S. and Pavithran, C., *Effect of chemical treatment on the tensile properties of short sisal fibre-reinforced polyethylene composites*. *Polymer*, 1996. **37**(23): p. 5139-5149.
141. Salemane, M.G. and Luyt, A.S., *Thermal and mechanical properties of polypropylene–wood powder composites*. *Journal of Applied Polymer Science* 2006. **100**(5): p. 4173-4180.
142. Kuan, C.-F., Kuan, H.-C., Ma, C.-C.M. and Huang, C.-M., *Mechanical, thermal and morphological properties of water-crosslinked wood flour reinforced linear low-density polyethylene composites*. *Composites Part A: Applied Science and Manufacturing*, 2006. **37**(10): p. 1696-1707.
143. *Elastic modulus of rubber wood*. [cited 2018 June 18]; Available from: <http://www.wood-database.com/rubberwood/>.
144. Oksman, K. and Clemons, C., *Mechanical properties and morphology of impact modified polypropylene–wood flour composites*. *Journal of Applied Polymer Science*, 1998. **67**(9): p. 1503-1513.
145. Bengtsson, M., Baillif, M.L. and Oksman, K., *Extrusion and mechanical properties of highly filled cellulose fibre–polypropylene composites*. *Composites Part A: Applied Science and Manufacturing*, 2007. **38**(8): p. 1922-1931.
146. Ichazo, M.N., Albano, C., González, J., Perera, R. and Candal, M.V., *Polypropylene/wood flour composites: treatments and properties*. *Composite Structures*, 2001. **54**(2): p. 207-214.

147. Wei, L., McDonald, A.G., Freitag, C. and Morrell, J.J., *Effects of wood fiber esterification on properties, weatherability and biodurability of wood plastic composites*. Polymer Degradation and Stability, 2013. **98**(7): p. 1348-1361.
148. Wu, L., Lu, S., Pan, L., Luo, Q., Yang, J., Hou, L., Li, Y. and Yu, J., *Enhanced thermal and mechanical properties of polypropylene composites with hyperbranched polyester grafted sisal microcrystalline*. Fibers and Polymers, 2016. **17**(12): p. 2153-2161.
149. Xu, Y., You, M. and Qu, J., *Melt rheology of poly (lactic acid) plasticized by epoxidized soybean oil*. Wuhan University Journal of Natural Sciences, 2009. **14**(4): p. 349-354.
150. Haque, M.M., Ali, M.E., Hasan, M., Islam, M.N. and Kim, H., *Chemical Treatment of Coir Fiber Reinforced Polypropylene Composites*. Industrial & Engineering Chemistry Research, 2012. **51**(10): p. 3958-3965.
151. Abdelmouleh, M., Boufi, S., Belgacem, M.N. and Dufresne, A., *Short natural-fibre reinforced polyethylene and natural rubber composites: Effect of silane coupling agents and fibres loading*. Composites Science and Technology, 2007. **67**(7): p. 1627-1639.
152. Krishnan K, A., Jose, C., K. R, R. and George, K.E., *Sisal nanofibril reinforced polypropylene/polystyrene blends: Morphology, mechanical, dynamic mechanical and water transmission studies*. Industrial Crops and Products, 2015. **71**: p. 173-184.
153. Datta, J. and Kopczyńska, P., *Effect of kenaf fibre modification on morphology and mechanical properties of thermoplastic polyurethane materials*. Industrial Crops and Products, 2015. **74**: p. 566-576.
154. Pothan, L.A., Oommen, Z. and Thomas, S., *Dynamic mechanical analysis of banana fiber reinforced polyester composites*. Composites Science and Technology, 2003. **63**(2): p. 283-293.
155. Jeencham, R., Suppakarn, N. and Jarukumjorn, K., *Effect of flame retardants on flame retardant, mechanical, and thermal properties of sisal fiber/polypropylene composites*. Composites Part B: Engineering, 2014. **56**: p. 249-253.

156. Liu, L., Yu, Y. and Song, P.a., *Improved Mechanical and Thermal Properties of Polypropylene Blends Based on Diethanolamine-Plasticized Corn Starch via in Situ Reactive Compatibilization*. Industrial & Engineering Chemistry Research, 2013. **52**(46): p. 16232-16238.
157. Lu, N. and Oza, S., *Thermal stability and thermo-mechanical properties of hemp-high density polyethylene composites: Effect of two different chemical modifications*. Composites Part B: Engineering, 2013. **44**(1): p. 484-490.
158. Thummanukitcharoen, P., Limpanart, S. and Srikulkit, K., *Preparation of organosilane treated microcrystalline (SiMCC) and SiMCC/polypropylene composites*. Journal of Metals, Materials and Minerals, 2012. **22**(1): p. 13 – 19.
159. Luo, G., Li, W., Liang, W., Liu, G., Ma, Y., Niu, Y. and Li, G., *Coupling effects of glass fiber treatment and matrix modification on the interfacial microstructures and the enhanced mechanical properties of glass fiber/polypropylene composites*. Composites Part B: Engineering, 2017. **111**: p. 190-199.
160. Sirisinha, K., Boonkongkaew, M. and Kositchaiyong, S., *The effect of silane carriers on silane grafting of high-density polyethylene and properties of crosslinked products*. Polymer Testing, 2010. **29**(8): p. 958-965.
161. Luo, S., Cao, J. and McDonald, A.G., *Esterification of industrial lignin and its effect on the resulting poly(3-hydroxybutyrate-co-3-hydroxyvalerate) or polypropylene blends*. Industrial Crops and Products, 2017. **97**: p. 281-291.
162. Li, L. and Dou, Q., *Effects of malonic acid treatment on crystal structure, melting behavior, morphology, and mechanical properties of isotactic poly(propylene)/wollastonite composites*. Polymer Composites, 2010. **31**(6): p. 966-973.
163. Li, J., Song, Z., Li, D., Shang, S. and Guo, Y., *Cotton cellulose nanofiber-reinforced high density polyethylene composites prepared with two different pretreatment methods*. Industrial Crops and Products, 2014. **59**: p. 318-328.
164. Ebrahimi, M. and Moosavi, F., *The effects of temperature, alkyl chain length, and anion type on thermophysical properties of the imidazolium based amino acid ionic liquids*. Journal of Molecular Liquids, 2018. **250**: p. 121-130.

165. Vong, W.-T. and Tsai, F.-N., *Densities, Molar Volumes, Thermal Expansion Coefficients, and Isothermal Compressibilities of Organic Acids from 293.15 K to 323.15 K and at Pressures up to 25 MPa*. *Journal of Chemical & Engineering Data*, 1997. **42**(6): p. 1116-1120.
166. Nakagaito, A.N. and Yano, H., *The effect of fiber content on the mechanical and thermal expansion properties of biocomposites based on microfibrillated cellulose*. *Cellulose*, 2008. **15**(4): p. 555-559.





Table A-1 Cost of preparation of PW-MCC

Raw material	Cost (THB/g or mL)	Amount (g or ml)	Cost (THB/Kg)
PW sawdust	0.01	3500	17.5
Sodium hydroxide	0.25	1400	350
sodium hypochlorite	0.10	1400	140
Hydrochloric acid	0.11	8750	962.5
Total + Utility estimated for 4 h = 100 THB			1570.0

Table A-2 Properties of PW-MCC and Avicel® PH101

Properties	Unit	PW-MCC	Avicel® PH101
DP	-	375	318
CrI	%	60	56
Particle size	μm	30.56	27.27
Td	°C	311	326
Cost	THB/kg	1,570	5,750

Table A-3 Tensile strength of PP and PW-MCC/PP composites

Formula	Tensile strength (MPa)	Young's modulus (GPa)	Elongation at break (%)
PP	20.47±1.30	0.30±0.007	295±54.39
PMCC5	18.35±0.59	0.31±0.009	52±9.47
PMCC10	18.35±0.88	0.35±0.019	26±5.51
PMCC20	17.83±0.47	0.42±0.028	19±3.00
PMCC30	16.57±0.25	0.48±0.049	10±1.79

Table A-4 Flexural and impact properties of PP and PW-MCC/PP composites

Formula	Flexural strength (MPa)	Flexural modulus (GPa)	Impact strength (J/m)
PP	33±1.81	0.96±0.061	93.43±4.55
PMCC5	32±1.90	1.00±0.071	43.53±1.22
PMCC10	33±1.87	1.15±0.090	37.25±1.52
PMCC20	34±1.57	1.43±0.060	27.84±2.11
PMCC30	33±2.01	2.00±0.105	19.31±1.44

Table A-5 Density, MFI, and CTE properties of PP and PW-MCC/PP composites

Formula	Density (g/cm ³)	MFI (g/10 min)	CTE ($(\mu\text{m}/\text{m})/^{\circ}\text{C}$)
PP	0.893	16.39	205.84
PMCC5	0.908	15.80	203.06
PMCC10	0.923	14.20	186.16
PMCC20	0.954	12.80	169.84
PMCC30	1.006	10.18	126.63

Table A-6 Tensile strength of modified PW-MCC/PP composites

Formula	Tensile strength	Young's modulus	Elongation at break
	(MPa)	(GPa)	(%)
PMCC5MA	20.32±0.69	0.33±0.010	49±15.25
PMCC10MA	19.23±0.67	0.38±0.008	24±7.23
PMCC20MA	21.30±0.44	0.45±0.021	17±4.08
PMCC30MA	20.61±0.32	0.53±0.019	8±4.45
PMCC5S	19.27±0.22	0.30±0.01	9±0.64
PMCC10S	18.55±0.80	0.31±0.005	8±0.18
PMCC20S	18.05±0.83	0.32±0.013	8±0.44
PMCC30S	18.65±0.68	0.32±0.016	8±0.68
PMCC5B	19.25±0.85	0.35±0.006	27±9.58
PMCC10B	18.22±0.52	0.36±0.003	21±10.59
PMCC20B	15.43±0.17	0.37±0.005	12±1.74
PMCC30B	14.02±0.33	0.38±0.08	10±1.04
PMCC5H	20.21±0.25	0.34±0.08	47±15.32
PMCC10H	19.81±1.20	0.35±0.023	27±2.27
PMCC20H	16.47±0.70	0.32±0.004	25±1.46
PMCC30H	14.75±0.27	0.31±0.012	15±4.08
PMCC5L	19.32±0.48	0.32±0.023	63±14.03
PMCC10L	17.42±0.36	0.30±0.020	33±8.89
PMCC20L	16.47±0.38	0.33±0.012	14±2.25
PMCC30L	15.92±1.03	0.34±0.015	11±0.78

Table A-7 Flexural and impact properties of modified PW-MCC/PP composites

Formula	Flexural strength (MPa)	Flexural modulus (GPa)	Impact strength (J/m)
PMCC5MA	34±0.83	1.21±0.048	46.86±3.22
PMCC10MA	33±0.19	1.31±0.018	37.02±3.87
PMCC20MA	34±0.76	1.71±0.033	25.24±2.34
PMCC30MA	34±1.99	2.20±0.085	20.82±2.45
PMCC5S	28±2.62	1.14±0.041	31.6±2.33
PMCC10S	27±1.68	1.18±0.051	25.9±1.54
PMCC20S	27±0.61	1.21±0.023	24.0±2.56
PMCC30S	26±0.37	1.35±0.056	20.04±2.44
PMCC5B	29±0.61	1.16±0.024	31.36±3.65
PMCC10B	28±0.40	1.17±0.020	26.76±2.78
PMCC20B	26±0.81	1.27±0.046	17.24±2.22
PMCC30B	23±0.83	1.30±0.045	14.94±1.89
PMCC5H	31±0.78	1.03±0.042	47.23±1.22
PMCC10H	29±0.31	1.02±0.035	39.73±1.15
PMCC20H	26±0.75	0.94±0.042	29.80±1.77
PMCC30H	24±0.34	0.91±0.019	22.79±1.55
PMCC5L	32±0.63	1.20±0.022	53.3±2.86
PMCC10L	30±1.82	1.13±0.075	33.7±2.75
PMCC20L	27±0.83	1.12±0.040	27.5±3.55
PMCC30L	25±0.70	1.08±0.051	26.4±4.12

Table A-8 Density, MFI, and CTE properties of modified PW-MCC/PP composites

Formula	Density (g/cm ³)	MFI (g/10min)	CTE ($(\mu\text{m}/\text{m})/^{\circ}\text{C}$)
PMCC5MA	0.918	16.02	198.72
PMCC10MA	0.935	15.96	180.98
PMCC20MA	0.976	14.42	168.01
PMCC30MA	1.018	10.19	125.77
PMCC5S	0.920	22.32	165.02
PMCC10S	0.933	23.10	230.89
PMCC20S	0.961	23.45	237.89
PMCC30S	1.010	23.67	274.16
PMCC5B	0.906	16.53	214.02
PMCC10B	0.921	16.28	198.00
PMCC20B	0.946	15.50	152.41
PMCC30B	0.976	14.13	169.33
PMCC5H	0.907	18.90	187.46
PMCC10H	0.918	18.73	156.52
PMCC20H	0.939	17.73	198.60
PMCC30H	0.960	17.59	214.80
PMCC5L	0.899	20.23	207.93
PMCC10L	0.918	21.22	170.22
PMCC20L	0.946	23.12	190.68
PMCC30L	0.972	20.89	196.90

Table A-9 Water absorption of PP and the obtained PP composites

Formula	% of water absorption			
	7 day	14 day	21 day	28 day
PP	0	0	0	0
PMCC5	0.1475±0.0003	0.2104±0.0003	0.2333±0.0002	0.2649±0.0002
PMCC10	0.1697±0.0006	0.3115±0.0003	0.3675±0.0003	0.4792±0.0033
PMCC20	0.3651±0.0003	0.5415±0.0003	0.5929±0.0018	0.6776±0.0008
PMCC30	0.7009±0.0007	1.0716±0.0007	1.3379±0.0014	1.3796±0.0010
PMCC5MA	0.1581±0.0002	0.1927±0.0003	0.1806±0.0002	0.2230±0.0002
PMCC10MA	0.2402±0.0003	0.3032±0.0002	0.3449±0.0001	0.3655±0.0002
PMCC20MA	0.3732±0.0002	0.4965±0.0005	0.5651±0.0003	0.6325±0.0004
PMCC30MA	0.7743±0.0012	1.0412±0.0012	1.2056±0.0020	1.3987±0.0012
PMCC5S	0.1254±0.0003	0.1307±0.0003	0.2070±0.0008	0.2347±0.0001
PMCC10S	0.2059±0.0002	0.2574±0.0001	0.3229±0.0006	0.4225±0.0007
PMCC20S	0.3868±0.0001	0.4725±0.0005	0.5605±0.0007	0.6379±0.0010
PMCC30S	0.5840±0.0002	0.7300±0.0007	0.9828±0.0003	1.1283±0.0005
PMCC5B	0.1302±0.0002	0.1130±0.0002	0.1317±0.0004	0.1584±0.0002
PMCC10B	0.1346±0.0001	0.1652±0.0002	0.1807±0.0001	0.2004±0.0002
PMCC20B	0.1503±0.0003	0.2005±0.0004	0.2581±0.0003	0.3406±0.0004
PMCC30B	0.1854±0.0003	0.2984±0.0006	0.3497±0.0003	0.4001±0.0003
PMCC5H	0	0.0079±0.0005	0.0095±0.0004	0.0810±0.0003
PMCC10H	0.0860±0.0002	0.0933±0.0001	0.0950±0.0004	0.0979±0.0007
PMCC20H	0.1434±0.0004	0.1560±0.0003	0.1637±0.0004	0.1856±0.0003
PMCC30H	0.1726±0.0001	0.2210±0.0002	0.2620±0.0022	0.2956±0.0005
PMCC5L	0.0770±0.0003	0.1523±0.0004	0.1466±0.0001	0.1576±0.0003
PMCC10L	0.1520±0.0006	0.2099±0.0002	0.2389±0.0002	0.2792±0.0004
PMCC20L	0.2052±0.0002	0.3320±0.0003	0.3633±0.0006	0.4540±0.0003
PMCC30L	0.3081±0.0010	0.4342±0.0001	0.5215±0.0003	0.6210±0.0005

VITA

Miss Patcharaporn Chuayplod was born on November 21st, 1983 in Chiang Mai, Thailand. She received a Bachelor's Degree in Chemistry from the Department of Faculty of Science, Thammasat University in 2006. After that, she continued her Master degree at the Petrochemistry and Polymer Science program from Faculty of science, Chulalongkorn University in 2006 and received a Master degree of Science in Petrochemistry and Polymer Science in 2008. She has worked at IRPC Public Company Limited since 2009 in Research and Development department. She decided to further study in a Doctoral degree program in Materials Science at the Department of Materials Science, Faculty of Science, Chulalongkorn University in 2012 and graduated in 2018.

Publication

International Journal

- Chuayplod, P., and Aht-Ong, D, "Mechanochemical-assisted heterogeneous surface modification of parawood microcrystalline cellulose and its effect on the properties of polypropylene composites" World Journal of Engineering (accepted)
- Chuayplod, P., and Aht-Ong, D, "Mechanochemical Assisted Modification of Parawood Microcrystalline Cellulose using Silane Coupling Agent and Their Composites Properties" Key Engineering Materials (accepted)
- Chuayplod, P., and Aht-Ong, D, "A study of microcrystalline cellulose prepared from parawood (*Hevea brasiliensis*) sawdust waste using different acid types" Journal of Metals, Materials and Minerals (submitted)

International Presentation

- Chuayplod, P., and Aht-Ong, D, 2016. "Mechanochemical - assisted modification of parawood microcrystalline cellulose under heterogeneous conditions as reinforced materials in polypropylene composites" ICCE-24 24th Annual International Conference on Composites and Nano Engineering, Sanya, Hainan Island, China, Jul 17-23 (oral presentation)
- Chuayplod, P., and Aht-Ong, D, 2016. "Modification of parawood microcrystalline cellulose with silane coupling agent under mechanochemical process and their composites properties" 3rd International Congress on Advanced Materials (AM 2016), Bangkok, Thailand, Nov 27-30 (oral presentation)
- Chuayplod, P., and Aht-Ong, D, 2018. "Mechanochemical assisted modification of parawood microcrystalline cellulose with silane coupling agent and their composites properties" The 8th International Conference on Key Engineering Materials (ICKEM2018), Osaka, Japan, Mar 16-18 (oral presentation)